2mil

NASA TECHNICAL TRANSLATION NASA TT F-15,377

COSMIC RAY STUDIES ABOARD ARTIFICIAL EARTH SATELLITES

N.L. Grigorov el al., Editors

Translation of "Izucheniye kosmicheskikh luchey na iskusstvennykh sputnikakh zemli", "Nauka" Press, Moscow, 1973, 172 pages.

NATIONAL AERONAUTICS AND SPACE ADMINISTRATION
WASHINGTON, D.C. 20546 MAY 1974

STANDARD TITLE PAGE

1. Report No. NASA TT F-15,377	2. Government Accession No.	3. Recipient's Catalog No.
4. Title and Subtitle: COSMIC RAY STUDIES ABOARD ARTIFICIAL EARTH SATELLITES		5. Report Date: April 1974 6. Performing Organization Code
7. Author(s): N. L. Grigorov, et al., Editors		8. Performing Organization Report No. 10. Work Unit No.
9. Performing Organization Name and Address: SCITRAN, Box 5456, Santa Barbara, CA 93108		11. Contract or Grant No. NASw-2483 13. Type of Report and Period Covered: Translation
12. Sponsoring Agency Name and Address: National Aeronautics and Space Administration, Washington, D.C. 20546		14. Sponsoring Agency Code

15. Supplementary Notes

Translation of "Izucheniye kosmicheskikh luchey na iskusstvennykh sputnikakh zemli", Moscow, "Nauka" Press, 1973, 172 pp.

16. Abstract

This volume includes studies characterizing the general outlook for and results of specific investigations in the field of cosmic ray physics, performed using artificial Earth satellites. The major portion of the collection is made up of articles presenting the results of experiments made aboard the Proton 1, 2, 3 scientific space stations (measurements of hydrogen and carbon effective interaction sections, energy spectrum of primary cosmic ray particles of high and superhigh energies, study of the chemical composition of cosmic rays and high-energy electron fluxes in near-Earth cosmic space). Several articles in the collection relate to methodological questions of cosmic ray study aboard artificial Earth satellites (AES).

17. Key Words (Selected by Author(s))	18. Distribution Statement: Unclassified - Unlimited		
19. Security Classif. (of this report): Unclassified	20. Security Classif. (of this page): Unclassified	21. No. of Pages: 228	22. Price

PRECEDING PAGE BLANK NOT FILMED

TABLE OF CONTENTS

PRECEDING PAGE BLANK NOT FILMED

PROSPECTS FOR STUDYING HIGH-ENERGY COSMIC RAY PARTICLES ABOARD HEAVY AES

N. L. Grigorov

Cosmic ray study carried out by various methods has shown that /3* cosmic rays consist of a flux of atomic nuclei (hydrogen $\sim$ 83%, helium $\sim$ 16%, heavier about 1%) having very different energies — from $\sim 10^8$ eV to $\sim 10^{20}$ eV. Their energy distribution is described by a power law of the form $I (\geq E) = AE^{-\gamma}$, where $\gamma = 1.6 - 1.7$ in the energy interval $10^{10} - 10^{15}$ eV, and $\gamma = 2.2$ for particle energies $E > 10^{15}$ eV. If the energy is expressed in 10^9 eV, then $A = 8 \cdot 10^3$ $m^{-2}sec^{-1}sr^{-1}$.

Primary cosmic ray protons interacting with the nuclei of air atoms lose their energy. As a result, the flux of protons of given energy decreases by a factor of 2.5 in an atmospheric layer 100 g/cm^2 thick. Consequently, at sea level (1000 g/cm^2), the nucleon (proton and neutron) flux will be lower by $2.5^{10} \underline{\sim} 10^4$ than at the edge of the atmosphere. Cosmic ray particle studies are often conducted at mountain elevations ($\sim$ 700 g/cm^2) in order to reduce

*Numbers in the margin indicate pagination in the original foreign text.

somewhat the effect of high-energy particle absorption in the atmosphere. Although in this case the nucleon intensity increases by about a factor of 16 in comparison with the intensity at sea level, it still remains 600 times lower than that of the cosmic ray primary particles of the same energy.

The complex nuclei which comprise the primary cosmic rays collide with atomic nuclei in an air layer which is several tens of grams per square centimeter thick, and break down into their component nucleons. Therefore, the cosmic ray nuclear component is practically not recorded in the atmosphere at heights below 20 - 25 km.

If the solution of any physical problems requires experimentation with high-energy particles, the question arises of where these experiments should be conducted.

The fluxes of primary particles with energies 10^{12}, 10^{13}, 10^{14} eV, respectively, are equal to 300; 6; 0.1 particles/$m^2 \cdot hr \cdot sr$. The particle flux reaches mountain altitudes weakened in intensity by a factor of nearly 10^3. Therefore, tremendous installations, tens of square meters in area, are built at mountain elevations to record particles with energy 10^{12} - 10^{13} eV. It has not yet been possible to record particles with energies 10^{14} eV in the lower part of the atmosphere by direct methods. It would appear that a way out of this situation would be to construct installations of still larger area, /4 say 10^3 m^2. However, difficulties of a fundamental nature arise in this case.

The high-energy particles passing through the atmosphere collide with atomic nuclei and lose part of their energy in the creation of new particles — mesons. Therefore, in the depth of the atmosphere, high-energy nucleons are nearly always accompanied by secondary particles. When recording nucleons at mountain elevations using equipment of large area, mesons will be recorded along with the nucleons. Separation of the high-energy nucleons from the mixed

particle flux is possible at the cost of reduction of the recorded particle flux (which is small to start with) by tens or hundreds of times [1]. Therefore, "pure" experiments with cosmic ray particles of known nature with particle energies 10^{13} eV or higher become practically impossible in the lower part of the atmosphere.

The situation is essentially different when working with primary cosmic ray particles. If the equipment has working area ~ 0.5 m^2, and angular aperture about 0.4 sr, such an instrument will record one particle an hour for particle energy 10^{13} eV, and one particle in two days for energy 10^{14} eV. During several months of measurements, we can record several thousand particles with energy 10^{13} eV, and hundreds of particles with energy 10^{14} eV, under conditions of "pure" primary particle beams, i.e., particles of precisely known nature.

The ionization calorimeter method, proposed by the author in 1954 [2], has been widely used in recent years for measuring cosmic ray particle energy.

In this method, we use the principle of total primary particle energy absorption in a thick layer of matter. The equipment utilizing this principle is quite heavy. Specifically, for an absorbing layer thickness of about 500 g/cm^2 in the example considered above, the equipment weight reaches 3 - 4 tons. Thus, we come to the inevitable conclusion that recording of cosmic ray nucleons with energies 10^{13} - 10^{14} eV by direct methods requires the use of equipment weighing at least several tons and conducting measurements in the course of several months near or beyond the edge of the atmosphere. It is quite obvious that these conditions can be satisfied only by using heavy artificial Earth satellites.

The considerations mentioned above formed the basis for the first experiments with high-energy cosmic ray particles initiated aboard the Proton 1, 2, 3 AES. It is appropriate to examine the

relationship between the results obtained from the Proton AES and the tasks which still await their solution. This examination appears to us to be useful, since it may shed some light on the question: does the new direction in cosmic ray studies, initiated aboard the Proton AES, have any promise? /5/

In these experiments, we studied the dependence of the effective inelastic interaction section of protons with light atomic nuclei (hydrogen, carbon) in the energy range 20 - 600 GeV. The objective of the experiment included measurement of σ^{in}_{p-C} with accuracy of a few percent in a wide energy interval, extending far beyond the limits achievable during the same time period on existing accelerators.

It is well known that the results of the measurements conducted showed a small increase of σ^{in}_{p-C} by 20 $\pm$ 5%, with proton energy variation from 20 to 600 GeV (see present volume). The second task posed in the experiments aboard the Proton 1, 2, 3 AES concerned study of the primary cosmic ray particles themselves in the energy range 10^{10} - 10^{14} eV, by direct methods. In these studies, an attempt was made for the first time to study cosmic ray chemical composition in the energy interval 10^{12} - 10^{13} eV.

The results obtained showed that the energetic distribution of the protons and heavier nuclei in the particle energy interval 10^{12} - 10^{13} eV is different — with increase of the particle energy in this interval, the proton flux decreases more rapidly than the heavy nuclei flux (see page 47 of present volume). This result leads to the inevitable conclusion that there is a change of cosmic ray chemical composition in the energy interval 10^{12} - 10^{13} eV, which is in conflict with the prevalent concept (without adequate experimental foundation) of constant cosmic ray chemical composition over a wide energy interval 10^{9} - 10^{15} eV.

The program of studies aboard the Proton AES included study of primary cosmic ray electron component energetic spectrum. Measurements made aboard the Proton 1 and 2 AES showed that in near-Earth cosmic space, at heights 200 - 600 km, there is a flux of electrons with energies of hundreds and thousands of MeV, which is comparable in intensity with the primary cosmic ray flux.

Determination of the section increase, anomaly in the proton spectrum in the energy interval 10^{12} - 10^{13} eV, and intense high-energy electron fluxes in near-Earth cosmic space was the subject of further investigation aboard the Proton 4 space station, for which equipment radically different from that installed aboard the Proton 1, 2, 3 AES was developed (see present volume, p. 69).

Orbital complex moment theory predicts increase of the total and inelastic effective nucleon-nucleon collision sections with increase of the colliding particle energy. However, this increase is very small. Thus, with transition from energies of 20 GeV to 1000 GeV, σ^{in}_{p-p} increases by 20%. In order to record this increase reliably, σ^{in}_{p-p} must be measured with an accuracy no less than 5% for proton energy 10^{12} eV.

Bearing in mind the fundamental importance of verifying the validity of the theoretical analyses, one of the most important problems of the immediate future is to measure σ^{in}_{p-p} with an accuracy no less than 5% in the energy interval 50 - 100 GeV. This problem is entirely solvable if the measurements are made aboard a heavy AES and the experiment is directed toward resolution of this question. To obtain the necessary statistical accuracy, it is sufficient to use equipment with the following parameters: instrument geometric factor $\sim 10^3$ cm^2 · sr, target (carbon and polyethylene) thickness $\sim$100 g/cm^2, measurement time no less than 100 days. /6

Experiments performed aboard the Proton 1, 2, 3 AES showed that the dependence of the effective inelastic interaction section of protons with carbon nuclei σ^{in}_{p-C} on proton energy E in the energy interval 20 - 600 GeV can be approximated by a function of the form

$$\sigma^{in}_{p-C}(E) = \sigma_0 (1 + a \ln E/20),$$

where $a \simeq 0.06$, for measurement of E in GeV. A very important question arises: to what energies is this growth law valid?

The experiments made aboard the Proton AES showed that visibility of the measurements performed is important when measuring the effective sections. Two requirements must be satisfied in order to provide this visibility:

a) the measurements should be made aboard oriented AES;

b) the experiment should be visualized, i.e., equipment should be used which permits "seeing" the primary particle, its interaction in the target, and the avalanche in the ionization calorimeter.

Contemporary experimental equipment — spark chambers, electron optical converters (EOC) — makes it possible, in principle, to accomplish the required visualization of the experiment with transmission of the information over telemetry channels. In these experiments, the important question of the dependence of the effective inelastic interaction section for high energies from 10^{12} to 10^{13} eV on the atomic weight of the target nuclei may be resolved at the same time. This question cannot be resolved on opposing beam accelerators and will remain the prerogative of cosmic ray physics in the next few decades.

On of the most important problems of high-energy physics, which was posed more than a decade ago as the result of cosmic ray study, is that of the origin of fireballs.

The multiperipheral theory, considering interactions between colliding high-energy nucleons as exchange of virtual π-mesons, leads to the conclusion that, as a result, there should arise massive globs of matter — fireballs — with a mass of 3 - 4 nucleon masses, subsequent disintegration of which yields the experimentally required particles. With increase of colliding particle energy, the number of these globs increases in proportion to the logarithm of the impinging particle energy, which leads to secondary particle dependence of the type $n_s \sim \ln E$. /7

In the colliding nucleon center-of-mass system, the fireballs travel relative to one another with mean value of the Lorentz factor $\bar{\gamma} = 2 - 3$. This circumstance leads to the characteristic pattern of observed particle distribution as a function of their divergence angles and energies.

In spite of the fact that the fireball question has been discussed for more than ten years [3 - 7], convincing experimental data supporting their existence have not yet been obtained. The complexity of the problem solution lies in the fact that the results obtained for particle energies $10^{11} - 10^{12}$ eV can be described without resorting to fireballs [8].

Resolution of the question of the formation of systems with large masses is of fundamental importance, and can be obtained by studying the interaction of particles with superhigh energies $10^{13} - 10^{14}$ eV. According to the multiperipheral theory, at such energies, three fireballs, each with mass 3 - 4 GeV, should sometimes arise. Interactions of this type will show up as three groups of particles, each of which consists of about eight charged particles. If interactions of this type are discovered, and it is shown that the number of groups increases with increase of the primary particle energy, then this phenomenon can no longer be described by alternative schemes of the hydrodynamic or statistical model type.

Conduct of the corresponding experiments, requiring work with ultrahigh energy particles and use of the nuclear photoemulsion technique to obtain the required angular resolution and measure the secondary π^0-meson particle energy, is possible only aboard heavy AES. There is little doubt that in the near future, orbital scientific stations with qualified personnel on board will come into being. Under these conditions, the conduct of studies with equipment including an ionization calorimeter, system of space chambers, and nuclear emulsions becomes quite realistic.

If there is periodic replacement by orbital station personnel of the exposed emulsions, observations can be made of hundreds of interactions of particles with energies 10^{13} eV and tens of interactions of particles with energies 10^{14} eV, i.e., we can obtain unique experimental data which cannot be obtained at the present time by any other techniques.

In such an experiment, a detailed study can be made at the same time, in most convincing fashion, of primary cosmic ray chemical composition in the energy interval 10^{13} - 10^{14} eV, and the shape of the energy spectrum of the various nuclei groups in the superhigh energy. energy interval can be studied, i.e., we can obtain experimental data of fundamental importance for the theory of particle acceleration in /8
astrophysical objects. In the same experiment, we can seek the processes characteristic for the interaction of complex nuclei at superhigh energies. New phenomena may be discovered in this completely open region of study.

In studying the processes taking place during interaction of particles with superhigh energies 10^{14} - 10^{15} eV by indirect methods — using extensive atmospheric showers and high-energy muons — some anomalies have been discovered which do not fit into the framework of the generally accepted notions. Thus, at one time it was suggested that there is direct multiple generation of muons in strong interactions of particles with superhigh energies [9]. The theoretical

possibility of such a process at superhigh energies $\sim 10^{15}$ eV, when at small colliding particle distances $\sim 10^{-17}$ cm, the weak interactions may become of the order of the strong interactions, was noted in [10].

In recent years, the interest in this problem, which is of fundamental importance for elementary particle physics, has increased in connection with the experimental data on angular distribution of cosmic ray muons with energies $\sim 3 \cdot 10^{12}$ eV at sea level [11].

If the μ-meson energy E_μ satisfies the inequality $E_\mu \cos\theta \gg 10^{11}$ eV, the dependence of the intensity of muons with energies E_μ on the angle θ with the vertical, will obey the law

$$I(\theta) \sim \frac{1}{\cos\theta},$$

if the muons arise as a result of π- or K-meson decay.

The experimental data obtained in [11] indicate deviation from the $(\cos\theta)^{-1}$ law in the direction of approach to isotropy for large angles θ. In this connection, the hypothesis on the possibility of direct muon generation (in about 2% of the interactions) was proposed in [11].

It should be noted that, even if the hypotheses of [11] are confirmed experimentally, they will not be proof of the existence of direct multiple muon generation in nucleon interactions. It is sufficient to assume the birth of a hypothetical particle, disintegrating with formation of muons and having a lifetime tens of times shorter that that of the π- or K-mesons, for the experimental data to obtain their natural explanation.

The question of the possibility of multiple muon generation during collision of particles with energies $10^{14} - 10^{15}$ eV can be clarified only by observing processes in dense media, where the

probability of π^- or K-meson decay is approximately 10^5 times less than in the atmosphere at high altitudes.

For studying such processes with adequate statistical justification, it is necessary to use equipment weighing about 100 tons, /9
injected into near-Earth cosmic space aboard a heavy AES. In such an installation, using the principle of the ionization calorimeter of large thickness for primary particle energy measurement, a system of spark chambers for detecting primary and secondary particles, and charge detectors, it is possible in the course of a year to observe many thousand interactions of particles with energies 10^{14} eV, hundreds of interactions of particles with energies 10^{15} eV, study in detail the chemical composition of primary cosmic rays with energies 10^{15} eV, and observe the processes of multiple generation of superhigh energy muons if they exist in nature and occur with probability $\sim 10^{-1} - 10^{-2}$. In these experiments, it becomes possible to study by direct methods the typical interaction processes of the particles responsible for extensive atmospheric showers, and give an unambiguous treatment of this phenomenon, which has been the subject of more than twenty years of study.

These problems are of direct importance for high-energy particle physics, astrophysics, and cosmic ray physics. There can be little question that they will be resolved in the next few years with the aid of heavy AES.

References

1. Babayan, Kh. P., N. L. Grigorov, G. G. Dulyan, V. A. Sobinyakov, Ch. A. Tret'yakova and V. Ya. Shestoperov. Izvestiya AN SSSR, seriya fiz., Vol. 30, 1966, p. 1617.

2. Grigorov, N. L., V. S. Murzin and I. D. Rapoport. ZhETF, Vol. 34, 1958, p. 506.

3. Niu, K. Rep. No. 11 from the Institute for Nuclear Studies. Univ. of Tokyo, July 20, 1958.

4. Cocconi, G. Phys. Rev., Vol. 111, 1958, p. 1969.

5. Kraushaar, W. J. and L. I. Marx. Phys. Rev., Vol. 93, 1954, p. 326.

6. Dobrotin, N. A. and S. A. Slavatinskiy. Izvestiya AN SSSR, seriya fiz., Vol. 30, 1966, p. 1566.

7. Mensovich, M. and Ye. Gerulya. Izvestiya AN SSSR, seriya fiz., Vol. 31, 1967, p. 1398.

8. Grigorov, N. L., Ye. I. Daybog, I. L. Rozental' and V. Ya. Shestoperov. Yadernaya fizika, Vol. 9, 1969, p. 597.

9. Vernov, S. N., V. I. Tulupov, B. A. Khrenov and G. B. Khristiansen. Proceedings of International Conference on Cosmic Rays, Vol. 2. Mosocw, Izdatel'stvo AN SSSR, 1960, p. 169.

10. Markov, N. A. Giperony i K-mezony [Hyperon and K-Mesons]. Fizmatgiz, 1958, p. 243.

11. Bergeson, H. E., I. W. Keuffel, M. O. Larson, et al. Phys. Rev. Letters, Vol. 21, 1968, p. 1089.

MEASUREMENT OF EFFECTIVE INELASTIC INTERACTION SECTIONS OF PROTONS WITH CARBON AND HYDROGEN NUCLEI IN THE ENERGY INTERVAL 20 - 600 GeV ABOARD PROTON 1, 2, 3 SPACE STATIONS

N. L. Grigorov, V. Ye. Nesterov, I. D. Rapoport,
I. A. Savenko and G. A. Skuridin

Introduction

Measurements of strongly interacting high-energy ($E \gtrsim 10^{12}$ eV) /10 particle fluxes at mountain elevations carried out by various methods in recent years have indicated that at such high energies, the inelastic interaction section of protons with air nuclei σ^{in} is at least 10 - 25% larger than for particle accelerator energies [1, 2, 3]. These estimates were obtained by indirect methods, and naturally require verification by direct measurements.

It is very difficult to ensure the required statistical accuracy of a few percent in measuring the effective inelastic interaction section of nucleons with light atomic nuclei at mountain altitudes because of the small high-energy particle flux. Moreover, in the lower part of the atmosphere, ions constitute a large fraction ($\sim$ 30%) of the strongly interacting particle flux. This situation "contaminates" the primary particle beam and selection of only the neutral

primary particles (neutrons) reduces by at least a factor of three the flux, already small, of particles which can be used for measuring σ^{in}.

These difficulties can be avoided if we measure σ^{in} beyond the limits of the atmosphere aboard heavy AES. In this case, the high-energy proton flux increases by 10^3 - 10^4 times in comparison with the proton flux at mountain altitudes. Moreover, in this case, we can ensure quite "clean" primary proton beams. These considerations have stimulated the conduct of σ^{in} measurements aboard heavy AES, in spite of the serious technical difficulties associated with such measurements. We have made such σ^{in} measurements aboard the Proton 1, 2, 3 space stations. We used the multipurpose SEZ-14 instrument to measure the effective inelastic section σ^{in} of protons with target (carbon and polyethylene) nuclei. (This instrument was used not only to measure σ^{in}, but also to study the shape of the primary cosmic ray particle energy spectrum in the energy interval from $\sim 10^{10}$ to $\sim 10^{14}$ eV.) The basis of the σ^{in} measurement was the "beam knockout" method, which is widely used in cosmic ray particle studies.

The essence of this method is that we first measure the particle /11
flux I_{nt} passing through detectors which define the instrument angular aperture, and an inelastic interaction detector without a target in the particle path. Then we measure the particle flux I_t passing through the same detectors and a target without interaction therein, with the target located in the particle path.

In both cases, the particles are selected on the basis of the same characteristic after passing through the detectors, target, and interaction detector. Under these conditions,

$$I_t = I_{nt} \cdot e^{-x/\lambda}, \qquad (1)$$

where x is the target thickness in g/cm^2; λ is the range in g/cm^2 for inelastic particle interaction in the target; λ and σ^{in} are connected by the known relation: $\sigma^{in} = A/\lambda N_{Av}$, where A is the atomic weight of the target nuclei, N_{Av} is the Avogadro number. In the case of measurements in cosmic space, when not only protons (Z= 1), but also helium nuclei (Z = 2) and heavier nuclei are present in the primary cosmic ray flux, for measurement of the effective proton inelastic interaction section it is necessary to have a detector which separates the protons from the entire cosmic ray particle flux.

I. Equipment

A schematic of the SEZ-14 instrument is shown in Figure 1. It consists of two identical halves, on each of which measurements of σ^{in} can be made independently. This results in improved reliability, the possibility of monitoring equipment sensitivity stability, and increase of the measurement statistics.

Each half of the SEZ-14 instrument consists of the following detectors.

The ionization calorimeter for measuring proton energy consists of nine steel plates, each 5.5 cm thick. Between the plates there are plastic scintillators 1 - 10, each 1.5 cm thick, which are viewed by two FEU-49 (FEU-III) photomultipliers, connected to a common load. The overall thickness of the absorber in the ionization calorimeter, equal to 2.7 λ_{Fe} (λ_{Fe} is the proton interaction range in iron), provides, on the average, release of 50% of the primary proton energy in the ionization calorimeter.

The amplitude of the FEU-III signal, proportional to the energy released in the ionization calorimeter, acts on a series of integral amplitude discriminators having various triggering thresholds E_i

(i = 1 - 9), uniformly distributed on a logarithmic scale in the energy interval from $E_1 \simeq 10^{10}$ to $E_9 \simeq 10^{14}$ eV.

Above and below the ionization calorimeter are located scintillation counters made from plastic scintillators I and II, which cover the entire area of the ionization calorimeter. The upper counter I /12

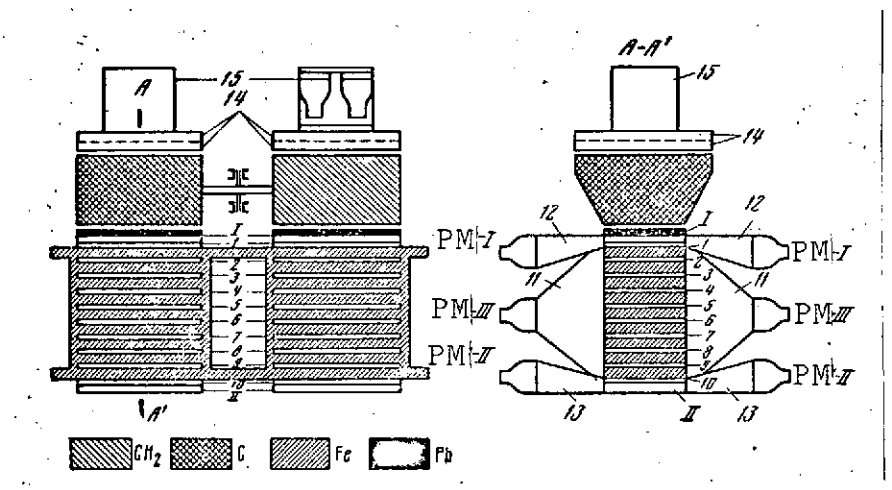

Figure 1. Schematic of SEZ-14 instrument:
1 - 10 — plastic scintillators of ionization calorimeter; 11 - 13 — diffusers for gathering scintillation light; 14 — proportional counters; 15 — direction detector; I — interaction detector; II — lower scintillation counter

serves to limit the solid angle in the limits of which primary particles are recorded. At the same time, it performs the functions of an inelastic proton interaction detector (ID) in the carbon and polyethylene targets located above it.

A lead layer 2.5 cm thick is located above the interaction detector I, for better detection of interactions. The lower scintillation counter II serves only to limit the solid angle. Both counters are constructionally identical, and in each of them the scintillators are viewed by two FEU-49, located on opposite sides and connected to a common load.

The diffusers 11 - 13, whose inner surfaces are painted with white enamel with low light absorption coefficient, are used for better light collection.

Above the targets are located two large proportional counters (PC) 14, which serve to separate the singly charged particles from the primary cosmic ray flux.

The selection of protons of given energy was accomplished as follows: It was required that the following signals appear in all the detectors within the limits of the coincidence circuit resolution time.

a) In each of the two proportional counters, the pulse amplitude was in the "window" $V_{min} \leq V \leq V_{max}$ ($V_{min} \simeq 0.2\ V_{prob}$, $V_{max} \simeq 2.7\ V_{prob}$, where V_{prob} is the most probable amplitude of the pulse created in the proportional counter by a singly charged relativistic particle). In this case, there is generated a signal, arbitrarily designated Z_1, corresponding to passage of one singly charged particle through both proportional counters. Under these conditions, the relativistic α particle (Z = 2) can imitate a singly charged particle with probability no greater than 2.5%. /13

b) In the interaction detector, the pulse amplitude was in the "window" $V_{min} \leq V \leq V_{max}$ ($V_{min} \simeq 0.4\ V_{prob}$, $V_{max} \simeq 1.7\ V_{prob}$, where V_{prob} is the most probable amplitude of the pulse created in the interaction detector by a singly charged relativistic particle). In this case, there is generated a signal, arbitrarily designated N_1, corresponding to passage of one singly charged particle through the interaction detector.

The relativistic α particle can imitate a singly charged particle in the interaction detector with probability not exceeding 2%.

c) In the lower scintillation counter there must be a signal with amplitude $V \geq 0.4\ V_{prob}$.

d) In the ionization calorimeter there must be released the energy corresponding to triggering of the i^{th} amplitude discriminator ($i = 1 - 9$). In this case, there is generated a signal, arbitratily designated E_{C_i}, corresponding to simultaneous triggering of the i^{th} amplitude discriminator and the two scintillation counters I and II. The resolution time of the coincidence circuits generating this signal is $\sim 1 \cdot 10^{-6}$ sec.

Then all the "simple" signals Z_1, N_1, E_{C_i} travel to a coincidence circuit with resolution time $\sim 6 \cdot 10^{-6}$ sec, where there is generated a signal, arbitrarily designated $Z_1N_1E_{C_i}$, which is fed to the scaling circuit — "operative memory".

The complex signal $Z_1N_1E_{C_i}$ means that at the moment of release in the ionization calorimeter of the energy E_{C_i}, one singly charged particle passed through both proportional counters and the interaction detector. (Detailed description of the construction and characteristics of all the SEZ-14 detectors is given in [4]).

The number of $Z_1N_1E_{C_i}$ events per unit time is a measure of the intensity of protons with energy $E \geq E_i$ passing through the apparatus. Thus, as a result of measurements without targets, the quantity I_{nt} is determined, while with targets, the quantity I_t is determined, which in accord with Expression (1) determine the value of σ^{in}.

Aboard the Proton 3 station, the described SEZ-14 apparatus was supplemented by directional Cherenkov counters, which discriminated the singly charged particle $Z = 1$, and performed the functions of a

detector of the direction of motion of that singly charged particle which, in passing through the proportional counters and interaction detector, generated the signal $Z_1 N_1 E_{C_i}$.

These direction detectors (DD) were located above the proportional counters, and each included four Cherenkov counters 15 (see Figure 1). Each counter consisted of a plexiglass detector 16 cm in diameter and 3 cm thick, and a PM-49. Al four PM-49 operated into a common load. /14

Since the DD reduced significantly the instrument relative aperture, the measurements with them were only of a monitor nature. Therefore, the DD in the SEZ-14 apparatus aboard Proton 3 were connected into the recording system so that proton selection could be carried out without the DD as well (by the second half of SEZ-14), i.e., the complex signals $Z_1 N_1 E_{C_i}$ could be recorded by the same technique as aboard Proton 1 and 2. Moreover, both halves of SEZ-14 recorded the signals $Z_1 N_1$ DD E_{C_i}, meaning that the signal $Z_1 N_1 E_{C_i}$ coincides with the pulse from the DD.

II. Results of Measurement of Effective Inelastic Interaction Section of Protons with Carbon Nuclei σ_{p-C}^{in}

A. Measurements Without DD

In the SEZ-14 apparatus, satisfaction of at least one of the following conditions was required for inelastic interaction recording.

1. Formation in the target of at least two charged particles ($n_s \geq 2$), with ranges $R \geq 28$ g/cm^2 Pb + 5 g/cm^2 of plastic scintillator. In this case, generation of any particles with lifetime $\tau \lesssim 10^{-10}$ sec, yielding γ quanta during their decay, may not occur.

2. Formation of at least one particle with lifetime $\tau \lesssim 10^{-10}$ sec, yielding during its decay γ quanta with total energy $E_\gamma \gtrsim 500$ MeV. In this case, charged particles may be absent.

3. Charge exchange of a proton into a neutron under the condition $n_s = 0$. In this case, generation of the electron-photon component may not occur.

Control experiments, made on the ITEP (Institute of Theoretical and Experimental Physics) accelerator, showed that even for proton energy E = 5 GeV, the probability W of interaction recording in the SEZ-14 apparatus is quite high: $93 \pm 4\%$ for particles entering the instrument from the proportional counters, and $81 \pm 5\%$ for protons entering through the SEZ-14 lower base [5]. In the latter case, the proportional counter performs the functions of an interaction detector.

With increase of the energy, the mean multiplicity n_s increases quite rapidly, and we can expect that for $E \gtrsim 20$ GeV, the recording interaction probability is close to 100% (this is indicated, specifically, by the σ^{in}_{p-C} values which we obtained).

The targets were made interchangeable in order to conduct measurements of the proton intensity I_{nt} without targets, and I_t with various targets under the same conditions. The graphite target, and then the polyethylene target, were alternately positioned within the limits of the instrument working aperture periodically with an interval of 6 - 12 hours. Then both targets were removed from the /15
instrument working aperture and the intensity I_{nt} was measured. After this, the entire measurement cycle was repeated.

In order to exclude the slow apparatus sensitivity variation which can arise during long-duration instrument operation, we determined the mean intensities during a measurement seance lasting 6 - 12

hours with fixed target position, and took the ratios $\langle I_{nt}/I_t \rangle$ obtained in adjacent measurement seances. Then these ratios were averaged throughout the entire flight, the quantity $\langle |I_{nt}/I_t| \rangle$ was determined, and the mean square deviation from the average was taken as the measure of the $\langle |I_{nt}/I_t| \rangle$ error.

The error determined in this way included both statistical errors (for the energy levels E_1, E_2, E_3 they introduce a small contribution to the overall error), and all the uncontrollable factors which influence the event counting rate (change of instrument orientation relative to the Earth, influence of the Earth's magnetic field on PM sensitivity, and so on).

A special analysis of the information obtained aboard the Proton 2 AES showed that the quantities I_{nt}/I_t have a normal distribution. Using the mean value $\langle |I_{nt}/I_t| \rangle$, obtained with the graphite target, we determined σ^{in}_{p-C}.

The preliminary results of σ^{in}_{p-C} measurements aboard the Proton 1 and 2 AES have already been reported and published in [6, 7].

The processing of all the available primary information relating to σ^{in} measurements (aboard Proton 1, 2, 3) has now been completed. The desire to obtain data on the magnitude of the effective inelastic interaction section of protons with protons required more exact account for the apparatus factors, primarily more precise calculation of the effective target thickness (particularly of the carbon target, because of its complex configuration).

Moreover, we took into account the differences in target thickness (reaching several percent) aboard each Proton AES. The values of $\bar{x}^g_C$ (effective graphite target thicknesses in g/cm^2 aboard the different AES for measurements without direction detector) and

the average amount of carbon $\bar{x}_C^p$ and hydrogen $\bar{x}_H^p$ along the particle path in the polyethylene targets are presented in Table 1. /16

TABLE 1

Satellites	Polyethylene target			Graphite target	
	$\bar{x}^p$	$\bar{x}_C^p$	$\bar{x}_C^p$	$\bar{x}_H^g$	$x_C=x_C^g-x_C^p$
Proton 1	36.1	30.9	5.2	33.8	2.9
Proton 2	35.8	30.7	5.1	33.1	2.4
Proton 3	36.7	31.5	5.2	34.1	2.9

Using the effective target thicknesses shown in Table 1, we obtained the values of σ_{p-C}^{in} from the measurements performed without the DD on each half of the SEZ-14 aboard the Proton 1, 2, 3, AES. They are shown in Figure 2. We see from this figure that all the σ_{p-C}^{in} values obtained on the first and second halves of the Proton 1 SEZ-14, first half of the Proton 2 SEZ-14, and the second half of the Proton 3 SEZ-14 yield values which agree well with one another in the measurement error limits. Therefore, the values of σ_{p-C}^{in}, relating to similar energy values obtained in different series of experiments, can be averaged.

The values of σ_{p-C}^{in} averaged with account for error "weight" are shown in Table 2.

Here, the errors are mean square values and include both statistical and all apparatus errors which affect apparatus sensitivity during the measurement time.

The question of systematic errors will be examined in the discussion of corrections.

TABLE 2

E, GeV	σ^{in}_{p-C}, mbarn	E, GeV	σ^{in}_{p-C}, mbarn
22	208 ± 4	200	253 ± 3.5
62	226.5 ± 2.5	610	240 ± 7

The measurement of σ^{in}_{p-C} made on the second half of the Proton 2 SEZ-14 [6] yields relative increase of σ^{in}_{p-C} with increase of E, which is the same as from the other measurements, but the absolute value of σ^{in}_{p-C} is 10% lower than indicated by the data obtained on the first half of the Proton 2 SEZ-14, and on the other Proton AES.

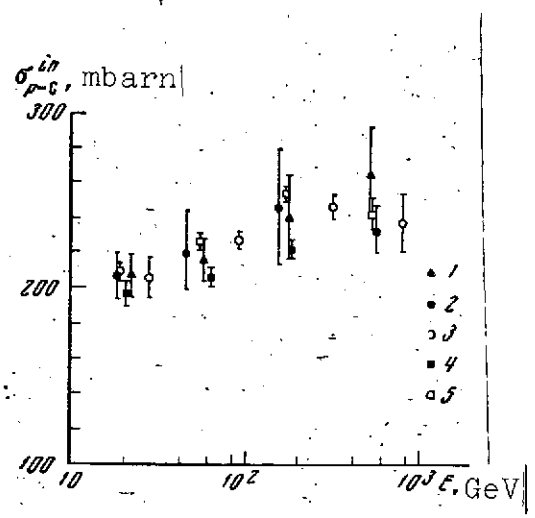

Figure 2. Results of σ^{in}_{p-C} measurements by different halves of the the SEZ-14 aboard Proton 1, 2, 3 AES: 1 — Proton 1, first half of SEZ-14; 2 — same, second half; 3 — Proton 2, first half; 4 — same, second half; 5 — Proton 3, second half; the abscissa axis is primary proton energy, the ordinate axis is σ^{n}_{pi-C} in mbarn

/17

The availability of more complete information on the scientific equipment operation made it possible to explain the reasons for the systematic low values of σ^{in}_{p-C} obtained on the second half of the Proton 2 SEZ-14. It was found that on the second half of the SEZ-14, during a significant part of the entire apparatus operating time, there was marked increase of the count rate of double coincidences CN_0 (coincidence of pulses from the interaction detector and lower scintillation counter), which enter into the generation of the signal $Z_1N_1E_{C_i}$. A possible reason for the count rate increase could be increased noise of one of the interaction detector photomultipliers, which would lead to

high channel loading, and, as a consequence, loss of $Z_1N_1E_{C_i}$ event counts (as a result of the "dead time" of the amplitude discriminators which form the signal N).

Special analysis of the information obtained showed that during those time periods when the CN_0 count rate exceeded significantly the normal value, the $Z_1N_1E_{C_i}$ count rate was less than normal, and its decrease with the targets was less than without the targets, which then led to decrease of the measured value of σ^{in}_{p-C}. In order to make certain that the low values of σ^{in}_{p-C}, in the measurements made on the second half of the Proton 2 SEZ-14, were connected with the anomalously high CN_0 signal count rate, we selected only those measurement seances in which the CN_0 signal count rate increase was not very large. The value of σ^{in}_{p-C} obtained from these seances was 5% higher than from all the measurement seances, including the seances with anomalously high CN_0 signal count rate. Therefore, prior to finding the method for introducing the corrections to the magnitudes of the ratios $\langle|I_{nt}/I_t\rangle|$, which determine the value of σ^{in}_{p-C}, we excluded the data of the second half of the Proton 2 SEZ-14 from consideration.

In order to obtain the final data on the value of σ^{in}_{p-C} for various proton energies, it is necessary to introduce into the measured effective section values several corrections, due to apparatus and systematic effects.

In the following, we examine the corrections for proton absorption in the target structure, random coincidences, and δ electron formation.

1. Correction for proton interactions in the duraluminum target structure. The correction was determined by calculation, using for

particle accelerator energies the values of the effective inelastic interaction section of protons with Al nuclei, equal to 400 mbarn. In order to account for these interactions, the measured value of $\langle I_{nt}/I_t \rangle$ must be multiplied by 0.975. This yields a 6% correction to σ^{in}_{p-C}.

2. Correction due to random coincidences of low-energy cosmic ray protons with energy release in the ionization calorimeter. The /18
essence of this correction is associated with the following. Signals of the $Z_1N_1E_{C_i}$ type may be created not only by true protons, which provide energy release E_i in the ionization chamber, but also by random coincidences of low-energy (1 - 10 GeV) cosmic ray protons passing through the proportional counters and interaction detector (signal Z_1N_1) with energy release E_i in the ionization calorimeter caused by any high energy particle.

Random coincidences of this type will constitute the same fraction of the true $Z_1N_1E_{C_i}$ events for all energies E_i, as long as the proton energy spectrum is similar to the spectrum of all cosmic ray particles, i.e., at least up to $E = 10^{12}$ eV. Thus, $I_{ra}(E_i)/I_{tr}(E_i) = \text{const}$, where $I_{ra}(E_i)$ and $I_{tr}(E_i)$ are the intensities of the $Z_1N_1E_{C_i}$ events, due, respectively, to random coincidences and the true flux of protons yielding energy release E_i in the ionization calorimeter. The measured intensity is equal to $I_{meas} = I_{tr} + I_{ra}$. The value of σ_{p-C} is determined by the magnitude of the measured ratio:

$$\frac{I^{nt}_{meas}}{I^{C}_{meas}} = \frac{I^{nt}_{tr}}{I^{C}_{tr}} + \frac{I^{nt}_{ra}}{I^{C}_{ra}} = \frac{I^{nt}_{tr}}{I^{C}_{tr}} \cdot \frac{1 + I^{nt}_{ra}/I^{nt}_{tr}}{1 + I^{nt}_{ra}/I^{nt}_{tr} K}, \qquad (2)$$

where

$$K = \frac{I^{nt}_{tr}/I^{C}_{tr}}{I^{nt}_{ra}/I^{C}_{ra}} .$$

We see from (2) that $(I_{nt}/I_C)_{meas} = (I_{nt}/I_C)_{tr}$, only for K = 1. Therefore, random coincidences will not distort the quantity σ^{in}_{p-C} only when, first, interactions in the target of low-energy cosmic ray particles yielding random coincidences are recorded with 100% effectiveness and, second, the true value of σ^{in}_{p-C} is constant throughout the entire energy interval (from the energy of protons yielding a contribution to the random coincidences to the measured energies E_i). However, as our experiments on a proton beam with energy E = 5 GeV [5] showed, for this energy the effectiveness of proton interaction recording in a target by the interaction detector of the SEZ-14 instrument is less than 100%. Therefore, we would expect that

$$\frac{I^{nt}_{ra}}{I^{C}_{ra}} < \frac{I^{nt}_{tr}}{I^{C}_{tr}}$$

i.e., K > 1, and $(I^{nt}/I_C)_{meas} < (I^{nt}/I_C)_{tr}$. Consequently, because of the existence of random coincidences, the measured value σ_{meas} will be less than the true value σ_{tr}.

Moreover, if σ_{tr} is independent of E, then K = const, and $\sigma_{meas}(E_i)/\sigma_{tr}(E_i)$ = const. If, however, $\sigma_{tr}(E)$ increases with increase of E, then K(E) will also increase with increase of E, since /19 I^{nt}_{ra}/I^{C}_{ra} is independent of E. This leads to a situation in which the measured increase of σ(E) will be weaker than the increase of $\sigma_{tr}(E)$.

The influence of random coincidences on σ under the experimental conditions aboard the Proton AES may be determined on the basis of the following arguments: $I_{ra}(E_i, \theta) = A(E_i) F_{cr}(\theta)$, where $F_{cr}(\theta)$ is the flux intensity of all cosmic ray particles at the latitude θ, $A(E_i)$ is a parameter proportional to the flux of all particles which yield in the ionization calorimeter a fixed energy release E_i which depends on the geometric and radiotechnical characteristics of the apparatus.

For fixed E_i, the value A = const, and $I_{meas}(E_i, \theta) = I_{meas}(E_i) + I_{ra}(E_i, \theta) = I_{tr}(E_i) + A(E_i) F_{cr}(\theta)$. With change of the latitude of the observation location from $\theta = 0°$ to $\theta \geq 50°$, the quantity F_{cr} changes by about a factor of 10, i.e., $F_{cr}(\theta \geq 50°)/F_{cr}(\theta = 0°) = 10$. The experimental data obtained aboard the Proton 2 and 3 AES showed that $I_{meas}(E_i, \theta \geq 50°)/I_{meas}(E_i, \theta = 0°) = 1.2$, and is independent of E_i (as it should be, if the dependence on θ is associated only with random coincidences). Recalling that $I_{tr}(E_i)$ will not depend on θ (if $E_i \gtrsim 20$ GeV) and $F_{cr}(\theta \geq 50°)/F_{cr}(\theta = 0°) = 10$, we find that $I_{tr}(E_i) = 0.98 \times I_{meas}(E_i, \theta = 0°)$, i.e., measurements in the equatorial region yield an intensity which is practically undistorted by random coincidences.

Hence, it follows that $I_{ra}(E_i, \theta) = I_{meas}(E_i, \theta) - I_{tr}(E_i) \simeq I_{meas}(E_i, \theta) - I_{meas}(E, \theta = 0°)$.

From these measurements, we can obtain for each latitude θ the intensity I_{ra} without target and with graphite target, and determine the ratio I_{ra}^{nt}/I_{ra}^{C}:

$$\frac{I_{ra}^{nt}}{I_{ra}^{C}} = \frac{I_{meas}^{nt}(E_i, \theta) - I_{meas}^{nt}(E_i, \theta = 0°)}{I_{meas}^{C}(E_i, \theta) - I_{meas}^{C}(E_i, \theta = 0°)}.$$

If this ratio is averaged over all θ values with account for satellite stay time at the various latitudes, we obtain $\langle|I^{nt}_{ra}/I^{C}_{ra}|\rangle$, which determines the correction to σ owing to random coincidences. It is easy to show that the correction to σ owing to random coincidences is

$$\frac{\Delta\sigma}{\sigma_{meas}} = \frac{\sigma_{tr} - \sigma_{meas}}{\sigma_{meas}} =$$

$$\frac{1}{\ln\left(\langle|\frac{I^{nt}_{meas}}{I^{C}_{meas}}|\rangle\right)} \ln \frac{1 - \langle|I^{nt}_{ra}/I^{nt}_{meas}|\rangle}{1 - \langle|\frac{I^{nt}_{ra}}{I^{nt}_{meas}}|\rangle \left(\langle|\frac{I^{nt}_{meas}}{I^{C}_{meas}}|\rangle \Big/ \langle|\frac{I^{nt}_{ra}}{I^{C}_{ra}}|\rangle\right)} .$$

Averaging over the available data obtained aboard Proton 2 for various energy thresholds, the correction owing to random coincidences was found to be $\Delta\sigma/\sigma_{meas} = 10 \pm 4\%$.

The large error in the correction magnitude leads to the corrected values of σ^{in}_{p-C} having, in addition to mean square errors amounting to ∿ 2 - 3%, large systematic error (the same for all energies), equal to ± 4%.

At the same time, the data on σ obtained only from that part of the information which relates to low latitudes (in the equatorial region) will not contain errors associated with random coincidences (and consequently, will not have the ± 4% systematic error), but will have large mean square errors because of using only part of the information obtained. Nevertheless, as we see from Table 3, the large mean square errors for the equatorial σ measurements are less than the systematic errors in σ^{in}_{p-C} arising with introduction of the random coincidence correction.

TABLE 3*

E, GeV	σ^{in}_{p-C}, mbarn	$\lvert\Delta\sigma\rvert$, mbarn	σ^{in}_{p-C}, mbarn
22	229±4	9	236±8
62	254±2,5	10	254±5
200	278±3,5	11	286±8
610	264±7	10,5	290±13

*Translator's note: Commas represent decimal points.

Table 3 presents in the second column the averaged σ^{in}_{p-C} values corrected for random coincidences (averaged over all the measurements aboard Proton 1, 2, 3). The mean square error was obtained by averaging the data before introducing the random coincidence correction. The third column shows the modulus of the systematic error in the corrected σ values, which arises when introducing the random coincidence correction. The fourth column shows the averaged values of σ_{p-C}, obtained aboard Proton 1, 2, 3 as a result of measurements only in the equatorial region. The errors are mean square.

We see from Table 3 that the σ^{in}_{p-C} values corrected for random coincidences agree to within the mean square measurement errors with the σ measurements at the equator, which do not contain errors due to random coincidences. Moreover, we see that the "equatorial" σ^{in}_{p-C} measurements have better accuracy of the absolute σ^{in}_{p-C} values; therefore, we shall use only these measurements in the following.

3. Corrections to σ^{in}_{p-C} owing to δ electrons. The magnitude of the correction to σ^{in}_{p-C} owing to δ electrons constitutes from 2.4% (for E = 22 GeV) to 4.3% (For E > 100 GeV). (The determination of of this correction is presented in more detail later, in examining the physical effects which influence the measured quantity σ^{in}_{p-C}). /21

TABLE 4

E, GeV	σ^{in}_{p-C}, mbarn	E, GeV	σ^{in}_{p-C}, mbarn
22	216±7	200	260±7
62	231±5	610	263±12

After introducing the corrections for δ electrons and for interactions in the duraluminum target structure to the average σ values obtained from measurements at the equator (last column of Table 3), we obtained the final σ^{in}_{p-C} values shown in Figure 3 and Table 4.

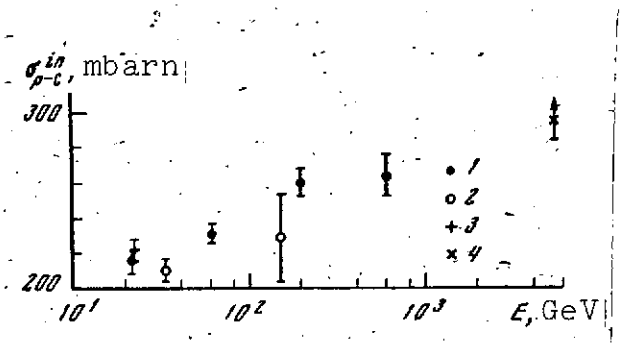

Figure 3. Dependence of σ^{in}_{p-C} on proton energy: 1 — mean σ^{ni}_{p-C} values from results of measurements aboard Proton 1, 2, 3 AES after introducing all the corrections; 2 — measurements of σ^{in}_{p-C} by direction detector aboard Proton AES; 3 — accelerator data [10]; 4 — lower limit of the σ^{in}_{p-C} section obtained by indirect methods [11]

B. Measurement with Direction Detector (DD)

Measurement of σ^{in}_{p-C} using a direction detector has the following characteristic features.

The thin Cherenkov counters used in the direction detectors preclude the possibility of recording a single singly charged particle leaving the ionization calorimeter and passing through the interaction detector and proportional counters. Therefore, events of the Z_1N_1 DD E_{C_i} type are due to primary protons entering the instrument only through its "entry window", and passing through the detectors in the following sequence: DD, PC, ID, and ionization calorimeter. In this case, interactions are recorded only by the interaction detector.

As was previously noted, the direction detectors reduced the SEZ-14 relative aperture by a factor of ten. Therefore, the measurement errors with the DD are significantly larger than without them, particularly at high energies when the measurement error is determined by the statistics of the protons being recorded. /22

In order to reduce the σ^{in}_{p-C} measurement errors at an energy of 150 GeV, we determined σ^{in}_{p-C} using measurements with both graphite and polyethylene targets. (In the polyethylene target, about 80% of all interactions take place on carbon nuclei.) In the latter case, we assumed that σ^{in}_{p-C} = (28.7 ± 1.7) mbarn, in accordance with the results obtained in measurements without the DD (see below). These σ^{in}_{p-C} values, obtained on the same SEZ-14 half with the graphite and polyethylene targets, were averaged with account for error "weight". These data are shown in the second column of Table 5. For energies of 18 and 50 GeV, the σ^{in}_{p-C} value indicated in the second column of Table 5 was obtained using measurements only with the graphite target. The third column shows the values of σ^{in}_{p-C} measurement on the same half of the Proton 3 SEZ-14 without DD, using only equatorial measurements. In the data shown in Table 5, corrections were introduced for the δ-electrons (to the results of measurements both without and with the DD), and for interactions in the target structure (only in the measurements without DD).

Corrections to results of measurements with DD.

1. The Cherenkov counters in the DD were arranged so that the primary protons traversing in the instrument solid angle do not pass through the massive duraluminum elements of the target structure; therefore, it is not necessary to introduce a correction into the results of σ^{in}_{p-C} measurements made with DD for interaction with the target structure elements (the correction is 6%).

TABLE 5

E, GeV	σ^{in}_{p-C} (with DD)	σ^{in}_{p-C} (without DD
18	215±7,6	215±10
50	195±12	230±7
150	228±25	259±10

2. No correction was introduced to the data obtained with DD for random coincidences, since there was no Z_1N_1 DD E_{C_i} event intensity dependence on geomagnetic latitude owing to random coincidences.

3. The same corrections for δ electrons were introduced into the results of measurements performed with DD as into the results of measurements without DD.

The mean σ^{in}_{p-C} value obtained in measurements with DD, as a result of averaging the data for the first two energy thresholds (E_1 and E_2) and equal to $\langle\sigma^{in}_{p-C}\rangle = 210 \pm 6$ mV, is for 34 GeV mean energy. /23 This value of σ and also the value obtained with DD for 150 GeV energy are shown by the circles in Figure 3. We see from the figure that the results of σ^{in}_{p-C} measurement with DD are in agreement with the results of measurements without DD (particularly for the 20 - 30 GeV energy, where the measurement errors with DD are still quite small).

III. Measurement of Effective Inelastic Proton-Proton Interaction Section σ^{in}_{p-p} in Energy Interval 20 - 600 GeV

The magnitude of the effective inelastic proton-proton interaction section σ^{in}_{p-p} was determined from measurements of the proton

fluxes of different energies passing without interaction through the carbon target (I^C), and the polyethylene target I^{CH_2}.

Since the amount of carbon per square centimeter in the polyethylene target was less than in the graphite target by the magnitude $\overline{\Delta x}_C = \overline{x}_C^g - x_C^p$ (see Table 1), the σ_{p-p}^{in} value was determined from the expression:

$$\sigma_{p-p}^{in} = \frac{1}{\overline{x}_H N_{Av}} \ln \left\langle \frac{I^C}{I^{CH_2}} \right\rangle + \frac{\Delta \overline{x}_C \sigma_{p-C}^{in}}{\overline{x}_H A_C}, \quad (3)$$

where $\overline{x}_H$ is the average amount of hydrogen in grams per square centimeter along the particle path in the polyethylene target; A_C is the atomic weight of carbon; σ_{p-C}^{in} is the effective inelastic interaction section with carbon nuclei, taken from measurement results with the graphite target.

The mean value of the intensity ratio $\langle I^C/I^{CH_2} \rangle$ was determined as follows. For two adjacent measurement seances with the carbon and polyethylene targets, we determined the ratio during the measurement seance of the intensities I^C and I^{CH_2}, and these ratios I^C/I^{CH_2} were averaged over all adjacent seance pairs. We determined the average value of $\langle I^C/I^{CH_2} \rangle$ and the mean square deviation from the average, which we took as the measure of the $\langle I^C/I^{CH_2} \rangle$ error.

The following corrections were made to the σ_{p-p}^{in} value determined using (3). /24

1. Correction for the δ electrons to the measured σ_{p-p}^{in} value was calculated, just as the correction to σ_{p-C}^{in}. These corrections ranged from 2.2% (for E - 22 GeV) to 4.0% (for $E \geq 100$ GeV), and were introduced into the results of σ_{p-p}^{in} measurements performed both without and with DD.

2. Correction for interactions in the duraluminum target structure was not introduced, since the graphite and polyethylene target structures were identical and the influence of these interactions was automatically excluded in calculating the ratio I^C/I^{CH_2}.

3. In order to avoid the need for introducing corrections to σ^{in}_{p-p} owing to random coincidences, we used only the results of measurements without DD in the vicinity of the equator. (We note that if we use all the information and introduce a correction for random coincidences equal to + 10%, we obtain the same result as when using only the near-equatorial measurements).

The final data, after introducing the indicated corrections and averaging the results of measurements made using both halves of the SEZ-14 apparatus aboard the Proton 1, 2, 3 AES, are shown in Table 6.

TABLE 6*

E, GeV	σ^{in}_{p-p}, mbarn	E, GeV	σ^{in}_{p-p}, mbarn
22	27,7±3,6	610	44,3±9,3
62	28,2±2,3	18	26,9±4,5
200	32,1±3,8	50	35,1±5,7

*Translator's note: Commas represent decimal points.

The last two rows are for measurements with DD. The weighted mean value for these two energies is $\sigma^{in}_{p-p} = 30 \pm 3.5$ mbarn, and is for an energy of $3.4 \cdot 10^{10}$ eV.

We see from Table 6 that the measurements with and without DD agree well with one another and with the particle accelerator data for the corresponding energy.

Figure 4 represents the σ^{in}_{p-p} measurement results. We see from the figure that the results of our measurements do not contradict the possibility of the same σ^{in}_{p-p} increase as is observed for σ^{in}_{p-C} with transition from partical accelerator energies $\sim$ 20 GeV to energies $\sim$ 200 GeV.

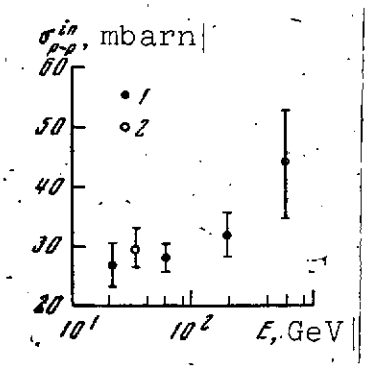

Figure 4. Dependence of σ^{in}_{p-p} on proton energy from results of measurements aboard Proton 1, 2, 3 AES after introducing all the corrections: 1 — measurements without DD; 2 — measurements with DD

/25

IV. Discussion of Results

We see from Figure 3 that with transition from proton energy $2 \cdot 10^{10}$ eV to $2 \cdot 10^{11}$ eV, the effective inelastic interaction section with carbon nuclei increases by 20 $\pm$ 5% (the probability that this increase is random for the measurement errors obtained is $2 \cdot 10^{-6}$).

It is obvious that the observed increase cannot be ascribed to measurement errors. Therefore, it is advisable to evaulate the possible methodological effects which could lead to the observed increase, and also the physical processes of trivial nature which are capable in principle of increasing the measured σ^{in}_{p-c} values.

A. Systematic Effects

1. With increase of particle energy, the SEZ-14 angular aperture for the protons being recorded may increase, and, as a consequence of this, the effective target thickness may increase.

The angular aperture increase is associated with the fact that when a primary proton passes through the proportional counters and interaction detector so that the avalanche generated by the proton exits through the side surface of the ionization calorimeter, this

proton may be recorded if at least one secondary particle enters the lower scintillation counter. The higher the proton energy E, the more secondary particles in the avalanche and the higher the probability of a scattered particle reaching the lower scintillation counter ("overcount" phenomenon).

With such broadening of the solid angle Ω in the limits of which primary protons are recorded, the effective path $\bar{x}_c$ traveled by the particles in the target will increase, the probability of interaction while passing through the target will increase, which will imitate increase of σ^{in}_{p-C}. This effect may be evaluated under the extreme assumption: each particle passing through the proportional counters and interaction detector, no matter what the angle at which it entered the ionization calorimeter, will be recorded if the energy E_i released in the calorimeter is sufficient to trigger the i^{th} amplitude discriminator. It is obvious that this assumption yields the maximal possible proton "overcount" and, therefore, the maximal possible increase of the effective target thickness $\bar{x}_c$. Calculation showed that for isotropic angular distribution of the primary protons, the "overcount" phenomenon increases effective target thickness by only 2.8% in comparison with the value used.

Thus, the "overcount" phenomenon can increase the measured section by a maximum of 3%, and cannot explain the observed 20% increase.

2. The absence of constant Proton satellite orientation relative to the vertical led to a situation in which events of the $Z_1N_1E_{C_i}$ type, recorded without DD, in many cases could be created by particles entering through the SEZ-14 lower base. The first possibility is the following. If the primary particle is a proton, then such a proton, after releasing in the ionization calorimeter the E_i part of its energy, may leave the calorimeter without accompaniment by other particles, enter the interaction detector, and pass through the

/26

proportional counters. In this case, a $Z_1 N_1 E_{C_i}$ signal is generated. If measurements are made with a target, such a "reverse-traveling" proton (or any other strongly interacting particle) creates, during interaction in the target, a shower, which will be recorded by the proportional counters (i.e., for such reverse-traveling, strongly interacting particles, the proportional counters will serve as an "interaction detector"). If the PC recorded showers with 100% probability, then all interactions in the targets of reverse-traveling protons and other high-energy particles would be recorded, and for these particles, the correct value of σ^{in} would be measured; however, the measured σ^{in} value would not be ascribed to particles with energy E_i released in the ionization calorimeter, but rather to particles with energy $<< E_i$.

Therefore, if σ^{in} did not depend on E, the reverse-traveling particles would not distort the measurement results. However, low-energy particles (a few GeV) create, during interaction in the targets, showers consisting of such a small number of particles that these showers are recorded by the PC with probability less than 100%. For such reverse-traveling particles, the measured value σ^{in}_{meas} will be less than the true value σ^{in}_{tr}. Therefore, the measured σ^{in} value for all primary proton particles and reverse-traveling particles will also be less than σ^{in}_{tr} in this case.

As E_i increases, the energy of the reverse-traveling protons will also increase and, consequently, the probability of the PC recording their interactions in the targets will increase. Therefore, the measured section will increase, approaching σ^{in}_{tr}. If σ^{in}_{tr} = const, the reverse-traveling particles could imitate increase of σ^{in}, with increase of E only under the condition that for smaller E the measured section $\sigma_{meas} < \sigma_{tr}$, and with increase of E the value of $\sigma^{in}_{meas} \rightarrow \sigma^{in}_{tr} = 215 \pm 5$ mbarn [11].

Comparison of our results with particle accelerator results (which we take to be true) shows that for minimal energy, $E \sim 20$ GeV $\sigma_{meas} = \sigma_{tr}$ (to within 5 - 7 mbarn). Comparison of measurement results without DD ($\sigma = 216 \pm 7$ mbarn) and with DD ($\sigma = 210 \pm 6$ mbarn) leads to the same conclusion. (Reverse-traveling particles are not present in the measurements with DD.)

There is a second possibility for creation of $Z_1N_1E_{C_i}$ events by /27 particles exiting through the lower base of the instrument.

A high-energy primary particle (of any nature) enters the ionization calorimeter through the lower base at a large angle to the instrument axis, so that the avalanche created by the particle exits through the side surface of the ionization calorimeter. However, in the avalanche there are many pions with energies of several hundred MeV, traveling at angles $\theta \sim 1$ relative to the primary particle direction of motion. One such pion may pass through the interaction detector and proportional counters. In this case, the reverse-traveling particles will be basically pions with energies of several hundred MeV. (For $E > 10^9$ eV $\theta < 0.3$ and the pion will travel along the avalanche; for $E \leq 10^8$ eV the pion range will be small and it will not depart very far from the avalanche.)

Such pions will be absorbed during interaction with the graphite target nuclei, and these interactions will be recorded by the proportional counters with probability close to 100%. In examining the mechanism of signal formation $Z_1N_1E_{C_i}$ by cosmic ray particles entering the SEZ-14 through the lower base, the section σ^{in}_{p-C} for reverse-traveling particles will correspond to the inelastic interaction section of pions with energy of hundreds of MeV with the carbon nuclei, and it will not change with primary particle energy change. Therefore, this $Z_1N_1E_{C_i}$ event formation mechanism cannot lead to σ^{in}_{p-C} increase with increase of E_i.

3. Nonlocal showers are those interactions of primary cosmic ray particles (protons, heavy nuclei) in the matter surrounding the SEZ-14 apparatus, as a result of which the most energetic particles enter the ionization calorimeter and release in the calorimeter the energy E_i, while the secondary particles of comparatively low energy enter the proportional counters, interaction detector, and lower scintillation counter. If a single particle enters both the PC and ID, a $Z_1N_1E_{C_i}$ signal arises, which imitates a proton which releases in the ionization calorimeter the energy E_i. The presence (or absence) of a target may influence nonlocal shower secondary particle entry into the PC (and to a lesser degree into the ID), since the latter is protected from below by the entire thickness of the ionization calorimeter, and from above by a layer of lead about 30 g/cm^2 thick), and thereby alter the intensity of the $Z_1N_1E_{C_i}$ events, i.e. influence the magnitude of the measured section σ^{in}_{p-C}.

It is not possible to calculate this phenomenon in practice. However, from the measurement results we can evaluate the nature of the influence of the quantity σ of both nonlocal showers and all the background processes leading to the appearance of $Z_1N_1E_{C_i}$ events.

Most of the Proton AES material surrounding the SEZ-14 instrument was located at the sides. This material, and also the ionization calorimeters themselves (the ionization calorimeter of the first SEZ-14 half was a source of nonlocal showers for the second SEZ-14 half, and vice versa), were nonlocal shower sources. Since both nuclear and electron-photon showers have marked secondary particle divergence directivity for the indicated arrangement of the material, the fraction of nonlocal showers imitating $Z_1N_1E_{C_i}$ events will increase relatively when the SEZ-14 instrument is turned with its "entry window" toward the Earth and all the material is located above the proportional counters. (In general, for such instrument orientation, only the reverse-traveling particles, nonlocal showers, and

/28

all those background events which lead to the formation of the complex $Z_1N_1E_{C_i}$ signal are recorded, since in this case direct high-energy proton flux is not recorded — it is shielded by the Earth). Therefore, the dependence of I_{nt}/I^C, I_{nt}/I^{CH_2} on the energy E_i, measured with the instrument "entry window" oriented toward the Earth, yields the characteristic of the influence of this entire complex of background events on increase of σ. In order to clarify how the indicated relations depend on the instrument orientation relative to the Earth, we used the Z_1N_1 DD E_{C_i} event count rate as an indicator of SEZ-14 orientation, since with the instrument oriented with "entry window" toward the Earth ("downward" orientation) the event count stopped, and with orientation toward the zenith ("upward" orientation) the Z_1N_1 DD E_{C_i} count rate was maximal.

Using these guide lines, we selected from all the information obtained aboard Proton 3, those time intervals when the instrument was oriented "upward" and "downward", and for these time intervals we determined the $Z_1N_1E_{C_i}$ event count rate (on the second SEZ-14 half without and with targets, and also the average values of I_{nt}/I^C and I_{nt}/I^{CH_2} for these two orientations for the energy thresholds $E_1 \simeq 20$ GeV, $E_2 \simeq 60$ GeV, $E_3 \simeq 200$ GeV, and $E_4 \simeq 600$ GeV.

The total time, in the course of which the specified instrument orientation was observed, was not long, and the accuracy of the intensity ratios obtained is not high. Since the measure of the section change with energy increase is the ratio of the quantity I_{nt}/I^C for E_i ($i \geq 2$) to the quantity I_{nt}/I^C for the energy E_i, in order to increase the accuracy, we averaged the ratios

$$\frac{\ln\left(\frac{I_{nt}}{I^C}\right)_{E_i}}{\ln\left(\frac{I_{nt}}{I^C}\right)_{E_1}} \text{ and } \frac{\ln\left(\frac{I_{nt}}{I^{CH_2}}\right)_{E_i}}{\ln\left(\frac{I_{nt}}{I^{CH_2}}\right)_{E_1}},$$

relating to the same energy E_i. The results are shown in Table 7.

TABLE 7*

	SEZ-14 orientation "up"	SEZ-14 orientation "down"
$\frac{\sigma(E_2)}{\sigma(E_1)}$	1,15±0,09	1,08±0,09
$\frac{\sigma(E_3)}{\sigma(E_1)}$	1,31±0,11	1,17±0,12
$\frac{\sigma(E_4)}{\sigma(E_1)}$	1,35±0,19	1,05±0,22

*Translator's note: Commas represent decimal points.

Although the errors are large, we can still conclude from the data of Table 7 that all the background events taken together ("downward" orientation) do not yield σ increase greater than the true protons ("upward" orientation). /29

All orientations of the SEZ-14 instrument were involved in the dependence of σ^{in}_{p-C} and σ^{in}_{pp} on E, presented in Figures 3 and 4. Consequently, the obtained section increase with proton energy increase is only the lower bound of the increase. The true increase may be somewhat greater than shown in these figures.

B. Physical Effects

1. δ electrons. In the SEZ-14 apparatus, a shower of two charged particles was recorded as an interaction. Therefore, among the recorded interactions, some portion consists of δ electrons. On the basis of the conditions of particle recording by the interaction detector, the energy of the δ electrons entering the detector must be quite high — several MeV.

We calculated the probability W_δ (E) that a proton with energy F creates in a graphite target a delta electron, which will be

recorded as a second particle. In the calculation, we accounted for the probability of recording electrons of different energies in the interaction detector.

E, eV	$6\cdot10^9$	10^{10}	$2\cdot10^{10}$	$4\cdot10^{10}$	$9.4\cdot10^{10}$	$\geq10^{11}$
W_δ (E)	0.4	0.6	1.1	1.3	1.6	1.7
$\frac{\Delta\sigma}{\sigma_{meas}}$	-1.2	-1.8	-3.2	-3.6	-3.8	-4.1

Owing to these delta electrons, the measured value σ_{meas} will be greater than the true value σ_{tr} by the magnitude $\Delta\sigma$. The calculated values of W_δ (E) and $\Delta\sigma/\sigma_{meas}$ are shown above.

The value of W_δ, due to muons with $\overline{E}_\mu \simeq 6 \cdot 10^8$ eV, was determined experimentally at sea level (from the viewpoint of delta electron formation, muon energy $6 \cdot 10^8$ eV is equivalent to proton energy $E = 6 \cdot 10^9$ eV). /30

We obtained a value of W_δ (with graphite target thickness x_C = 26 g/cm^2) equal to $0.5 \pm 0.17) \cdot 10^{-2}$. We have presented previously in [8, 9] preliminary data obtained with low statistical accuracy $W_\delta = (0.16 \pm 0.27) \cdot 10^{-2}$. We see that the experimental value of W_δ agrees well with the calculated value, which indicates correct account for the experimental factors, principally the probability of recording δ electrons. This provides a basis for using the calculated value of the correction $\Delta\sigma/\sigma_{meas}$ for proton energies E > $6 \cdot 10^9$ eV. It may be seen that when E increases from $1 \cdot 10^{10}$ eV to 10^{11} eV, the measured section can increase by only $\sim$ 3%, owing to the δ electrons. However, the nature of the increase (fast for $10^{10} \leq E \leq 4 \cdot 10^{10}$, and slow for $E > 4 \cdot 10^{10}$ eV) has an entirely different form than that observed experimentally (see Figure 3).

2. Quasielastic scattering. If, in our measurements, secondary particles — products of quasielastic interactions of primary protons with carbon nuclei — were recorded, then with increase of the proton energy, the probability of recording these secondary particles would increase (if only because of reduction of the divergence angle in the laboratory coordinate system), and this could lead to increase of σ^{in}_{meas}. Let us evaluate the maximal possible contribution of quasielastic scattering to the measured quantity σ^{in}_{p-C}.

It is obvious that, as a result of quasielastic scattering, there cannot arise a secondary particle (nucleon) with energy $\geqq E_{rn}(t)$, where $E_{rn}(t)$ is the kinetic energy of the recoil nucleon arising for elastic scattering with transfer of the four-momentum t. Therefore, the maximal probability of secondary particle recording will occur if the transferred momentum is communicated to a single proton. In order for this proton to enter the interaction detector, its range must be no less than 28 g/cm^2 Pb, i.e., the kinetic energy $E \geqq 150$ MeV. This value of E corresponds to $|t| = 0.3$ (GeV/c)^2. Therefore, secondary particles in the quasielastic scattering case under the present conditions can be recorded if $t \geqq 0.3$ (GeV/c)^2, and a single proton carries away the transferred momentum.

For primary proton energy 23 GeV, the quasielastic scattering section for carbon nuclei with momentum transfer $t \geqq 0.3$ (GeV/c)^2 amounts to only 1.7 mbarn [10]. If we consider that with transfer of this momentum to a target-nucleus neutron, quasielastic scatterings will not be recorded, we find that the maximal contribution to σ^{in}_{p-C} of quasielastic scattering of protons with energy $\sim$ 20 GeV amounts to 0.9 mbarn.

Another way to record quasielastic scattering is possible — complete disintegration of the nucleus and recording of "evaporative" neutrons. However, the probability of recording them under our conditions is so small that their contribution to the section can be only $\sim$ 0.1 mbarn. /31

Thus, if with increase of the primary proton energy there is no increase of the total quasielastic scattering section or broadening of the primary proton scatter cone, the contribution of quasielastic scattering to the measured σ increase is no more than 0.9 mbarn, i.e., no more than 0.5%.

B. Comparison with Other Results

We see from the above analysis that the observed σ^{in}_{p-C} increase cannot be explained by trivial physical processes (δ electrons, quasielastic scattering).

The question naturally arises of the degree to which this increase in the high-energy proton interval contradicts (or agrees with) the available data on behavior of the inelastic interaction section of protons (nucleons) with the light nuclei in the cosmic ray particle energy interval ranging from hundreds to thousands of GeV.

Measurement of the effective inelastic interaction section of cosmic ray particles having energy of hundreds of GeV with atomic nuclei has been made by many authors, primarily at mountain elevations [12 - 17]. In these studies, the inelastic interaction section of all cosmic ray particles (nucleons and pions) with Fe atomic nuclei was measured. By inelastic interaction they meant those interactions in which the primary particle transferred to π^0 mesons a significant part of its energy (from several to tens of percent). In each of the cited studies, the effective section was measured with statistical accuracy $\sim$ 7 - 10% for particle energies of several hundred GeV.

Therefore, the question of σ^{in} increase or invariability was resolved by comparing the measured section with accelerator measurement results (different apparatus and different technique). The effective section was not measured in any of the studies performed in cosmic rays, other than the present investigation, using the

same apparatus and technique over a wide energy interval — from particle accelerator energies up to hundreds of GeV. In the studies [12 - 17] made in cosmic rays, no account was taken for the difference in the inelastic interaction sections of pions and nucleons, in spite of the fact that the interaction section was measured of particles, among which pions constitute $\sim$ 30%. Therefore, it is not clear which data the measured section should be compared with. However, if we account for the pion fraction in the particle flux at those altitudes at which the measurements were made, account for the difference in the effective sections of pions and nucleons with energy $\sim$ 100 GeV obtained in cosmic rays in [18], and introduce into the results of [12 - 17] the corresponding correction, then the corrected sections will exceed by about 10% the values obtained for particle /32
acceleration energies [11]. The single available study on cosmic rays in which the primary particles were neutrons with mean energy $\bar{E}$ = 100 GeV [18], gave σ^{in}_{p-C} = 216 $\pm$ 20 mbarn. This result does not contradict our data.

No direct measurements are available in the nucleon energy range $E > 10^{12}$ eV. However, we can obtain relations which permit measuring the lower limit of the effective inelastic interaction section of nucleons with air atom nuclei for energies $(2 - 5) \cdot 10^{12}$ eV, with quite good statistical accuracy. A detailed analysis of the experimental data on methods and results of determining the lower effective inelastic interaction section limit is presented in [11]. We shall cite the final results from that study.

The first method — comparison of the relative fluxes of strongly interacting particles I_{si} (E), traveling without accompaniment by other particles, and of all particles of the same energy I_{na} (E) (regardless of accompaniment by secondary particles) — yields for inelastic proton interaction in air the range $\lambda \lesssim 75 \pm 5.5$ g/cm^2 for $E \gtrsim 6 \cdot 10^{12}$ eV. Hence, $\sigma^{in}_{p-C} \geqq 280 \pm 21$ mbarn [11].

The second method — comparison of the absolute fluxes of single nuclear-active particles with the flux of protons of the same energy incident on the top of the atmosphere — yields $\sigma^{in}_{p-C} \geq 300 \pm 13$ mbarn for particles with $E \gtrsim 5 \cdot 10^{12}$ eV [11]. (The interaction section with air nuclei was scaled to the interaction section with carbon nuclei, using the law $\sigma \sim A^{2/3}$.)

We see that both methods lead to σ^{in}_{p-C} increase, exceeding considerably the measurement error. We obtain the mean σ^{in}_{p-C} value for $\bar{E} = 5.5 \cdot 10^{12}$, by averaging the results of both methods:

$$\langle \sigma^{in}_{p-C} \rangle = 294 \pm 11 \text{ mbarn.}$$

This value is also shown in Figure 3 by the x symbol. The entire ensemble of data obtained on the σ^{in}_{p-C} dependence on E in the $20 \leq E \leq 600$ GeV interval can be described by a single empirical relation

$$\sigma^{in}_{p-C} = \sigma_0 \left(1 + a \ln \frac{E}{20}\right),$$

where $\sigma_0 = 216 \pm 17$ mbarn, $a = (6.8 \pm 1.2) \cdot 10^{-2}$.

Conclusions

1. Measurements of the effective inelastic interaction sections of protons with carbon nuclei in the energy interval from 20 to 600 GeV yield σ^{in}_{p-C} increase by at least $20 \pm 5\%$, with transition from 20 to 200 GeV energy. Systematic and physical effects can explain no more than 4% increase. /33

2. Measurement of the effective inelastic proton-proton interaction section in the energy interval 20 - 600 GeV were made with 8 - 20% accuracy. The relation obtained does not contradict the similar section increase obtained for σ^{in}_{p-C} in the same energy interval.

3. The available experimental data on effective inelastic interaction sections of cosmic ray particles with light atomic nuclei for energies of a few hundred GeV and for energies of several thousand GeV do not contradict the results obtained aboard the Proton 1, 2, 3 space stations.

References

1. Grigorov, N. L., V. A. Sobinyakov, V. Ya. Shestoperov and A. V. Podgurskaya. Zhurnal eksperimental'noy i teoreticheskoy fiziki (ZhETF), Vol. 33, 1957, p. 1099.

2. Dovzhenko, O. I, G. T. Zatsepin, Ye. A. Murzina, S. I. Nikol'skiy and V. I. Yakovlev. Proceedings of International Conference on Cosmic Rays. Moscow, Izdatel'stvo AN SSSR, 1960, p. 144.

3. Babayan, Kh. P., N. L. Grigorov, E. A. Mamidzhanyan, V. A. Sobinyakov and V. Ya Shestoperov. Izvestiya AN SSSR, seriya fiz., Vol. 29, 1965, p. 1552.

4. Grigorov, N. L., G. P. Khakhidze, V. Ye. Nesterov, I. D. Rapoport, I. A. Savenko, A. V. Smirnov, A. F. Titenkov and P. P. Shishkov. Kosmicheskiye issledovaniya, Vol. 5, No. 3, 1967, p. 383.

5. Akimov, V. V., V. S. Borisov, G. V. Veselova, L. L. Gol'din, L. N. Kondrat'yev, V. Ye. Nesterov, I. D. Rapoport, N. G. Ryabova and G. K. Tumanov. Trudy vsesoyuznoy konf. po fizike kosm. luchey (Proceedings of All-Union Conference on Cosmic Ray Physics), Part 1. Moscow, FIAN, No. 1, 1968, p. 96.

6. Grigorov, N. L., V. Ye. Nesterov, I. D. Rapoport, I. A. Savenko and G. A. Skuridin. Kosmicheskiye issledovaniya, Vol. 5, No. 3, 1967, p. 420.

7. Basilova, R. N., N. L. Grigorov, V. Ye. Nesterov, I. D. Rapoport, I. A. Savenko and G. A. Skuridin. Izvestiya AN SSSR, seriya fiz., Vol. 31, 1967, p. 1450.

8. Grigorov, N. L., V. Ye. Nesterov, I. D. Rapoport, I. A. Savenko and G. A. Skuridin. Trudy mezhdunarodnoy konferentsii po kosmicheskim lucham (Proceedings of International Conference on Cosmic Rays). Calgary, Canada, 1967, p. 512.

9. Grigorov, N. L., V. Ye. Nesterov, I. D. Rapoport, I. A. Savenko and G. A. Skuridin. Izucheniye chastits kosmicheskikh luchey vysokikh energiy na ISZ "Proton" (Study of High-Energy Cosmic Ray Particles Aboard the Proton AES). Preprint, Moscow, NIIYaF, Moscow State University, 1967.

10. Belletini, G,, G. Cocconi, A. N. Diddens, et al. Nucl. Phys., Vol. 79, 1966, p. 609.

11. Grigorov, N. L. Izmereniya effektivnykh secheniy neuprugogo vzaimodeystviya chastits kosmicheskikh luchey s atomnymi yadrami v oblasti energiy bolee 250 GeV (Measurement of Effective Inelastic Interaction Sections of Cosmic Ray Particles with Atomic Nuclei in the Energy Interval Above 250 GeV). Preprint, Moscow, NIIYaF, Moscow State University, 1969.

12. Denisov, Ye. V., V. G. Denisova, V. M. Kim, A. Ye. Morozov and S. A. Slavatinskiy. Izvestiya AN SSSR, seriya fiz., Vol. 31, 1967, p. 1466.

13. Andronikashvili, E. P., et al. Izvestiya AN SSSR, seriya fiz., Vol. 32, 1968, p. 326.

14. Andronikashvili, E. P., et al. Izvestiya AN SSSR, seriya fiz., Vol. 31, 1961, p. 1455.

15. Garibashvili, D. I., et al., Izvestiya AN SSSR, seriya fiz., Vol. 31, 1967, p. 1458.

16. Akashi, et al. Canadian Journal of Physics, Vol. 46, 1968, p. 660.

17. Denisov, Ye. V. Izvestiya AN SSSR, seriya fiz., Vol. 32, 1968, p. 398.

18. Alakoz, A. V., V. N. Bolotov, M. I. Devishev, L. F. Klimanova and A. P. Shmelev. Izvestiya AN SSSR, seriya fiz., Vol. 32, 1968, p. 394.

ENERGY DISTRIBUTION OF PRIMARY COSMIC RAY PARTICLES IN THE 10^{10} - 10^{14} eV ENERGY INTERVAL MEASURED ABOARD PROTON 1, 2, 3 SPACE STATIONS

N. L. Grigorov, V. Ye. Nesterov, I. D. Rapoport,
I. A. Savenko and G. A. Skuridin

Introduction

The study of the primary cosmic ray particle energy spectrum /34
shape and, particularly, the chemical composition in the high-energy region is of direct importance for two basic aspects of cosmic ray physics: astrophysical and nuclear physical. In the first case, the spectrum and chemical composition are those basic characteristics which are directly associated with the mechanism of particle acceleration and propagation in galactic space. In the second case, the spectrum and chemical composition are those characteristics which enter critically into the various models which interpret the processes of ultrahigh-energy particle interaction with atmospheric matter.

It is obvious that the most direct way to investigate primary cosmic rays involves studies conducted at those altitudes where the cosmic ray flux and composition have not yet been distorted by their interaction with atmospheric matter, i.e., either at balloon altitudes

or beyond the bounds of the atmosphere aboard AES. Studies of this type in the high-energy particle region were initiated aboard the Proton AES.

The basic results of high-energy particle study conducted aboard the Proton 1, 2, 3 AES have now been analyzed. We shall report the results obtained relating to two basic aspects:

1) the form of the all-particle spectrum without determination of their charge (ionization burst spectrum) in the energy interval from 10^{11} to 10^{14} eV;

2) the form of the proton spectrum in the energy interval from 10^{10} to 10^{13} eV.

The basic instrument used in studying the form of the energy spectra was the SEZ-14 instrument, described in detail in [1]; therefore, we shall not discuss the principles of its operation. We simply note that the SEZ-14 aboard Proton 3 was supplemented by two direction detectors (DD), located above the proportional counters (PC) (see Figure 1, page 14 of the present volume). Each of these detectors was a telescope consisting of two plastic scintillators with dimensions $37 \times 37 \times 1.5$ cm^3, between which were located four plexiglass Cherenkov counters, 16 cm in diameter and 3 cm thick. The total area of the Cherenkov counters in each DD was 800 cm^2. These /35
Cherenkov counters were used as motion direction detectors for the particles passing through the proportional counters, and as particle selectors with respect to charge. The DD reduced the SEZ-14 instrument relative aperture by a factor of nine; therefore, they were used differently in the two halves.

In the first half of the SEZ-14 instrument, the DD was connected to generate a coincidence signal from the sensors determining the instrument angular aperture. In this case, a signal exceeding $\sim 0.4\ V_{prob}$, where V_{prob} is the most probable pulse created by a

μ-meson at sea level, was required from the Cherenkov counter. Ionization bursts E_i were recorded in the same fashion as aboard the Proton 1 and 2 AES (since E_i is a "simple" signal which does not include coincidences with other signals); in addition, events of the type Z_1N_1 DD E_{C_i}, Z_1N_2 DD E_{C_i}, analogous to the events $Z_1N_1E_{C_i}$ and $Z_1N_2E_{C_i}$, aboard the Proton 1 and 2 AES, were recorded, but with the requirement for the presence of an impulse from the Cherenkov counter.

In the second half of the SEZ-14 instrument, the DD served as a charge meter: amplitudes of the Cherenkov counter impulses lying in a "window" extending from 0.4 V_{prob} to $\sim 2V_{prob}$, were selected, and only these pulses were used to generate the complex signals Z_1N_1 DD E_{C_i}. The signals from the Cherenkov counter were not used to generate the "master" pulse, therefore, it was possible to conduct parallel measurements with and without the DD, i.e., we could measure the intensities of the events $Z_1N_1E_{C_i}$, $Z_1N_2E_{C_i}$, as was done aboard the Proton 1 and 2 AES.

Measurement Results

§1. All-Particle Energy Spectrum

The all-particle energy spectrum is simply the spectrum of the ionization bursts caused in the ionization calorimeter by all cosmic ray particles, regardless of their nature, location of entry into the ionization chamber, and direction of travel.

We should note that if the chemical composition is independent of particle energy, the heavy nuclei flux in the high-energy region constitutes about 40% of the flux of all particles of given energy.

If we consider that the interaction range in iron for heavy nuclei is somewhat less than the proton range, and for this reason the heavy nuclei will release in the ionization calorimeter a

relatively larger part of their energy than the protons, then the nuclear share in generation of the recorded bursts constitutes about 60 %.

If a primary particle with energy E_0, $E_0 + dE_0$ strikes an elementary area $dS_i = dx_i \cdot dy_i$ (the subscript i denotes the number of the ionization calorimeter face), and with probability W (u, Z) releases the energy fraction $u = E_r/E_0$, then for a power-law primary particle spectrum $I(E_0)\, dE_0 = A/E_0^{\gamma})\, dE_0$, the number of the ioniza- /36
tion bursts corresponding to the energy release E_r, $E_r + dE_r$, recorded per unit time, will be

$$N(E_r)\,dE_r = \frac{A\,dE_r}{E_r^{\nu}} \sum_i \underbrace{\int dx_i \int dy_i}_{S_i} \int_0^{2\pi} d\alpha \int_0^{\pi/2} d\beta \cos\beta \sin\beta \times \left| \times \int_i^0 u^{\nu-1} W(u, Z)\,du. \right| \qquad (1)$$

where α and β are the angles at which the primary particle crosses the i^{th} ionization calorimeter face; Z = Z (x, y, α, β) is the total path traveled by the primary particle and the avalanche which it generates in the ionization calorimeter.

We denote

$$\sum_i \underbrace{\int dx_i \int dy_i}_{S_i} \int_0^{2\pi} d\alpha \int_0^{\pi/2} \cos\beta \sin\beta\, d\beta = \pi \sum_i S_i = \Gamma_{gl}$$

Γ_{gl} is the global geometric factor (in our case, $\Gamma_{gl} = \pi (S_1 + S_2 + S_3)$ $cm^2 \cdot sr$, where S_1, S_2, S_3 are the areas of the base and two sides of the ionization calorimeter).

Then the expression for $N(E_r)\, d E_r$ can be rewritten in the form:

$$N(E_r)\,dE_r = \frac{A\,dE_r}{E_r^{\nu}} \Gamma_{gl} \overline{u^{\nu-1}},$$

where

$$\overline{u^{\nu-1}} = \frac{\sum_i \int dx_i \int dy_i \int d\alpha \int \cos\beta \sin\beta\, d\beta \int_0^1 u^{\nu-1} W(u, Z)\,du}{\Gamma_{gl}} \qquad (2)$$

and

$$N(\geqslant E_{r1}) = \frac{1}{(\gamma-1)} \frac{A}{E_{r1}^{\gamma-1}} \Gamma_{gl} \overline{u^{\gamma-1}} \quad (3)$$

or

$$\frac{N(\geqslant E_{r1})}{\Gamma_{gl}} = \frac{A}{(\gamma-1)} \frac{1}{\left\{\frac{E_{r1}}{(\overline{u^{\gamma-1}})^{\frac{1}{\gamma-1}}}\right\}^{\gamma-1}} = I(\geqslant E), \quad (3a)$$

where

$$E = - \frac{E_{r1}}{(\overline{u^{\gamma-1}})^{\frac{1}{\gamma-1}}}.$$

Thus, to obtain the absolute flux of the primary particles creating bursts with energy release E_r in the ionization calorimeter, it is necessary to refer the measured burst intensity $N(\geqq E_r)/\Gamma_{gl}$ /37 to the energy of the first particles $E_0 = \frac{E_r}{(\overline{U^{\gamma-1}})^{\frac{1}{\gamma-1}}}$.

Previously [3], we took as $(\overline{u^{\gamma-1}})^{\frac{1}{\gamma-1}}$ the mean energy release $\bar{u}$, corresponding to the ionization calorimeter mean thickness $\bar{Z}$ for isotropic irradiation of the calorimeter by the particles. In this case, $\bar{Z}$ = 220 g/cm^2 Fe, $\bar{u}$ = 0.30.

A more exact calculation performed by Titenkov, in accordance with [2], yields for $\gamma - 1 = 1.7$ $(\overline{u^{\gamma-1}})^{\frac{1}{\gamma-1}} = 0.26$, i.e., $E_0 = 3.9\ E_r$ (in place of $3.3\ E_r$ in our previous publications [3]).

The gain of the PM-49 instrument used to record the light flash in the ionization calorimeter was selected so that the triggering threshold of the first amplitude discriminator was ten times greater than the pulse created by a single muon passing through the entire ionization calorimeter, whose thickness was 386 g/cm^2. It follows from this that the energy release E_1, corresponding to the first threshold V_1 is

$$E_1 = 10 \cdot 1.3 \cdot 1.5 \cdot 10^6 \cdot 386 \text{ g/cm}^2 = 7.5 \cdot 10^9 \text{ eV}.$$

Therefore, when recording ionization bursts by the first threshold, the primary proton energy $E_{0,\ 0.1} = 3.9\ E_1 = 29$ GeV.

With each subsequent threshold E_i, there is compared the primary proton energy $E_{0,i} = 29\ V_i/V_1$ GeV, where $V_{i|}$ is the pulse amplitude corresponding to the discriminator triggering threshold. However, this "correlation" of the discriminator thresholds does not take into account the possible photomultiplier sensitivity variations as a result of the effect on the photomultipliers of large vibrational overloads in the initial stage of the flight.

Therefore, we utilized the latitude effect of the protons recorded by the first threshold, i.e., the dependence of the $Z_1N_1E_{C_i}$ event count rate on geomagnetic rigidity R.

The results of these measurements are shown in Figure 1, from which we see that the threshold rigidity for protons corresponding to triggering of the first discriminator of the second half of the SEZ-14 is equal to 11 GeV/c, or the kinetic energy $E_1 = 10$ GeV (theoretical value of E_1 corresponds to 15 GeV). However, on the average, when recording ionization bursts, less energy by a factor of two is released than when recording protons, i.e., the first threshold will correspond to mean proton energy $2 \cdot 10 = 20$ GeV (theoretical value is 29 GeV). Thus, for the second half of the Proton 2 SEZ-14 instrument, $E_i = 20\ V_i/V_1$ GeV.

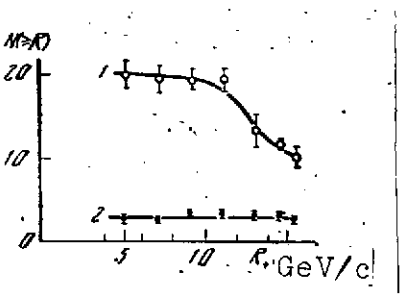

Figure 1. Count rate of events $Z_1N_1E_{C_1}$ (1) and $Z_1N_1E_{C_2}$ (2) of second half of SEZ-14 instrument aboard Proton 2 versus geomagnetic rigidity

/38

Ionization bursts of given magnitude E_i are created not only by protons, by also by heavy nuclei. Moreover, for nuclei, the quantity $u^{\overline{\gamma-1}}$ will depend on the atomic weight A of the nucleus. We considered only the dependence of the interaction range of a primary nucleus of atomic weight A with Fe atomic nuclei, assuming that the cascade shape is independent of A.

Under this assumption, we found that

$$\frac{\bar{u}(A=4)}{\bar{u}(A=1)} = 1.1; \quad \frac{\bar{u}(A=14)}{\bar{u}(A=1)} = 1.25 \quad \frac{\bar{u}(A=30)}{\bar{u}(A=1)} = 1.33.$$

With account for the fraction of different nuclei $\alpha(A_i)$ and $\bar{u}(A_i)$, we relate the given energy release E_i to the mean particle energy $E_{0,i}$, where

$$E_{0,i} = \frac{20}{\Sigma\alpha(A_i)\frac{\bar{u}(A_i)}{\bar{u}(A=1)}} \frac{V_i}{V_1} = 19\frac{V_i}{V_1}\ \text{GeV}$$

The energetic "correlation" of the first discriminator to the latitude effect could not be accomplished for all the instruments, but only for those SEZ-14 halves in which the threshold was low enough to record protons with $E \lesssim 15$ GeV. Therefore, "correlation" of the energy scale of all the instruments was accomplished as follows.

For each k^{th} instrument, the energy threshold $E_{k,i}$, corresponding to the amplitude $V_{k,i}$ of the pulse, triggering the i^{th} discriminator can be expressed in terms of $E_{k,2}$ — the energy threshold of the second amplitude discriminator

$$E_{k,i} = E_{k,2}\frac{V_{k,i}}{V_{k,2}}. \qquad (4)$$

In order to determine $E_{k,2}$, we plotted the ionization burst count rate N_k ($\geq V_{k,i}$) for each instrument as a function of the i^{th} discriminator triggering amplitude $V_{k,i}$. The results are presented

in Figure 2, from which we see that all the integral spectra $N_k(\geqslant V_{k,i})$ have a power-law form with the same spectrum exponent, i.e., $N_k(\geqslant V_{k,i}) = \frac{B_k}{(V_{k,i})^{\gamma-1}}$, but several different values of B_k. This difference is associated with different photomultiplier gain. The equality $N_k(\geqslant E_{k,2}) = N(\geqslant E_2)$ must be satisfied, meaning that with the correct determination of the energy scale, the energy spectra measured by all the instruments will yield the same intensity of particles of the same energy. Therefore, /39

$$E_{k,2} = E_2\left[\frac{N(\geqslant E_2)}{N_k(\geqslant E_{k,2})}\right]^{\frac{1}{\gamma-1}}, \quad (5)$$

where E_2 is the second energy threshold on the second half of the Proton SEZ-14 for recording ionization bursts, and $N(\geqslant E_2)$ is the burst count rate corresponding to this threshold.

Using the data of Figure 2, Expressions (5) and (4), and radiotechnical calibration, i.e., the values of $V_{k,i}$, we plotted the energy spectra of all particles for each SEZ-14 half (k = 1 - 6). The results of six independent series of ionization burst spectra measurements made aboard the Proton 1, 2, 3 AES are shown in Figure 3.

The absolute intensity of all particles recorded based on the number of ionization bursts $I(\geq E_i)$ was determined using the magnitude of the geometric factor Γ_{gl} and the Expressions (3) - (5). /40

We see from Figure 3 that the measured integral all-particle spectrum in the energy range $5 \cdot 10^{10} - 10^{14}$ eV can be approximated by a power function of the form $I(\geqslant E) = AE^{-(\gamma-1)}$ with $\gamma - 1 = 1.73 \pm 0.05$. The error in the exponent $\gamma - 1$ is due, not to the statistics of the observed ionization bursts, but rather to the experimental point scatter, the reason for which may be the low stability of the individual amplitude discriminator thresholds.

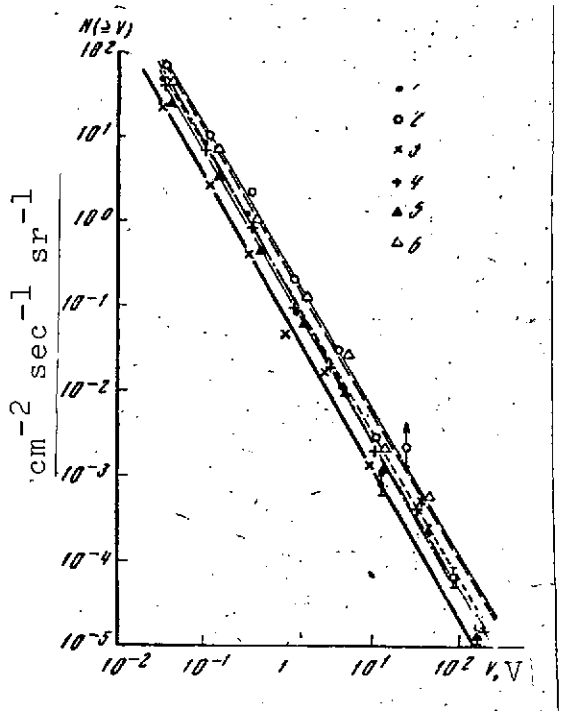

Figure 2. Ionization burst count rate versus amplitude V of signal coming from SEZ-14 ionization calorimeter installed aboard Proton 1, 2, 3, AES:

1 — Proton 1, first half; 2 — Proton 1, second half; 3 — Proton 2, first half; 4 — Proton 2, second half; 5 — proton 3, first half; 6 — Proton 3, second half

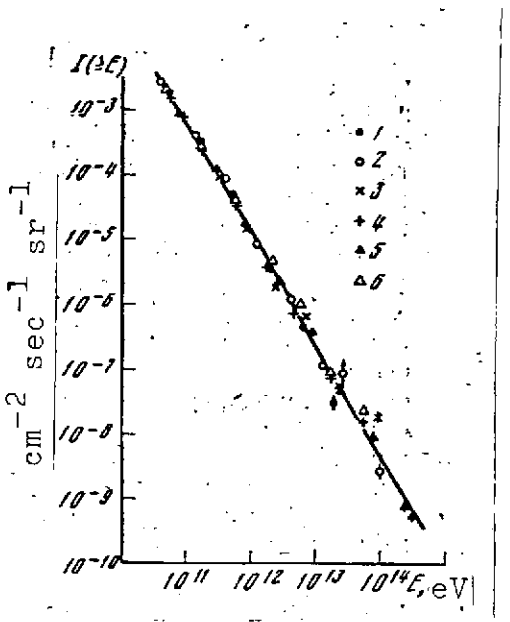

Figure 3. Integral all-particle energy spectrum. Notations same as in Figure 2.

All the experimental points for particle energy $E \sim (3 - 5) \cdot 10^{14}$ eV lie somewhat below the approximating function with $\gamma - 1 = 1.73$, which can be considered an indication of possible increase of the exponent for particle energies $\geq 10^{14}$ eV. However, we cannot assign serious importance to this fact, since when recording ionization bursts of corresponding particle energies $\sim 3 \cdot 10^{14}$ eV, the amplitude of the signal taken from the photomultiplier anode reaches values of 150 V. Therefore, we cannot be certain that the intensity decrease for $E \sim 3 \cdot 10^{14}$ eV is not the result of disruption of the linear relationship between the light flash magnitude and pulse amplitude.

§2. Primary Cosmic Ray Proton Energy Spectrum

Singly charged particles of given energy were separated in the SEZ-14 on the basis of pulse amplitudes in both proportional counters. Cases of triggering of the i^{th} energy release discriminator in the ionization calorimeter accompanied by triggering of both scintillation counters were assigned to the proton recording category if the pulses in both proportional counters did not exceed 2.7 V_{prob} (where V_{prob} is the most probable value of the pulse amplitude created by muons at sea level).

In the previous proton spectra analyses, we used only those cases in which in the upper scintillation counter — the interaction detector — the pulse amplitude corresponded to passage through the detector of a single particle, i.e., we used events of the type $Z_1N_1E_{C_i}$ [4]. As is well known, the spectrum of these events in the energy interval $E \gtrsim 10^{12}$ eV experienced marked increase of the exponent from about 1.7 (for $E < 10^{12}$ eV) to about 2.5 in the energy interval $2 \cdot 10^{12} - 10^{13}$ eV.

Reverse current particles may play a definite role in selection of the events $Z_1N_1E_{C_i}$. Although calculations made in [3] showed that we cannot explain quantitatively the observed proton spectrum slope change by the reverse current of particles from the ionization calorimeter into the interaction detector and proportional counters, nevertheless, the general tendency for increase of this effect with energy increase stimulated us to seek an approach to the experimental data which would permit significant reduction of the possible reverse current influence on the proton spectrum. /41

To this end, we relaxed the requirement for single particle passage through the interaction detector, i.e., all particles with charge Z = 1 were recorded, regardless of the pulse amplitude in the

interaction detector. Technically, this was accomplished by separate measurement of the intensity of events with fixed energy release E_i, when the pulse amplitude in the proportional counters corresponded to a singly charged particle and a single particle was in the interaction detector, i.e., events $Z_1N_1E_{C_i}$. (These cases were assigned their own telemetry channels, since they were later used to measure the effective inelastic interaction sections.) We also measured independently the number of cases with the same energy release E_i, with the same impulse in the proportional counters, but with number N of particles in the interaction detector exceeding 2 ($N_2 \geq 2$). Thus, events $Z_1N_1E_{C_i}$ and $Z_1N_2E_{C_i}$ were recorded separately. The sum of the intensities of these events is independent of the reverse particle current from the ionization calorimeter to the interaction detector. In order to reduce the probability of scattered reverse current particles entering the proportional counters and thereby reducing the number of protons recorded, we plotted the proton spectrum (intensity of the sum of events $Z_1N_1E_{C_i} + Z_1N_2E_{C_i}$) only from those measurement seances in which the carbon or polyethylene targets were located between the proportional counters and the interaction detector.

The intensities $I(Z_1N_1E_{C_i} + Z_1N_2E_{C_i})$ were measured on the first and second halves of the Proton 2 SEZ-14 and on the second half of the Proton 3 SEZ-14. The results of these independent series of measurements, made by three different instruments, are shown in Figure 4. This figure also shows along the ordinate axis the $Z_1N_1E_{C_i} + Z_1N_2E_{C_i}$ event count rate (right hand scale, experimental points 1, 2, 3). The energy thresholds of the different instruments were referred to the same scale using the result of measurement of the ionization bursts E_i.

We see from Figure 4 that all three series of measurements without DD yield results which agree well with one another and, just as

when recording only the $Z_1N_1E_{C_i}$ events [4], yield a change of γ, the proton spectrum exponent, in the interval $E \geq 2 \cdot 10^{12}$ eV. Thus, this change of γ is not associated with the reverse particle current from the ionization calorimeter into the DD.

The solid line in Figure 4 represents the function

$$I(\geqslant E) = A\left(\frac{100}{E}\right)^{1,62} \frac{1}{\left[1+\left(\frac{E}{1500}\right)^2\right]^{0,35}}, \quad (6)$$

where E is proton energy in GeV;
A is a normalizing coefficient.
We have noted previously that because of "overcount" [3], the absolute proton flux intensity from the measurements of the $Z_1N_1E_{C_i}$ event count rate, and also the $Z_1N_1E_{C_i} + Z_1N_2E_{C_i}$ event count rate may be too high by several fold.

/42

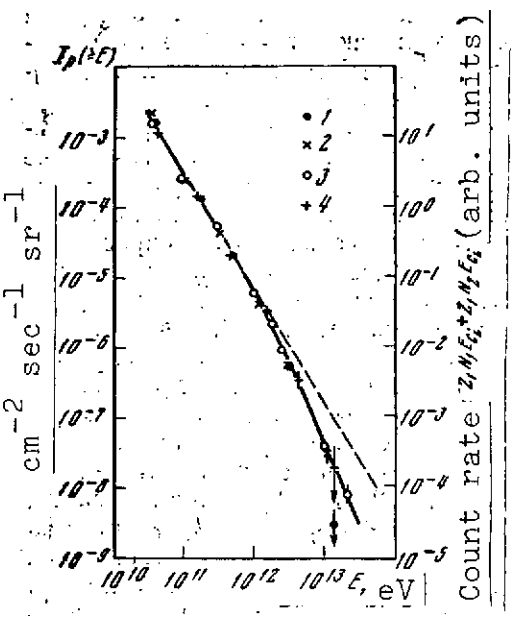

Figure 4. Integral proton energy spectrum; events $Z_1N_1E_{C_i} + Z_1N_2E_{C_i}$
1 — first half of Proton 2 SEZ-14; 2 — second half of same; 3 — second half of Proton 3 SEZ-14; 4 — events Z_1N_1 DD $E_{C_i} + Z_1N_2$ DD E_{C_i} (first half of Proton 3 SEZ-14, measured with DD)

We were able to estimate the magnitude of the "overcount" when recording particles with energy $\sim$ 10 GeV after analyzing the available information on cosmic ray particle count rate using the SEZ-14 telescope, consisting of the interaction detector and the lower scintillation counter. The geometric factor of this telescope was $\sim$ 800 cm^2 · sr. The count rate at high latitudes was $\sim$ 220 - 250 sec^{-1}, and at the equator — 75 sec^{-1}, i.e., the absolute cosmic ray particle flux intensities measured by this telescope at

high latitudes was 0.28 - 0.31 $cm^{-2} \cdot sec^{-1} \cdot sr^{-1}$, and at the equator — 0.09 $cm^{-2} \cdot sec^{-1} \cdot sr^{-1}$.

Thus, at high latitudes, the average intensity corresponds to the literature data, while at the equator it is four times the true cosmic ray particle flux. Consequently, the "overcount" (when recording double coincidences) amounts to a factor of about four. When measuring the all-particle flux at the equator, using the same SEZ-14 telescope, with the additional requirement that the particles pass through the DD, the measured intensity was 0.04 - 0.045 $cm^{-2} \cdot sec^{-1} \cdot sr^{-1}$, i.e., inclusion of the DD into the all-particle recording system reduces the "overcount" by a factor of two. The imposition of the requirement for fixed energy release in the ionization calorimeter (as is the case when measuring the events Z_1N_1 DD E_{C_i} and Z_1N_1 DD E_{C_i}) /43 should reduce still further the probability of "addition".

Therefore, at the present time, the most reliable determination of the absolute high-energy primary proton flux can be obtained from measurement of the Z_1N_1 DD E_{C_i} + Z_1N_2 DD E_{C_i} event intensity.

Analysis of the information obtained showed that $I(Z_1N_1$ DD E_{C_i} + Z_1N_2 DD $E_{C_i})$ is independent of target position; therefore, in order to increase the statistics (particularly necessary for proton energies $E > 5 \cdot 10^{12}$ eV), we present the Z_1N_1 DD E_{C_i} + Z_1N_2 DD E_{C_i} event intensity, obtained as the mean intensity value from all the measurements, with and without targets.

In order to obtain the absolute proton flux intensity, the measured count rate was divided by 14 $cm^2 \cdot sr$. The geometric factor of the SEZ-14 instrument with DD is less by a factor of nine than without the DD, i.e., $\Gamma = 47$ $cm^2 \cdot sr$; from muon flux measurements at sea level without and with the DD, we determined the probability of

recording a singly charged particle by the proportional counters and the direction detector: this probability was $\eta = 0.6$; with account for shading of the SEZ-14 entry window by the Earth (coefficient 0.5) $\Gamma \cdot \eta \cdot 0.5 = 14$ cm^2 · sr.

The results of proton flux measurement based on the sum of the intensities Z_1N_1 DD E_{C_i} + Z_1N_2 DD E_{C_i} are shown in Figure 4 (crosses). The absolute proton fluxes obtained from the intensity of the events Z_1N_1 DD E_{C_i} + Z_1N_2 DD E_{C_i} are plotted on the left scale; the intensities $Z_1N_1E_{C_i}$ + $Z_1N_2E_{C_i}$ were normalized to the intensities of the events Z_1N_1 DD E_{C_i} + Z_1N_2 DD E_{C_i} at the point $E = 10^{11}$ eV; the normalization coefficient was found to be equal to one third, i.e., the "overcount" in the events $Z_1N_1E_{C_i}$ + $Z_1N_2E_{C_i}$ yields a factor of about three.

We see from Figure 4 that measurements with and without the DD yield the same proton spectrum shape:

$$I_p(\geqslant E) = 3 \cdot 10^{-4} \left(\frac{100}{E}\right)^{1.62} \frac{1}{\left[1+\left(\frac{E}{1500}\right)^2\right]^{0.35}} \text{cm}^{-2} \cdot \text{sec}^{-1} \cdot \text{sr}^{-1} \qquad (6a)$$

where E is measured in GeV.

An important characteristic of the measurements with DD is the fact that in this case, protons entering the SEZ-14 instrument only from the DD side are recorded. They pass through the proportional counters and then enter the ionization calorimeter. Particles entering the SEZ-14 instrument through the lower base and yielding a signal Z = 1 in the proportional counter are not recorded. We verified this as follows.

Using the indications of the three-component magnetometer installed aboard the Proton 3 AES, we selected those time intervals when the SEZ-14 instrument had its "entry window" facing the Earth.

Counting of the events Z_1N_1 DD E_{C_i} and Z_1N_2 DD E_{C_i} terminated each time the instrument was oriented in this way, relative to the Earth.

In spite of the fact that the conditions of proton spectrum measurement with and without the DD are different, the shapes of the spectra obtained by the different methods coincide. This means that the observed increase of the spectrum exponent in the energy interval $E > 2 \cdot 10^{12}$ eV is not associated either with the possibility of recording reverse-traveling particles (without DD) or with the reverse stream (as was the case in the preliminary measurements of only $Z_1N_1E_{C_i}$ [3]. /44

§3. Discussion of Results

1. Absolute high-energy particle flux intensities

The fluxes of protons with energy $E \geq 15$ GeV have been determined in several experiments performed aboard balloons, using nuclear photoemulsions.

The proton flux I_p ($E \geq 15$ GeV) = 96 ± 13 $m^{-2} \cdot sec^{-1} \cdot sr^{-1}$ was obtained in [5], and 86 ± 12 $m^{-2} \cdot sec^{-1} \cdot sr^{-1}$ was obtained in [6]. The proton flux I_p ($E \geq 15$ GeV) = $83 + 12$ $m^{-2} \cdot sec^{-1} \cdot sr^{-1}$, i.e., the mean value for I_p ($E \geq 15$ GeV) = $88 + 7$ $m^{-2} \cdot sec^{-1} \cdot sr^{-1}$, was obtained in [7]. If we extrapolate our measured proton spectrum using (6) to energies $E = 15$ GeV, and equate I_p (≥ 15 GeV) = 88 ± 7 $m^{-2} \cdot sec^{-1} \cdot sr^{-1}$, we obtain the value for the coefficient A: $A = (4 \pm 0.3) \cdot 10^{-4}$ $cm^{-2} \cdot sec^{-1} \cdot sr^{-1}$. Our measurements yield $A = 3 \cdot 10^{-4}$ $cm^{-2} \cdot sec^{-1} \cdot sr^{-1}$, i.e., they are in agreement with the data obtained in the low-energy proton interval. The basic indeterminacy in the value of A obtained in our experiments is associated with inaccuracy of the energy "correlations" with respect to the cosmic ray latitude effect.

2. Comparison of proton and all-particle energy spectra

If we approximate the all-particle spectrum by a power-law function of the form $I\ (\geq E) = B\ (100/E)^{\gamma-1}$, where E is measured in GeV, we see from Figure 3 that $B = 6 \cdot 10^{-4}$ cm^{-2} $\cdot$ sec^{-1} $\cdot$ sr^{-1}, and $\gamma - 1 = 1.73 \pm 0.05$.

For the proton spectrum measured with DD under conditions of minimal "overcount" of particles from directions exceeding the limits of the solid angle defined by the SEZ-14 geometry, we obtained the Expression (6), where E is measured in GeV and $A = 3 \cdot 10^{-4}$ cm^{-2} $\cdot$ sec^{-1} $\cdot$ sr^{-1}. We see from these data that in the particle energy interval $10^{11} - 10^{12}$ eV, the ratio of the all-particle flux and the proton flux of the same energy $I\ (\geq E)/I_p\ (\geq E) = 2$ (for $E < 1000$ GeV), i.e., it is in good agreement with the expected ratio. (We noted previously that about 50% of the recorded bursts will be created by nuclei with $Z \geq 2$, and 50% by protons.)

We note that the ratio $I\ (\geq E)/I_p\ (\geq E) = 2$ obtained is independent of the energy correlation inaccuracies, since these inaccuracies alter the values of B and A to the same degree. The question arises of whether or not the observed all-particle spectrum contradicts the fact that the proton spectrum experiences a break at $E \sim$ 2000 GeV, while the spectrum of all nuclei with $Z \geq 2$ remains power-law with a single spectral exponent over the entire measured energy interval. /45

In order to answer this question, we calculated the expected burst spectrum under the assumption that the $Z \geq 2$ nuclei burst spectrum has the form $I_Z\ (\geq E) = A \cdot (100/E^{1.62})$, while the proton burst spectrum has the form (6). Under these assumptions, the observed burst spectrum will have the form:

$$I(\geq E) = A \cdot (100/E)^{1,62}\left\{\Gamma + \frac{1}{[1+(E/1500)^2]^{0,35}}\right\} \quad (7)$$

where $A = 3 \cdot 10^{-4}$ cm^{-2} $\cdot$ sec^{-1} $\cdot$ sr^{-1}. This function is shown by the solid line in Figure 3. We see from Figure 3 that (7) describes well the experimental all-particle spectrum. Thus, the proton spectrum exponent change for $E \gtrsim 2000$ GeV does not contradict the observed all-particle spectrum.

Thus, representation of the integral all-particle spectrum in the energy interval $10^2 \leq E \leq 10^5$ GeV by a single power-law function with exponent $\gamma - 1 = 1.73$ is approximate, and apparently does not reflect the actual, more complex superposition of spectra of particles of different nature (protons and heavy nuclei).

3. Comparison of measured spectra with high-energy nucleon spectra in the atmosphere

For a long time it was thought that the high-energy nucleon spectra in the atmosphere at different heights contradict the primary particle spectrum, i.e., they are purely power-law with integral spectrum exponent $\gamma - 1 = 1.6 - 1.7$. This idea was based on three assertions:

a) independence of nucleon effective inelastic interaction section on their energy;

b) independence of nucleon interaction inelasticity on their energy;

c) purely power-law form of the primary cosmic ray spectrum.

In recent years, several studies have been made of the energy spectra of strongly interacting particles and high-energy γ quanta at various altitudes in the atmosphere [8 - 14]. In spite of the difference in the methods used, in most of the studies it was found

that in the particle energy interval $\geq 10^{12}$ eV, the integral spectrum exponent $\gamma - 1 = 1.85 - 2$, i.e., somewhat larger than for the primary particles. With strict satisfaction of the three conditions listed above, $\gamma - 1$ cannot change. Consequently, the available experimental data indicate that certain of the listed characteristics are weak functions of particle energy. /46

Experiments aboard the Proton AES showed that σ^{in} changes by $\sim 18\%$ with transition from E = 20 GeV to E = 200 GeV, i.e., assumption "a" is not satisfied exactly. According to our primary particle spectra measurements, condition "c" is also not satisfied.

In this connection a question arises: what will the nucleon component spectra be like at various altitudes in the atmosphere, if we assume that the primary particle spectrum and σ^{in} are like those measured aboard the Proton AES? Does not a conflict with the available experimental data arise in this case?

In order to answer this question, we calculated the vertical nucleon flux spectra at various atmospheric depths x (g/cm^2) under the following assumptions:

a) the primary proton spectrum has the form shown in Figure 4;

b) the $Z \geq 2$ nuclei spectrum has a power-law form

$$I_Z(\geq E) = 3 \cdot 10^{-4} (100/E)^{1,62} \text{ cm}^{-2} \cdot \text{sec}^{-1} \cdot \text{sr}^{-1},$$

c) during collision with the air atom nuclei, the primary cosmic ray particle nuclei partially fragment into nucleons (the fraction of nucleons retaining the original energy is 50%);

d) the nucleons have mean inelasticity coefficient K = 0.55.

At the depth x, the primary protons and the nucleons arising from heavy nucleus breakup contribute to the nucleon flux. Since the

range for heavy nuclei interaction in air is short, we can consider in the first approximation that the nucleon flux at the top of the atmosphere consists of two components:

$$F(\geqslant E, x=0)=F_p(\geqslant E, x=0)+F_Z(\geqslant E, x=0),$$

where $F_p(\geqslant E, x=0)$ is defined by (6a), and

$$F_Z(\geqslant E, x=0)=C(100/E)^{1.62}\ \text{cm}^{-2}\cdot\text{sec}^{-1}\cdot\text{sr}^{-1};$$

F_p are primary protons; F_z are nucleons from nuclear fragmentation; E is nucleon energy in GeV.

Since for $E \leq 10$ GeV/nuc, the fraction of nucleons packed in the nuclei amounts to $\sim 40\%$ of the free proton flux with the same energy [15], and since we have assumed that during fragmentation, half the nucleons retain the original energy, then $C = 0.5 \cdot 0.4 \cdot 3 \cdot 10^{-4} = 0.6 \cdot 10^{-4}$.

In the calculation, we took the range for inelastic interaction with air atom nuclei $\lambda = 83$ g/cm^2, in accordance with the σ^{in}_{p-C} value obtained in experiments aboard the Proton 1, 2, 3 AES for proton with $E \geq 200$ GeV [2].

The nucleon flux F (E, x) with energy E, E + dE at the depth x (g/cm^2) was calculated by successive approximations: /47

$$F(E, x)=e^{-\frac{x}{\lambda}}dE\sum_{n=0}^{\infty}\left(\frac{x}{\lambda(1-K)}\right)^n F_c\left[\frac{E}{(1-K)^n}\right]\frac{1}{n!}, \qquad (8)$$

where K is the coefficient of inelasticity.

The calculation results are shown in Figure 5 by the solid lines. The experimental data of various authors are also shown in this figure.

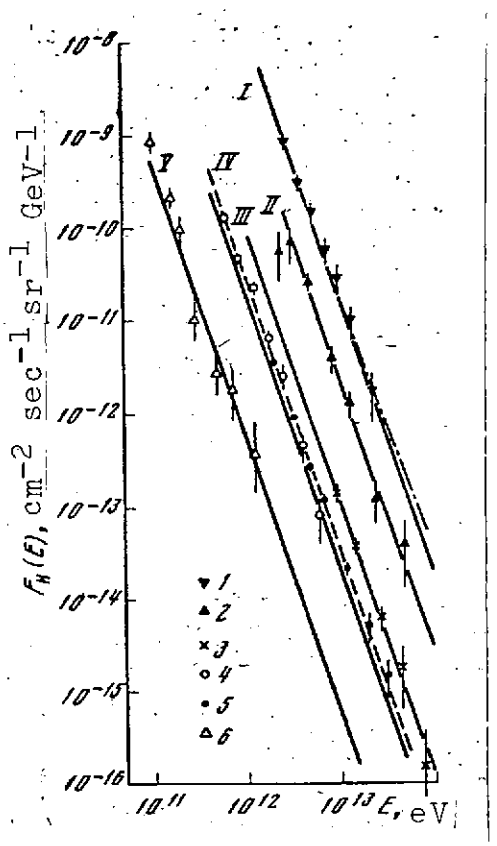

Figure 5. Nucleon energy spectra at various depths in the atmosphere: I — x = 20 g/cm^2 (dash-dot line is calculated γ quanta spectrum, point for E = $3.5 \cdot 10^{12}$ eV is normed to the calculated spectrum); II — x = 200 g/cm^2; III — x = 530 g/cm^2; IV — x = 700 g/cm^2 (dashed line is the same spectrum shifted with respect to energy 20% to the right); V — neutron spectrum for x = 1000 g/cm^2, calculated under the assumption that the neutron flux constitutes 50% of the nucleon flux; 1 — nucleon spectrum (x = 20 g/cm^2), determined from the γ quantum spectrum [10] under the assumption $E_H = 3.5\ E_\gamma$ 2 — nucleon spectrum (x = 200 g/cm^2) obtained from the γ quantum spectrum [11] under the assumption $E_H = 3\ E_\gamma$; 3 — nucleon spectrum (x = 530 g/cm^2) obtained from the γ quantum spectrum [12] under the assumption $E_H = 3.5\ E_\gamma$; 4 — spectrum of all nuclear-active particles (x = 700 g/cm^2), determined using an ionization calorimeter [8]; 5 — spectrum of all nuclear active particles (x = 700 g/cm^2), determined from ionization burst measurement [9]; 6 — neutron spectrum at depth x = 100 g/cm^2 [13]

We see from Figure 5 that the available experimental data agree well with the expected nucleon component spectra at all atmospheric depths, calculated from primary proton and complex nuclei energy distribution measurement aboard the Proton 1, 2, 3 AES.

As was noted in [3], in order to match the measured σ^{in}_{p-C} and the single high-energy nucleon flux [9], it is necessary to assume that the primary proton integral spectrum exponent in the energy interval /48 E > 10^{12} eV has a value of $\sim$ 2.3 - 2.5.

The fact that the primary cosmic ray spectrum is not purely power-law, while the nuclear spectrum is power-law, leads to a situation in which, as we can see from Figure 5, the high-energy nucleon spectra in the depth of the atmosphere will not be purely power-law. A consequence of this will be the fact that the nucleon absorption range in the atmosphere will be a very weak function of energy: for $E \sim 10^{11}$ eV, $L_n = 109$ g/cm^2; for $E = 10^{12} - 10^{13}$ eV, $L_n = 101$ g/cm^2.

For higher energies, L_n again increases somewhat if the nuclear spectrum exponent remains unchanged up to primary particle energies $\geqq 10^{15}$ eV. There are experimental indications of weak decrease of L_n with transition from nucleon energies of $E \sim 10^{10}$ eV to $E \sim 10^{12} - 10^{13}$ eV.

Thus the decrease of L_n with increase of nucleon energy finds its natural explanation without assumptions on change of the basic characteristics of the elementary interactions act.

References

1. Grigorov, N. L., G. P. Kakhidze, V. Ye. Nesterov, I. D. Rapoport, I. A. Savenko, A. V. Smirnov, A. F. Titenkov and P. P. Shishkov. Kosmicheskiye issledovaniya, Vol. 5, No. 3, 1967, p. 383.

2. Grigorov, N. L., V. Ye. Nesterov, I. D. Rapoport, I. A. Savenko and G. A. Skuridin. Present volume, page 11.

3. Grigorov, N. L., V. Ye. Nesterov, I. D. Rapoport, I. A. Savenko and G. A. Skuridin. Proceedings of International Conference on Cosmic Rays, Calgary, Canada. Preprint, Moscow, IPM [Institute of the Problems of Mechanics], 1967.

4. Grigorov, N. L., V. Ye. Nesterov, I. D. Rapoport, I. A. Savenko, G. A. Skuridin and A. F. Titenkov. Izvestiya AN SSSR, seriya fiz., Vol. 31, 1967, p. 1225.

5. Daniel, R. R. and N. Sreenivasan. Proc. Intern. Conf. on Cosmic Rays. Jaipur, 3, 1963, p. 60.

6. Daniel, R. R. and V. L. Bhatt. Proc. Intern. Conf. on Cosmic Rays. Jaipur, 3, 1963, p. 56.

7. Gangubi, S. N., N. Kameswara and M. S. Swanei. Nuovo Cimento, Vol. 30, 1963, p. 33.

8. Yerofeyeva, I. N. Proceedings of All-Union Conference on Cosmic Rays, Part 1. Moscow, FIAN, Vol. 1, p. 90.

9. Babayan, Kh. P., N. G. Boyadzhan, N. L. Grigorov, E. A. Mamidzhanyan, V. A. Sobinyakov, Ch. A. Tret'yakova and V. Ya. Shestoperov. Izvestiya AN SSSR, seriya fiz., Vol. 31, 1967, p. 1425.

10. Bowler, et al. Nature, Vol. 209, No. 5023, 1966, p. 567.

11. Apanasenko, A. V., L. T. Baradzey, et al. Izvestiya AN SSSR, seriya fiz., Vol. 32, 1968.

12. Japan-Brazil Emulsion Group. Canad. Journal of Physics, Vol. 46, 1968, p. 660.

13. Ashton, F., G. King, E. A. Mamidzhanyan, et al. Izvestiya AN SSSR, seriya. fiz., Vol. 33, 1969, p. 1557.

14. Yakovlev, V. I. Dissertation, Moscow, FIAN, 1969.

15. Ginzburg, V. L. and S. I. Syrovatskiy. Proiskhozhendiye kosmicheskikh luchey [Origin of Cosmic Rays]. Moscow, Izdatel'stvo AN SSSR, 1963.

APPARATUS FOR STUDYING COSMIC RAYS ABOARD THE PROTON 4 SCIENTIFIC STATION

N. L. Grigorov, I. D. Rapoport, I. A. Savenko,
L. F. Kalinkin, and G. P. Kakhidze

Introduction

The Proton-4 automatic scientific station was launched on November 16, 1968, into near-Earth orbit with apogee 495 km and perigee 255 km, providing long station lifetime. The task of the Proton 4 station included continuation of high- and superhigh-energy cosmic radiation studies initaated aboard the Proton 1, 2, 3 heavy artificial Earth satellites (AES). /49

The major portion of this program involves investigation of cosmic ray energy and charge spectra, and investigation of the most important characteristics of high-energy particle interaction with atomic nuclei as a function of energy. Another portion of the program is associated with seeking in the primary cosmic rays, hypothetical fundamental particles with fractional electric charge (quarks), and recording of high-energy electrons in near-Earth space.

In the following, we describe the scientific equipment complex installed aboard the Proton 4 space station.

A wide-aperture energy and charge spectrometer (IK-15) was constructed to measure particle energy and charge spectra, and study nuclear interaction characteristics; this spectrometer constituted the major part of the apparatus. Two other instruments were designed to perform the second part of the program: high-energy electron flux measurement was accomplished by an SEZ-12 instrument; quark recording was accomplished by an SEZ-13 instrument. Both instruments are improved modifications of installations used aboard the earlier Proton stations.

I. Particle Energy and Charge Spectrometer (IK-15) for Studying High-Energy Cosmic Radiation

One of the most urgent problems of astrophysics is the study of high- and superhigh-energy particle fluxes in cosmic space, determination of their composition, energy spectrum, and the characteristics of their interaction with matter.

The systematic development of experimental studies in this direction makes it possible to approach the solution of the very important problem of high-energy cosmic radiation particle origin, and explanation of their propagation processes in the Galaxy. At the same time, the same circle of questions is of great interest in studying the properties of the elementary particles which have been discovered in the high-energy interaction processes. The cosmic radiation particles permit considerable broadening of the energy interval of nuclear studies, which can be conducted on accelerators only up to 10^{10} - 10^{11} eV. The cosmic ray energy spectrum extends considerably beyond this limit, and makes it possible to conduct effective studies of this nature up to 10^{15} - 10^{16} eV — the practical limit is determined only by the decaying nature of the spectrum and the ability of the latest experimental equipment to utilize the weak high-energy particle fluxes. /50

The latter situation is one of the major difficulties accompanying the conduct of cosmic ray experiments. It requires long exposures

of the equipment beyond the Earth's atmosphere and the use of sufficiently fast radiation detectors. At the same time, the physical variety of the branching processes, which take place in matter during high-energy particle passage, leads to inevitable methodological complication of the experiment and the need for multiple methodological variations with the objective of sufficiently precise study of the phenomena. Also complicated is the composition of the cosmic radiation itself — both in the nature and energy of the particles and the isotropic nature of the spatial distribution. Under these conditions, the achievement of adequately definite and reliable results is possible only by means of a systematic investigation, consistently developed into a series of goal-directed experiments.

The first step, preparing the required methodological bases for the development of cosmic ray studies in the high-energy interval, was the development of the ionization calorimeter method for measuring particle energy $\geq 10^{14}$ eV [1]. While retaining definite analogy with the calorimetric method and being based on the principle of particle energy absorption in a block of matter with subsequent measurement of the absorbed energy using the ionization effect, this method requires the use of a large amount of absorbing matter and the construction of a complex and heavy detecting device [2]. Therefore, initiation of the use of this method for direct study of primary cosmic radiation beyond the limits of the atmosphere is closely associated with the development and construction of heavy AES, which are opening up a new era in cosmic space exploration for scientific studies.

The first series of experiments conducted to study high-energy primary cosmic radiation was carried out aboard the Proton 1, 2, 3 /51 scientific stations. These studies involved determination of the charge composition in the energy interval near 10^9 eV/nuc [3, 4]; measurement of the overall cosmic radiation energy spectrum up to 10^{14} eV (protons up to 10^{13} eV) [5 - 13]; measurement of the effective inelastic nuclear interaction section of high-energy protons with light nuclei, such as carbon and hydrogen [5, 6, 8, 10, 14 - 19]; study of the electron component [5, 6, 20, 21]; search for quarks

[22, 23]; recording the gamma quanta in the primary cosmic radiation flux [24]. The basic apparatus was an ionization calorimeter with relatively small absorber volume (thickness about three ranges for nuclear interaction and cross section 0.25 m^2 [25], which limited the measurement accuracy.

The next step in the development of these experiments aboard the Proton satellites was directed primarily toward increasing energy measurement range and accuracy.

The Proton 4 scientific station was equipped with radiation detectors of considerably wider relative aperture, which permitted realizing the program noted above in the primary particle energy up to 10^{15} eV. At the same time, the more complex and differentiated ionization calorimeter configuration, with a large amount of absorbing matter (Figure 1), not only made possible more exact measurement of particle energy, but also permitted tracing the process of sequential energy absorption in the calorimetric material. The range of

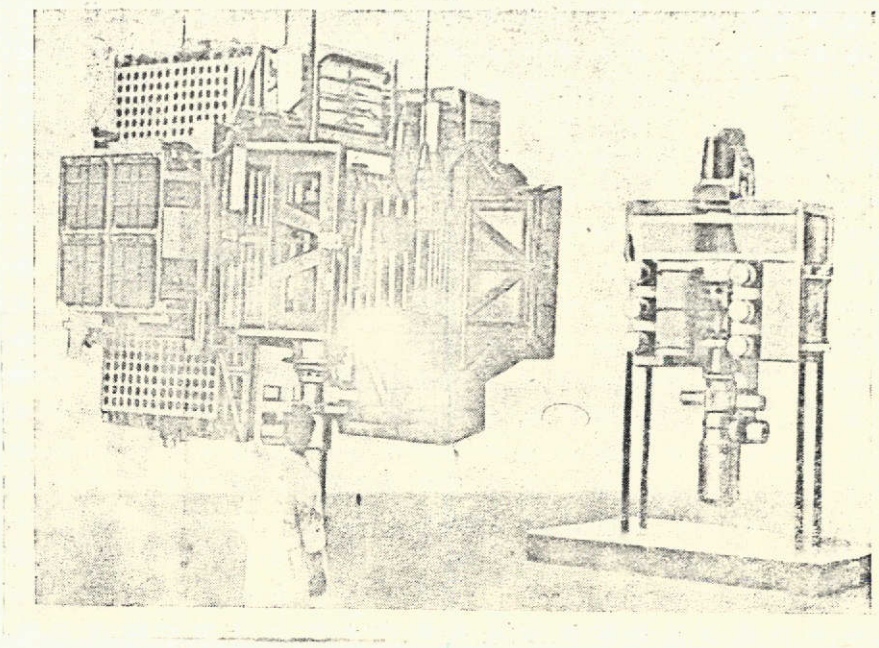

Figure 1. General view of Proton 4 station scientific apparatus complex (left) in comparison with that of the preceding Proton stations (right)

nuclear investigations was also broadened. In addition to measuring particle inelastic interaction sections with light nuclei (carbon, hydrogen), provision was made for analogous measurements on heavier nuclei (iron and lead) and wider study in this energy interval of the act of impinging particle collision with the target nucleus was undertaken.

In the following, we present a description of the instrument installed aboard the Proton 4 scientific station and intended for performing these studies — this instrument is designated IK-15. It can be classified as a high-energy particle spectrometer for studying cosmic radiation in the interval 10^{11} - 10^{15} eV.

1. Schematic of IK-15 Spectrometer

The instrument consists of the following basic components (see Figure 2):

1) ionization calorimeter for measuring energy;

2) rccorded particle charge detectors (DD1, DD2, PC2, PC11);

3) targets for studying nuclear interactions;

4) detectors of particle interaction with target atomic nuclei (PC3, PC4, PC7 - PC10);

5) auxiliary radiation detectors for generating recording control command.

During operation of the instrument in cosmic radiation flux, the following are accomplished:

a) global recording of particles from all directions;

b) selection of particles in a relatively narrow solid angle in the direction passing through all the radiation detectors.

The recording of particles in the global flux is accomplished only by the ionization calorimeter, which permits in this case carrying out global measurements of the energy spectrum of all particles. Thanks to the large mean effective recording area and large "viewing" angle (the effective solid angle in this case is equal to approximately 2 π steradians), these measurements cover the largest possible energy interval. The relative aperture is one of the essential ionization calorimeter parameters, since it determines the upper recorded particle energy limit. For given absorber thickness, the relative aperture is determined by its cross section and, in the final analysis, by the permissible apparatus weight. The geometric factor of the ionization calorimeter for global flux recording under the assumption of 50% shadow of the instrument by the Earth is $\Gamma_{gl} = \pi (S_x + S_y + S_z) = 1.4 \cdot 10^5$ cm^2 · sr, where S_x, S_y, S_z are the calorimeter face areas. Quite effective particle recording in global flux up to 10^{15} eV is possible with this relative aperture and an exposure time of about 100 days. For comparison, we note that the relative aperture of the ionization calorimeter of the SEZ-14 instruments aboard the Proton 1, 2, 3 AES was $2.7 \cdot 10^4$ cm^2 · sr, for global particle recording.

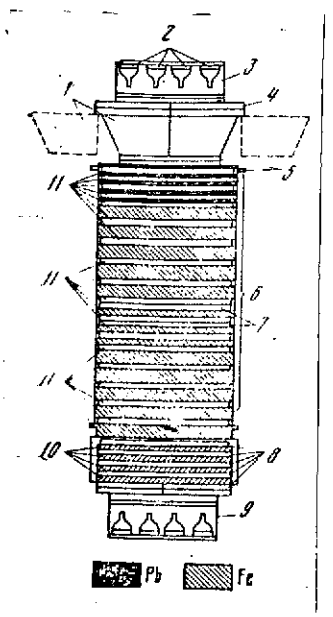

Figure 2. Schematic of IK-15 charge and energy spectrometer: 1 — targets; 2 — Cherenkov counters; 3 — charge detector DD1; 4 — proportional counter PC2; 5 — interaction detectors — proportional counters PC3, PC4; 6 — ionization calorimeter; 7 — proportional counters PC5, PC6; 8 — proportional counters PC7 - PC11; 9 — charge detector DD2; 10 — thin graphite targets; 11 — ionization chambers IK-1 to IK-16

Recording in a selected direction is accomplished in a considerably smaller solid angle, determined by the charge detector on one side, and by the proportional counters at the exit from the ionization

calorimeter on the opposite side. Since the ionization calorimeter is symmetric in this direction relative to the entrance and exit, it was advisable for maximal utilization of the flux in this solid angle to install two charge detectors: DD1 for particles entering the calorimeter from one side, and DD2 for particles coming from the opposite side. In order to differentiate these directions, the charge detectors DD1 and DD2 were given selective sensitivity. Each of these detectors, roughly speaking, records particles entering the instrument only from one side and, therefore, they serve at the same time as detectors of the direction of particle entry into the instrument.

Particle separation in this solid angle is accomplished by selecting coincidences of the electrical signals from one of the charge detectors (DD1 or DD2) with the signals of the proportional counters PC3 or PC4, PC5 or PC6, and one of the counters PC7 - PC11. The geometric factor of this "telescope" is considerably smaller than in the first case, and amounts to 420 $cm^2 \cdot sr$ (we recall that the corresponding geometric factor of the SEZ-14 instrument aboard Proton 3, operating together with the direction detector, was 47 $cm^2 \cdot sr$). Therefore, the possible energy measurement interval in this solid angle is smaller (up to $\sim 10^{14}$ eV). However, the accuracy of these measurements within the given solid angle is considerably higher, and particle charge measurements and study of the nuclear processes in /54 the target and calorimeter material are possibly only for this separated flux.

Let us examine the recording of a particle entering the instrument through DD1. Below DD1 is located the two-layer PC2, performing multiple control particle charge measurements. Then follow the interchangeable carbon and polyethylene targets with thickness equal to $\sim 1/4$ of the range for nuclear interaction. The carbon and polyethylene targets replace one another periodically, and part ($\sim 1/3$) of the time measurements are conducted without targets (the targets are removed from the ionization calorimeter entrance window).

Detection of interaction in the targets is made by PC3 and PC4 by recording the secondary particle showers which arise as a result of interaction. In the first five lead absorbing layers (2.5 cm thick each), there is intense electron-photon avalanche development, due to decay of the neutral π-mesons generated in the act. The energy transferred to these particles can be determined from the indications of the four ionization chambers IK-1 to IK-4, located between the layers. A more sensitive ionization detector PC4 is located below the first lead layer in order to record weaker ionization effects. The overall thickness of the lead part of the calorimeter is sufficient, on the average, for electron-photon shower development at the maximal planned primary particle energy. Thus, the upper lead part of the calorimeter is intended for separation and measurement of the energy of the first electron-photon avalanche arising as a result of the first act of particle interaction with the target nucleus.

The further particle interactions and transformations take place in the following 13 iron absorber layers with total thickness 855 g/cm^2, scattering of energy in which is monitored by the ionization chambers IK-5 - IK-16 located here. The presence of the iron and lead layers, monitored by individual ionization detectors, makes it possible to measure the particle interaction sections on heavy nuclei. In this case, the proportional counters PC7 - PC11 at the calorimeter exit serve to restrict the solid angle, in the limits of which primary flux recording takes place.

A particle entering the instrument from the DD2 side crosses the control PC11 (analog of PC2), and enters a block of layered targets. Here are located four thin graphite layers, each 2.26 g/cm^2 thick, with a proportional counter after each layer (PC7 - PC10) as an interaction detector. In view of the low probability of secondary particle multiplication processes in a thin layer, we can determine from the proportional counter indications, the multiplicity of the secondary particles generated in the interaction act on the graphite nucleus. The subsequent processes in the ionization calorimeter do not differ from the case examined above of particle entry into the

instrument from the DD1 side. The counters PC3 and PC4 limit the solid angle for the flux recorded from the DD2 size. /55

In addition to combined operation of the charge and energy detectors, autonomous particle recording by DD1 and DD2, apart from the ionization calorimeter, is accomplished in the IK-15 instrument, which makes it possible to determine the particle charge spectrum in the energy interval 10^9 - 10^{10} eV/nuc.

Let us turn to a more detailed description of the design features and basic parameters of the IK-15 functional components.

2. Ionization Calorimeter

Absorber. The amount of absorbing matter in the ionization calorimeter determines energy measurement accuracy and, therefore, is one of the important instrument parameters. The maximal thickness of the IK-15 absorber in the direction determined by the charge detectors (Figure 2) is 855 g/cm^2 of iron and 140 g/cm^2 of lead, which amounts to 7.5 nuclear interaction ranges. On the average, about 90% of the primary particle energy is absorbed in this amount of material. We recall that the calorimeter thickness of the SEZ-14 instruments, installed aboard the Proton 1, 2, 3 AES, was only 386 g/cm^2 Fe, which constituted about three nuclear interaction ranges [25]. In that calorimeter, the protons released, on the average, 50% of their energy. For global particle recording aboard the Proton 1, 2, 3 AES, the average absorber thickness in the calorimeter was 220 g/cm^2 Fe, and, in this case, the protons released $\sim$ 30% of their energy. Aboard the Proton 4 station, the average absorber thickness for global particle recording is around 400 g/cm^2, i.e., about three nuclear interaction ranges. The average fraction of the particle energy absorbed in this case is close to 50%.

Energy measurement accuracy depends essentially not only on the amount of absorbing matter in the ionization calorimeter, but also

on the number of detectors measuring the ionization created in the absorber. The thickness of an individual absorber layer was selected close to that which is necessary on the average for maximum development of the electron-photon avalanche arising in the layer as a result of nuclear interaction of a particle with minimal limiting energy in the interval being recorded ($\sim 10^{11}$ eV).

On the basis of these considerations, the absorber was divided into 13 layers of iron. For constructional reasons, the iron layers were made of different thickness — from 4.8 to 9.8 cm.(the absorber layers were thinner in the middle part of the calorimeter because of the necessity for locating the additional telescope counters PC5 and PC6). The general construction of the absorber is shown in Figure 3. The major portion of the absorber is made of iron. The advisability of selecting iron as the absorber material was pointed out in [2]. /57 In addition, the iron calorimeter absorber forms a quite strong load-carrying structure, which reinforces the entire apparatus.

Ionization chambers. The ionization chamber was made from 1.5-mm-thick stainless steel in parallelepiped form, with external dimensions 900 × 1045 × 33.8 mm (Figure 4). The chamber was divided by rigid partitions into 15 sections with common gas filling. The dimensions of each section were 30 × 60 mm, length 945 mm. Sectioning stiffens the structure and permits reducing the time for collection of the charges formed in the gas. The internal electrodes were made from 1-mm-diameter steel filaments stretched along the sections. The filaments were loaded to 40 kg by means of springs. The filament ends were attached to cermet insulators mounted on two supports. All the filaments were electrically connected to a common collector, with the lead exiting through a feed-through insulator. High voltage is applied to the electrode, and the electrical signal arising upon particle passage is taken out through this lead. The chamber is welded. A high degree of chamber housing hermeticity is achieved using argon-arc vacuum welding. The chamber capacity was degassed prior to filling by evacuation at a temperature of +200° C to 10^{-4} mm Hg for one day. The degree of chamber hermeticity achieved can be

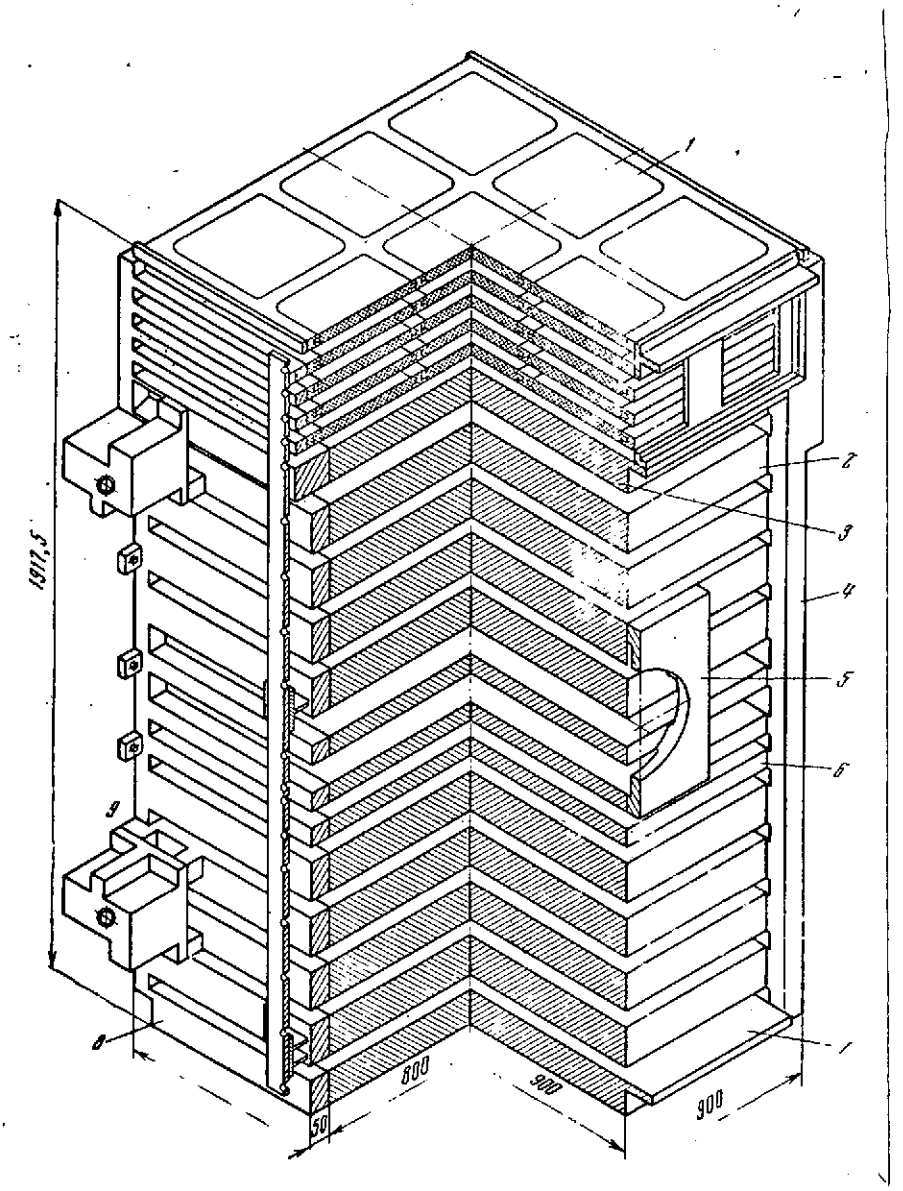

Figure 3. Absorber of IK-15 ionization calorimeter (upper five layers lead, remaining layers iron):

1 — lead filter; 2 — type-1 plate; 3 — type-2 plate; 4 — right side panel; 5 — adapter; 6 — type-3 plate; 7 — type-4 plate; 8 — left side panel; 9 — attach bracket

characterized by the inleakage magnitude $\sim 10^{-5}$ liters · μm Hg/sec. The total chamber volume is 27.5 liters, the working area is 0.8 m^2. The structure weighs 26 kg.

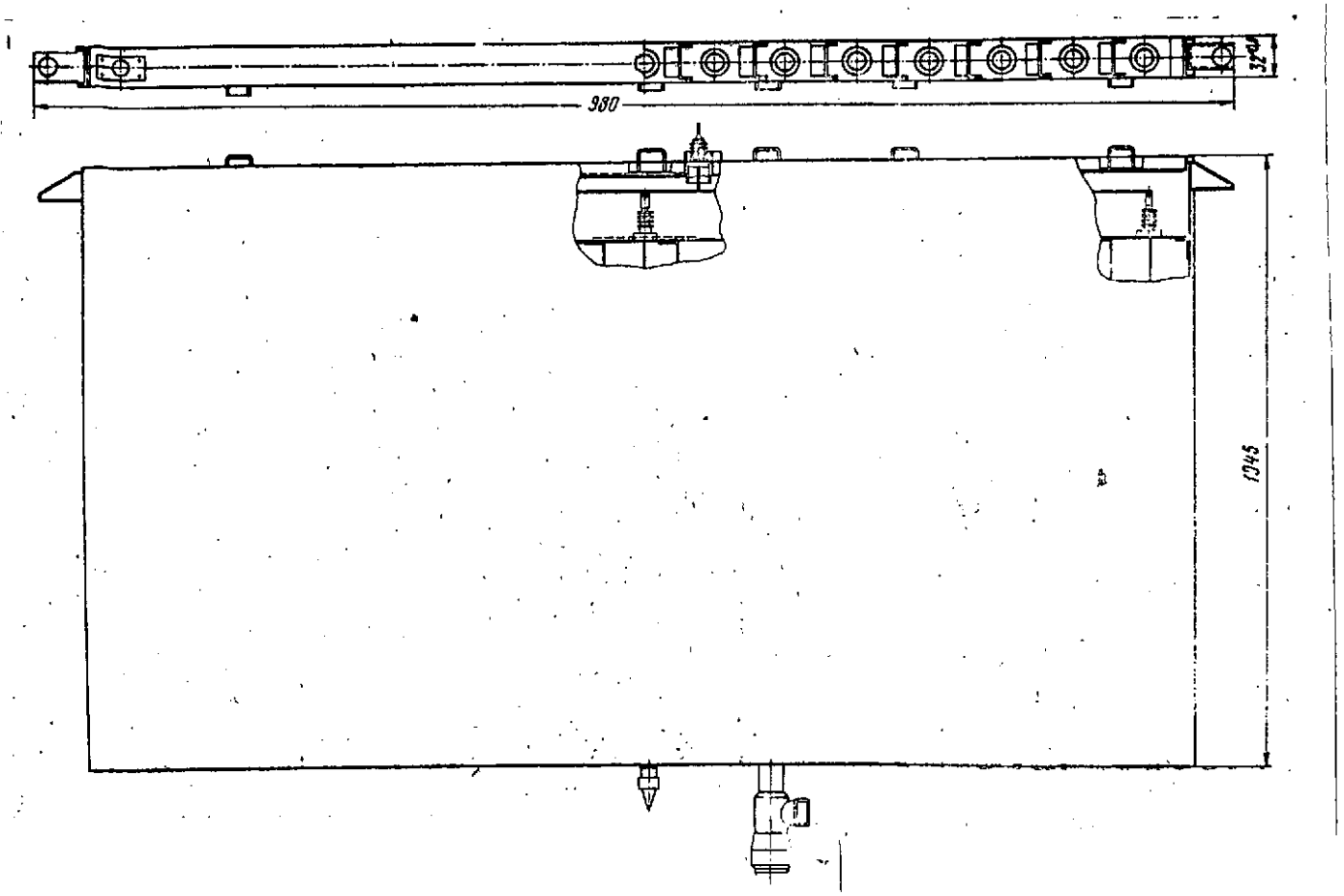

Figure 4. Construction of ionization chambers (IK-1 to IK-16)

The chamber is equipped with a special value for evacuation and gas filling. Provisions are also made on the housing for attachment fittings which make it possible to mount the chamber in the calorimeter and mate it with the electronic units.

The ionization chambers are filled with xenon with the addition of 5% nitrogen to a total pressure of 790 mm Hg. The use of a gas with high density (incomparison with argon, for example) makes it possible to increase the ionization effect created in the chamber by fast charged particles. The addition of nitrogen shortens the charge collection time and stabilizes the amplitude of the electrical impulses in relation to possible oxygen impurities. The total thickness of the gas layer in the chamber in the direction perpendicular to its plane is 18.3 mg/cm^2. A fast singly charged particle crossing

the chamber in this direction creates in the gas $1.3 \cdot 10^3$ ion and electron pairs losing to ionization about 28 KeV. The recordable part of the electron component collects under the influence of the electrical field on the inner electrode (chamber filament) in a few microseconds, and creates here an electrical impulse of negative polarity with amplitude proportional to the energy released in the gas. If the charge formed in the gas were collected completely, it would create in the singly charged ionizing particle case a voltage pulse with amplitude 0.8 μV (the electrical capacity of the chamber is 268 ± 2 pF).

The operating voltage on the ionization chamber was determined from the following considerations. /59

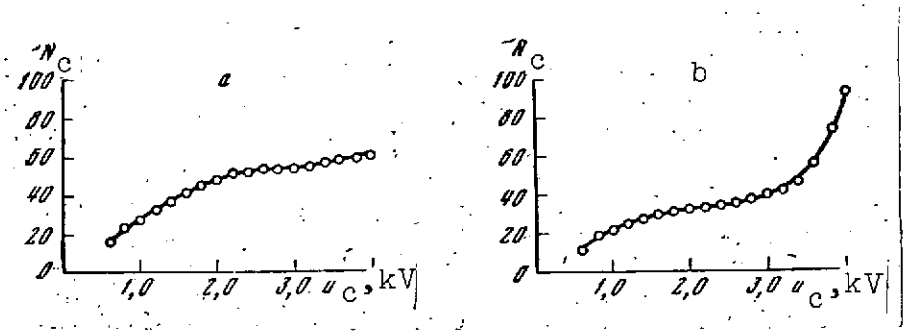

Figure 5. Relative magnitudes of electrical impulse amplitudes at ionization exit chamber from α particles as function of chamber working voltage:

a — particle tract direction from midpoint of section side wall toward inner electrode; b — particle track direction from midpoint of section upper wall toward inner electrode

Figure 5a shows a curve expressing recorded impulse amplitude versus ionization chamber voltage. Here, Pu^{239} α-particles deposited on the side wall of a standard chamber section (the sections had dimensions identical to those of the section in the working chamber) were used as the ionization source. In this case, the worst conditions for charge collection are realized, since the region with minimal electrical field intensity is subjected to ionization. With an operating voltage of 1750 V established on the chamber, recording of 85% of the charge is accomplished under conditions of α-particle

impulse amplitude "saturation" (Figure 5). The "saturation" region is reached in the interval 2.2 - 3.0 kV. At voltages exceeding 3 kV, secondary processes leading to gas amplification begin to show up. An analogous curve is shown in Figure 5b for the case when the ion column is created by α-particles along the perpendicular to the plane of the chamber — from the midpoint of the section upper wall to its filament. This is the most favorable case for charge collection, since the ion column crosses the region with maximal electrical field intensity.

For the selected 1750 V operating voltage, conditions are realized under which ion recombination along the track does not occur for weakly ionizing singly charged relativistic particles and minimal charge collection time is achieved. Figure 6 shows the duration τ_ϕ of the impulse front observed from an α-particle emitted from the section side wall versus chamber operating voltage magnitude. The impulse front duration measurement was based on the time interval between signal levels 0.1 and 0.9 of the peak value. We see from Figure 6 that, with increase of the operating voltage above 1800 V, the value of τ_ϕ decreases only slightly. At the same time, this operating voltage magnitude is significantly less than the value at which gas amplification begins to show up.

/60

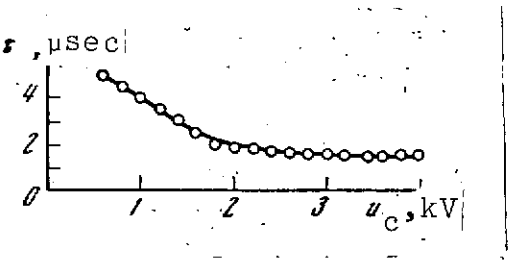

Figure 6. Duration of α-particle impulse front as function of chamber operating voltage (particle track direction from side wall of section toward inner electrode)

Proportional counters. Proportional counters are sensitive ionization detectors which permit reliable recording of small ioniza- effects, beginning with a single singly charged relativistic particle. Proportional counters of large area for studying high-energy particles in cosmic space were first developed for the Proton 1, 2, 3 scientific stations.

The proportional counters perform a different role in the IK-15 system: they form a "telescope" which limits the solid angle of the system when recording single particles (PC4 - PC7), and make it possible to establish passage through the filter of a primary particle without shower accompaniment, acting as interaction detectors (PC3, PC7 - PC10. As previously mentioned, the counters PC2 and PC11 below the DD detectors monitor the charge of the primary particles being recorded.

The variety of counter functions led to differences in their construction, although the general configuration of these detectors is the same.

The construction of the counters PC8 - PC10 is shown in Figure 7. These counters, with working area 1.25 m^2, contain 17 sections with section dimensions 30 × 60 mm. The overall gas volume of the counter of this type is 51 liters. The counter weighs 35.6 kg. The counter dimensions correspond to the dimensions of the divided filters between which they are positioned as interaction detectors.

The construction of the counters PC4 - PC7, located below the calorimeter absorbing layers is analogous. Their working area is 0.8 m^2; each contains 15 sections of the same dimensions. The overall gas volume of the counter of this type is 27.5 liters, weight is 25.5 kg. The counters PC4 - PC10 each have a single electrical lead. The counters PC2, PC3, PC11 have a large gas gap 50 mm high; moreover, they are dual-layer counters which permit ionization measurements of high accuracy and identification of single singly charged particles. One counter of this type, PC11, is shown in Figure 8. This counter is divided into two layers, each of which has two electrical leads /62 for recording ionization impulses. In each layer, they are 15 sections of dimensions 50 × 83 mm each. The two layers have common gas filling. The overall counter working area is 1.54 m^2. In essence, the counter contains in a common housing four sectional proportional counters. The counter PC2 is of analogous construction. It consists of two layers with 16 sections in each layer with four electrical

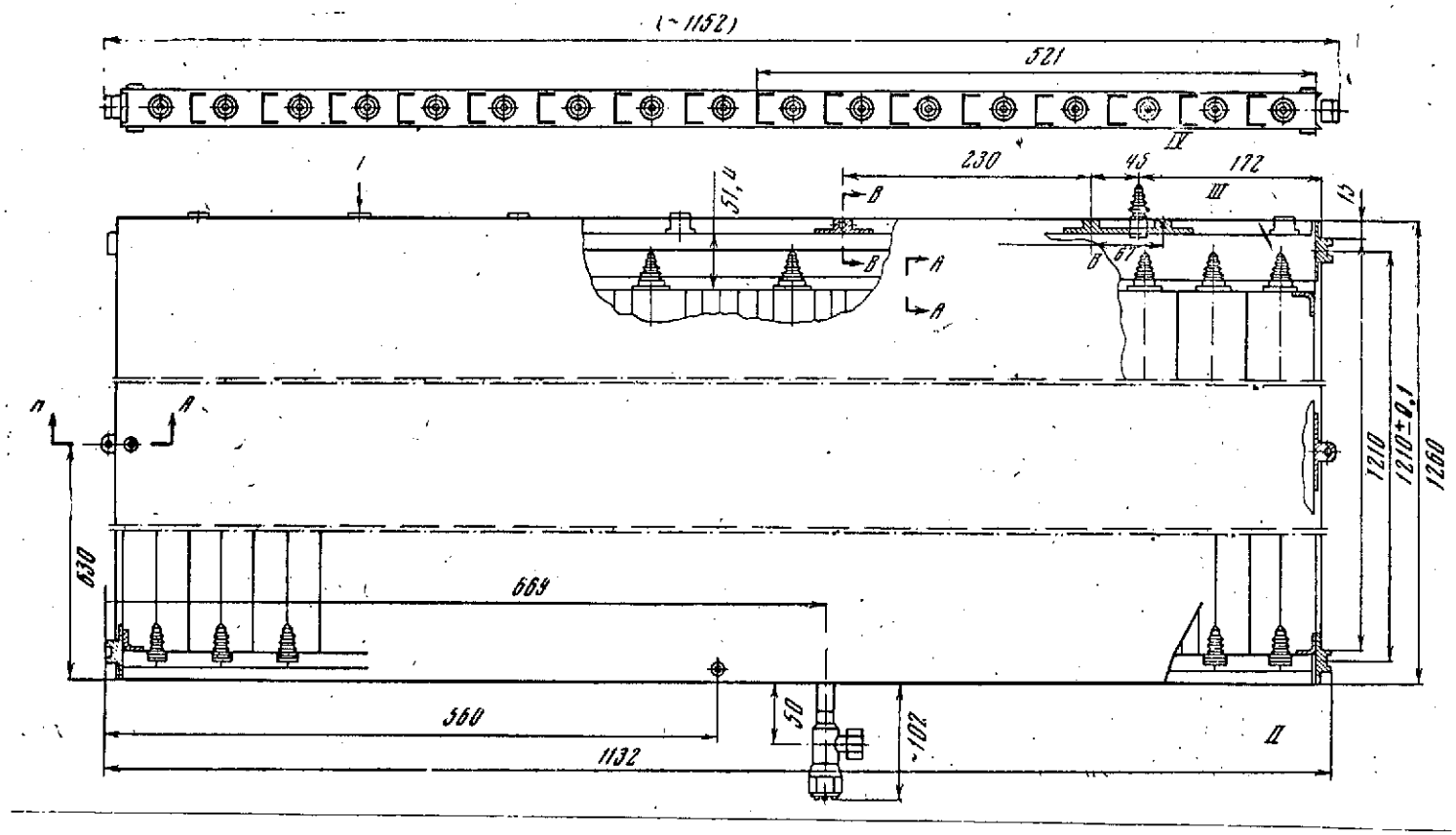

Figure 7. Construction of proportional counters PC8 - PC10

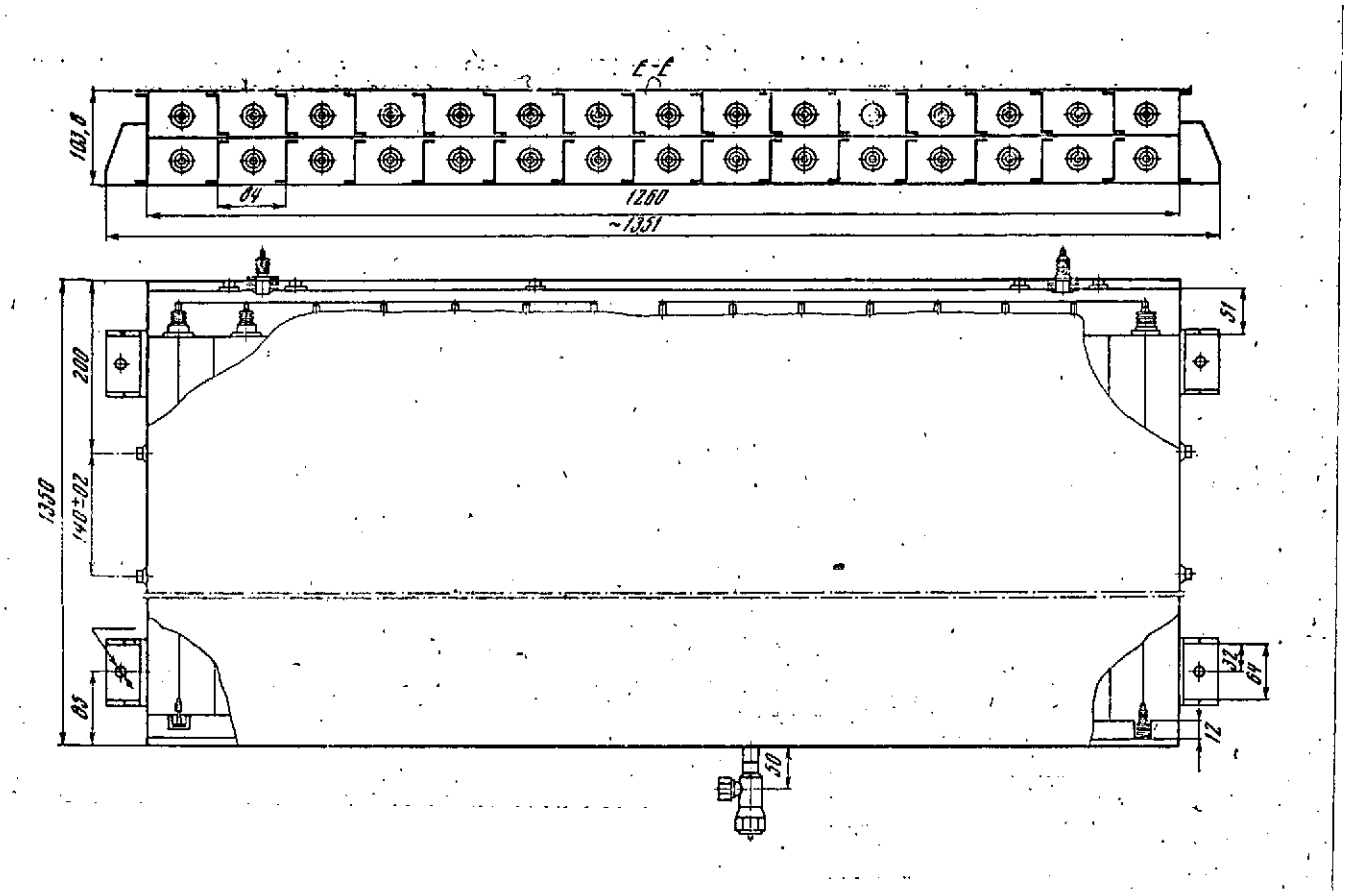

Figure 8. Construction of proportional counter PC11

leads. The proportional counter PC3 is two-layer with a single electrical lead from each layer. In each layer there are nine sections of 50 × 83 mm each. The counter working area is ∿ 0.8 m^2.

Along each section of every counter, a 0.1-mm-diameter tungsten filament is stretched (with tension 0.4 kg) to serve as the inner electrode. The filament is attached to two insulators (see Figures 7, 8). The filaments of all sections of a single layer or part of the sections, as in the PC2 and PC11 counters, are joined electrically and have a lead passing through a feed-through insulator for voltage supply and electrical impulse recording. The housings of all the counters are made from 1.5-mm-thick stainless steel, using the same technique and the same degassing procedure as the ionization chambers. Tests have shown that with the use of this technology both the proportional counters and the ionization chambers remain operable and maintain their sensitivity up to a year without refilling.

The proportional counters are filled with argon with 10% methane addition to a total pressure of 270 - 300 mm Hg. a quite high gas amplification factor is achieved at this pressure and 1.6 - 1.7 kV voltage on the counters. When a fast singly charged particle passes through the counter in the direction perpendicular to its plane, a voltage impulse with most probable amplitude ∿ 1 mV appears on the counter lead. Figure 9 shows an experimentally obtained plot of gas amplification factor (GAF) in the proportional counter versus supply voltage.

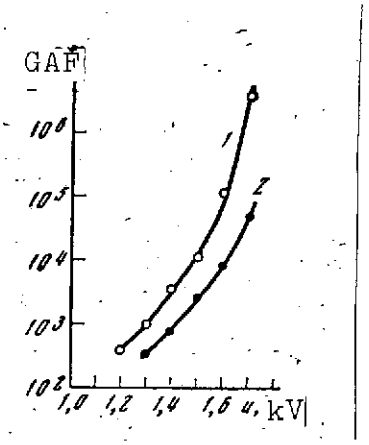

Figure 9. Counter gas amplification factor versus operating voltage:

1 — for pressure 240 mm Hg; 2 — for pressure 300 mm Hg

/64

Ionization detector adjustment and ionization impulse measurement. The ionization detector unit includes: ionization chamber or proportional counter, high-voltage source (transformer) for chamber (counter) supply, electronic impulse amplifier, and (in the proportional counter units) two additional amplitude discriminators — threshold devices to discriminate the "window" corresponding to the ionization effect of a single singly charged particle. The unit is a structural whole, and its adjustment is accomplished as part of the system, together with the subsequent electronic metering circuits.

Adjustment of the proportional counter unit sensitivity is accomplished by varying the voltage on the counter, the gas pressure in the counter, and the gain in the electronic circuits. The amplifier has two amplification stages. The first stage with gain 20 is sufficient for output of signals to the next metering device. The second (gain ∿ 30) is required to excite the amplitude discriminators. The adjustment of the PC unit is accomplished using a natural source of fast singly charged particles — μ-mesons, constituting the hard component of cosmic radiation at sea level.

Figure 10, I(a) shows the amplitude spectrum of μ-meson impulses recorded at the proportional counter PC2 (upper left quarter)

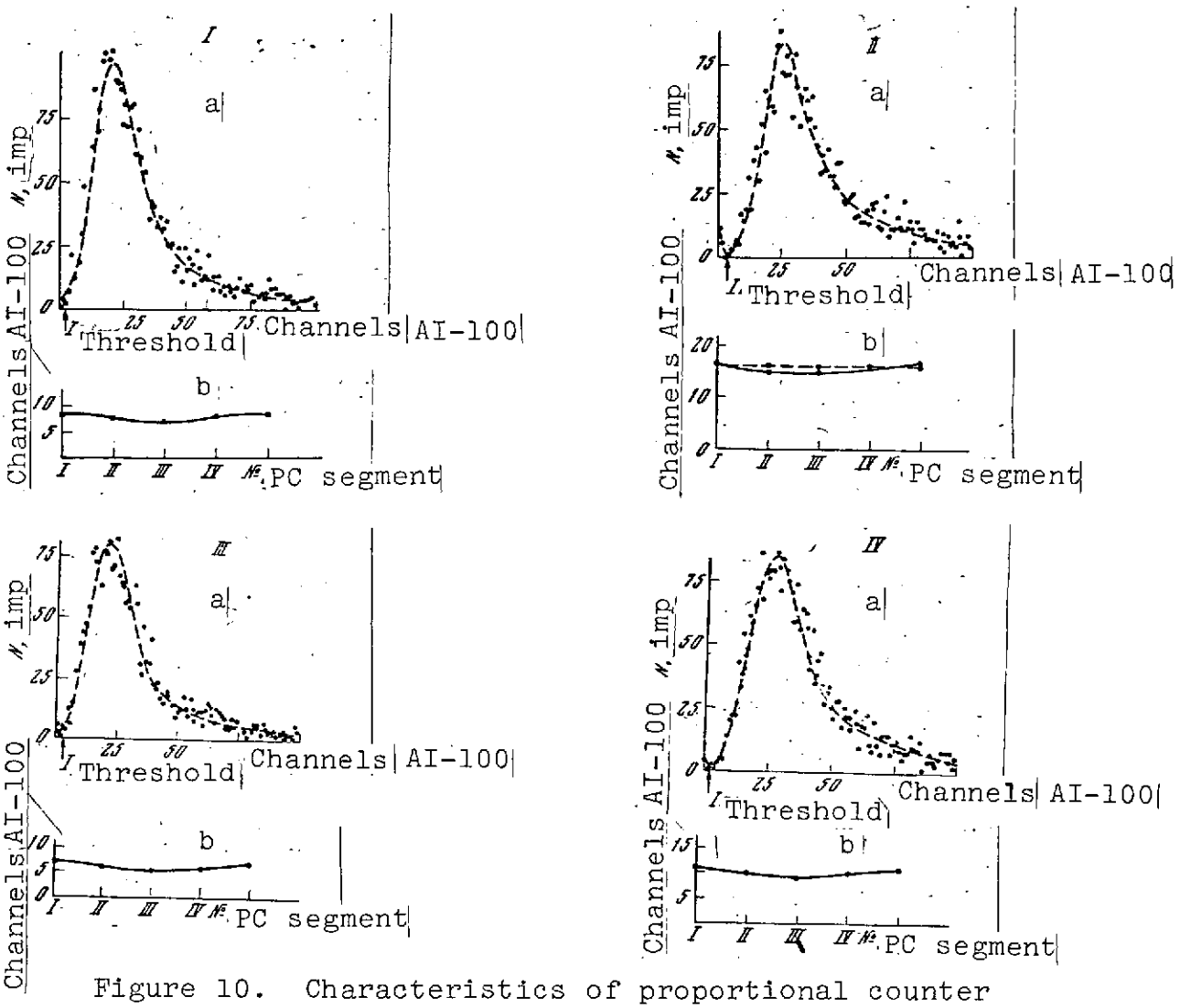

Figure 10. Characteristics of proportional counter PC2:

a — μ-meson amplitude spectrum at sea level at counter output; b — distribution of counter sensitivity over five segments; I — upper left quarter of counter; II — upper right quarter of counter; III — lower left quarter of counter; IV — lower right quarter of counter

amplifier output. The abscissa is the AI-100 impulse amplitude analyzer channel number, the ordinate is the number of impulses recorded in the corresponding channels. The spectrum illustrates the amplitude scatter at the impulses coming from the given detector output when fast singly charged particles pass through the detector. The triggering threshold of the first discriminator, required for the detector to record any singly charged particle (this threshold corresponds to an amplitude of ∿ 200 μV at the porportional counter

output), is indicated on the abscissa axis. The most probable spectrum amplitude corresponds to ∿ 1 mV at the amplifier input.

Figure 10, I(b) shows results of tests of counter sensitivity uniformity over its area, broken down into five equal segments. The amplitude spectrum recorded on the given segment was determined for each segment, the most probable amplitude values are shown on the graph. We see from Figure 10, I(b) that the counter sensitivity nonuniformity over its area, referred to the average value, does not exceed 10%.

Analogous spectra and sensitivity nonuniformity characteristics for various parts of counters PC2 and PC3, and also for counter PC4, are shown in Figure 10, II, III, IV, Figure 11, I, II, and Figure 12.

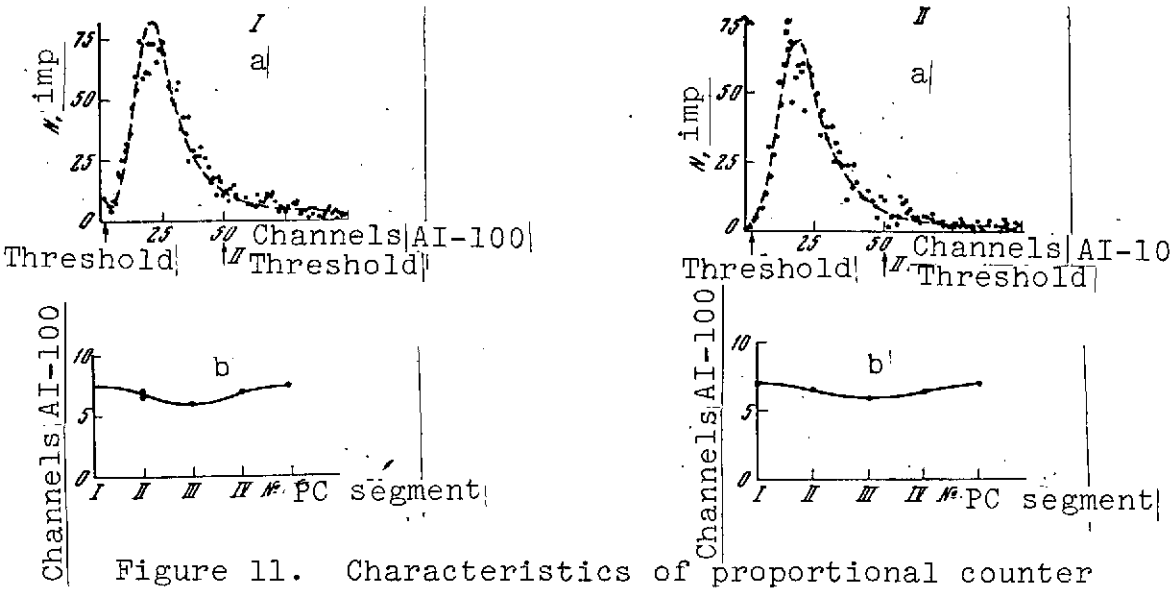

Figure 11. Characteristics of proportional counter PC3:

I — upper half of counter; II — lower half of counter; a, b — same as in Figure 10

In connection with the objective of the PC3 and PC4 counter units, which act as interaction detectors, correct adjustment of the "window", which permits discrimination of single singly charged particle passage from passage of several particles, takes on particular importance in these units. Critical here is the establishment of the triggering threshold of the second amplitude discriminator, which /65

sets the upper limit of the "window". A satisfactory compromise was found in the relationship between the second discriminating threshold and the probable amplitude in the spectrum, which is indicated in Figures 11, I, II and Figure 12. With this adjustment, the effectiveness of single singly charged particle recording in the "window" limits is 75%, while the probability of recording two particles as a single particle is less than 20 %. /66

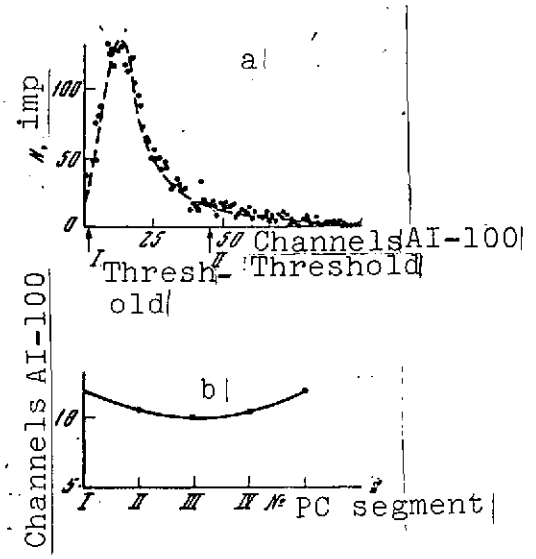

Figure 12. Characteristics of proportional counter PC4:
a, b — same as in Figure 10

Adjustment of the ionization chamber unit involves setting the required electronic amplifier sensitivity. The lower limit of recordable amplitudes is bounded by amplifier input self-noice ($\lesssim$ 15 μV). Here, reliable recording can be initiated with the ionization effect created by simultaneous passage of 50 - 60 fast singly charged particles. With account for this value and also the threshold sensitivity of the following measuring circuits ($\sim$ 5 mV), the gain is set at 250 - 300.

Two techniques for calibrating the electronic circuits were adopted in order to correlate the recorded impulse amplitudes with the ionization effect created in the detector: calibration by a "reference" charge and calibration by voltage pulses. /67

The first technique involves applying a charge equivalent to definite energy release in the ionization detector gas to the amplifier input circuit through a small calibrating capacitor ($\sim$ 5 pF). The second technique involves applying to the amplifier input voltage pulses simulating the impulses generated by the detectors for given energy release in the gas. In both cases, quite exact simulation of the calibrating pulse shape is essential for equivalent recording. Figure 13 shows as an illustration the pulse shapes observed at the

ionization chamber amplifier output for calibration by charge (a) and voltage pulse (b) in comparison with the pulse from an α-particle (c) emitted from the side wall of one of the sections. Analogous pulse shapes observed at the output of the proportional counter amplifiers are shown in Figure 14.

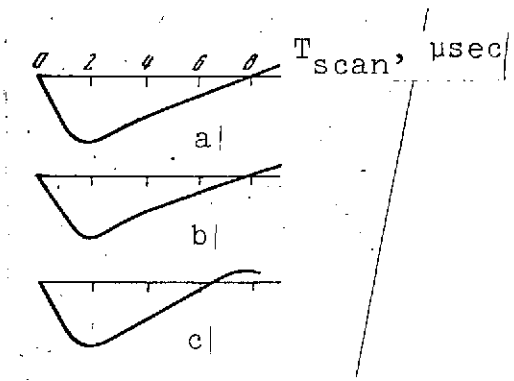

Figure 13. Shapes of pulses observed at ionization chamber amplifier output:

a — from calibrating signal for calibration based on charge; b — for calibration by voltage impulses; c — from α-particles

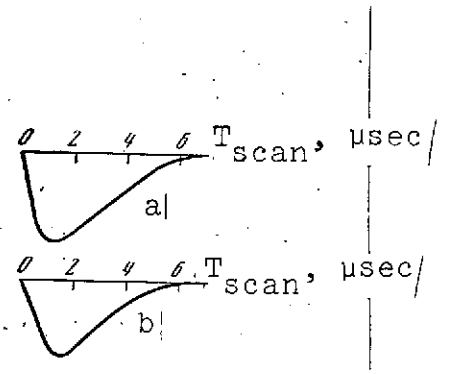

Figure 14. Shapes of pulses observed at proportional counter amplifier output:

a — from μ-mesons; b — from calibrating voltage impulses

The pulses from the amplifier output are directed to a multichannel amplitude meter. Each ionization detector output channel (except for counters PC5 and PC6, which serve only for control signal generation) is equipped with individual amplitude analyzers. Certain channels are equipped with two analyzers to increase the measurable amplitude dynamic range (the channels of proportional counters PC4, PC7 - PC10 are of this type). The amplitude analyzer performs double analog-numerical conversion of the recorded pulse amplitude into code /68 and transmission of the code to the telemetry system. The amplitude analyzer also performs temporal selection (with resolution time 5 - 6 μsec) of the recorded pulses and amplitude analysis of the input pulse; storage of the code corresponding to the pulse with subsequent transmission to the telemetry system is accomplished only in the presence of an enabling command in the form of a control pulse generated by the IK-15 logic unit. Linear pulse transmission without significant

amplitude distortions upon control command is the first operation carried out in the analyzer.

The second operation entails logarithmic transformation of the amplitude of the impulse selected for recording into six-place binary code. With account for the adopted amplitude quantization step of $\sim$ 10%, the analyzer permits amplitude measurements in the dynamic range up to $\sim 10^3$. A second conversion into two-place octal code is accomplished in the subsequent output circuits. At the output of each of these places, there are eight quantized voltage levels (from 0 to 6 V), which are transmitted directly to the telemetry system. Amplitude recording of the pulses measured by a single analyzer is accomplished by two telemetry channels. The information on the amplitude of each recorded pulse is retained until the arrival of the next pulse. At the moment of arrival of a command for pulse transmission, preliminary "clearing" of the memory unit is performed.

In all, the IK-15 amplitude and measuring unit includes 42 amplitude analyzers for measuring the amplitudes of the pulses coming from the proportional counters, ionization chambers, and Cherenkov counters in the charge detectors.

Figure 15 shows the amplitude-number calibration characteristic of the proportional counter circuit. The calibration was performed by calibrating voltage pulses applied to the PC amplifier input. The input amplitude values are shown along the abscissa axis to logarithmic scale, and the corresponding values of the numerical code generated at the amplitude analyzer output are shown along the ordinate axis. We see from the graph that the amplitude variation range is 800. The measurements begin with amplitudes comprising 0.2 of the most probable value I_{prob} corresponding to fast singly charged particle passage, and reach amplitudes corresponding to passage of 160 particles. This is the ionization measurement range for the proportional counter. If two measureing circuits are available, the measurement range expands to ionizations corresponding to $2 \cdot 10^4$ particles.

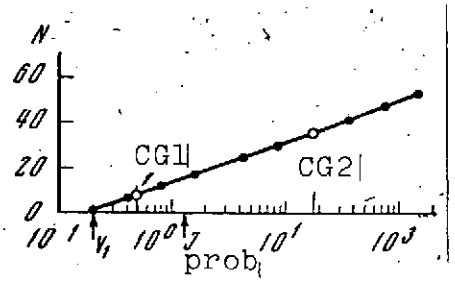

voltage at PC amplifier input, mV

Figure 15. Typical amplitude-number characteristics of circuit for recording pulses from proportional counter

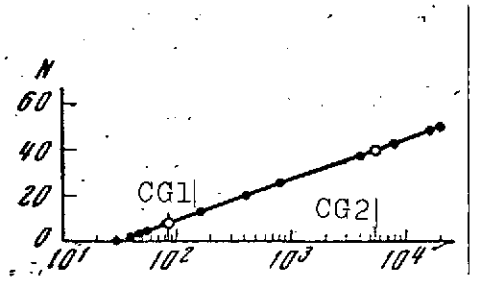

m, particles

Figure 16. Typical amplitude-number characteristic for circuit for recording pulses from ionization chamber

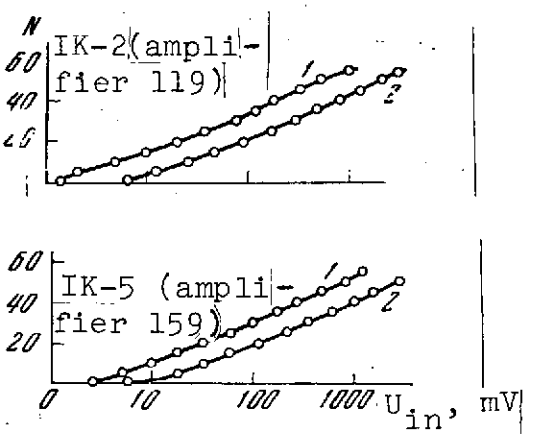

Figure 17. Actual amplitude-number characteristics of circuits for recording pulses from ionization chambers IK-2 and IK-5:

1 — for calibration based on charge; 2 — for calibration by voltage pulses

The ionization chamber measurement circuits components have similar characteristics. Figure 16 shows the amplitude characteristic of the ionization chamber circuit. Here, the calibration voltage pulse amplitudes at the amplifier input are expressed as the number of fast singly charged particles creating equivalent ionization in the chamber gas (abscissa axis). We see from the figure that measurements can be carried out here for the ionization effects created by simultaneous passages of from 40 - 50 particles, up to $2 \cdot 10^4$ particles.

/69

For certain ionization detector components, the characteristic does not have the ideal form presented in Figures 15, 16. Shown as an illustration are the characteristics of the IK-2 and IK-5 measurement circuits (Figure 17); curves 1 correspond to circuit calibrations based on charge, curves 2 correspond to calibrations by voltage pulses; the ordinate axis is the number of pulses at the amplitude-number converter output. Characteristics 1 and 2 do not differ

significantly in form, indicating equivalence of the two calibration techniques. Their shift along the abscissa is associated with the scaling coefficient difference, which must be taken into account in referring the arbitrary amplitude values shown along the abscissa axis to the amplifier input.

Calibration generators which could be activated and deactivated on command from the Earth were provided in order to check for sensitivity change of the amplification circuits and metering devices during the experiment. The calibration voltage pulses are applied to the input of each amplifier in the ionization chamber and proportional counter systems. The magnitudes of these calibration amplitudes (CG1 and CG2) are indicated on the amplitude characteristics of Figures 15 and 16. /70

3. Charge Detectors

The DD charge detector is one of the essential functional components of the IK-15 spectrometer. As indicated by the name, its basic task is to determine the nature of the cosmic radiation particle being recorded by the instrument by measuring its charge. The principle of these measurements is based on recording the Cherenkov radiation excited by a relativistic charged particle in a transparent medium. The intensity of this radiation depends quadratically on the transiting particle charge. This principle is widely used in experimental studies of primary cosmic radiation composition, specifically, it was used for these same purposes aboard the preceding Proton scientific stations.

The primary procedural and technical difficulty in its realization in application to the IK-15 spectrometer involved the necessity for creating a detector which exceeded considerably in effective area all preceding experiments of similar nature.

The basic idea of the DD design was to configure a detector of large area from a large number of small Cherenkov counters which had been tested systematically during previous experiments in space. The

following "stepped" instrument structure was adopted: four Cherenkov counters were combined into a section forming a completely autonomous instrument; four sections operating into a common measurement output constitute the DD. The presence of the four independent sections ensures high reliability of the instrument as a whole.

Figure 18 shows a plan view of the general configuration of DD1, consisting of four sections. The sections are mounted in a common frame 2. The frame crosspieces provide quite rigid support for each

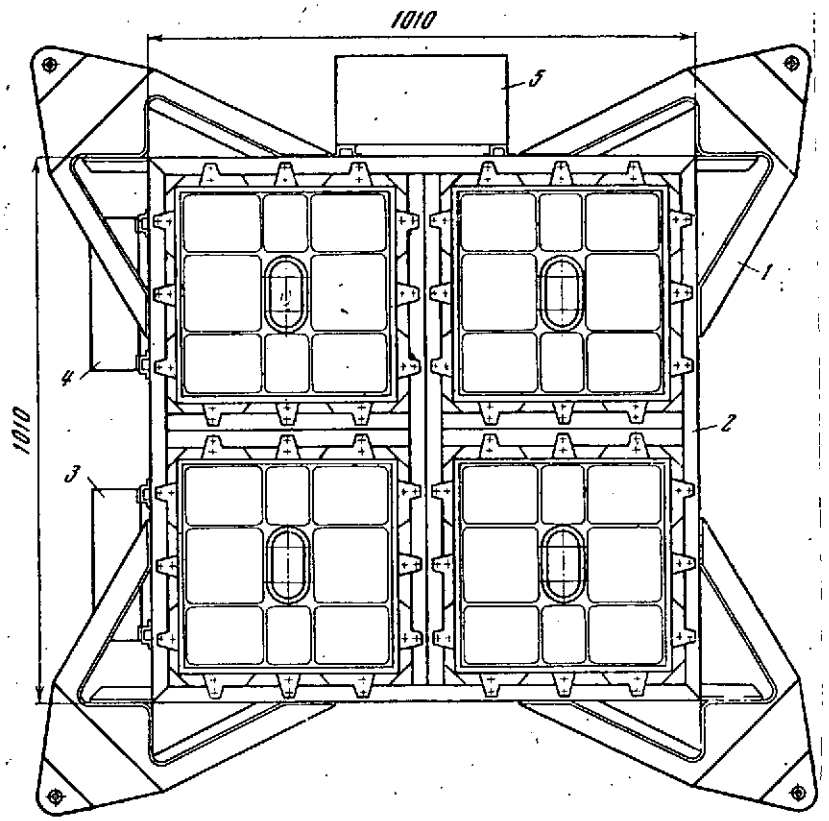

Figure 18. Configuration of DD1 charge detector sections (top view):

1 — detector supports; 2 — common frame; 3, 4, 5 — electronic units

of the sections. The DD1 is attached by four welded supports 1 to the ionization calorimeter above the continuous filter unit. The DD electronic units (3, 4, 5) are mounted on the side surface of the frame. The configuration of DD2 is similar with one essential difference: mounting of DD2 on the IK-15 is accomplished using two welded supports.

A schematic of one section with indication of the corresponding geometric dimensions is shown in Figure 19. The section consists of four Cherenkov counters, joined by two common scintillation counters, forming the "telescope". Coincidence of pulses coming from both counters at the moment of particle passage through the telescope serves as a signal for selection and amplitude analysis of the impulse at the combined output of the section Cherenkov counters. The dimensions shown make it possible to estimate the relative aperture of the entire DD instrument. The geometric factor of the DD is 1960 $cm^2 \cdot sr$, which exceeds by 18 times the relative aperture of the charge detector used in [3].

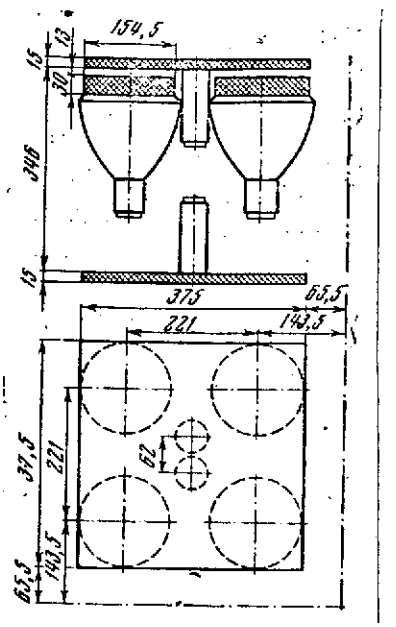

Figure 19. Schematic of one DD charge detector section

/72

Let us examine in more detail the construction of the scintillation and Cherenkov counters. Each scintillation counter consists of a radiator and two PM-53 photomultipliers. The scintillation counter radiator is made from a plastic scintillator using polystyrene with the addition of p-terphenyl. The radiator has the form of a plate with dimensions 375 × 375 × 15 mm. All the radiator surfaces are polished, the side surfaces are, in addition, coated with white enamel for diffuse scattering of the light, which permits increase of the radiator light output.

Structurally, the scintillation counter is made in the form of a plate, on which the scintillation counter housing is mounted. The radiator is located in this housing. For protection against mechanical damage during vibration, the radiator is packed between two pads fabricated from 2-mm-thick rubber, and a 2.5-mm-thick rubber pad is provided around the perimeter between the housing and the radiator; the radiator is held down by a cover. Gaskets made from paronit

material are provided between the housing, cover, and plate to ensure light tightness; recording of the light impulses is accomplished by two photomultipliers (PM) which are in optical contact with the radiator through a light guide. To obtain good optical contact, the contacting surfaces of the PM, light guides, and radiators are coated with silicone vaseline and lapped together carefully. Mounting of the PM-53 photomultiplier, together with the high-voltage dividers, is accomplished with the aid of a special framework, which is designed to protect the PM against extraneous light and prevent mechanical damage.

The Cherenkov counter (Figure 20) consists of the radiator 1 and PM-49 photomultiplier. The radiator is made from plexiglass in the form of a 154.5-mm-diameter cylinder, 30 mm high. The radiator surface contacting the PM-49 is polished, all the other radiator surfaces are matte and coated with black enamel to absorb the Cherenkov radiation arising in the radiator from cosmic particles entering the instrument from the PM.

The Cherenkov counter radiator and PM-49 photomultiplier are mounted in a special housing. The new Cherenkov counter design utilized the PM-49 housing which had been used aboard Proton 1, 2, 3, and which had proved to be a convenient and reliable unit. The housing protects the PM against extraneous light and mechanical damage, /73
and also ensures reliable optical contact of the PM with the radiator. The photomultiplier, radiator, and electronics mounted on the housing form an individual electronic unit.

Mounting of the photomultiplier and radiator is accomplished as follows. The photomultiplier is supported in the housing with its shell resting on a gasket 3 made from vacuum rubber bonded to the clamping ring 4. Clamping of the photomultiplier to the radiator is /74
accomplished by three screws 5 which pass through threaded sleeves 6 and are connected with the clamping ring.

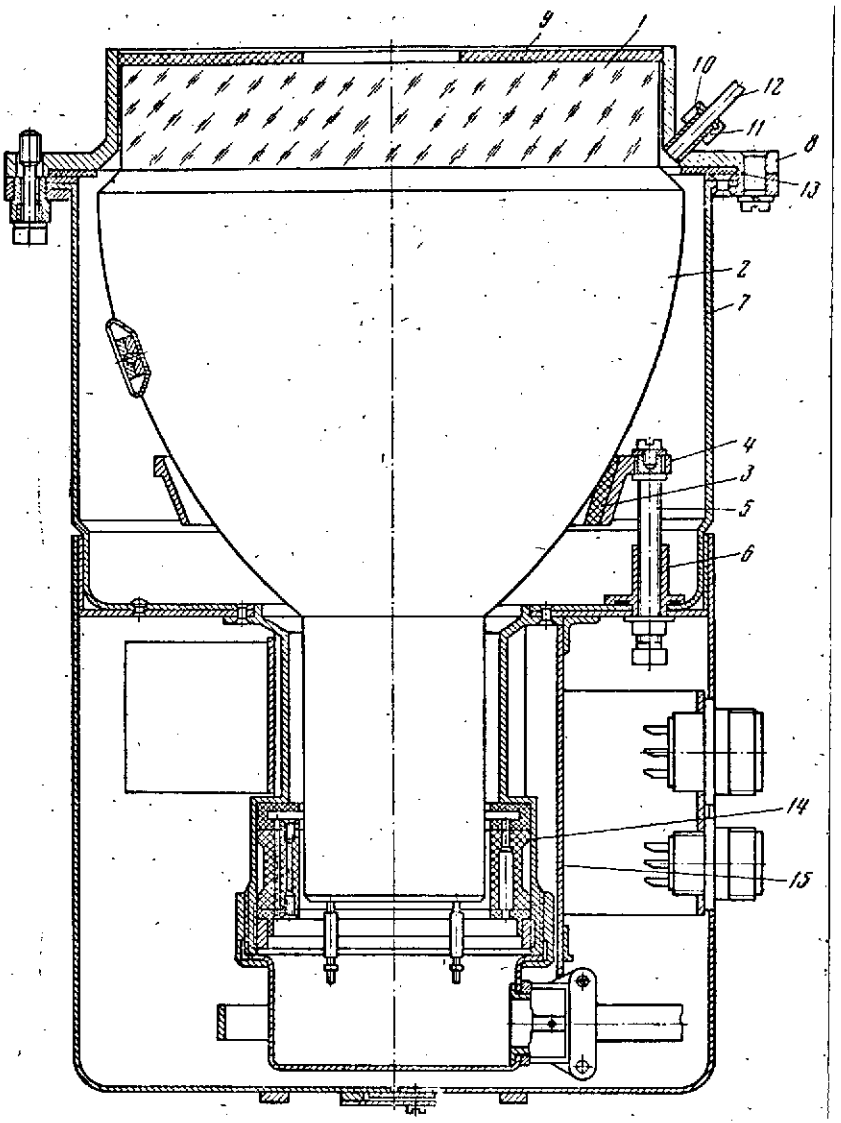

Figure 20. Cherenkov counter

The radiator and optical contact are mounted on the photomultiplier. For reliable contact, the photomultiplier and radiator contacting surfaces are coated with silicone vaseline and lapped to one another, after which the cover 8 with vacuum rubber gasket 9| is installed on the light-tight housing 7. The vacuum rubber provides reliable protection of the radiator surface against mechanical damage during vibratory loads.

In the cover 8 there is a threaded sleeve 10 with nut 11 for attaching the lightguide 12 coming from the light generator. The

light generator generates calibration light pulses which are applied to the photomultiplier during adjustment of the Cherenkov counter from the automatic sensitivity adjustment system.

All details of the light-tight housing are black anodized or oxidized (depending on the material). The rivets, attach screws and sleeves passing through the light-tight housing wall are coated with black glyptal lacquer. The light-tight vacuum rubber gasket 13 is provided where the light-tight housing joins the cover 8. In the upper part of the light-tight housing adapter, there is installed the plexiglass drum 14 with built-in voltage divider for power supply to the photomultiplier dynodes. The electronic units which transform the high-voltage power for supplying the photomultiplier and pulse amplifier are mounted on the shell 15.

The anodes of the four PM-49 in one DD section are connected together, and form the common signal output of the Cherenkov counters of that section. The pulses from this output are amplified by a common amplifier (gain about 160) and discriminated by a common output threshold device (threshold $Z_0 \sim 1.5$ mV), which is triggered by passage through the counter of any charged particle, including a singly charged particle. The Cherenkov counter sensitivity is established by selecting the voltage on the PM-49 (1.4 - 1.5 kV) so that the most probable amplitude of the pulses excited by passage of a singly charged particle will amount to 5 mV on the PM anodes. The choice of such a low amplitude level for the singly-charged particle ($Z = 1$) makes it possible under these conditions to record amplitudes over a quite large dynamic range (up to $Z \sim 50$) in the limits of the photomultiplier amplitude characteristic linear segment.

Passage of a singly charged particle through the Cherenkov counter is accompanied by considerable scatter of the excited pulse amplitudes. Figure 21a shows typical amplitude spectra, recorded at the PM output with μ-meson passage (the ordinate is the number of pulses recorded in the corresponding channel). The spectrum span (width) determines the detector resolution for recording particles /75

of different charges. In the case of combined operation of four PM into a common output, the width of the overall amplitude spectrum depends significantly on matching all the PM sensitivities. Even with proper initial adjustment of all the PM, in the course of time there will inevitably be drift of the sensitivity of each of them and general detuning of the section.

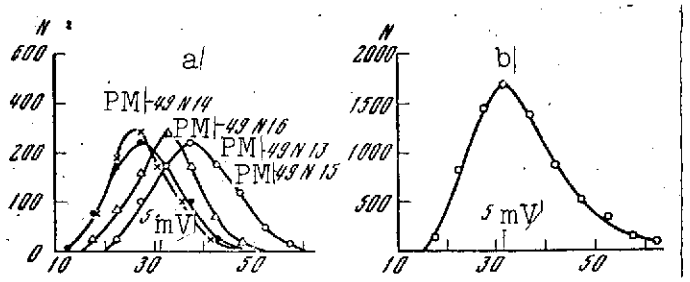

Analyzer channels

Figure 21. Amplitude spectra of μ-meson pulses for four Cherenkov counters of one section prior to their adjustment (a) and form of their combined spectrum after automatic sensitivity adjustment (b)

Therefore, periodic autotuning of section PM sensitivity is necessary. This requirement applies even more to the entire DD detector, which combines 16 Cherenkov counters. A potentiometric system for PM sensitivity autotuning is provided in the DD detector. Four reference light pulse generators (each section is serviced by an individual light generator) are activated twice a day on command from the Earth. The reference light pulses are directed with the aid of flexible lightguides to the PM-49 photochathodes. The intensity of these light flashes is regulated so that for normal PM adjustment they excite on the PM anode pulses with amplitude in the range 200 - 215 mV.

After 20 minutes, the time required for light generator stabilization, the mechanism which rotates the potentiometers regulating PM supply voltage is activated. At the same time, the commutator of this same mechanism connects the output of each of the photomultipliers being tuned in turn to a comparison circuit, in which, on the basis of the reference signal level, a command is generated which controls the mechanism for rotating the corresponding potentiometer. After checking and correcting the sensitivity of all 16 PM, the autotuning system is deactivated. Autotuning of PM sensitivity relative

to one another is accomplished by this system to within ± 5%, which is quite adequate for amplitude spectra matching.

Figure 21b shows the form of the amplitude spectrum recorded from μ-mesons with combined operation of the four Cherenkov counters of a section when PM-49 sensitivity adjustment was accomplished with the indicated degree of accuracy. Prior to autotuning, the amplitude spectra from the same counters had the form shown in Figure 21a. /76

The general form of the amplitude spectrum recorded by four DD sections operating into a common output when using autotuning is shown in Figure 22b, in comparison with the spectrum recorded by a single section (Figure 22a).

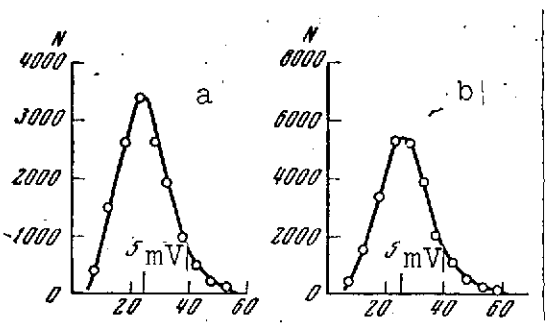

AI-100 channels

Figure 22. μ-meson pulse amplitude spectrum at output of one DD section (a) in comparison with amplitude spectrum obtained from combined output of 16 Cherenkov counters with sensitivity autotuning (b)

The amplitudes of the Cherenkov counter pulses coming from each section are summed after preamplification in a common circuit, and are then discriminated by six threshold devices, tune to levels corresponding to passage of particles with charges $Z_2 \geqslant 2, Z_3 \geqslant 6, Z_4 \geqslant 10, Z_5 \geqslant 20, Z_6 \geqslant 30, Z_7 \geqslant 50$. Triggering of the discriminator Z_i simultaneously with the appearance of pulses from two scintillation counters indicates passage within the limits of the solid angle of a particle section with charge $\geq Z_i$. In this case, the DD electronic unit generates a triple coincidence signal $c_2 Z_i$. The count rates of these signals are recorded by the corresponding telemetry channels, and these data contain information on cosmic radiation charge composition in the energy interval 10^9 - 10^{10} eV/nuc.

More precise amplitude measurements of the DD pulses are accomplished with the aid of the amplitude analyzers described above.

Here, use is made of two analyzers, which permit measurement over a wide range: measurement of charges up to Z ∿ 7 is accomplished with the aid of the first (sensitive) analyzer, the second expands the measurement range to Z ∿ 50. Figure 23 shows the corresponding amplitude-number characteristics of these analyzers (the abscissa is the voltage pulse amplitude, referred to the PM-49 anode). Measurement of the amplitudes in these analyzers is accomplished only on the corresponding command from the IK-15 logic unit. Generation of this command is associated with passage of a particle of sufficiently high energy in the limits of the solid angle formed by the detector DD and proportional counters PC3 -PC10.

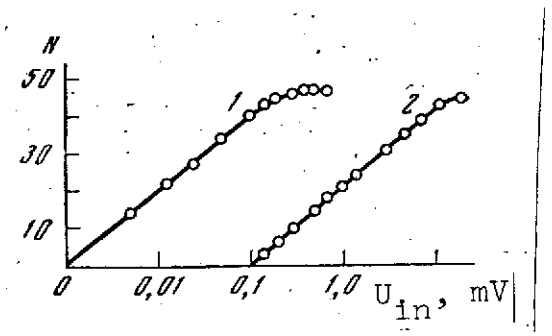

Figure 23. Amplitude-number characteristics of DD1 charge detector pulse recording system:

1 — sensitive channel; 2 — "coarse" channel

The detector DD also participates in generation of this command. /77 A signal τ indicating coincidence of the pulses from the counters PC3 (or PC4), PC5 (or PC6), PC7 - PC10 enters the DD electronic unit. A corresponding signal $z_0\tau$, indicating coincidence of the pulse τ with the pulse $c_2 z_0$, is generated in the DD electronic circuits. The signal $z_0\tau$ indicates passage of a particle in the solid angle noted above.

Another auxiliary signal, which is required for joint operation of the DD with the ionization calorimeter, is generated in the DD electronic circuits in the case of single singly charged particle (proton) passage through the instrument. This signal z_1, together

with the signal τ, forms the coincidence signal $z_1\tau$, indicating proton passage through the IK-14 in the limits of the specified solid angle.

4. Targets

Each of the "thick" targets (graphite and polyethylene), located below the charge detector DD1, is made structurally in the form of two halves located opposite one another (Figure 24). Filter alternation is accomplished by sequential displacement of these halves in the direction of the system operating window or beyond the limits of this window. Each half is mounted in an individual box of identical construction for both halves. The more dense carbon target is distributed uniformly in the box in three separate layers (Figure 25). The polyethylene target fills the entire box volume in five layers (Figure 26).

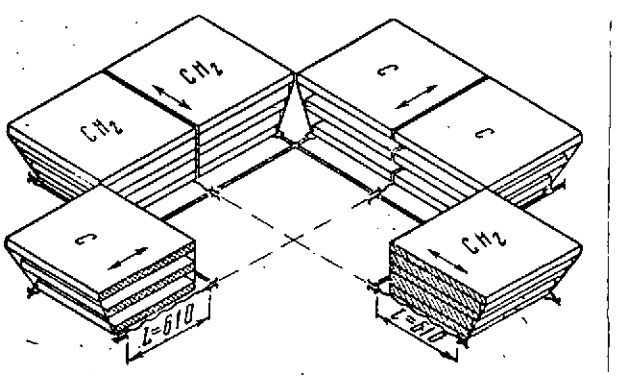

Figure 24. Relative positioning of target blocks and direction of their displacement

The total thickness of the carbon target is 22.3 g/cm^2, that of the polyethylene target is 26 g/cm^2. The excess of polyethylene target matter in comparison with /79 the carbon target amounts to 3.7 g/cm^2, and is due to the hydrogen atoms.

Alternation of the carbon and polyethylene targets is accomplished twice a day on command from the Earth. The basic configuration is that when all the targets are withdrawn beyond the limits of the system working aperture. In the next stage, the polyethylene /80 target is inserted. Then it is replaced by the carbon target. Then measurements are again conducted with the targets removed.

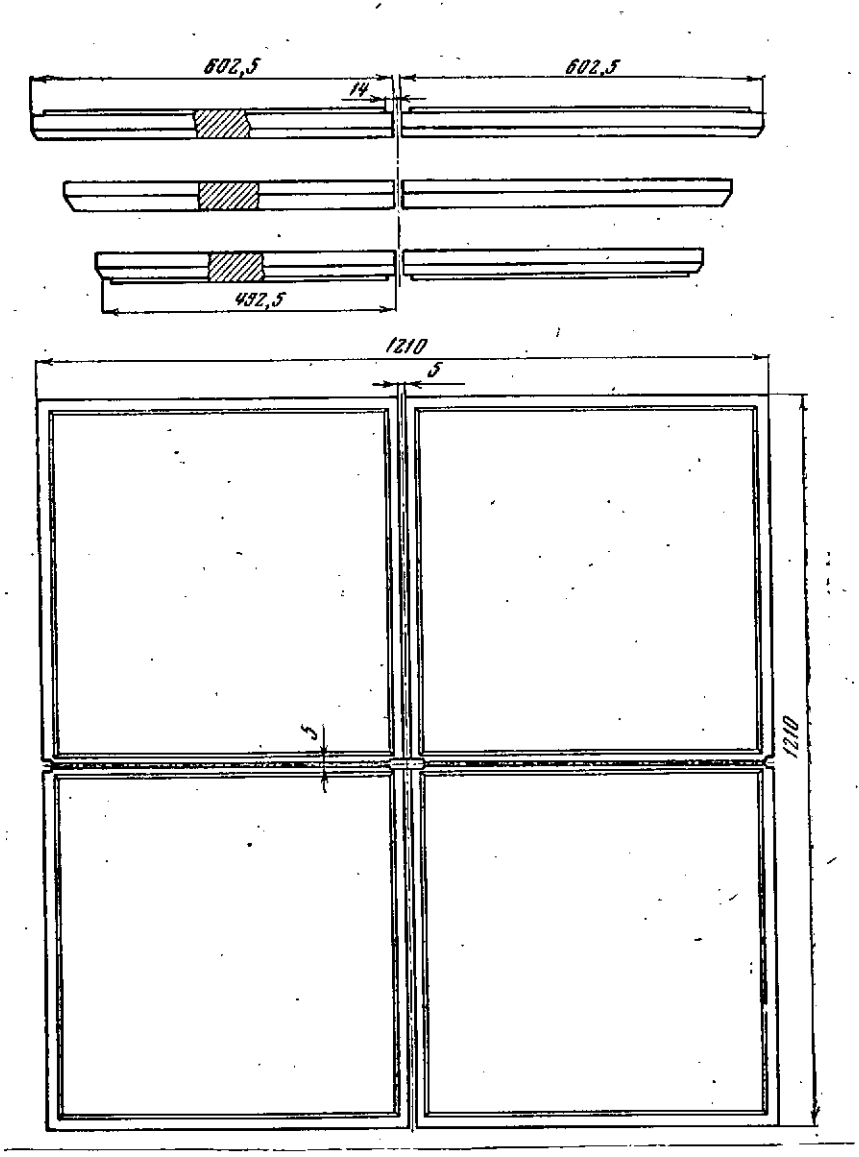

Figure 25. Cross section of carbon target

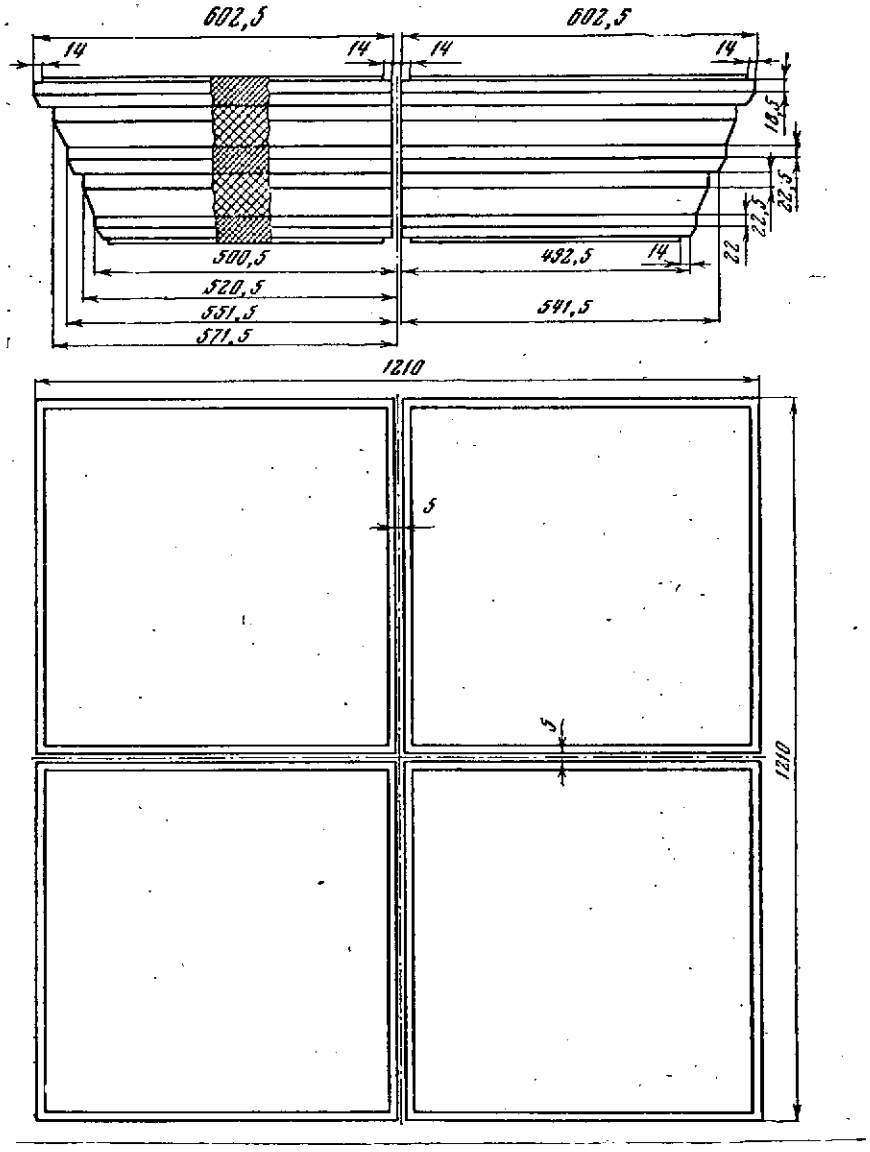

Figure 26. Cross section of polyethylene target

The thin divided carbon targets are stationary. They are used with the detector DD2 activated. Here, there are in all four carbon layers, each 2.26 g/cm^2 thick.

5. Interaction Detectors

The two-layer proportional counter PC3, located beneath the "thick" target, makes it possible, on the basis of the ionization effect created in this counter, to discriminate cases of single singly charged particle (proton) transit without interaction in the target from cases of inelastic interaction with formation in the target of a shower of several secondary charged particles. In the first case, the amplitude of the pulse from PC3 lies in the limits of the "window" between the first and second amplitude discriminator thresholds. In the second case, the amplitude of the output signal goes beyond the limit of the "window", which serves as an indication of interaction.

If charged particles do not arise in a nuclear interaction but only π^0-mesons occur, then such interactions can be recorded on the basis of the ionization effect in the proportional counter PC4 as a result of electron-photon avalanche development in the lead filter located above this counter. Therefore, simultaneous presence of pulses from counters PC3 and PC4, with amplitudes in the limits of the "window", can serve as an indication of absence of interaction in the target. The IK-15 electronic unit identifies such cases specifically, and generates on the basis of pulses from PC3 and PC4 a special signal N_1, indicating absence of interaction in the target with passage of a single singly charged particle. We can also estimate the magnitude of the ionization effect in counters PC3 and PC4 from the indications of the corresponding amplitude analyzers.

The proportional counters located between the thin divided targets act as interaction detectors. A special signal analogous to N_1 is not generated for these counters; we can evaluate the absence or

presence of interaction here by the indications of the corresponding amplitude analyzers.

6. Auxiliary Radiation Detectors

Passage of a primary particle through the ionization calorimeter may be accomplished by the appearance of secondary particles, which are scattered in the reverse direction. These particles may strike the corresponding detectors and distort the proton spectrum shape. In order to study such phenomena, evaluate their probability, and clarify their role in the measurements, in the upper part of the IK-15 instrument on the DD1 side there are located shower indicators, as /81 which we use the four lower scintillation counters, forming part of DD1 and connected in pairs in the double coincidence scheme C_iC_j. Coincidence of the pulses C_i and C_j, arriving simultaneously from several counters at the moment of recorded particle passage through DD1 and the ionization calorimeter, indicates passage through the detectors of several shower particles. The counters PC2 (when DD1 is working) and PC11 (when DD2 is working) serve to determine the number of such particles.

The auxiliary proportional counters PC5 and PC6, mounted in the central part of the ionization calorimeter, participate together with the other detectors in the selection of those primary particles which pass through one of the charge detectors DD and the ionization calorimeter. The counters are adjusted so that their output threshold devices trigger only with passage through the counter of more than ten shower particles.

7. Measurement Principle and Electronic Recorder

Two measurement techniques form the basis of particle recording in the IK-15 spectrometer. The first consists in selection of recorded events of a quite narrow class (for example, protons with energy $\geq E_i$) with subsequent measurement of the rate of occurrence

of the identified events. The second technique involves individual measurements of the amplitudes of the pulses from the sensors for each recorded case. The first technique is used for recording frequent events, the second is used for quite rare events, when individual telemetry measurements can be made.

The first technique includes recording of global high-energy particle fluxes. In these measurements, only a single detector is used — the ionization calorimeter. The pulses from all the ionization chambers are summed, with respect to amplitude in a common circuit, at the output of which amplitude discrimination of the pulses, based on 10 levels E_i (i = 1 - 10) approximately equally spaced on a logarithmic scale, is accomplished. Measurement of the event recording rate in the channels of these discriminators makes it possible to determine the intensity of particles with energy $\geq E_i$, and establish the shape of the energy spectrum in the interval 10^{11} - 10^{16} eV.

Recording of the cosmic radiation proton component is a measurement of the same type. On the basis of the signals $z_1\tau$, arriving from the charge detector DD1, we identify protons which do not experience interaction in the target (signal N_1) and pass in the limits of the calorimeter solid angle with energy release $\geq E_i$. The required particle selection is accomplished on the basis of coincidence of the signals $z_1\tau$, N_1, E_i. Recording of the events as a function of the channels selecting these coincidences makes it possible to determine /82 the proton energy spectrum and measure their effective interaction section with carbon and hydrogen nuclei by comparing the fluxes recorded in the presence or absence of the targets.

Measurements of this same type are associated with particle separation on the basis of charges $\geq z_i$ in the detectors DD1 and DD2, with subsequent recording of the c_2z_i event occurrence rate.

Let us turn to measurements of the second type. Individual measurements in the global flux are made only in relation to the overall energy release in the ionization calorimeter for quite rare particles with energy release $\geqq 10^{14}$ eV. In the case of such energy release amplitude, analysis is performed of the signals coming from the output circuit which sums the pulses from all the ionization chambers. The amplitude analyzer intended for this purpose has an amplitude range of more than 10^3.

For particles $z_0\tau$, recorded in the limits of the solid angle, individual recording is performed with amplitude analysis of all the detectors DD, PC, IK (except for PC5, PC6), beginning with energy release in the ionization calorimeter $E_0 \gtrsim 10^{13}$ eV. In the case of coincidence of the signals $z_0\tau$ and E_0, a command M is generated which permits passage and analysis of the pulses in the amplitude analyzers of all the detectors. On this same command, measurement is performed in a special analyzer of the overall energy release in the calorimeter, and the presence of signals from the shower indicators DD1 is noted, i.e., recording is performed of the coincidence pulses MC_iC_j, where C_j, C_i are the signals from the corresponding pair of scintillators DD1 ($i, j = 1 - 4$).

For individual recording of particles in the lower energy interval (with energy release $\geqq 10^{12}$ eV), selective recording of the events is performed by dividing the frequency of their recording in the ratio 1 : 43. For the events selected in this fashion, a command MB is generated which permits amplitude measurements in the channels of all the detectors.

Generation of all the indicated control and recording signals is accomplished in the IK-15 electronic recorder, containing 21 blocks. The transformer circuits which supply the amplifiers and high-voltage transformers of the ionization chamber and proportional counter

components are concentrated in a special block. Distribution of the power from the onboard source to all the IK-15 electronic blocks is accomplished in the other block. Reception and execution of the commands for turning on and off the equipment, and turning on and off the reference generators, are also accomplished here. The circuits for automatic control of filter motion, activated on command from the Earth, are concentrated in four separate blocks.

A special commutator is supplied for reception and execution of commands for changing the IK-15 operating regime. Activation of both detectors DD1 and DD2, or operation of only one of them together with the ionization calorimeter, is possible on commands transmitted from /83
the Earth. Deactivation of the detectors DD1 and DD2 and autonomous operation of the ionization calorimeter to record the particle energy spectrum in the global flux is also possible.

II. High-Energy Electron Spectrometer (SEZ-12)

In the primary cosmic radiation composition, the high-energy electron flux is very small, and amounts to $\sim 10^{-2}$ of the overall particle flux. Nevertheless, study of the electron component is of considerable interest, particularly in connection with the question of origin of this component. Measurement of high-energy electron intensity in cosmic space and determination of their energy spectrum can provide essential information in this regard.

The question of intensity of electrons with energies above 10^7 eV in near-Earth cosmic space at altitudes of 10^2 - 10^3 km has become of particular interest in recent years in connection with experiments to study the electron flux undertaken aboard the Proton 1 and 2 AES [20]. The results obtained in these experiments permitted making certain assumptions on high-energy electron behavior in near-Earth space. Therefore, it is important to verify and refine these data in subsequent experiments.

The basic difficulty in studying the primary cosmic ray electron component lies in the smallness of the electron flux and the procedural complexity of identifying the electrons on the background of the dominating relativistic proton flux.

The SEZ-12 instrument, designed for discrimination and measurement of electron intensity and energy spectrum, was installed aboard the Proton 4 space station. It is an improved version of the instrument used earlier aboard the Proton 1 and 2 AES. /84

Instrument schematic. The instrument contains the following basic elements (Figure 27).

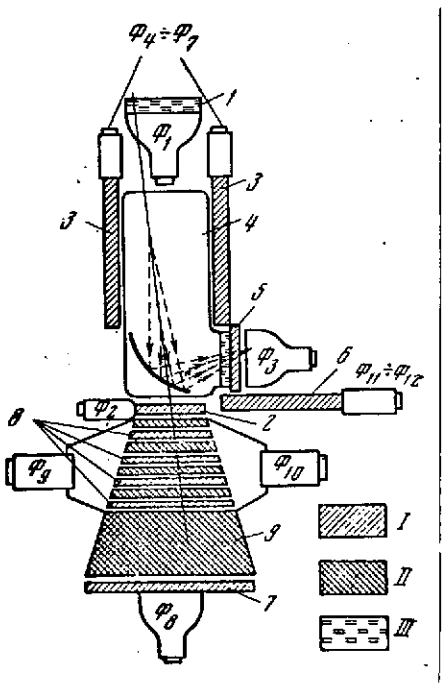

Figure 27. Schematic of SEZ-12 high-energy electron spectrometer:

$\Phi_1 - \Phi_{12}$ — photoelectron multipliers; I — plastic scintillator; II — lead; III — plexiglass

1. Cherenkov counter with plexiglass radiator 1 (PCC), which is the upper counter of the telescope. Amplitude selection of the pulse from the output of this detector, accomplished wtih the aid of the differential window AB, makes it possible to discriminate single singly charged relativistic particles arriving from the upper hemisphere in the telescope solid angle. The integral threshold unit B monitors detector operation.

2. Scintillation counter 2, which is the lower control (LC) counter of the telescope. All the pulses from the output of this counter, with amplitude exceeding the threshold A and corresponding to fast charged particle passage through the scintillator, are recorded.

3. Gas Cherenkov counter 4 (GCC) with additional scintillator 5 ahead of the PM photocathode. The differential amplitude analyzer at the counter output separates the amplitude interval (AB) associated with singly charged particle passage through the Cherenkov counter, and discriminates cases of charged particle passage through the scintillator 5. The integral discriminators A and B are also used to monitor counter operation.

4. Scintillation counter in cylindrical form 3, which protects the GCC against the background of charged particles traveling outside the telescope aperture by anticoincidence selection (ACC).

5. Scintillation counter 6 (ACP) which protects the GCC against the background of charged particles traveling downward by anticoincidence selection.

6. Particle energy detector 8 (ED), which is a scintillation variant of the ionization calorimeter. The amplitudes of the pulses from the ED output are proportional to the electron energies. The integral thresholds E_1 - E_5 correspond to the following approximate electron energy values:

$$E_1 = 155 \text{ MeV}; \quad E_2 = 525 \text{ MeV}; \quad E_3 = 2.0 \text{ GeV};$$
$$E_4 = 9.0 \text{ GeV}; \quad E_5 = 76 \text{ GeV}.$$

7. Lead alloy filter 9 for absorbing the electron-photon showers formed by electrons in the energy detector.

8. Scintillation counter 7 — "marker" (O) — which records particles passing through the filter.

Separation of the electrons from the charged particle flux is accomplished as follows. Separation of the single singly charged particles — electrons and protons — from the multiple charged nuclei takes place in the plexiglass Cherenkov counter. Further /85

separation of the electrons from the protons takes place in the gas Cherenkov counter as a result of the difference in the Cherenkov radiation onset thresholds ($\sim$ 6 MeV for electrons, and $\sim$ 10 GeV for protons). Protons with energies exceeding the threshold value are recorded by the "marker" directly or on the basis of the products of nuclear interaction in the matter of the energy detector and filter, while electrons of not too high energies form in the energy detector and filter electron-proton showers which are absorbed in the matter and do not yield signals in the "marker".

In comparison with preceding SEZ-12 instrument variants, the following changes and additions were introduced into the construction of the instrument installed aboard the Proton 4 station.

1. In place of the scintillation counter used previously as the "upper control" detector of the telescope, we used a Cherenkov counter with plexiglass radiator. The radiator had the form of a disk 155 mm in diameter and 30 mm thick. The geometric factor of the telescope, just as that of the instrument installed aboard the Proton 2 station, was 2.4 $cm^2 \cdot sr$. All the radiator surfaces, other than the upper end, were polished, while the upper end was unpolished and coated with black paint to improve particle recording directivity. Installation on the instrument of this Cherenkov counter, together with the gas Cherenkov counter, leads to considerable reduction of the probability of the instrument recording upward traveling particles. In addition, when using the plexiglass Cherenkov counter as the upper control detector of the telescope, there is reduced background loading by low-energy radiation, since it records electrons with energy $\geq 10^5$ eV and protons with energy $\geq 10^8$ eV.

2. A plastic scintillator plate, made in the form of a disk with diameter 155 mm, equal to the diameter of the PM photocathode, and thickness 10 mm, was mounted ahead of the gas Cherenkov counter PM photocathode. With the aid of this scintillator, it is possible to identify cases of PM triggering from particles traveling outside the telescope solid angle and causing Cherenkov radiation in the

plexiglass window of the GCC ahead of the PM and in the front glass of the PM tube. In passing through the scintillator, these particles will create at the PM output, signals far exceeding in amplitude the pulses associated with Cherenkov radiation in the gas. Amplitude selection of the signals from the GCC with the aid of the differential "window" AB, whose upper threshold corresponds to scintillation recording, permits excluding these background triggering cases.

3. A plastic scintillator plate (ASP), with dimensions 500 × 500 × 30 mm^3, was located below the gas Cherenkov counter PM. The ASP signals are recorded by two PM-16, installed in optical contact with the scintillator. In order to reduce light losses, the scintillator surface is polished, and the interior of its enclosure is coated /87 with white light-reflecting paint. The two PM installed on the plate were sufficient for recording particles passing through any point of the plate. The ASP signals were connected in anticoincidence with the telescope pulses, which protects the GCC PM from triggerings caused by background particles traveling outside the instrument solid angle. A general view of the instrument is shown in Figure 28.

4. Analysis of results of measurements made aboard the Proton 1 and 2 AES showed the advisability of introducing certain changes into the logic of the instrument electronic circuit operation. For example, information on detector loading was necessary, in order to establish stability of individual detector operation and the operating regimes of the related electrical devices. In addition, recording of the count rates of the coincidences and anticoincidences of the detector signals in various combinations was necessary for determining the role of random coincidences of this sort.

Recorder. Figure 29 shows a block diagram of the electronic logic circuits associated with the detectors and selection of the required coincidences (CC is a coincidence circuit) and anticoincidences (CA is an anticoincidence circuit). The arrows indicate parameters going to the telemetry system. These parameters have the following content.

I. Measurement of individual detector loading:

PCC (AB) — count of PCC pulses in differential window (AB);

PCC (B) — count of PCC pulses above integral threshold B;

LC — count of LC pulses above integral threshold A;

GCC (A) — count of GCC pulses above integral threshold A;

GCC (B) — count of pulses above integral threshold B;

ASP — count of ASP pulses above integral threshold A;

O — count of O pulses above integral threshold A;

E_1 — count of ED pulses above integral threshold E_1;

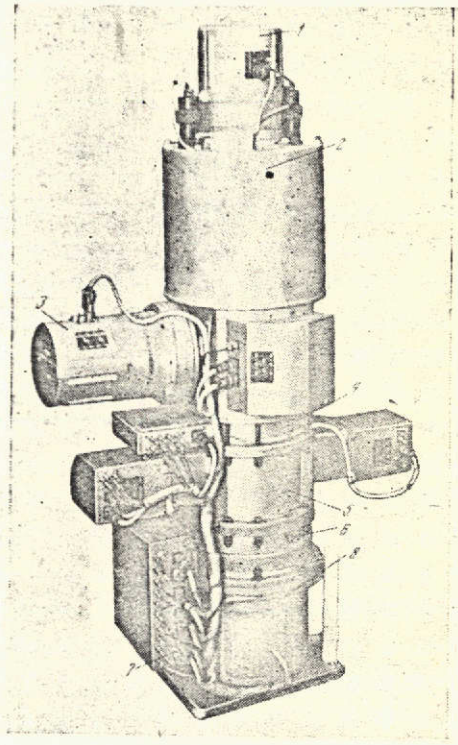

Figure 28. SEZ-12 instrument:

1 — telescope "upper control" counter; 2 — anticoincidence cylinder; 3 — GCC PM; 4 — telescope "lower control" counter; 5 — energy detector; 6 — lead alloy filter; 7 — one instrument electronic block; 8 — "marker" counter

E_2 — count of ED pulses above integral threshold E_2.

Hereafter, we use the following notations for coincidences and anticoincidences:

AB — coincidence of signals A and B;

$A\bar{B}$ — anticoincidence of signals A and B (B is the inhibiting pulse).

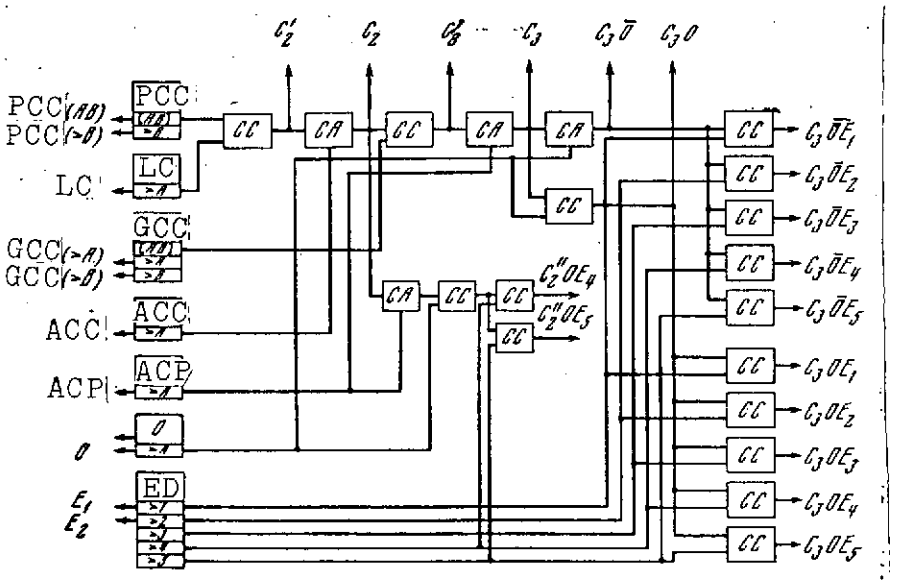

Figure 29. Block diagram of SEZ-12 instrument logic electronic circuits

II. Measurement of loads in coincidence and anticoincidence channels.

$C_2' = PCC\ (AB) \cdot LC;$

$C_2 = C_2' \cdot \overline{ACC};$

$C_3' = C_2 \cdot GCC\ (AB);$

$C_3 = C_3'\ ACP;$

$C_3\overline{O};$

$C_3O;$

$C_3\overline{OE}_i\ (i = 1 - 5);$

$C_3OE_i\ (i = 1 - 5);$

$C_2''OE_e = C_2 \cdot \overline{ACP} \cdot O \cdot E_e\ (e = 4, 5).$

The basic parameter characterizing recording of electrons is the parameter $C_3\overline{OE}_i$. The remaining events play a secondary role and serve as a check of instrument operation and the measurement conditions: detector loading, detector stability, influence of ramdom coincidences, and so on. /88

The total number of parameters telemetered is 28. Some monitor parameters with relatively low count rates were recorded together on a single telemetry channel.

Preliminary adjustment of the instrument involves selection of the electronic circuit (discriminator) component tirggering thresholds and the operating regimes of all the PM. The values of the threshold magnitudes were determined approximately as a result of studies on models of the instrument detectors. They were selected so that the signal at the PM anode, appearing as a result of particle passage through the detector, triggered the discriminator with an acceptable voltage on the PM. The individual components and detectors of the instrument were initially adjusted individually, and then conbimed adjustment of all the components was performed. The components and instrument as a whole were subjected to climatic and vibration tests. During these tests, the operating regimes of the PM and the discriminator thresholds were varied in the allowable limits.

The operation of the instrument as a whole was checked on the basis of cosmic ray μ-meson count rate at sea level.

The value of the instrument geometric factor $\Gamma = 2.4 \pm 0.1$ cm^2 · sr was determined from the μ-meson count rate and by calculation. The effectiveness of singly charged particle recording by the telescope was determined from measurement in μ-meson flux, and was found to be $\varepsilon = 0.43 \pm 0.1$.

The overall instrument weight is 185 kg, overall dimensions are $1500 \times 880 \times 460$ mm^3, power supply required is 9 W.

III. Spectrometer for Particles with Fractional Electrical Charge (SEZ-13)

In 1964, Gell-Man and Schweig [26] advanced the hypothesis on existence of three types of fundamental particles ("quarks") which have unusual properties: their electrical charge is less than that of electrons. With the aid of these fundamental particles, we can construct the entire spectrum of the presently known strongly interacting "elementary" particles, and indicate their basic properties.

Attempts have been made in the course of several years to detect quarks in accelerator experiments. These experiments have yielded negative results. It is possible that the quark mass is such that the proton energy which can be obtained on accelerators is not sufficient for generation of a pair of quarks, or that the section for generation of these particles is very small. The search for quarks /89
in cosmic rays was also initiated. Several experiments were conducted at sea level and at mountain elevations to detect quarks and evaluate their possible flux.

The detection of quarks in cosmic rays at sea level and on mountain tops by electronic equipment may be complicated significantly by the shower-type accompaniment of high-energy particles. Quarks can also arise in collisions of high-energy cosmic ray particles with atoms of the interstellar medium. In this case, during their travel in the Galaxy, they will cover such great distances that the secondary particles which arise simultaneously with the quarks will separate to distances which exclude simultaneous entry into the instrument of two or more particles. Also possible is the existence in cosmic space of relict quarks, which are most likely to be detected beyond the limits of the atmosphere. This source of quarks may be more significant than their generation in the atmosphere. For these reasons, the search for quarks in primary cosmic rays was carried out for the first time aboard the Proton 3 cosmic station [22, 23].

The wide relative aperture SEZ-13 instrument was developed for this purpose. The primary cosmic ray particle charge is measured in the SEZ-13 instrument. Proportional counters, in which the electrical pulse is proportional to the square of the charge of a relativistic particle passing through the counter, are used to measure the charge. The charge measurement is accomplished simultaneously by 12 proportional counters, in order to reduce the probability of imitation of a particle with charge e/3 and 2e/3 by particles with charge equal to one (as a result of fluctuations of the ionization losses of charged particle energy and the gas amplification factor in the proportional counter, and also as a result of difference of the particle trajectories in the counter).

A general view of the instrument is shown in Figure 30. The proportional counters of area 0.45 m^2 each form a "telescope" with geometric factor $\Gamma = 3000$ $cm^2 \cdot sr$. The total amount of matter for a particle passing through in the solid angle amounts to 11.5 g/cm^2.

The instrument operated aboard the Proton 3 station for 1500 hours. As a result of the analyzed information, an estimate was made of the upper limit of the possible flux of quarks with charge 1/3 e $\sim 2.5 \cdot 10^{-9}$ $cm^{-2} \cdot sec^{-1} \cdot sr^{-1}$, and with charge 2/3 e $\sim 2.5 \cdot 10^{-8}$ $cm^{-2} \cdot sec^{-1} \cdot sr^{-1}$ [27, 28, 29].

An estimate was also made of the upper limit of the effective cross section for quark generation during interaction with the interstellar gas nuclei of cosmic ray particles with energy $\geq 10^{11}$ eV: σ (1/3 e) $\leq 1.4 \cdot 10^{-30}$ cm^2, if the charge is equal to e/3, and σ (2/3 e) $\leq 1.4 \cdot 10^{-29}$ cm^2, if the charge is equal to 2/3 e [27, 28, 29].

The measurements made aboard the Proton 3 station showed that for high detector loadings (10^4 imp/sec), there arises a definite number of cases when the telemetry indications do not relate to a single particle. Impulses above the specified threshold are sometimes observed in the recording channels; zero pulse amplitude values are sometimes observed in the proportional counters. An advanced SEZ-13 instrument was constructed to eliminate these drawbacks, and was installed aboard the Proton 4 cosmic station. /91

Figure 30 shows the arrangement of the proportional counters and electronic units, which are mounted in a special frame. Six dual PC are used in the instrument. The magnitude of the gas gap in each half is 5 cm. Each half is divided into seven sections, with inner electrode in each section made from 0.1+-mm-diameter tungsten filament. The electrodes of each half have common electrical output.

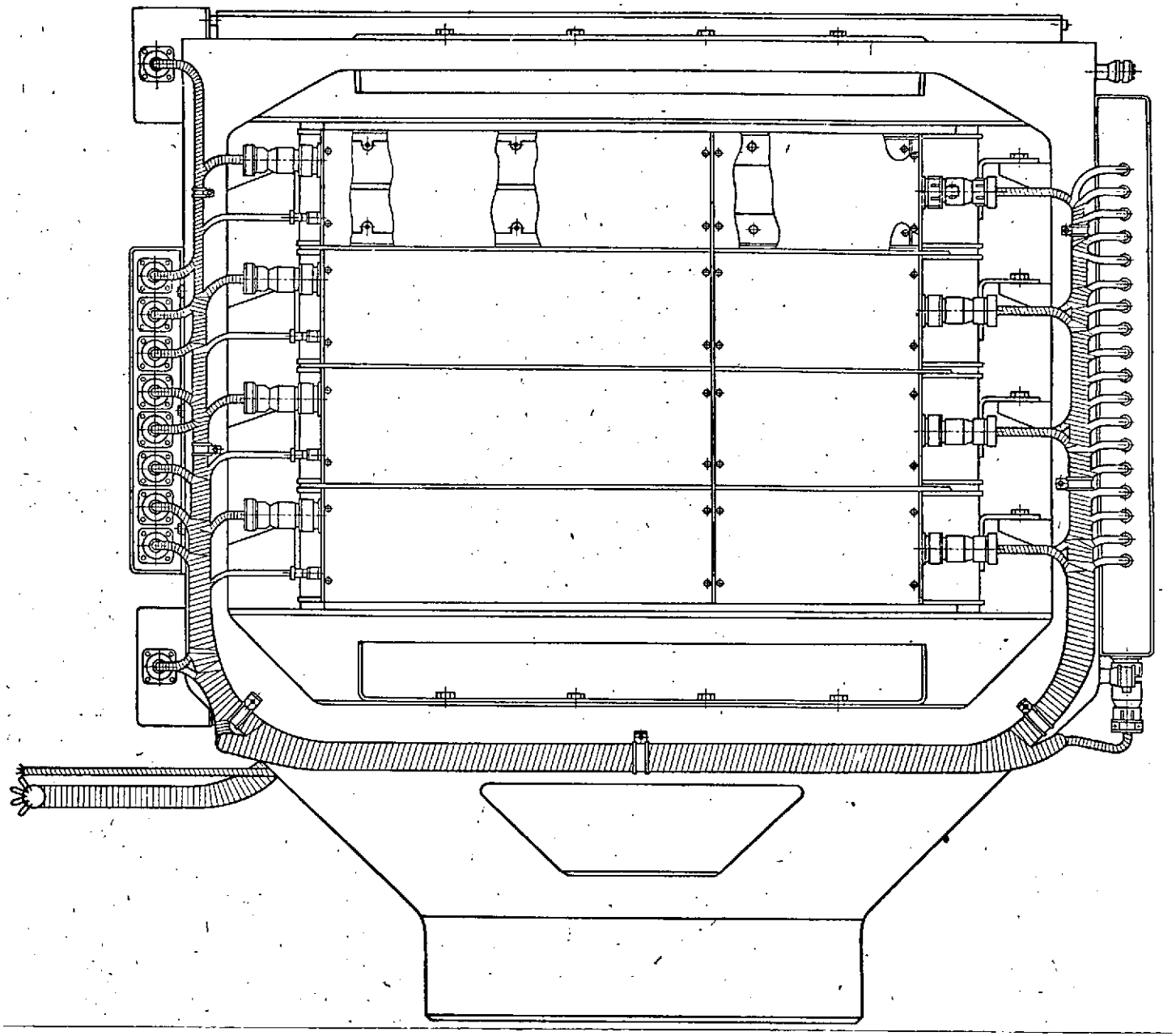

Figure 30. General view of SEZ-13 instrument installed aboard Proton 4 cosmic station

This installation thus consists of 12 independent proportional counters which are functionally combined pairwise by a common structure. The two upper and two lower counters are turned 90° relative to the middle counters, so that the filaments in these counters are positioned at right angles to the filaments in the middle counters, if we view the counters from above. Each counter is filled with argon, with the addition of 10% methane, to a total pressure of 280 mm Hg. The operating voltage on the counter filaments is 1750 V. Under these conditions, a singly charged relativistic particle yields a probable impulse amplitude of about 3000 μV.

The electrical pulses travel from the proportional counters to amplifiers. A block diagram of the electronic recording system is shown in Figure 31. Each PC is equipped with an amplifier with gain 1000. The pulses from the amplifier output travel on command through

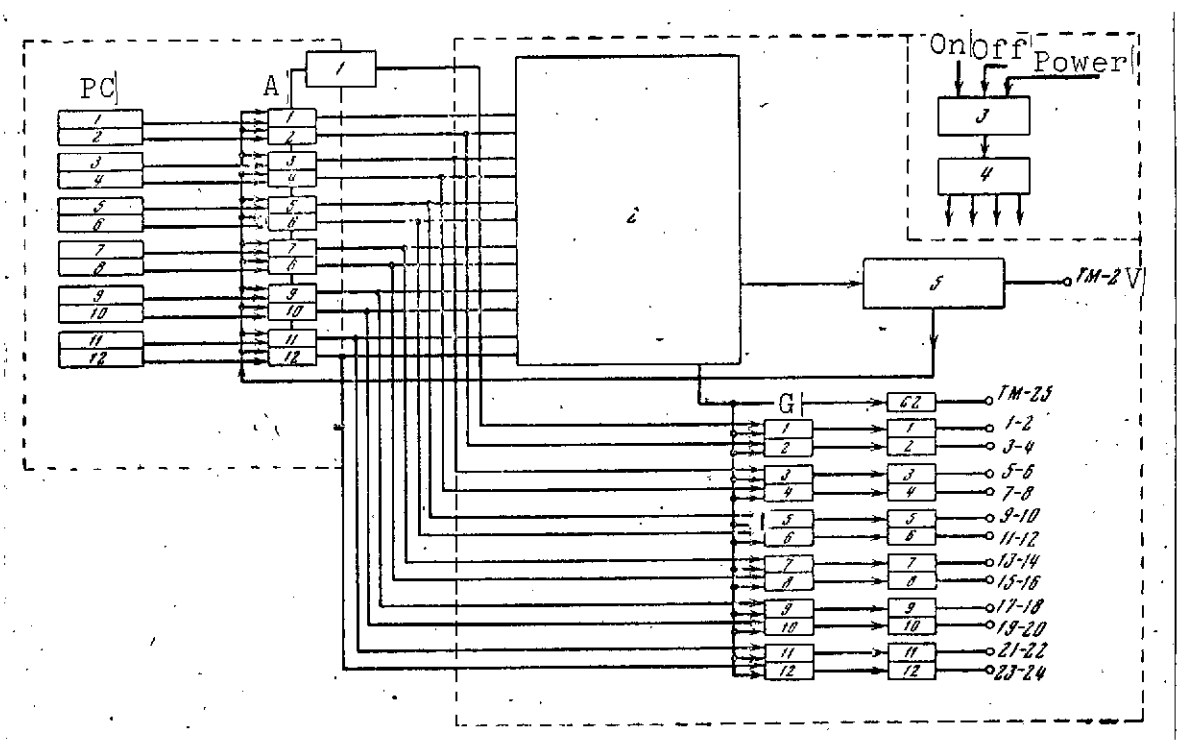

Figure 31. Block diagram of electrical recording system of the SEZ-13 instrument:

1 — summer; 2 — controller; 3 — on-off relay; 4 — voltage transformer; 5 — internal calibration unit

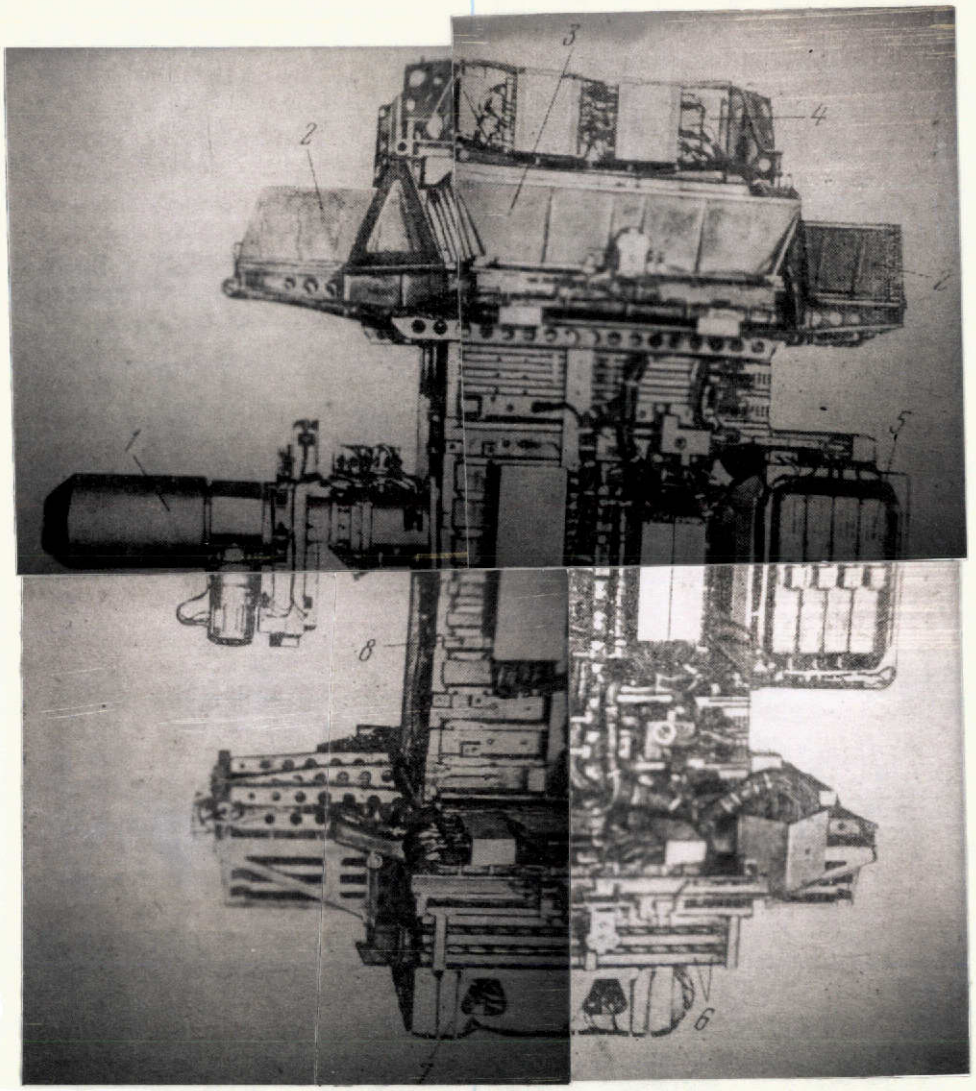

Figure 32. Proton 4 station scientific equipment complex:

1 — instrument for recording electrons (SEZ-12); 2 — graphite target; 3 — polyethylene target; 4 — charge detector (DD1); 5 — instrument for recording quarks (SEZ-13); 6 — thin graphite targets; 7 — charge detector (DD2); 8 — ionization calorimeter (IK-15)

the linear gates G1 - G12 and are measured with respect to amplitude by the amplitude analyzers C2 - 1 to C2 - 12. The pulse amplitude information is directed to the telemetry channels TM1 - TM24.

The control command is generated in the controller by amplitude discrimination of the pulses arriving from the amplifier output. A

command is generated if the pulse amplitudes in all 12 counters correspond to passage of a particle with charge less than one.

In order to calibrate the instrument, the recording command is also generated with passage of singly charged particles (protons) with division of the frequency of these events in the ratio 1 : 2^{19}. In these cases, the amplitudes of the pulses corresponding to a singly charged particle are recorded. Triggering of the calibration pulse, whose amplitude corresponds to particles with charges 1/3 e, 2/3 e, 1 e, takes place with this same average frequency. Additional transmission of a calibration pulse with zero amplitude serves to determine the electronic amplifier self-noise level.

Non-overloading pulse amplifiers, which make it possible to avoid the false triggerings observed in the preceding version of the instrument associated with amplifier overloading, were used in the SEZ-13 instrument installed aboard the Proton 4 station (Figure 32). The circuits for amplitude discrimination selection of the pulses being recorded in the controller were also improved. /92 /93

The general technical data on the instrument are: weight 200 kg, dimensions 1020 × 930 × 920 mm^2, power required 16 W, number of output telemetry channels 26.

References

1. Grigorov, N. L., V. S. Murzin and I. D. Rapoport. ZhETF, Vol. 34, 1958, p. 506.

2. Grigorov, N. L., I. D. Rapoport, I. A. Savenko and G. A. Skuridin. Kosmicheskiye issledovaniya, Vol. 2, No. 5, 1964, p. 724.

3. Volodichev, N. N., N. L. Grigorov, Yu. V. Mineyev, O. B. Kislyakov, V. Ye. Nesterov, I. D. Rapoport, I. A. Savenko, A. V. Smirnov and B. M. Yakovlev. Kosmicheskiye issledovaniya, Vol. 5, No. 1, 1967, p. 119.

4. Volodichev, N. N., N. L. Grigorov and I. A. Savenko. Kosmicheskiye issledovaniya, Vol. 5, No. 3, 1967, p. 431.

5. Grigorov, N. L., V. Ye. Nesterov, I. D. Rapoport, I. A. Savenko and G. A. Skuridin. Investigation into High-Energy and Ultra High-Energy Particles and the Electron-Photon Component of Primary Cosmic Rays Aboard Proton-1 Satellite. Report at the 9th International Conference on Cosmic Rays, London, September, 1965. Preprint, Moscow, NIIYaF, Moscow State University, 1965.

6. Grigorov, N. L., V. Ye. Nesterov, I. D. Rapoport, I. A. Savenko and G. A. Skuridin. Investigation of Primary Cosmic Rays Aboard the Proton-1 Scientific Station. Report at 11th International Astronautics Congress, Athens, 1965.

7. Grigorov, N. L., V. Ye. Nesterov, I. D. Rapoport, I. A. Savenko, G. A. Skuridin and A. F. Titenkov. Kosmicheskiye issledovaniya, Vol. 5, No. 3, 1967, p. 395.

8. Grigorov, N. L., V. Ye Nesterov, I. D. Rapoport, I. A. Savenko and G. A. Skuridin. Report at 10th International Conference on Cosmic Rays, Canada, June, 1967. Preprint, Moscow, NIIYaF, Moscow State University, 1967.

9. Grigorov, N. L., V. Ye. Nesterov, I. E. Rapoport, I. A. Savenko, G. A. Skuridin and A. F. Titenkov. Izvestiya AN SSSR, seriya fiz., Vol. 31, No. 8, 1967.

10. Volodichev, N. N., N. L. Grigorov, V. Ye. Nesterov, I. D. Rapoport, I. A. Savenko, G. A. Skuridin and A. F. Titenkov. Izucheniye chastits kosmicheskikh luchey vysokoy i sverkhvysokoy energii i khimicheskogo sostava v oblasti ochen' tyzahelykh yader na nauchnykh kosmicheskikh stantsiyakh "Proton-1" i "Proton'2" (Study of High and Superhigh-Energy Cosmic Ray Particles and Chemical Composition in the Very Heavy Nuclei Region Aboard the Proton 1 and 2 Cosmic Stations). Report at All-Union Conference on Cosmic Rays, Alma Ata, October, 1966. Preprint, Moscow, NIIYaF, Moscow State University, 1966.

11. Akimov, V. V., N. L. Grigorov, V. Ye. Nesterov, I. D. Rapoport, I. A. Savenko, G. A. Skuridin and A.F. Titenkov. Collection: Kosmicheskiye luchi (Cosmic Rays), No. 13. Moscow, Nauka Press, 1972.

12. Grigorov, N. L., V. Ye. Nesterov, I. D. Rapoport, I. A. Savenko and A.F. Titenkov. Trudy vsesoyuznoy konferentsii po kosmicheskim lucham v Tashkente (Proceedings of All-Union Conference on Cosmic Rays at Tashkent), Mosocw, FIAN, 1969.

13. Grigorov, N. L., V. Ye. Nesterov, I. D. Rapoport, I. A. Savenko and G. A. Skuridin. The Study of Energy Spectrum of Primary Cosmic Ray Particles of High and Ultra-High Energies from the "Proton" Series of Satellites. Report at 11th International Conference on Cosmic Rays, Budapest, August, 1969. Preprint, Moscow, NIIYaF, Moscow State University, 1969.

14. Basilova, R. N, N. L. Grigorov, G. P. Kakhidze, O. M. Kovrizhnykh, V. Ye. Nesterov, I. A. Savenko, G. A. Skuridin and A. F. Titenkov. Izvestiya AN SSSR, seriya fiz., Vol. 31, 1966, p. 610.

15. Grigorov, N. L., V. Ye. Nesterov, I. D. Rapoport, I. A. Savenko and G. A. Skuridin. Izvestiya AN SSSR, seriya fiz., Vol. 31, 1967, p. 1450.

16. Grigorov, N. L., V. Ye. Nesterov, I. D. Rapoport, I. A. Savenko and G. A. Skuridin. Kosmicheskiye issledovaniya, Vol. 5, No. 3, 1967, p. 420.

17. Akimov, V. V., N. L. Grigorov, V. N. Nesterov, I. D. Rapoport, I. A. Savenko and G. S. Skuridin. Collection: Kosmicheskiye luchi (Cosmic Rays), No. 13. Moscow, Nauka Press, 1972. /94

18. Akimov, V. V., N. L. Grigorov, V. Ye Nesterov, I. D. Rapoport and I. A. Savenko. Proceedings of All-Union Conference on Cosmic Rays at Tashkent. Moscow, FIAN, 1969.

19. Grigorov, N. L., V. Ye. Nesterov, I. D. Rapoport, I. A. Savenko and G. A. Skuridin. Measurements of Effective Cross Sections of Inelastic Interaction of Protons with Carbon and Hydrogen Nuclei in the 20 - 600 GeV Energy Range Aboard the Proton 1, 2, 3 Satellites. Report at 11th International conference on Cosmic Rays, Budapest, August, 1969. Preprint, Moscow, NIIYaF, Moscow State University, 1969.

20. Grigorov, N. L., Yu. S. Klintsov, B. Ye Nesterov, I. D. Rapoport, I. A. Savenko and B. M. Yakovlev. Izvestiya AN SSSR, seriya fiz., Vol. 31, 1966, p. 1773.

21. Grigorov, N. L., S. I. Voropaev, L. F. Kalinkin, V. A. Labutin and I. A. Savenko. Collection: Kosmicheskiye luchi (Cosmic Rays), No. 13. Moscow, Nauka Press, 1972.

22. Grigorov, N. L., G. P. Kakhidze, I. D. Rapoport and I. A. Savenko. Collection: Kosmicheskiye luchi (Cosmic Rays), No. 13. Moscow, Nauka Press, 1972.

23. Grigorov, N. L., G. P. Kakhidze, I. D. Rapoport and I. A. Savenko. Proceedings of All-Union Conference on Cosmic Rays at Tashkent. Mosocw, FIAN, 1969.

24. Grigorov, N. L., L. F. Kalinkin, V. Ye. Nesterov, Ye. A. Pryakhin, I. A. Savenko, Ye. A. Sysoyev and I. V. Estulin. Kosmicheskiye issledovaniya, Vol. 5, No. 1, 1967, p. 124.

25. Grigorov, N. L., G. P. Kakhidze, V. Ye. Nesterov, I. D. Rapoport, I. A. Savenko, A. V. Smirnov, A. F. Titenkov and P. P. Shishkov. Kosmicheskiye issledovaniya, Vol. 5, No. 3, 1967, p. 383.

26. Gell-Mann, M. Phys. Letters, Vol. 8, 1964, p. 124.

27. Grigorov, N. L., G. P. Kakhidze, I. D. Rapoport and I. A. Savenko. Report at All-Union Conference on Cosmic Ray Physics, Alma Ata, 1966. Collection: Kosmicheskiye luchi (Cosmic Rays), No. 11. Moscow, Nauka Press, 1969.

28. Grigorov, N. L., G. P. Kakhidze, I. D. Rapoport and I. A. Savenko. Report at All-Union Conference on Cosmic Ray Physics, Novosibirsk, 1967. Collection: Kosmicheskiye luchi (Cosmic Rays), No. 11. Moscow, Nauka Press, 1972.

29. Grigorov, N. L. ,G. P. Kakhidze, I. D. Rapoport and I. A. Savenko. Report at International Conference on Cosmic Ray Physics, Budapest, 1969. Acta Phys. Acad. Sci. Hung.,, Vol. 29, Suppl. 3, 1970, p. 37.

CALIBRATION OF SEZ-14 INSTRUMENT INSTALLED ABOARD PROTON 1, 2, 3 COSMIC STATIONS ON ITEF [INSTITUTE OF THEORETICAL AND EXPERIMENTAL PHYSICS] SYNCHROTRON

V. V. Akimov, V. S. Borisov, G. V. Veselova, L. L. Gol'din, L. N. Kondrat'yev, V. Ye. Nesterov, I. D. Rapoport, N. G. Ryabova, and G. K. Tumanov

Introduction

The effective inelastic interaction sections of protons with /95
hydrogen nuclei in the energy interval from 10^{10} to 10^{12} eV were measured aboard the Proton 1, 2, 3 AES. The measurements were made by the "beam knock-out" method, using an SEZ-14 instrument [1]. Increase of the section by 20% was recorded with proton energy increase from 10^{10} to 10^{12} eV [2].

In order to determine the possible experimental errors, it is of interest to conduct measurements of the effective inelastic interaction sections of protons with hydrogen nuclei on proton accelerators, using the same instrument and the same technique used aboard the Proton satellites.

The first calibration measurements, whose results are presented below, were made at 5 GeV energy on the ITEF proton synchrotron. The authors intend to carry out analogous measurements on the accelerator at higher energies in the future.

A schematic of the experimental setup is shown in Figure 1. The study was made in the secondary beam of elastically scattered protons. The scattered protons emitted at an angle of 13° to the direction of the internal beam, were focused by two magnetic lenses, analyzed by a SP-12 magnet

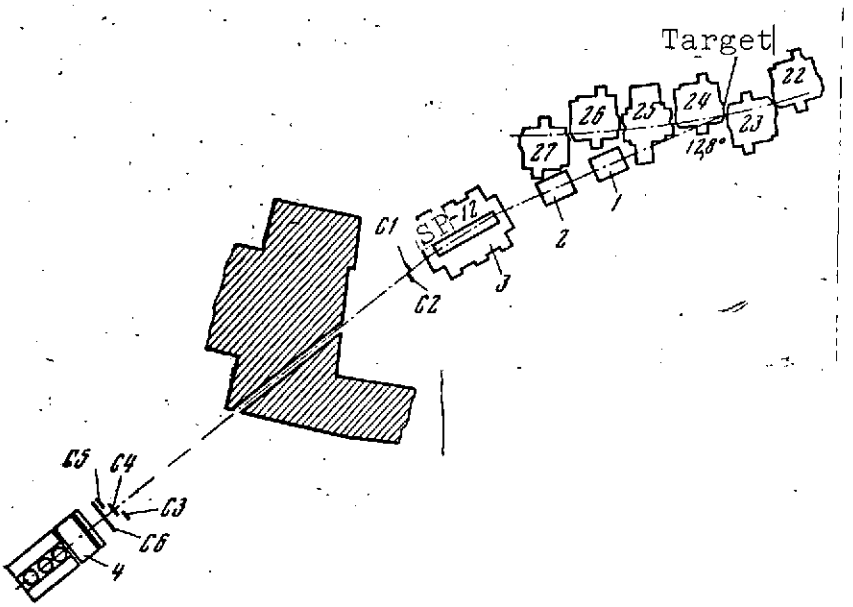

Figure 1. Schematic of experimental setup:
1, 2 — magnetic lenses; 3 — deflecting magnet;
4 — SEZ-14 instrument; C1 - C6 — scintillators of the scintillation telescope

(rotation angle 15°), traveled first to the telescope, consisting of scintillation counters with path length 16.6 meters [3], and then to the SEZ-14 instrument. The combination of signals $(C_1 + C_2) \times (C_3 + C_4 + C_5) \times C_6$ gave the monitor signal M. The scintillation telescope count (M) served as a check during the measurements. All the recorded signals were applied to scalers through gate circuits, which were activated only during that time when the beam was pointed at the target and the primary beam energy had the required value.

The measurements were made with constant proton energy ("plateau" cycle). The duration of particle impact on the target was 150 - 200 msec. The π-meson impurity content in the beam did not exceed 2%.

The SEZ-14 instrument was mounted on a special positioner, with the aid of which the instrument could be positioned at any angle to the proton beam. Measurements were made first of all with the instrument "entry window" facing the beam, i.e., the protons first /96
passed through the proportional counters and then through the targets, interaction detector, calorimeter, and the lower scintillation counter.

Measurement of effective inelastic interaction sections of 5 GeV protons with hydrogen nuclei. For measurement of the effective sections, we used the same signals $Z_1N_1E_{C_1}$ [1, 2] as used in the measurements aboard the Proton satellites, i.e., we identified protons which had not experienced interaction during passage through the graphite target. However, for separating particles which had passed through the scintillation telescope from the background particles, $Z_1N_1E_{C_1}$ were used in coincidence with the scintiallation telescope signal M, i.e., the signals $Z_1N_1E_{C_1}M$ were recorded. Z_1 means that the particle electrical charge recorded by the two proportional counters is equal to one; N_1 means that a single particle with unit charge passes through the interaction detector — the scintillation counter located after the 26.2 g/cm^2-thick graphite target; E_{C_1} means that energy $\geq E_1$ was released in the ionization calorimeter and at least one particle passed through the lower scintillation counter (signal C), which defined the solid angle. In this case, the threshold E_1 corresponded to the energy release of a single relativistic particle. The introduction of coincidences with the scintillation telescope signal M permitted, in addition, exclusion of the influence of random coincidences under condition of high detector background loadings at /97
the time of particle impact on the target.

The basic difficulty in calibrating the SEZ-14 instrument using the accelerator proton beam was the fact that the instrument, designed for studying cosmic rays, was not intended for operation under high loading conditions. However, the introduction of any changes into the instrument was not possible, on the basis of the very essence of the experiment. Therefore, in making the measurements, careful adjustment of particle impact on the internal target was made in order that the impact duration be maximal and no marked changes of particle intensity take place during impact. Moreover, for continuous monitoring of the count loss magnitudes in each instrument detector during the measurement process, the signals Z_1M, N_1M, E_1M, CM were recorded (the count loss magnitude could be evaluated on the basis of the count rate ratio Z_1M/M, N_1M/M, E_1M/M, CM/M).

A special experimental data reduction technique was developed in order to exclude the influence of count losses on the results obtained.

The maximal count losses in the SEZ-14 instrument occurred in the proportional counter (signal Z_1). Even for good measurement seances, the ratio Z_1M/M varied from 0.5 to 0.8. In our case, the effectiveness of formation of the signal Z_1 for a singly charged particle recorded by two proportional counters was 0.8. The number of recorded $Z_1N_1E_{C_1}M$ events was normed by the number of simultaneously recorded events Z_1M, in order to exclude the influence of signal Z_1 count losses on the effective section measurements in the normal position of the instrument. This normalization would be incorrect if there was reverse current in the proportional counter. By reverse current, we mean scattering of particles formed as a result of interaction in the carbon or iron into the aft hemisphere in the laboratory coordinate system. Estimates of the reverse current magnitude [4] make it possible to consider that such reverse current is absent for proton energy 5 GeV. Then it was necessary to make certain that

either in the measurement process count losses of the signals N_1, E_1, C are absent or, if they do occur, they have no influence on the effective section measurement results. To this end, we plotted the dependence of the N_1 signal count losses (ratio N_1M/M) on the Z_1 signal count losses (ratio Z_1M/M). We see from Figure 2 that for $Z_1M/M \geq 0.75$, there are no signal N_1 count losses. Losses of signal E_1 counts do not affect the magnitude of the measured effective section, since they are independent of the filter position (filter insertion does not influence the overall calorimeter loading); the scintillation counter does not experience overloading (Figure 3). Therefore, we

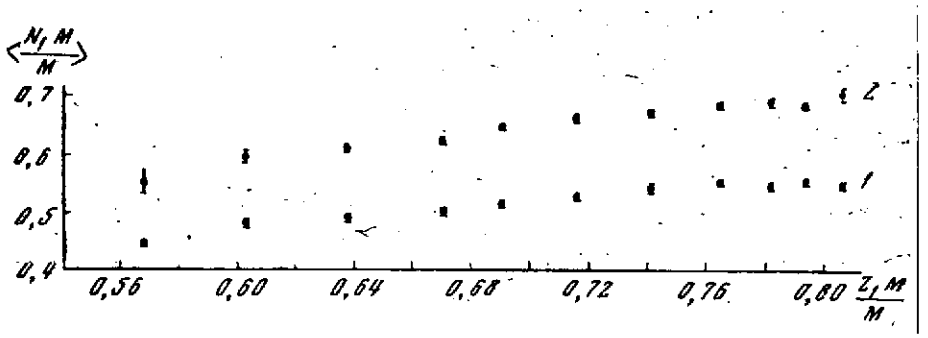

Figure 2. $\langle N_1M/M \rangle$ as a function of $\langle Z_1M/M \rangle$:

1 — with filter; 2 — without filter

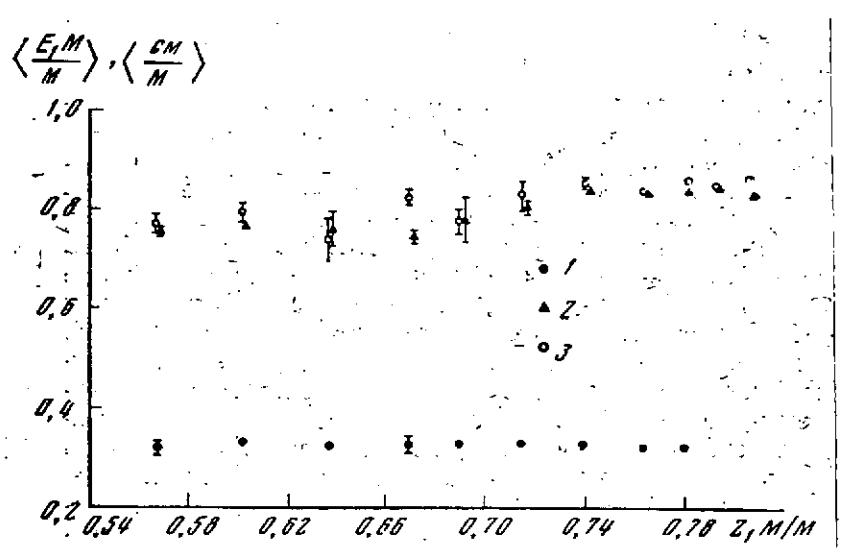

Figure 3. $\langle E_1M/M \rangle$ and $\langle CM/M \rangle$ as a function of $\langle Z_1M/M \rangle$:

1 — $\langle E_1M/M \rangle$ with filter; 2 — $\langle E_1M/M \rangle$ without
3 — $\langle CM/M \rangle$ without filter

selected, first of all, those series of readings when $Z_1M/M \geq 0.75$. For the selected series, we calculated the mean values of $I = Z_1N_1E_{C_1}M/Z_1M$ separately for measurements without target I_0 and with graphite target I_C. The ratio of these quantities was $I_0/I_C =$ /99
1.298 ± 0.014. For a considerable part of the measurements, $Z_1M/M <$ 0.75. In the analysis, it was found that if the measurements are sorted on the basis of the magnitude of the signal Z_1 counting losses (the entire range of Z_1M/M variation was broken down into 11 intervals), then the percentage signal N_1 counting losses in each of the selected intervals is the same for measurements without target and with the graphite target (Figure 4). Therefore, with this data sampling, signal count losses have no effect on the magnitude of the ratio I_0/I_C and, consequently, no influence on the magnitude of the measured effective section. This made it possible to average the quantities I_0 and I_C separately for each of the 11 intervals shown in Figure 4, and calculate their ratio I_0/I_c.

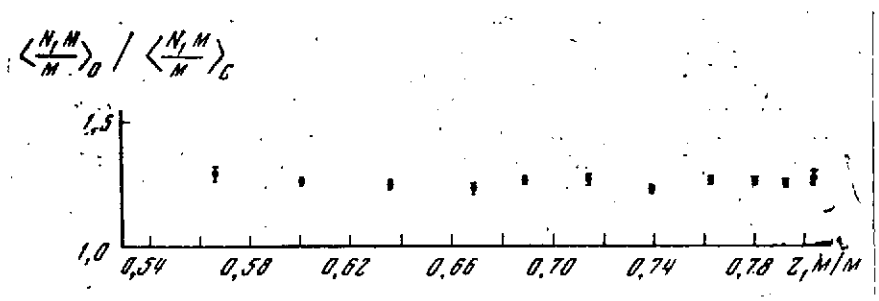

Figure 4. $\langle N_1M/M\rangle_0/\langle N_1M/M\rangle_c$ as function of $\langle Z_1M/M\rangle$

The calculation results are shown in Figure 5. Then all the I_0/I_C values obtained were averaged, with account for the weight of each value. The resulting ratio was $I_0/I_C = 1.308 \pm 0.011$, and the magnitude of the effective inelastic interaction section of protons with energy 5 GeV with carbon nuclei was $\sigma_{p-C} = 204 \pm 6$ mb. This

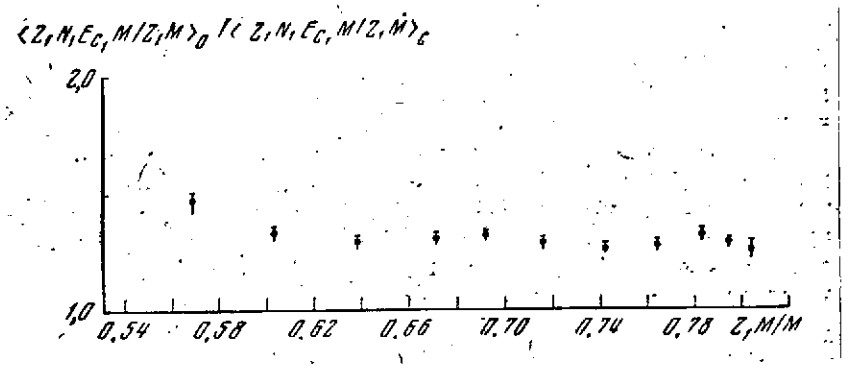

Figure 5. Quantity $\langle Z_1 N_1 E_{C_1} M/Z_1 M\rangle_0 / \langle Z_1 N_1 E_{C_1} M/Z_1 M\rangle_C$ for various values of $Z_1 M/M$

ratio is somewhat low because of the low multiplicity of secondary particles with energy 5 GeV (n_s = 1.6). The primary contribution to this reduction is made by the case when, as a result of interaction, only a single charged particle reaches the interaction detector and the lower scintillation counter. This effect may be estimated roughly if we use the multiplicity distribution of [5], from which it follows that for energy 5.7 GeV, only a single fast charged particle (proton with energy $\geq$ 500 MeV or π-meson with energy $\geq$ 80 MeV) is formed in approximately 30% of all interactions, the remaining particles have less energy. The minimal energy of these fast single particles is close to the energy which is necessary for the particles to reach the interaction detector. Therefore, if the angular and energetic distribution of these single particles generated during interactions /100 were such that they all would create the signal $Z_1 N_1 E_{C_1}$ with the same probability as would protons with energy 5 GeV, then the measured effective section would be too low by 30%.

However, comparison of the σ_{p-C} value obtained with that measured for energy 21.5 GeV [6] shows that the SEZ-14 instrument, even for small particle multiplicity which existed in the present experiment with proton energy 5 GeV, measures quite accurately the effective inelastic interaction section of protons with carbon nuclei in

the case of particle entry into the instrument from the direction of its "entry window". The magnitude of the section reduction in this case amounts to 8 ± 6%. This is evidence of effectiveness interaction recording high. The understating of the section by less than 30% may be explained by the fact that not all the fast single particles formed as a result of interaction create the signal C. Part of this particles depart through the calorimeter side surface, and part create in the calorimeter avalanches which reach the lower scintillation counter with lower probability than avalanches from protons with energy 5 GeV (it should be noted that the probability of creation of the signal C by a proton with energy 5 GeV, traveling along the instrument axis, is approximately 30%). Moreover, part of the fast single particles are accompanied by π^0-mesons, and yield a signal N_2 in the interaction detector.

In order to evaluate the influence of the indicated effects on the magnitude of the obtained section understatement, we found the magnitude of the effective section from the signal N_1M. To this end, we measured the ratio $\left(\frac{N_1M}{M}\right)_0 \Big/ \left(\frac{N_1M}{M}\right)_C$, whose magnitude was equal to 1.243 ± 0.004, which corresponds to the section $\sigma_{p-C} = 166 \pm 3$ mbarn.

We see that reduction of the limitations on the departure angle and energy of the individual secondary particles leads to increase of the unmeasured part of the section, but even in this case the section understatement is less than 30%, which does not contradict the arguments presented above on reasons for measured section understatement.

Instrument angular sensitivity diagram. During calibration of the SEZ-14 instrument, the angular sensitivity diagram of the instrument was measured (Figure 6). To this end, the instrument was set with aid of a positioning device at various angles to a proton beam. We see from Figure 6 that, for proton energy 5 GeV, the instrument actual aperture coincides with the geometric aperture (50°). Thus, the "overcount" due to widening of the instrument aperture because

of particle scattering in the instrument can be neglected for energy 5 GeV. We also see from Figure 6 that, in the case of particle entry into the instrument from behind, i.e., from the direction of the lower scintillation counter (in this case, the instrument was turned 180° to the beam), recording of events $Z_1N_1E_{C_1}M$ takes place. In this case, the counting rate of such events amounts to about 25% of the counting rate for the normal instrument position, when the particles enter the instrument from the direction of the "entry window". These events are apparently the result of cases when the proton passes through the entire instrument without interaction therein, or when only a single particle from the avalanche formed in the calorimeter passes through the interaction detector and proportional counter.

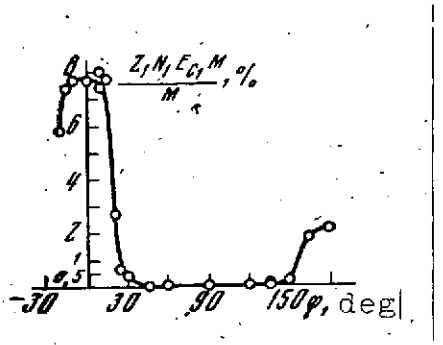

Figure 6. SEZ-14 instrument angular sensitivity diagram when recording events $Z_1N_1E_{C_1}M$ with proton energy 5 GeV

/101

Measurements by instrument turned 180° relative to the proton beam. As was noted previously, as a consequence of satellite rotation, particles may enter the instrument from behind (from the direction of the scintillation counter), and recording of the events $Z_1N_1E_{C_1}$ may introduce some contribution to the measured effective section, depending on the change of the counting rate of this signal with the carbon filter in place (in this case, the proportional counter acts as interaction detector), and also on the relationship of the counting rate of this signal with particle passage through the instrument from the front and from the back. Therefore, when calibrating the instrument, it was necessary to determine the ratio of the $Z_1N_1E_{C_1}M$ signal counting rate, without the filter, to the counting rate with the filter, and the quantity σ_{p-C} corresponding to this ratio for the case of particle passage from the direction of the scintillation counter.

In the case of measurements with the instrument turned 180° to the beam, the maximal counting losses arose in the C signal formation channel; therefore, normalization was made to the number of CM pulses recorded. In order to determine the magnitude of the section with this instrument position, we used the average values of $I = Z_1N_1E_{C_1}M/CM$, which were measured with and without the graphite filter in place. The value of the ratio I_0/I_C was equal to 1.245 ± 0.016, which corresponds to an effective section $\sigma_{p-C} = (167 \pm 10)$ mbarn.

Analysis of measurement results with particle into the instrument from the direction of the lower scintillation counter. In order to extrapolate the section measurement results for 5 GeV into the higher energy region, it is necessary to understand what causes the formation of the signals $Z_1N_1E_{C_1}M$ with the instrument turned 180° to the beam. In the latter case, the intensity of the events $Z_1N_1E_{C_1}M$ for the seances without counting losses constitutes 5% of the intensity of the protons incident on the instrument, and is still less in the presence of counting losses. /102

According to calculations, 4.5% of the protons incident on the instrument pass through the entire instrument without interaction. If we consider that the probability of formation of the signal $Z_1N_1E_C M$, in the case of single singly charged relativistic particle passage through all the detectors is equal to $\sim 1/2$, then half the particles forming the signal $Z_1N_1E_{C_1}M$ will interact with the carbon nuclei like protons with energy 5 GeV incident on the instrument at o°. In order to clarify the question of whether the electrons leaving the calorimeter yield a contribution to the formation of the signal $Z_1N_1E_{C_1}M$, we fabricated a lead filter whose thickness for nuclear interactions was equal to the thickness of the graphite filter, and we measured the amplitude distribution of the impulses in the proportional counters with this filter; in this case, control was provided

by the signal N_1M. Within the limits of statistical accuracy ($\sim$ 10%), the obtained amplitude distribution agreed with the corresponding spectrum with the carbon filter. Thus, the second component forming the signal $Z_1N_1E_{C_i}M$ consists of nuclear-active particles, generated during interaction.

In the case of measurement with the instrument turned 180° to the beam, the number of events in which at least one particle is recorded by the interaction detector amounts to 40% of the number of protons striking the instrument. Of such events, approximately half represent single singly charged particles (signal N_1M), and in half of the cases, the signal N_2M is generated — number of singly charged particles $\geq$ 2. Measurements were made in this same instrument position of the counting rate ratio without the filter and with the carbon filter for the signals $Z_1^*N_1E_{C_1}M$, where Z_1^* is a differential window in the proportional counter narrower than Z_1 (the lower thresholds of the windows Z_1^* and Z_1 coincided [$\sim$ 15 MV], while the upper threshold of the window Z_1^* [100 mV] was lower by a factor of two than for the window Z_1 [200 mV]).

For measurement of this ratio, based on the signal $Z_1^*N_1E_{C_1}M$, normalization (as in the $Z_1N_1E_{C_1}M$ case) by the number of recorded CM impulses was made. The ratio I_0^*/I_C^* was equal to 1.318 ± 0.018, which corresponds to a section $\sigma_{p-C} = 210 \pm 10$ mbarn.

The difference in the sections obtained for the signals $Z_1N_1E_{C_1}M$ and $Z_1^*N_1E_{C_1}M$ can be explained both by wide-window recording of two and three particles, formed as a result of interaction, and by the creation by a single particle after interaction (in those cases when, as a result of interaction, only a single particle which can reach

the proportional counters is formed) of an impulse whose magnitude exceeds the upper threshold of the narrow window as a consequence of the large ionizing capability of this particle.

Conclusions

As a result of analysis of the data obtained, we can draw the following conclusions. /103

1. In the case of proton incidence from the "entry window" direction, the SEZ-14 instrument, even for the low generated particle multiplicity existing in the present experiment (n_s = 1.6 for E = 5 GeV), measures quite accurately the effective inelastic interaction section of protons with carbon nuclei. The magnitude of the section understatement in this case amounts to 8 $\pm$ 6%.

2. In the case of proton incidence on the SEZ-14 instrument from the opposite direction, the measured effective section for proton energy 5 GeV is 18% low in comparison with the value measured with normal instrument position relative to the proton beam. On the basis of the measurements made for energy 5 GeV, we can conclude that, if the measurements were made aboard the Proton AES with this energy, the influence of particles entering the instrument from the opposite direction because of satellite rotation would lead to reduction of the measured effective section by about 4% in comparison with the value measured with particle entry into the instrument from the direction of its "entry window".

Thus, the low section value obtained during calibration is caused basically by low multiplicity of the particles generated during interactions. This makes it possible to consider that for proton energy 15 GeV, corresponding to the first recording threshold in the case of measurements aboard satellites, the section underestimation will be less than for 5 GeV because of increase of the average generated particle multiplicity.

The authors wish to thank N. L. Grigorov for his unfailing interest and valuable discussions, I. A. Savenko and Yu. V. Trigubov for assistance in the study, B. A. Yakovlev, B. M. Volchenkov, E. T. Martusov, and A. S. Tsupikov for assistance in the measurements, and also the accelerator operating group for the opportunity presented for carrying out the low particle intensity measurements.

References

1. Grigorov, N. L., G. P. Kakhidze, V. Ye. Nesterov, et al. Kosmicheskiye issledovaniya, Vol. 5, No. 3, 1967, p. 383.

2. Grigorov, N. L., V. Ye. Nesterov, I. D. Rapoport, et al. Kosmicheskiye issledovaniya, Vol. 5, No. 3, 1967, p. 420.

3. Birger, N. G., V. S. Borisov, G. K. Bysheva, L. L. Gol'din, et al. Yadernaya fizika, Vol. 6, No. 2, 1967, p. 344.

4. Grigorov, N. L., V. Ye. Nesterov, I. D. Rapoport, et al. Kosmicheskiye issledovaniya, Vol. 5, No. 3, 1967, p. 395.

5. Johnson, William R. Phys. Rev., Vol. 99, 1955, p. 1049.

6. Bellettini, G., G. Cocconi, A. N. Diddens, et al. Nucl. Phys., Vol. 79, 1966, p. 609.

STUDY OF HIGH-ENERGY ELECTRONS IN NEAR-EARTH COSMIC SPACE ABOARD PROTON 1 AND 2 AES

N. L. Grigorov, L. F. Kalinkin, E. I. Kogan-Laskina, and I. A. Savenko

The study of high-energy electrons in cosmic rays is of great /104
scientific interest, since it aids in obtaining answers to several important questions of astrophysics and cosmic ray physics. Specifically, there is a connection between the characteristics of the cosmic ray electron component and factors such as the structure of the galactic magnetic field, cosmic ray propagation in this field, radiation modulation in the solar system, nature of processes in cosmic ray sources, and so on. In recent years, particular attention has been devoted to measurements of electron fluxes with energies above 10^7 eV in near-Earth cosmic space at altitudes of 10^1 - 10^3 km. The results from study of high-energy electrons at the indicated altitudes may clarify certain peculiarities of the behavior of these particles in the Earth's magnetic field.

Equipment for measuring the fluxes and energy spectrum of electrons with energies $\gtrsim$ 20 MeV in the cosmic radiation was installed aboard the Proton 1 and 2 scientific cosmic stations.

A schematic of the instrument is shown in Figure 1. The instrument is a telescope formed by scintillation (1, 2) and gas Cherenkov

(3) counters. Separation of the electrons from the protons was accomplished by the recording threshold of the gas Cherenkov counter ($\sim$ 6 MeV) for electrons and $\sim$ 10 GeV for protons) and was supplemented by absorption of the electron photon showers caused by electrons with energies $\lesssim$ 10 GeV, in a lead layer of total thickness $\sim$ 30 radiation units (4, 5). Electrons with energies $\lesssim$ 10 GeV were recorded by all the telescope counters telescope and did not cause triggering of the counter 6, located after the filter 5. Protons with energies up to $\simeq$ 10 GeV were not detected by the gas Cherenkov counters, while those with energies above 10 GeV were recorded by the counter 6 (directly or on the basis of the products of their interaction with the matter). The gas Cherenkov counter also determined the direction of motion of the recorded particles (from the first counter to the second). In order to protect against showers which could be generated by high-energy protons in the matter of the instrument itself and its surroundings, the gas Cherenkov counter was placed in the hollow plastic scintillator cylinder 7. The impulses from this detector were connected in anticoincidence with the signals from the telescope. The minimal recordable electron energy was determined by the ionization losses in the matter along the path from counter 1 to counter 2 and amounted to about 20-30 MeV. In the region $E_e \geq 500$ MeV amplitude analysis of the impulses from the scintillation shower calorimeter 4 (discriminators with integral thresholds) was used to measure the energies.

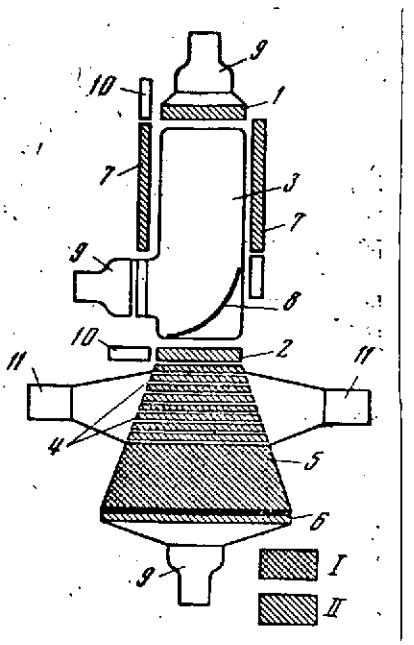

Figure 1. Schematic of instrument for measuring high-energy electrons aboard Proton 1 and 2 space stations:

1, 2 — telescope scintillation counters; 3 — gas Cherenkov counter; 4 — scintillation shower counter; 5 — lead alloy filter; 6 — scintillation counter recording radiation passing through the filter; 7 — scintillation anticoincidence counter; 8 — gas Cherenkov counter mirror; 9 — PM-49; 10 — PM-16; 11 — PM-52; I — lead; II — plastic scintillator

/105

In principle, the arrangement of the instrument installed aboard the Proton 2 AES was analogous to that used previously aboard Proton 1. The only difference was that the relative aperture of the instrument aboard Proton 2 was halved, by reducing the area of the telescope counter 2 (the geometric factor of the instrument aboard Proton 1 was $\Gamma = 5$ cm^2 · sr, that aboard Proton 2 was $\Gamma = 2.5$ cm^2 · sr). In this case, edge effects during particle passage through the shower calorimeter were eliminated, and particle energy determination became more reliable. Moreover, experience obtained during the experiment aboard Proton 1 was taken into consideration for proper selection of the preliminary scaling coefficients, and more rational choice of the parameters to be telemetered. For the data from Proton 2, we also had information on satellite geographic coordinates and orientation of the instrument axes in space. Comparison of the instrument indications aboard the two satellites showed that, with account for their relative aperture difference, the measurement results are quite similar. Therefore, in the sequel, we analyze in detail the information obtained in the experiment aboard Proton 2. Some preliminary results and their interpretation have been published previously [1]. /106

Figure 2 shows the latitude dependences of the relative counting rates of electrons and protons (shower calorimeter discriminator threshold corresponds to electron energy $\simeq$ 500 MeV). These results were obtained by averaging data for about 20 satellite orbits around the Earth (we took as the time origin for each orbit, the moment the orbit crosses the geographic equator with satellite motion from North to South). The differences of these dependences, which exceeds the error limits at high latitudes, indicates difference in the nature of these radiations. Figure 3 shows the global electron flux integral energy spectra in the near-equatorial and high geographic latitude $|\phi_{max}| = 63°$ regions. We see that the intensity dependence on energy is somewhat different in the different spectral regions: for the near-equator latitudes $\gamma - 1 \simeq 0.6$ for $E_e = 50$ MeV, and $\gamma - 1 \simeq 1$ for $E_e \simeq 5$ GeV (γ is the characteristic exponent of the differential /107

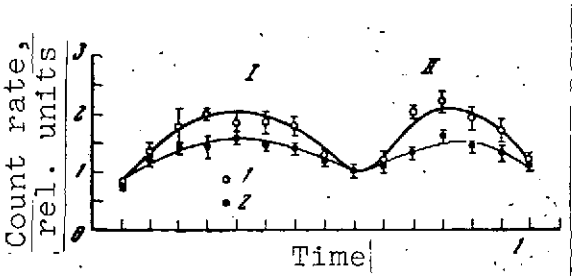

Figure 2. Latitude dependence of relative counting rates of electrons with energies $E_e \geq$ 500 MeV (1), and protons recorded at the same shower calorimeter threshold (2); curves are normalized to the equator region:

1 — southern hemisphere; 2 — northern hemisphere

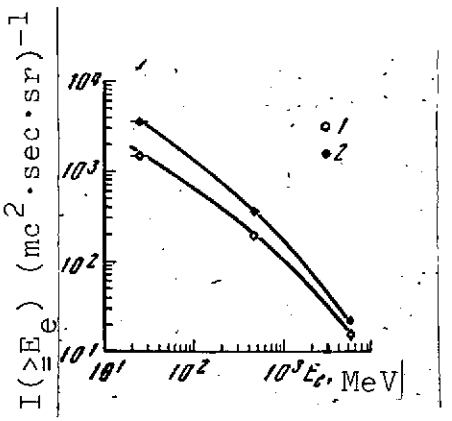

Figure 3. Integral energy spectrum of electrons in equatorial region (1), and at high latitudes (2), measured aboard Proton 2 AES (global flux)

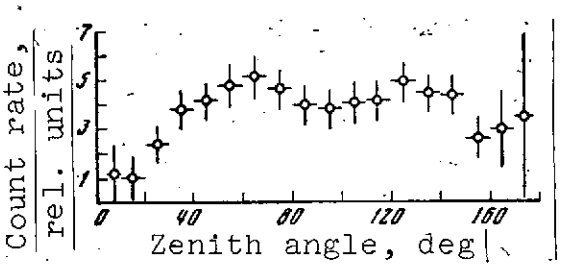

Figure 4. Distribution of electrons with energies $E_e \geq$ 500 MeV as function of angle formed by the instrument axis with the vertical for orbital segments with threshold magnetic rigidity $R \geq$ 10 GeV/c (Proton 2)

spectrum). This spectrum is far more "rigid" than that of the primary cosmic rays ($\gamma - 1 \simeq 1.7$). In the geomagnetic equator region, the electron flux with energy above 300 MeV was about 300 $(m^2 \cdot sec \cdot sr)^{-1}$. Figure 4 shows the distribution of electrons of such as a function of zenith angles for the satellite orbit segments with threshold magnetic rigidity $R \geq$ 10 GeV/c. Marked anisotropy of the radiation is not observed.

Most obvious among the results presented is the high recorded electron intensity. For comparison, we can note that the total primary cosmic ray intensity observed in the geomagnetic equator region amounts to 80 - 120 $(m^2 \cdot sec \cdot sr)^{-1}$ [2, 3]. It is true that we should note that, in the charged particle flux measurements in near-Earth space, it was found that the measured intensities exceeded by several times the values determined by the primary cosmic radiation.

Such results were obtained with equipment using various recording methods and carried aloft on balloons [4, 5], rockets [6], and satellites [7 - 10] (the sources cited are not exhaustive and are, basically, only illustrative).

The existence of this so-called excess radiation has now been reliably established. However, the nature and mechanism of its formation are still not very clear (naturally, in the balloon experiments the formation of secondary particles in the residual atmosphere was taken into account, and in the experiments performed aboard satellites, the region of space where the direct influence of the Earth's radiation bands might have an influence, were excluded from consideration).

The literature data presently available contain many indications that there is a significant relativistic electron fraction in the excess radiation composition.

It was found in [4], where Geiger counters were used as detectors, that the excess radiation flux amounts to about 500 $(m2 \cdot sec \cdot sr)^{-1}$ at the equator and about 1000 $(m^2 \cdot sec \cdot se)^{-1}$ in the Murmansk region. Approximately the same relationship is observed for the energy fluxes in the primary cosmic radiation at these latitudes. On this basis the authors of [4] suggest that the excess radiation consists basically of secondary electrons which are formed from the primary cosmic rays in electromagnetic cascades in the atmosphere. The connection between primary cosmic rays and excess radiation was examined in more detail in [8]. Studying the geographic distribution of the counting rate of a gas discharge counter located aboard the Kosmos 4 and Kosmos 5 satellites, the authors of [8] established a close correlation between measured radiation intensity and primary cosmic radiation. The longitudinal variation of the counting rate in the equatorial region, the connection with the magnetic rigidity, and the latitudinal variation pattern can all be explained in a natural fashion under the assumption of a genetic connection between the excess radiation and the primary cosmic rays at the point of observation. True, it could be noted that the detectors used in [4, 8] did not permit differentiation of the sort of recorded particles and, therefore, the conclusions apply to the excess radiation as a whole. /108

Identification of the nature of the particles comprising the excess radiation at heights of $\sim$ 300 km was made in [7]. Charged particle tracks in emulsions exposed during the flight of the second Soviet spacecraft were analyzed. It was found that the recorded radiation intensity exceeds the primary cosmic radiation intensity by a factor of three (in an interval covering one satellite orbit around the Earth). On the basis of specific ionization g/g_{min}, the excess particles can be subdivided into two groups: relativistic ($g/g_{min} < 1.4$), and "gray" ($g/g_{min} > 1.4$). The relativistic particles were not nuclear-active, and this made it possible to assume that they are electrons. Their fraction in the excess radiation is quite large — about half.

It is interesting to note that the data obtained in the experiment aboard Proton 2 are comparable with the results of [5], both in the particle flux values and in the intensity dependence on energy, although the conditions of these experiments differed markedly. In the latter study, performed aboard balloons with the aid of a telescope consisting of scintillation and Cherenkov counters interlayered with lead absorbers, the energy spectra of the "direct" and "return" albedo electrons in the energy range $10 - 10^3$ MeV were measured. (The "direct" albedo radiation arises in the matter of the atmosphere under the action of primary cosmic rays, and is directed upward from the Earth; the "return" albedo is the part of the "direct" radiation which returns to the atmosphere under the influence of the Earth's magnetic field.) Specifically, it was found that, at the geomagnetic latitude corresponding to the threshold rigidity 4.9 GeV/c, the electron fluxes with energies above 300 MeV are quite large, and consti- $I_{dir} \gtrsim 110$ and $I_{ret} \gtrsim 50$ $(m^2 \cdot sec \cdot sr)^{-1}$ for the "direct" and "return" albedo. The spectra were quite "rigid", the characteristic exponents of the differential spectra, approximated by a power-law

dependence of the intensity on energy, were $\gamma_{dir} = 1.29 \pm 0,06$ and $\gamma_{ret} = 1.44 \pm 0.09$, respectively. Thus, the measurements made in [5] indicate a natural source of intense electron fluxes with energy of hundreds of MeV, which were discovered in the measurements aboard the Proton AES [1].

At the same time, it was noted in [1] that the high electron flux intensity may be associated with the mechanism of electron capture and relatively long retention by the Earth's magnetic field.

The results of [11, 12] can be considered confirmation of this /109
concept. Fluxes of electrons with energies 100 - 1500 MeV were measured at altitudes corresponding to $\gtrsim$ 10 g/cm^2 residual atmosphere, using equipment including a telescope formed by scintillation and Cherenkov counters and a shower spark chamber as the basic element to discriminate electrons from the other particles. The measurements were made at a geomagnetic latitude where the cutoff geomagnetic formation momentum amounted to 3.5 GeV/c. The results deserving most attention are that at quite high altitudes large electron fluxes were recorded, and significant temporal variations of these fluxes were detected. The data obtained during equipment ascent aboard balloons grouped as follows (Figure 5, [11]). Two flights (July 6, 1967 and July 9, 1968) provided altitude-intensity relations agreeing with one another and with the calculated secondary electron intensity values: increase during ascent, maximum at an altitude corresponding to atmospheric depth $\sim$ 120 g/cm^2, and flux decrease by an order of magnitude at the maximal height. The latitudinal variation of intensity in the initial stage of the other two flights (June 14, 1967 and October 27, 1967) was also the same and up to heights of about 100 g/cm^2, agreed with the results of the first two flights. However, at higher altitudes a significant (by a factor of 2 - 3) intensity increase, in comparison with the measurements and calculated electron flux values mentioned above, was observed. The absolute magnitude of the additional flux was $\sim$ 600 (m^2 · sec · sr)$^{-1}$. The spectrum of this radiation, as in the previously mentioned cases, is also quite "rigid":

$\gamma = 1.6 \pm 0.4$. It is important to note that the appearance of the additional electron flux was not associated with change of the primary cosmic ray intensity measured by neutron monitors. The attempt by the authors of [11, 12] to associate the change of the electron flux magnitudes with the state of the Earth's magnetosphere was a natural one. In spite of the fact that the electron energies are quite high, the influence of magnetosphere state change on their /110
fluxes had already been observed experimentally in [13], where change of the intensities of electrons with energies 10 - 225 MeV by a factor of 2 - 3 was noted during nighttime and daytime measurements. In the case under discussion here, such an explanation was excluded, since all the flights were made at the same time of day. However, a correlation was found between the additional electron flux appearance and change of the geomagnetic field state, characterized by the three-hour K-index.

Taken together, the experimental data just discussed make it possible to note the following. Both in the stratosphere (at altitudes of 25 - 40 km), and at higher altitudes (200 - 600 km), significant fluxes of electrons of quite high energies ($E_e \gtrsim 10^7$ eV) are observed. The large "direct" albedo electron fluxes in the atmosphere, caused by primary cosmic ray interaction with atmospheric matter, lead to injection of these particles into near-Earth space. The significant variations in time of the secondary electron fluxes in the stratosphere, which are not

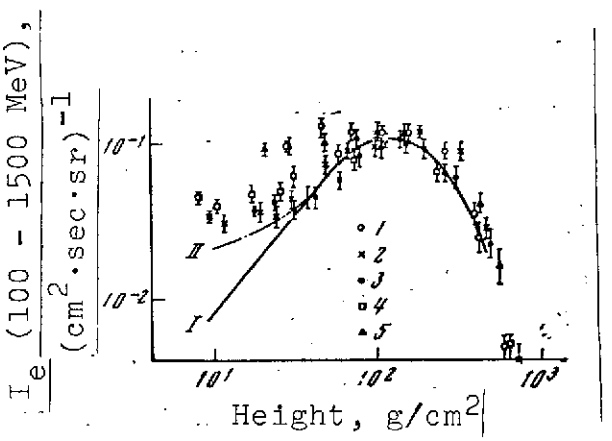

Figure 5. Intensities of electron fluxes with energies 100 - 1500 MeV at various heights in the atmosphere [11]: 1 — Apr. 14, 1967, 2 — July 9, 1968; 3 — July 6, 1967; 4 — Oct. 8, 1958; 5 — Oct. 27, 1967; I — calculated altitudinal variation of secondary electron flux generated in the atmosphere by proton-nuclear component of primary cosmic rays; II — sum of (I) and "return" albedo electron flux

associated with variations of the primary cosmic ray intensity, can be considered an indication of the existence in near-Earth space of a "reservoir" in which electrons of quite high energies accumulate, i.e., an indication of comparatively long-term retention of these particles by the Earth's magnetic field. During distrubance of the magnetosphere state, these particles "spill out" into the atmosphere.

However, it should be noted that at present there is no adequate explanation for the details of the mechanism of high-energy albedo electron trapping by the Earth's magnetic field, the duration of their retention in this field, and the direct causes of the "spilling".

It may be assumed that long-term observations at heights of $\sim 10^2 - 10^3$ km, with simultaneous measurements aboard balloons in the stratosphere, will make it possible to clarify the basic mechanisms of intense high-energy electron flux formation in near-Earth cosmic space and "injection" of this flux into the Earth's atmosphere.

The authors wish to thank Yu. S. Klintsov and O. B. Ben'kovskiy for their assistance in preparing the equipment for measuring high-energy electrons aboard the Proton scientific cosmic stations.

References

1. Grigorov, N. L., Yu. S. Klintsov, V. Ye. Nesterov, I. D. Rapoport, I. A. Savenko and B. M. Yakovlev. Izvestiya AN SSSR, seriya fiz., Vol. 30, 1966, p. 1773.

2. Charakhch'yan, A. N. and T. N. Charakhch'yan. ZhETF, Vol. 35, 1958, p. 1088.

3. McDonald, F., and W. Webber. Phys. Rev., Vol. 115, 1959, p. 194.

4. Bazilevskaya, G. A., A. N. Charakhch'yan, T. N. Charakhch'yan, A. N. Kvashnin, A. N. Pankratov and A. A. Stepanyan. Trudy FIAN, No. 100, 1967, p. 34.

5. Verma, S. D. Journ. Geoph. Res., Vol. 72, 1967, p. 915.

6. Van Allen, J. A. and A. V. Gangnes. Phys. Rev., Vol. 78, 1950, p. 50.

7. Grigorov, N. L., D. A. Zhuravlev, M. A. Kondrat'yeva, I. D. Rapoport and I. A. Savenko. Kosmicheskiye issledovaniya, Vol. 1, No. 3, 1963, p. 436.

8. Basilova, R. N., S. N. Vernov, V. Ye. Nesterov, N. F. Pisarenko, I. A. Savenko and P. I. Shavrin. Kosmicheskiye issledovaniya, Vol. 2, No. 2, 1964, p. 280. /111

9. Lin, W. C., D. Venkatesan and J. A. Van Allen. Journ. Geoph. Res., Vol. 68, 1963, p. 17.

10. Ginzburg, V. L., L. V. Kurnosova, Yu. I. Logachev, L. A. Razorenov and M. I. Fradkin. Collection: Iskusstvennye sputniki Zemli (Artificial Earth Satellites). Moscow, Izdatel'stvo AN SSSR, No. 10, 1961, p. 22.

11. Bezus, V. A., A. M. Gal'per, N. L. Grigorov, V. V. Dmitrenko, L. F. Kalinkin, V. G. Kirillov-Ugryumov, B. I. Lukov, A. S. Melioranskiy, Yu. V. Ozerov, I. A. Savenko, E. M. Shermanzon and I. L. Roxental'. Isvestiya AN SSSR, seriya fiz., Vol. 33, 1969, p. 1827.

12. Bezus, V. A., A. M. Gal'per, N. L. Grigorov, V. V. Dmitrenko, L. F. Kalinkin, V. G. Kirillov-Ugryumov, B. I. Luchkov, A. S. Melioranskiy, Yu. V. Ozerov, I. L. Rozental', I. A. Savenko and E. M. Shermanzon. Collection: Fizika elementarnykh chastits i kosmicheskikh luchei (Physics of Elementary Particles and Cosmic Rays). Moscow, Atomizdat Press, Vol. 2, 1969.

13. Jokipi, J. R., J. L'Heureux and P. Meyer. Preprint EFINS 67-45, May, 1967.

STUDY OF HIGH-ENERGY ELECTRONS IN THE STRATOSPHERE

V. A. Bezus, A. M. Gal'per, N. L. Grigorov, V. V. Dmitrenko, L. F. Kalinkin, V. G. Kirillov-Ugryumov, B. I. Luchkov, A. S. Melioranskiy, I. A. Savenko, and E. M. Shermanzon

A flux of electrons with energy $E_e \gtrsim 300$ MeV, exceeding by about /112 ten times the primary electron flux [2, 3], was recorded in a study by Grigorov et al. [1], made aboard the Proton 1 and 2 AES. Another peculiarity of the recorded flux was that it was noted not only at high latitudes, but also near the equator, varying in intensity by less than a factor of two ($4 \cdot 10^{-2}$ and $2.2 \cdot 10^{-2}$ [cm^2 · sec · sr]$^{-1}$) These measurements shows that within the limits of the Earth's magnetosphere there exist not only electrons of low and moderate energies ($\gtrsim$ 1 MeV), which form the radiation bands (see, for example, [4]), but also high-energy electrons ($E_e \gtrsim 100$ MeV).

During 1967 and 1968, we made measurements using equipment installed aboard high-altitude balloons to study the high-energy electron fluxes in the upper layers of the atmosphere. We measured the direct (toward the Earth) and albedo (from the Earth) electron fluxes in the energy interval 100 - 1500 MeV. The measurements were made at 46° geomagnetic latitude, where the cutoff momenta are about 3.5

GeV/c, and primary cosmic ratiation electrons in the measured energy interval cannot penetrate. Individual measurement results were published earlier in several papers [5 - 11].

Instrument Configuration and Operation

A block diagram of the recording instrument is shown in Figure 1. The instrument consists of the following components: Ch is a directional Cherenkov threshold detector with plexiglass radiator. Directivity of the counter is achieved by blackening the upper surface of the radiator and establishing the corresponding electronic circuit threshold, C_1, C_2, C_3 are polystyrene scintillation counters, SC is a multilayer spark chamber with lead plates acting as electrodes with overall thickness equal to 3.7 radiation lengths, A is a lead absorber, three radiation lengths thick, PR is a photorecorder which photographs the spark chamber in two orthogonal projections through a mirror system.

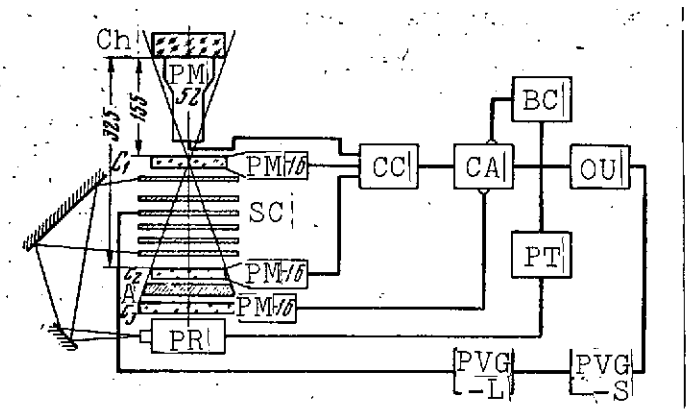

Figure 1. Block diagram of recording instrument: /113

Ch — Cherenkov counter; C_1, C_2, C_3 — scintillation counters; SC — spark chamber; A — lead absorber; PR — photorecorder; CC — coincidence circuit; CA — anticoincidence circuit; OU — output unit; PVG-S, PVG-L — "small" and "large" pulse voltage generators; BC — blocking circuit; PT — photorecorder trigger circuit

The instrument operates as follows. The electron being recorded triggers the counters Ch and C_1, and creates an electron shower in the spark chamber. The shower particles are recorded by the counter C_2 and absorbed in the block A, without reaching the counter C_3. Events of the type $CHC_1C_2\overline{C}_3$ are identified by an electronic circuit consisting of the triple coincidence circuit CC and the

anticoincidence circuit CA (a bar above a symbol means that the given counter is connected in anticoincidence). This identification technique excludes recording of protons and other penetrating particles whose ionization range for the threshold velocity in the Cherenkov counter $\beta_{thr} = 0.67$ exceeds the total amount of matter in the instrument. However, in addition to electrons, events of the type $ChC_1C_2C_3$ will cause nuclear cosmic particle interactions in SC and A, in which no charged product will reach C_3, and muons in the energy interval 55 - 80 MeV are stopped in block A. Final selection of the electronic cases among the recorded events is made on the basis of spark chamber photographs.

Further operation of the instrument involves recording the events identified by the CC and CA circuits. An impulse from the CA circuit triggers the output unit OU, triggering circuit of the photorecorder PR, and blocking circuit BC. The impulse from the OU triggers the small and large pulse voltage generators PVG-S and PVG-L, which generate the high-voltage pulse for the spark chamber. The chamber consists of five gaps separated by plates containing 0.7 radiation lengths of lead each. The upper 3-cm-high gap determines /114 the direction of the entering electron. The remaining gaps, each 1.5 cm high, record the electron shower. The chamber is filled with neon at 1 atm pressure. The upper and lower spark chamber electrodes are connected to ground, and a high-voltage pulse of amplitude 25 kV and duration 0.5 μsec with leading front duration 30 nsec, is applied to the midpoint of the chamber. The pulse delay is no more than 0.5 μsec.

All the electronic circuits, voltage transformers, and pulse voltage generators are made using nonfilament components. In the study, we used two instruments of the same type (A-2 and A-3), which were geometrically similar to one another and had effective area $S_2 = S_3 = 110$ cm^2, solid viewing angle $\Omega_2 = \Omega_3 = 110$ cm^2, and geometric factor 13.5 cm^2 · sr. The instrument energy requirement was about 12 W. Each instrument weighed about 45 kg. A detailed description of the equipment is given in [12].

Instrument Calibration

The characteristics of each instrument were measured during operation with cosmic muons, monochromatic electrons in the energy interval 100 - 1500 MeV (synchrotron of the Lebedev Physics Institute of the Academy of Sciences of the USSR [FIAN], linear accelerator of the Physicotechnical Institute of the Academy of Sciences of the UkSSR [PTI], and using protons with momentum 2 GeV/c (Joint Institute of Nuclear Studies).

1. Calibration of CH, C_1, C_2, C_3 Counter Telescope

Figure 2 shows the electron recording effectiveness (η_e) in the instrument A-3 as a function of electron energy. The electron recording effectiveness was measured directly in electron beams. The effectiveness η_e initially increases sharply from zero to E $\sim$ 100 MeV to a maximal value of about 0.3 for E $\sim$ 400 Mev, and then decreases gradually to zero. The decrease of η_e with increase of the energy takes place because of the increased probability of an electron avalanche passing through block A and reaching the "anticoincidence" counter C_3. We see from the curve shown in Figure 2 that the instrument records effectively electrons in the 100 - 1500 MeV interval.

Electron recording effectiveness as a function of the angle of of entry into the instrument is shown in Figure 3. This Figure shows one of the angular characteristics obtained for the A-3 instrument, recorded for electrons with energy 435 MeV passing through the center of the Ch counter radiator at the angle ϕ to the instrument axis in one projection, and with fixed angle $\psi = 0$ in the other orthogonal projection. The effectiveness changes very weakly in the angle interval $\pm$ 10°, and decreases sharply with increase of ϕ. The effectiveness of reverse flux (ϕ = 180°) recording is less than /115
$2 \cdot 10^{-4}$.

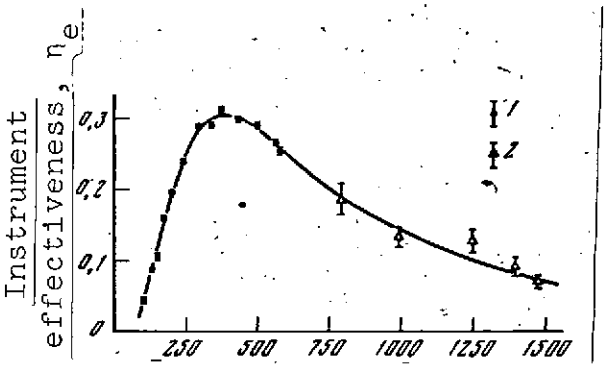

Electron energy E_e, MeV

Figure 2. Effectiveness of instrument recording of electrons as function of energy:

1 — FIAN synchrotron; 2 — PTI linear accelerator

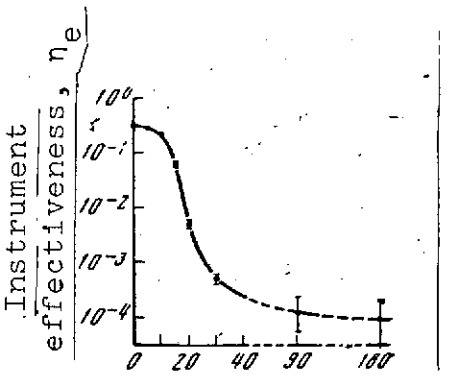

Angle of electron incidence on instrument, deg

Figure 3. Effectiveness of electron recording versus incidence angle

The geometric factor of the A-3 instrument, calculated from calibration measurements for electrons with energy 435 MeV, is $\Gamma = (14.5 \pm 1.0)$ cm^2 · sr.

2. Spark Chamber Calibration

When recording electrons and muons, it was shown that in the large spark chamber gap the sparks follow along the particle tracks up to a maximum angle, determined by the instrument aperture and equal to $\sim 20°$. The accuracy of particle angle measurement in the upper gap is $\sim 2°$.

Comparison of the shower curves obtained during calibration for electrons with energy 100 - 1500 MeV with the calculated curves or the shower curves obtained by other experimental methods showed that the spark chamber has effectiveness close to 100% [12] for recording of many particles.

The total number n of sparks in all five gaps serves as the characteristic of the electron shower in the spark chamber. Figure 4 shows the dependence of the average number $\bar{n}$ of sparks and the standard deviation σ_n of the number of sparks as a function of

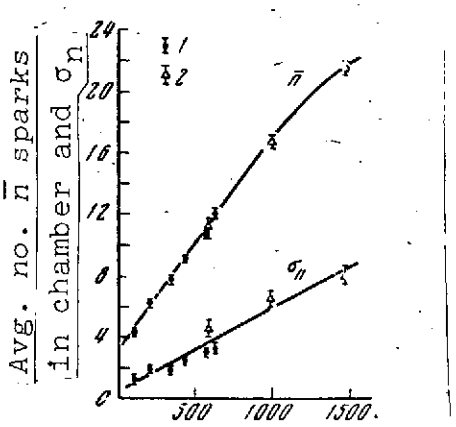

Figure 4. Average number n of sparks in spark chamber and mean square deviation σ_n of number of sparks versus electron energy:

1 — FIAN spectrometer; 2 — PTI linear accelerator

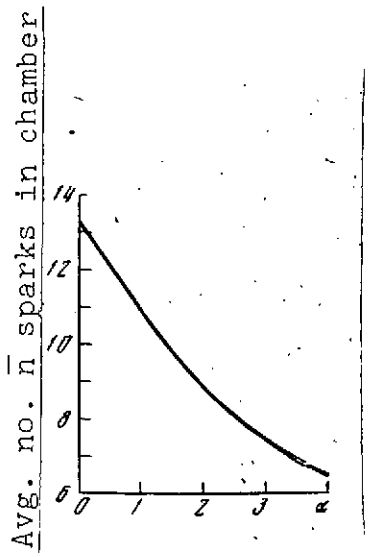

Figure 5. Average number $\bar{n}$ of sparks in showers versus differential energy spectrum exponent α

electron energy. We see that $\bar{n}$ increases linearly with energy increase in the 100 - 1000 MeV interval; for higher energies we observe some deviation from the linear relationship, which is most likely explained by the spark overlap in showers with a large number of particles. The relative error of individual electron energy measurement, based on number of sparks in the shower, is equal to approximately 70% for E = 200 MeV, and 50% for E = 1000 MeV. This large error arises because of fluctuations during initial development of the shower. However, the multilayer spark chamber can be used as a spectrometer for measuring electron group energy spectrum shape. As a result of calculation made on the basis of the calibration data shown in Figures 2 and 4, for an electron differential energy spectrum of power-law form $N(E) = CE^{-\alpha}$, we obtained the dependence of of the average number $\bar{n}$ of sparks in the showers on the value of the exponent α, shown in Figure 5 [13]. The statistical error in measurement of the spectrum exponent for a group of 100 showers is 10%.

/116

3. Imitation of Electron Events by Nuclear-Active Particles

During A-3 instrument operation in a proton beam with momentum 2 GeV/c, we determined the probability of electron event imitation by nuclear-active particles. The separated proton beam contained ∿ 95% protons and ∿ 5% $\pi^{\pm}$ mesons. It was shown that with probability $(3.0 \pm 0.8) \cdot 10^{-2}$, nuclear-active particle incident on the instrument causes triggering of the $CHC_1C_2\bar{C}_3$ counter telescope. Examination of the events recorded in the spark chamber showed that (0.180±0.022) of them are accompanied in the spark chamber by a shower pattern which does not differ in form from the showers generated by electrons. In the remaining cases, individual tracks or characteristic nuclear /117
interactions of the "star" for "fork" type and sudden track terminations were recorded. Thus, the probability of electron event imitation by nuclear-active particle with momentum 2 GeV/c is $(5.5 \pm 1.6) \cdot 10^{-3}$. Since with increase of the incident particle energy the probability increases that one of the nuclear interaction products will enter the "anticoincidence" counter C_3, the imitation probability will be lower for high energies.

Measurement Conditions

The measurements were made using controllable high-latitude balloons at 46° North geomagnetic latitude. In all, six direct electron flux measurements and two albedo electron measurements were made. Information on the flights made is shown in Table 1.

Each instrument was installed in a sealed, thermally insulated container in which there was also located a console with auxiliary instruments: clock, thermometer, vacuum gauge, compass, and plumb line, which were photographed simultaneously with the spark chamber. The instruments were activated on the ground before launching the balloon, and operated both during ascent, which usually lasted 1.5 - 2 hours, and during drift at maximal height. In all the measurements,

TABLE 1

Flight date	Launch time (world time)	Residual atmosphere, g/cm^2	Measurements made and No. of instrument used
June 14, 1967	2 h, 22 m	25.0	Electrons (A-3)
July 6	2 h, 53 m	19.0	Electrons (A-3)
Oct. 27	3 h, 28 m	20.0	Electrons (A-3)
Oct. 31	1 h, 47 m	16.0	Albedo electrons (A-3)
July 9, 1968	3 h, 16 m	8.7	Albedo electrons (A-2)
Oct. 8	2 h, 54 m	7.7	Electrons (A-3)
Oct. 19	4 h, 11 m	8.9	Electrons (A-3)

the temperature and pressure inside the container remained in the limits of 10 - 15° C, and about 1 atm. The altitude in the atmosphere at any moment of time could be determined from the barogram recorded during each flight.

In the albedo flux measurement case, the container with the instrument was rotated 180°.

Measurement Results

From the data obtained in flight, we determined the electron intensity and energy spectrum at various altitudes. /118

The electron intensity was calculated from the formula

$$I_e = \frac{N_e}{(T - \tau N)\overline{\Gamma\eta}},$$

where N_e is the number of particles recorded during the time T = 10 min, τ is the instrument blocking time, N is the total number of instrument triggerings during the time T, Γ is the instrument geometric factor, η is the recording effectiveness. Since the geometric factor and effectiveness are functions of energy, the value $\overline{\Gamma\eta}$ averaged over the recorded particle spectrum is substituted into the formula.

Figures 6 and 7 show the measured direct and albedo electron flux intensities. The altitude dependence of the secondary atmospheric electrons was calculated in [14]. Although the calculation was made for energies greater than 1 GeV, the comparison made in [14] between the calculated curve and the experimental data of [2], in which electrons with lower energies were measured, showed that the calculated relative altitude dependence remains the same in the energy interval 100 - 1000 MeV.

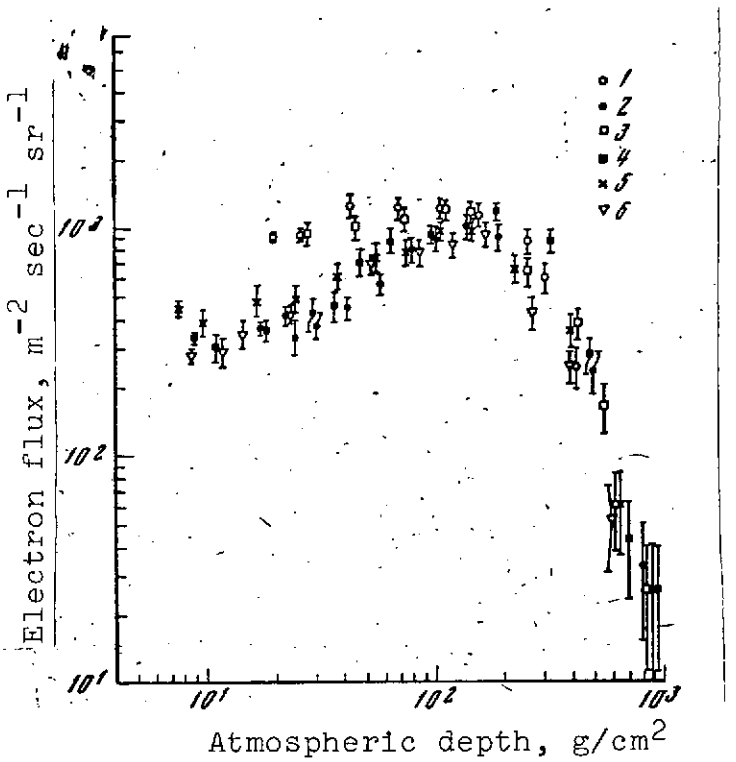

Figure 6. Altitude dependence of the direct (toward Earth) electron flux with energy 100 - 1500 MeV:

1 — May 14, 1967; 2 — July 6, 1967; 3 — Oct. 27, 1967; 4 — July 9, 1968; 5 — Oct. 8, 1968; 6 — Nov. 19, 1968

We should note some peculiarities in the altitude dependences of the recorded fluxes.

a) Altitude dependence of the direct (toward-the-Earth) electron flux with energy 100 - 1500 MeV. The results of all six measurements agree well with one another and with the theoretical dependence at large depths ($h \gtrsim 100$ g/cm^2) if the calculations of [14] and the data of the

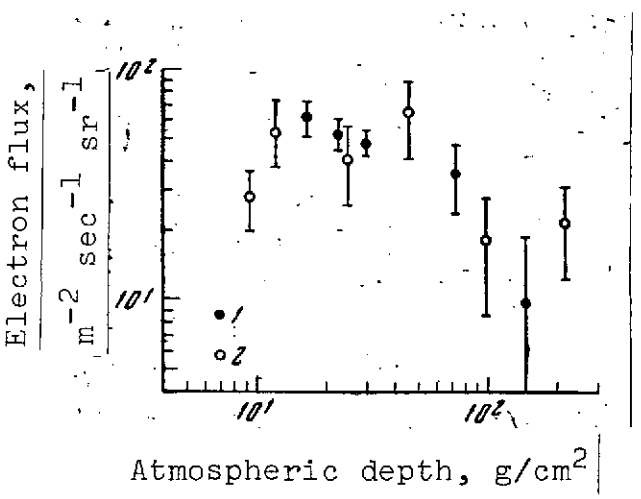

Figure 7. Altitude dependence of albedo electron flux with energy 100 - 1500 MeV:

1 — Oct. 31, 1967; 2 — July 9, 1968

present experiments are normed to h $\simeq$ 120 g/cm^2. Specifically, at the maximum ($\sim$ 120 g/cm^2), the measured flux intensity amounts to about 0.1 (cm^2 · sec · sr)$^{-1}$. At small depths (h $\lesssim$ 50 g/cm^2), the individual measurement results diverge markedly. The greatest discrepancy is observed for measurements made on June 14, 1967 and October 27, 1967, on the one hand, and on August 6, 1967 and July 9, 1968, on the other hand. While in the first two of these flights the intensity varies anomalously weakly with height, in the second two flights the measured intensity decreases with altitude, following more exactly the calculated variation. At altitudes h $\lesssim$ 20 g/cm^2, none of the flight results agree with the calculated flux [$\simeq 10^{-2}$ (cm^2 · sec · sr)$^{-1}$].

The discrepancy found goes far beyond the statistical error limit, and cannot be explained by the instrumental errors, since all the measurements were made on the same instrument (A-3), and the conditions inside the container were the same in all flights. An additional criterion of instrument operation correctness is the instrument counting rate for particles of non-electron nature — particles which do not create showers in the spark chamber. Such particles, constituting about 10% of the total number of instrument triggerings, may be muons, protons, and other particles which come to a stop or /120
interact in block A, or are recorded by the instrument as a result of count loss of the counter C_3. Figure 8 shows the altitude variation of the non-electron event counting rate in flights with "normal" (July 6, 1967, July 9, 1968) and "abnormal" (June 14, 1967, Oct. 27, 1967) electron fluxes. We see that at all altitudes, no marked difference is noted in the counting rates and, consequently, the instrument recording effectiveness was constant in all the flights. Figure 9 shows the altitude variation separately for electrons with energy E $\simeq$ 500 - 1500 MeV, which caused in the spark chamber showers with number of particles n $\geq$ 10. Once, again, in this energy interval in the June 14, 1967 and October 27, 1967 flights, we observe increased electron flux intensity, although the statistical errors are markedly higher here. This result indicates that particles, not

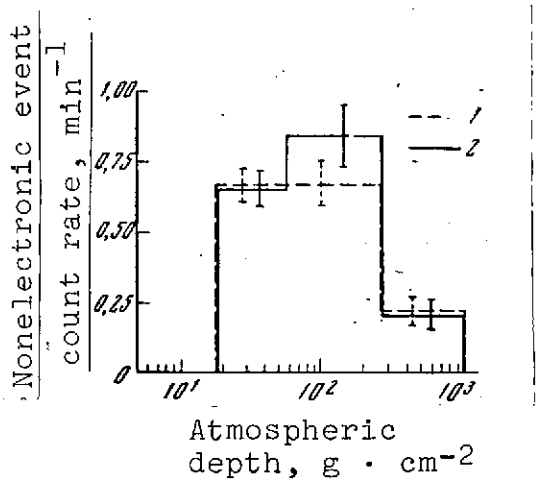

Figure 8. Altitude dependence of non-electron particle counting rate:

1 — June 14, 1967 and Oct. 27, 1967; 2 — July 6, 1967 and August 9, 1968

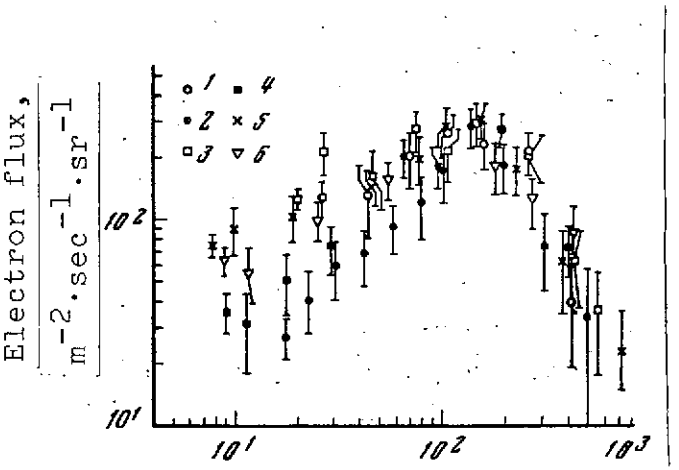

Figure 9. Altitude dependence of direct flux electrons with energy 500 - 1000 MeV:

Notations same as in Figure 6

only electrons with energy 100 - 200 MeV, whose daily variations were noted in [15, 16], but also electrons of higher energies (500 - 1000 MeV), whose variations were noted for the first time, participate in the electron flux varaitions which we discovered. /121

b) Altitude dependence of albedo electron flux with energy 100 - 1500 MeV. The results of albedo flux measurements made on October 31, 1967 and August 9, 1968 are shown in Figure 7. The albedo flux differs from the direct electron flux in both absolute intensity and altitude dependence. The albedo electron flux increases monotonically with altitude up to about 15 g/cm^2, where its maximum is apparently observed.

It should be noted that the albedo flux measurement is made particularly difficult by the background from the direct flux of high-energy gamma quanta, which are converted in block A and create a powerful electron shower, and in this case an impulse develops in the directional Cherenkov counter. Among the $ChC_1C_2\overline{C}_3$ telescope triggerings, only 20% of the cases are caused by albedo electrons.

Separation of albedo electrons from the background gamma quanta was possible, thanks to the presence of the spark chamber, in which it is possible to determine the electron shower development direction. It was apparently because of the strong background from electrons and gamma quanta of the direct flux that in [17], where only a counter telescope was used, the albedo electron flux recorded was higher by several fold, and the altitude variation of this flux repeated the strong altitude dependence of the direct electron-photon component flux.

In addition to intensity, at the various altitudes we measured the exponent α of the recorded flux differential energy spectrum.

In order to determine α, we calculated the average number $\bar{n}$ of sparks in the showers at the given altitude, and from the calculated dependence of $\bar{n}$ on α (see Figure 5), we determined the values of α_e. Figure 10 shows the altitude dependence of α_e. We see that the electron energy spectrum varies with depth in the atmosphere, which is a result of the different participation at different altitudes of the two basic secondary soft component generation processes: $\pi \to \mu \to e$ decay and $\pi^0 \to 2\gamma$ [18].

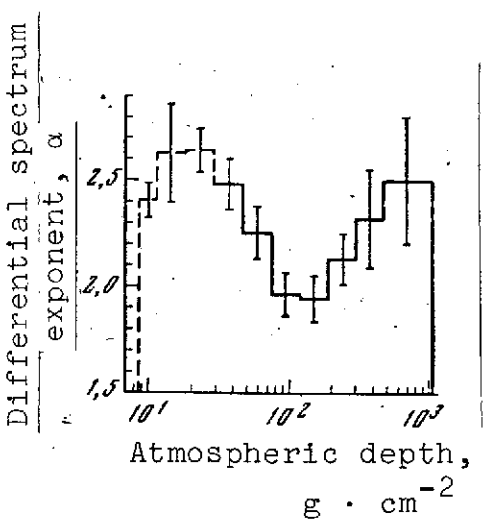

Figure 10. Altitude dependence of differential electron energy spectrum exponent α_e

/122

The exponents α_e measured for "normal" and "abnormal" fluxes agree everywhere, except at the high altitudes (less than 30 g/cm^2). At these altitudes, α_e of the "abnormal" flux is lower than for the "normal" flux, i.e., the "abnormal" flux has a more rigid spectrum.

Because of the limited albedo electron flux statistics, it was not possible to construct the albedo flux spectrum exponent altitude dependence. The exponent α_{alb} averaged over all altitudes is 1.6 ± 0.3.

Discussion of Results

The most interesting result of the measurements is the discovery of large direct electron flux variations in the upper layers of the atmosphere. Since significant primary cosmic ray intensity changes were not observed during the measurements, the secondary electron flux should not have changed noticeably. Therefore, increase of the recorded electron flux intensity could take place only as a result of the appearance of additional electron flux i_{add}, incident from outisde on the top of the atmosphere, whose magnitude is equal to the difference between the recorded and calculated secondary fluxes. The exponent α_{add} of the additional flux differential energy spectrum, calculated from the α_e difference for the "abnormal" and "normal" fluxes, was 1.56 ± 0.22.

The additional flux cannot be explained by variation of the double-albedo electron flux. The albedo and double-albedo electron fluxes were identical in magnitude, and the maximal albedo flux which we measured was $\sim 7 \cdot 10^{-3}$ $(cm^2 \cdot sec \cdot sr)^{-1}$, which is nearly an order less than the recorded additional fluxes. /123

Table 2 shows the direct electron fluxes and additional fluxes obtained in the six measurements made (in calculating the additional fluxes, it was considered that the secondary electron flux calculation inaccuracy [14] is 20%), and also quantities characterizing cosmic ray intensity, solar activity, and state of the Earth's magnetic field on the days of observation: number of Deep River neutron monitor counts M, number R_z of solar spots, overall magnetic field K_p-index (ΣK_p), and the change of the overall K_p-index on the day of measurement in comparison with the preceding day $(\Delta(\Sigma K_p))$. While ΣK_p characterizes the state of the magnetosphere, $\Delta(\Sigma K_p)$ shows whether the disturbance level is increasing or decreasing. We see from the values shown in Table 2 that the additional flux correlates only with

TABLE 2

Measurement date	$I_e \cdot 10^2$ $(cm^2 \cdot sec \cdot sr)^{-1}$ at h=25 g/cm^2	$I_{add} \cdot 10^2$ $(cm^2 \cdot sec \cdot sr)^{-1}$ at h=25 g/cm^2	M	R_Z	ΣK_p	$\Delta(\Sigma K_p)$
		Direct flux				
June 14, 1967	9.3 ± 0.9	6.3 ± 1.1	6625	31	23	+ 10
July 6	4.1 ± 0.4	1.1 ± 0.7	6634	97	14	- 10
Oct. 27	9.2 ± 0.7	6.2 ± 1.0	6679	125	18	+ 13
July 9, 1968	3.7 ± 0.5	0.7 ± 0.8	6489	91	9	- 4
Oct. 8	3.8 ± 0.5	0.8 ± 0.8			14	- 8
Nov. 19	4.2 ± 0.4	1.2 ± 0.7	6217		12	- 16
		Albedo				
Oct. 31, 1967	0.52 ± 0.08	–	6414	100	11	- 7
July 9, 1968	0.40 ± 0.15	–	6489	91	9	- 4

the parameters characterizing the magnetic field: the additional flux appears for large values of $\sum K_p$ and $\Delta(\sum K_p)$. This means that appearance of the additional flux is connected with magnetosphere transition from the quiet to the disturbed state.

Both the very fact of additional flux recording and their dependence on magnetosphere state lead us to the conclusion that electrons with energy greater than 100 MeV exist and accumulate in nearby near-Earth space. We can consider that such electrons fill the part of the inner electron belt nearest the Earth, and are weakly retained by the geomagnetic field. The additional fluxes which we recorded represent the "spilling" part of the trapped flux, and spilling takes place for comparatively small magnetic field disturbances. If the trapped flux is located on the shell L = 2, spilling should be observed at the middle latitudes, where our measurements were made, and should be absent at the high latitudes, where most of of the electron flux measurements in the 100 - 1500 MeV interval were made by other authors [2, 3, 15, 16, 19 - 24]. However, many

measurements of the electron flux in the same energy interval have been made at the middle latitudes [17, 21, 25, 26], and the fact that the additional electron flux was not detected in these studies is apparently explained by the fact that none of these measurements were made with such a disturbed magnetosphere ($\sum K_p \geqslant 18$, and $\Delta(\sum K_p \geqslant 10)$, as our measurements on June 14, 1967, and October 27, 1967.

While the measurement on July 9, 1968 yields the electron flux value for the quiet magnetosphere and the measurements on June 14, 1967 and October 27, 1967 yield the value for the disturbed magnetosphere, the measurements on July 6, 1967, October 8, 1968, and November 19, 1968 represent essentially an intermediate case: small disturbances took place on the days before the measurement (July 5, 1967, October 7, 1968, November 18, 1968) and terminated by the time of the flight, as indicated by the large negative values of the quantity $\Delta(\sum K_p)$. The time between termination of the "disturbance" and initiation of the measurements was 3 - 18 hours. Spilling was nearly completely terminated and an electron flux state returning to the "normal" state is recorded, although in the 500 - 1500 MeV interval (Figure 9), there is still marked excess above the "normal" state in the measurements on October 8, 1968 and November 19, 1968. /124

Electrons with energy greater than 100 MeV, having Larmor radius > 90 km, can be retained by the Earth's magnetic field, which follows from the fact of recording in the inner radiation belt on the shell with $L \sim 1.5$ of protons with energy $E_p \geq 110$ MeV, whose Larmor radius exceeds 400 km [4].

If the spilling part constitutes $\sim 10^{-2}$ of the trapped flux, the intensity of the latter must be no more than 1 - 10 $(cm^2 \cdot sec \cdot sr)^{-1}$, which is several orders of magnitude less than the electron flux intensity with energy 0.01 - 1 MeV, usually recorded in the radiation belts [27]. It appears that faster and more selective equipment, in comparison with that usually used for analysis of

radiation belt composition [27] is required for recording such flux on the background of considerably larger low-energy electron and energetic proton fluxes.

In conclusion, we wish to express our thanks to E. I. Pobedonostsev, V. A. Petukhov, and I. A. Prishaev for their assistance in carrying out the experiments.

References

1. Grigorov, N. L., Yu. S. Klintsov, V. Ye. Nesterov, I. D. Rapoport, I. A. Savenko and B. M. Yakovlev. Izvestiya AN SSSR, seriya fiz., Vol. 30, 1966, p. 1773.

2. Meyer, P. and R. Vogt. Phys. Rev. Let., Vol. 6, 1961, p. 193.

3. L'Heureux, J. and P. Meyer. Phys. Rev. Let., Vol. 15, 1965, p. 93.

4. Rosser, W. UFN, Vol. 85, 1965, p. 147.

5. Bezus, V. A., A. M. Gal'per, N. L. Grigorov, V. V. Dmitrenko, L. F. Kalinkin, V. G. Kirillov-Ugryumov, B. I. Luchkov, A. S. Melioranskiy, Yu. V. Ozerov, I. L. Rozental', I. A. Savenko and E. M. Shermanzon. Izvestiya AN SSSR, seriya fiz., Vol. 32, 1968, p. 1863.

6. Dmitrenko, V. V. and B. I. Luchkov. Trudy 5-y vsesoyuznoy yezhegodnoy zimney shkoly po kosmofizike (Proceedings of 5th All-Union Annual Winter School on Cosmophysics). Apatites, Polar Geophysical Institute of the Kola Branch of the Academy of Sciences of the USSR, 1968, p. 163.

7. Bezus, V. A., A. M. Gal'per, V. V. Dmitrenko, V. G. Kirillov-Ugryumov, B. I. Luchkov, Yu. V. Ozerov, I. L. Rozental', E. M. Shermanzon, N. L. Grigorov, L. F. Kalinkin, A. S. Melioranskiy and I. A. Savenko. Geomagnetizm i aeronomiya, Vol. 9, 1969, p. 540.

8. Gal'per, A. M. and B. I. Luchkov. Trudy 6-y vsesoyuznoy yezhegodnoy aimney shkoly po kosmofizike (Proceedings of 6th All-Union Annual Winter School on Cosmophysics). Apatites, Polar Geophysical Institute of the Kola Branch of the Academy of Sciences of the USSR, 1969, p. 132.

9. Bezus, V. A., A. M. Gal'per, N. L. Grigorov, V. V. Dmitrenko, L. F. Kalinkin, V. G. Kirillov-Ugryumov, B. I. Luchkov, A. S. Melioranskiy, Yu. V. Ozerov, I. L. Rozental', I. A. Savenko and E. M. Shermanzon. Collection: Elementarnye chastitsy i kosmicheskiye luchy (Elementary Particles and Cosmic Rays). Moscow, Atomizdat Press, Vol. 2, 1969, p. 3. /125

10. Bezus, V. A., A. M. Gal'per, N. L. Grigorov, V. V. Dmitrenko, L. F. Kalinkin, V. G. Kirillov-Urgyumov, B. I Luchkov, A. S. Melioranskiy, Yu. V. Ozerov, I. A. Savenko, I. L. Rozental' and E. M. Shermanzon. Izvestiya AN SSSR, seriya fiz., Vol. 33, 1969, p. 1827.

11. Bezus, V. A., A. M. Gal'per, V.V. Dmitrenko, V. G. Kirillov-Ugryumov, B. I. Luchkov, E. M. Shermanzon, Yu. V. Ozerov, I. L. Rosental', N. L. Grigorov, L. F. Kalinkin, A. S. Melioranskiy and I. A. Savenko. Proc. of XI Intern. Conf. on Cosmic Rays, 1969, Budapest. Acta Phys. Acad. Sci. Hung., Vol. 29, Suppl. 1, 1970, p. 761.

12. Gal'per, A. M., N. L. Grigorov, L. F. Kalinkin, V. G. Kirillov-Ugryumov, B. I. Luchkov, A. S. Melioranskiy, Yu. V. Ozerov, I. A. Savenko, I. L. Rozental' and E. M. Shermanzon. PTE, No. 3, 1969, p. 78.

13. Bezus, V. A., A. M. Gal'per, V. V. Dmitrenko, A. V. Kurochkin, B. I. Luchkov, Yu. V. Ozerov, E. M. Shermanzon and Yu. T. Yurkin. PTE, No. 3, 1969, p. 52.

14. Okuda, H. and I. Iamamoto. Report Ionosp. Space Res. Japan, Vol. 19, 1965, p. 322.

15. Jokipii, J. K., J. L'Heureux and P. Meyer. Journ. Geophys. Res., Vol. 72, 1967, p. 4375.

16. Webber, W. R. Journ. Geophys. Res., Vol. 73, 1968, p. 4905.

17. Verma, C. D. Journ. Geophys. Res., Vol. 72, 1967, p. 915.

18. Charakhch'yan, A. N. and T. N. Charakhch'yan. ZhETF, Vol. 35, 1958, p. 1088.

19. L'Heureux, J. Astrophys. J., Vol. 148, 1967, p. 399.

20. Webber, W. R. and Ch. Chotkowski. Journ. Geophys. Res., Vol. 72, 1967, p. 2783.

21. Simnet, G. M. Planetary and Space Science, Vol. 15, 1967, p. 1787.

22. Fanselow, J. L. Astrophys. J., Vol. 152, 1968, p. 783.

23. Israel, M. H. and R. E. Vogt. Phys. Rev. Let., Vol. 20, 1968, p. 1053.

24. Bewermann, K. P., C. J. Rise, E. C. Stone and R. E. Vogt. Phys. Rev. Let., Vol. 22, 1969, p. 412.

25. Schmoker, J. W. and J. A. Earl. Phys. Rev., Vol. 138, 1965, p. D-300.

26. Bland, C. J. Space Res., Vol. 5, 1965, p. 618.

27. Gorn, L. S. and B. I. Khazanov. UFN, Vol. 95, 1968, p. 353.

STUDY OF CHEMICAL COMPOSITION AND ENERGY SPECTRA OF GALACTIC COSMIC RAYS ABOARD AES

N. L. Grigorov, N. N. Volodichev, I. A. Savenko, and A. A. Suslov

Nuclei heavier than protons in cosmic rays were first discovered in 1947 by groups of researchers at Minnesota and Rochester Universities. Using a nuclear emulsion and Wilson chamber installed aboard balloons, they found in the primary flux nuclei of various elements up to charge ~ 40 [1, 2]. Since that time, the chemical composition and energy spectra of multiply charged primary cosmic radiation nuclei have become the objects of intense study. /126

In the present article, we discuss the result of measurements of nuclei fluxes with charges $Z \geq 1, 2, 4, 6, 16$ of primary cosmic rays of moderate energy, obtained aboard the Proton 2 cosmic station using an SEZ-1 Cherenkov spectrometer [3] in orbital segments with known satellite orientation. We selected trajectory segments in which the satellite rotated about its axes with rate not exceeding $1 - 2$ deg/sec^{-1}, which made it possible to calculate the cutoff geomagnetic rigidity values to within $\pm 10\%$. The rigidity values were calculated from the data of [4]. Among the available data, these conditions are satisfied by 16 measurement seances, lasting approximately 12 hours each. For the analysis, we selected data obtained

without instrument shading by the Earth. Table 1 shows the numbers of nuclei of the various groups recorded in the 16 measurement seances in the geomagnetic rigidity interval 3 - 16 GeV/c, and the time the satellite was in the no-shading zone. We note that the satellite was in this zone for less than 20% of the time.

TABLE 1*

t, hrs	N ($Z \geqslant 1$)	N ($Z \geqslant 2$)	N ($Z \geqslant 4$)	N ($Z \geqslant 6$)	N ($Z \geqslant 16$)
10,0	475 800	58 382	8732	6065	501

*Translator's note: Commas represent decimal points.

1. Primary Nuclear Group Flux Relations

The experimental data presented in this study were obtained during nearly a month of instrument operation. Therefore, we must be certain that in the course of this time the instrument operated stably, and that the same nuclear groups were measured. The intensity of the various nuclear groups measured by the instrument during this period can serve as a control of instrument operation. Since the satellite was not oriented and performed random rotations around its axes, we determined the average intensity over a quite long time interval in order to exclude the influence of instrument inlet aperture shielding by the Earth. Figure 1 shows the dependence of the averaged — with respect to direction and time (approximately a day) — intensity of nuclei with $Z \geqslant 1$, $Z \geqslant 2$, $Z \geqslant 4$, $Z \geqslant 6$ and $Z \geqslant 16$, on time in the course of satellite orbits 1 - 631. The statistical errors at each point in the scale of the figure do not exceed the dimensions of the points. The filled points were obtained by averaging the data over half a day, since information for the other half of the day was not available for one reason or another. We see that for the group $Z \geq 1$, this time is not sufficient, apparently because of the fact that in this group the primary nuclei are supplemented by secondary particles, whose distribution with respect to latitude and direction

/127

differs from the distribution for the primary particles [5 - 7]. Nevertheless, the mean square deviations of the day-long average intensities from the mean intensity values for each nuclear group do not exceed 1%. The constandy of the intensities for all the nuclear groups indicates quite convincingly stable values of the photomultiplier electrical thresholds and gain in the course of the long measurement time period.

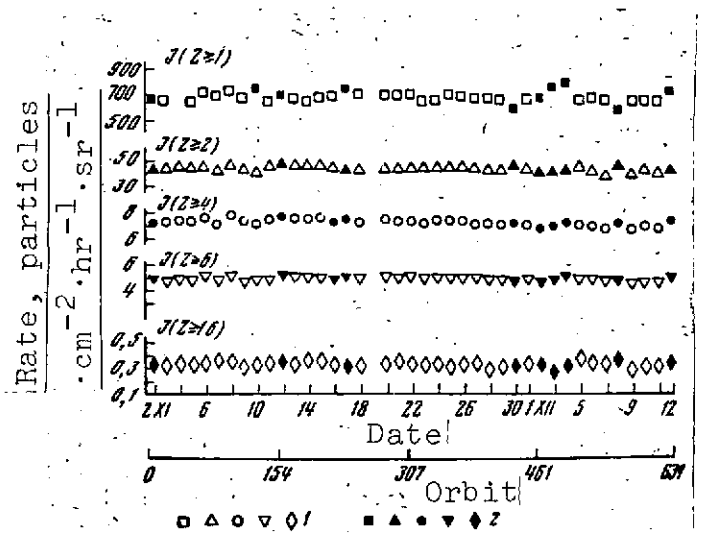

Figure 1. Dependence of averaged intensity of various nuclear groups on time in the course of orbits 1 - 631 of the Proton 2 AES:

1 — day-long average; 2 — half-day average

The evidence of stable instrument operation makes it possible to examine the data obtained by averaging them over a long time interval. Table 2 shows the average nuclear group flux ratios

TABLE 2*

R, GeV/c	$N(Z\geq 2)/N(Z\geq 6)$	$N(Z\geq 2)/N(Z\geq 16)$
3—6	10,6±0,2	113±10
6—10	10,6±0,3	123±21
10—16	11,0±0,5	91±9

*Translator's note: Commas represent decimal points.

$N(Z\geq 2)/N(Z\geq 6)$ and $N(Z\geq 2)/N(Z\geq 16)$ during 16 measurement seances, and the mean square deviations from the average values in each cutoff geomagnetic rigidity R range. Corrections for distortions due to the threshold devices and edge effects [8] are introduced into the ratios. We see that, to within experimental errors, the ratios of

the fluxes of nuclear groups with $Z \geqslant 2$, $Z \geqslant 6$, $Z \geqslant 16$ do not change with rigidity increase from 3 to 16 GeV/c.

2. Primary Cosmic Ray Nuclei Rigidity and Intensity Spectra

Using the data obtained, we plotted the integral rigidity spectra for particles with $Z \geqslant 1$, $Z \geqslant 2$, $Z \geqslant 6$, and $Z \geqslant 16$ (Figure 2). Here, the intensity values were determined by averaging in the threshold rigidity intervals 1 - 3; 3 - 6; 6 - 10; and 10 - 16 GeV/c the intensities obtained during the 16 measurement seances. In Figure 2, the intensity values found in this way lie in the middle of the corresponding rigidity intervals. An exception are the intensities determined for the rigidity 1 - 3 GeV/c, which relate to the effective rigidity values determined by the instrument threshold devices. Table 3 shows the nuclear group intensities obtained for kinetic energies E_{kin}, corresponding to the effective rigidity values.

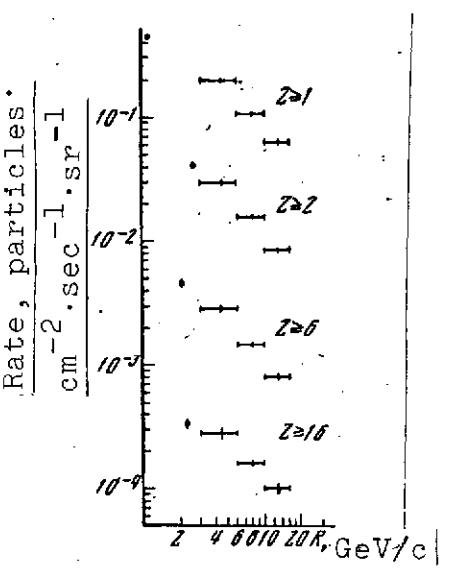

Figure 2. Integral rigidity spectra for particles with different charges

/129

The integral rigidity spectra exponents $\gamma - 1$, determined from our data

TABLE 3*

Nuclear group	E_{kin}, GeV/nuc	Particle rate, $m^{-2} \cdot sec^{-1} \cdot sr^{-1}$
$Z \geqslant 1$	$\gtrsim 0,5$	4420±80
$Z \geqslant 2$	$\gtrsim 0,7$	430±10
$Z \geqslant 6$	$\gtrsim 0,5$	47±2
$Z \geqslant 16$	$\gtrsim 0,6$	3,3±0,2

*Translator's note: Commas represent decimal points.

in the interval 6 - 16 GeV/c, are equal to 1.3 $\pm$ 0.1 for the nuclear groups with $Z \geq 2$ and $Z \geq 6$; 1.1 $\pm$ 0.1 for the group with $Z \geq 1$; and 1.0 $\pm$ 0.3 for the group with $Z \geq 16$. The errors of the $\gamma - 1$ values were due to the mean-square deviation of the intensities obtained in each measurement seance from the averaged intensity values. The somewhat smaller slope of the spectrum of particles with $Z \geq 1$, in comparison with the slope of the spectra of nuclei with $Z \geq 2$ and $Z \geq 6$, is apparently due to secondary particles, whose relative contribution to the primary nuclei fluxes increases with decrease of the latitude [5]. The reduction of the spectrum slope of nuclei with $Z \geq 16$ can be explained by the inadequate statistical basis for these nuclei. Considering these remarks, we can conclude that the integral rigidity spectra for all the primary nuclear groups represented here are similar, and the exponents $\gamma - 1$ of the integral spectra for these groups satisfy the value 1.3 $\pm$ 0.1. This agrees well with the $\gamma - 1$ values published in the literature for threshold rigidities 3 - 16 GeV/c [5, 9, 10].

3. Dependence of Nuclear Group Flux Ratio $L (3 \leq Z \leq 5)/S (Z \geq 6)$ on Rigidity

The light nuclear group fluxes $L (3 \leq Z \leq 5)$ were determined from the difference of the fluxes of nuclear groups with $Z \geq 4$ and $Z \geq 6$, with account for nuclear abundance in this group [5].

According to the calculations, the probability of recording α-particles after a threshold recording nuclei with $Z \geq 4$ did not exceed 10^{-7}. Table 4 compares the average nuclear group L and S flux ratios during 13 measurement seances for different threshold rigidity intervals. Corrections for distortions due to the threshold devices and edge effects were introduced into these ratios [8]. We /130 see from Table 4 that the quantity L/S increases from 0.28 $\pm$ 0.02 to 0.42 $\pm$ 0.03 with increase of the geomagnetic cutoff rigidity.

4. Discussion of Measurement Results

As noted above, the channel intended for registering particles with $Z \geq 1$ recorded both primary protons and nuclei and secondary singly charged particles. Figure 3 shows the integral rigidity spectra for these particles measured aboard the Proton 2 AES during orbits 45 - 52 of the satellite trajectory (points) and aboard the Kosmos 137 AES (solid curve) [11]. The measurements aboard Kosmos 137 were also made by a Cherenkov counter, a year after the measurements aboard Proton 2. With account for the statistical errors, we can consider that the results of the two series of measurements are quite close. The statistical error for the measurements aboard Kosmos 137 is shown below the solid curve.

TABLE 4*

R, GeV/c	L/S
3—6	0,28±0,02
6—10	0,39±0,03
10—16	0,42±0,03

*Translator's note: Commas represent decimal points.

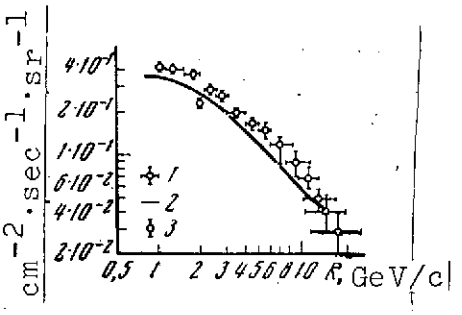

Figure 3. Integral rigidity spectra for particles with charge $Z \geq 1$:

1 — Proton 2; 2 — Kosmos 137; 3 — statistical error of measurements aboard Kosmos 137

The resulting integral spectra and nuclear group ratios as functions of rigidity indicate similarity of the integral spectra of nuclear groups with $Z \geq 2$, 6, 16 in the 3 - 16 GeV/c interval, which confirms the preliminary conclusions drawn previously on the basis of analysis of the information obtained aboard the Proton 1 and 2 AES [12 - 15]. The same conclusion has been drawn in several studies performed aboard balloons and satellites [5, 9, 16, 17]. However, studies have recently appeared in which the possibility of difference in the spectra of the different moderate-energy nuclear groups is noted.

Specifically, in [10, 18, 19], the values 1.32 ± 0.05; 1.40 ± 0.07; 1.46 ± 0.14, respectively, were obtained for the integral

spectra exponent of the nuclei of helium, the M-group ($6 \leq Z \leq 9$) and the VH-group ($Z \geq 20$) for 3 - 12 GeV/c geomagnetic cutoff rigidity. The authors of these studies state that their results do not exclude systematic increase of multiply charged nuclei spectra slope with increase of the charge. A similar conclusion was reached previously in [20], but it was not confirmed by later experimental data. If the conclusions drawn in [10, 18, 19, 20] are confirmed, a question inevitably arises: is the difference in the nuclear group spectra embedded during spectra formation in the cosmic ray sources, or is this the result of primary nuclei interaction with the hydrogen of the interstellar medium? Thus, improved determination of multiply charged nuclei is an urgent problem today.

The conclusion on similarity of the integral spectra of the various nuclear groups in the moderate-energy interval drawn in the present article confirms qualitatively the possibility of existence of the cumulative acceleration mechanism proposed in [21], in which the particles acquire identical momenta per unit charge, i.e., they are accelerated to the same rigidity, and their rigidity spectra are thus similar. The values obtained for the integral spectra exponents 1.3 ± 0.1 agree with the values 1.5 ± 0.2 given in the literature [5, 9, 10]. The values presented for $N (Z \geq 2)/N (Z \geq 6)$ and $N (Z \geq 2)/N (Z \geq 16)$ are close to the flux ratios of these groups for moderate energies obtained by other authors [5, 10, 19].

The intensity values for the nuclear groups obtained in the present study exceed, by a factor of two or more, the intensities measured by several investigators in the same time period aboard balloons [10, 18, 19, 22 - 24], and aboard "distant" satellites [25 - 28], although there are exceptions [25, 26, 29, 30].

The data on nuclear group fluxes obtained aboard "nearby" satellites (altitudes $\sim$ 200 - 600 km) are scanty. However, we should note the study [17], in which high intensities of the various nuclear groups were also obtained.

The high (in comparison with the galactic cosmic ray nuclear flux values accepted in the literature) intensity values obtained aboard the Proton 2 satellite can be explained, for example, by trapping of primary cosmic radiation nuclei into quasiperiodic orbits. An argument supporting this assumption is the similarity of the different nuclear group flux magnitude ratios from the Proton 2 satellite data to the corresponding ratios for galactic cosmic rays.

However, the instrument aboard the Proton 2 AES did not permit differentiating single particles from "shower" events. Therefore, the high intensities obtained may be due to recording of showers, although quantitative explanation of the effect, in this case, encounters major difficulties. We should emphasize that the high intensities measured aboard the Proton 2 AES for the different nuclear groups retain constant values over a long time period ($\sim$ 1.5 months). It seems to us that this effect is of considerable interest, and new experiments are required to clarify its nature. /132

The values for L/S = 0.28 - 0.42 in the present study agree with the results of several studies [10, 31 - 38], in which the values 0.2 - 0.4 were obtained for this ratio, which corresponds to thickness of matter traversed by the primary nuclei equal to 2 - 10 g/cm^2 [5, 9, 33] and cosmic ray lifetime $\sim 3 \cdot 10^8$ [9].

The increase of the nuclear group L and S flux ratio noted in the present study with geomagnetic cutoff rigidity increase (Figure 4) agrees qualitatively with the results of [24], in which increase of this ratio (more precisely L/M) from 0.18 $\pm$ 0.05 to 0.30 $\pm$ 0.03, with energy increase in the interval from 100 to more than 600 MeV/nuc, was obtained. In some studies [31, 32], no change of L/S with energy was found, while in [10, 33 - 38], decrease of this ratio with energy increase is noted for moderate energies, although, if we consider the measurement accuracy, it is more natural to speak in [33, 35, 36] of constancy of

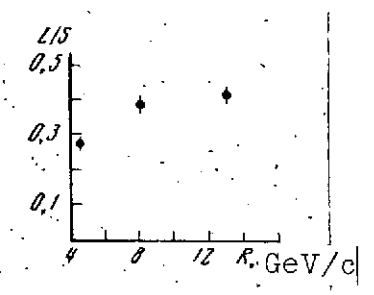

Figure 4. Ratio L/S versus rigidity

the ratio L/S with energy change. We should also note that study of the dependence of L/S on energy in the moderate-energy interval has been carried out aboard balloons, except for our investigation.

More precise determination of the nuclear group L and S flux ratio energy dependence is important for solving the question of selecting the particular cosmic ray origin model. If it is found that L/S increases with energy increase, this may support the unsteady galactic model, in accord with which most cosmic rays are formed during powerful and rare explosions in the galactic nucleus region. The frequency of such explosions is no greater than once in $\sim 10^8$ years [9, 39 - 41].

Decrease of L/S with energy increase will be an argument against the nonstationary galactic cosmic ray origin model [39, 40, 42]. Such dependence of L/S on energy can occur, for example, if nuclei /133
with low rigidity enter the trap in the source region, passing through as a result of the larger amount of matter, and in this case more L nuclei are formed by fragmentation [43], or, if the slow cosmic rays travel basically in the disk region, where the average interstellar gas density is higher, while the relativistic particles spend a significant part of the time in the more rarefied halo [40]. The question of acceptability of any particular model can be finally resolved after accounting for the ionization losses during primary nuclei propagation in interstellar space and establishing the fragmentation paramater energy dependence [39, 40, 42].

5. Prospects for Investigation

Several studies [5, 9] of Soviet and foreign experimenters have been devoted to investigation of primary cosmic ray composition and energy spectra. Prior to the advent of artificial satellites and space rockets, experiments of this sort were performed aboard balloons (primarily by the foreign investigators). These measurements made it possible to determine the energy spectra of the various nuclear groups as a function of primary cosmic ray charges, obtain

information on the chemical composition of nuclei of solar origin in the low-energy interval during powerful chromospheric bursts on the sun.

However, in view of the small number of balloon flights and large measurement errors, the data on cosmic ray nuclei chemical composition and energy spectra were far more scanty than the corresponding data on the cosmic ray proton component. This is explained by the fact that, in addition to the large statistical measurement errors associated with the small magnitudes of the cosmic ray multiply charged component fluxes, errors in comparing the data of different authors, obtained using different instruments, are possible. Additional discrepancies resulting from such comparison arise when extrapolating the flux values obtained from balloon experiments to the upper edge of the atmosphere.

When conducting measurements beyond the limits of the Earth's atmosphere, i.e., aboard satellites and space rockets, the drawbacks noted above, associated with balloon experiments, disappear to a considerable degree and, moreover, it becomes possible to conduct quite long-term and continuous observations of cosmic ray intensity. Such observations are very important in obtaining statistically valid measurement results when studying intensities in comparatively narrow energy intervals, or when recording heavy nuclei and very-high energy particles, when the intensity of the particles being recorded is very low.

From the data on primary cosmic ray chemical composition and /134
energy spectra and their changes as a function of time, we can obtain valuable conclusions on the processes of cosmic ray generation in the sources, propagation conditions in cosmic space, and the properties of this space (magnetic field structure, amount of matter traversed by the cosmic ray particles, and so on).

Most of the data published in the literature on primary cosmic ray composition and energy spectra agree satisfactorily with one another only for the nuclear groups based on charge. However, even

for the intensity ratios of the elements within a given nuclear group, the difference may reach a factor of two or more. At the same time, it is necessary to know these ratios for the various energies with far better accuracy, in order to analyze the correctness of any particular theory of cosmic ray origin, the mechanism of their generation, and in order to make a more detailed study of the conditions in cosmic space.

In order to solve these problems, it is necessary to make measurements using an instrument having the best possible charge amplitude resolution when recording cosmic ray nuclei with different charges Z.

Study of primary cosmic ray chemical composition and energy spectra is carried out by various methods: photoemulsions, n - p detectors, scintillation and Cherenkov counters, calorimeters, and so on. However, in the geomagnetic energy interval, use of scintillation and Cherenkov counters is advantageous, since in this case they have the following advantages, in comparison with the other methods:

1) possibility of creating adequately wide-aperture instruments with geometric factor $\Gamma \gtrsim 100$ cm^2 · sr, along with comparatively simple fabrication, adjustment, and measurement result analysis; as was noted above, this possibility is important in obtaining statistically valid measurement results when recording low-intensity radiations;

2) directivity of the Cherenkov radiation and insensitivity of the Cherenkov detector to low-energy particles, specifically, nuclear disintegrations; these characteristics make it possible to avoid the background of low-energy particles whose intensities may exceed by several orders that of the radiation being studied.

One of the disadvantages of the scintillation-Cherenkov counter method, in comparison, for example, with the photoemulsion method, is the "nonvisuality" of the events being recorded which, however,

can be compensated for to a considerable degree if differential amplitude analysis of the nuclei, based on individual charges, is made. If such an analysis is not made, and recording of the cosmic ray nuclear groups is accomplished by integral threshold devices (as /135 was the case in the SEZ-1 instruments aboard the Proton 1 and 2 satellites), then for correct interpretation of the measurement results in this case, proper correlation of the triggering threshold level in the given integral channel with the "threshold" value of the recorded particle charge is necessary.

The amplitude resolution of the recorded particles, with regard to charge when using the scintillation-Cherenkov counter method, can also be quite good. Thus, under laboratory conditions, when using instruments of the SEZ-1 type, the amplitude distributions of singly charged relativistic particles were obtained in the Cherenkov counter with relative halfwidth $p \approx 50\%$. For relativistic particles having charge Z, the distribution relative halfwidth will decrease in inverse proportion to Z. However, in order for such a relationship to be realized, it is necessary, when using in the Cherenkov counter "large" photomultipliers of the PM-49 type, to select photomultipliers with adequate uniformity of the sensitivity over the photocathode, and screen the photomultiplier from the Earth's magnetic field influence by a magnetic shield. When using as Cherenkov light detectors "small" photomultipliers, in which the photocathode dimensions and distance from the photocathode to the first dynode are much less than for the PM-49, it is necessary to ensure uniform light collection, regardless of the point of recorded particle passage in the detector.

It should be noted that the difficulties noted above are not fundamental. Simple calculations show that elimination of these difficulties, along with use of "good" instrument geometry, is quite possible with reasonable instrument dimensions, and makes it possible to carry out differential amplitude analysis of the cosmic ray nuclei on the basis of individual charges, up to and including the iron nuclear group. However, in this case it is necessary to perform simultaneous differential analysis of the recorded nuclei on the

basis of charge, using both Cherenkov and scintillation counters in order to avoid ambiguity in identification of events associated with Cherenkov radiation intensity dependence on energy near its "threshold".

An instrument of the SEZ-1 type, with use of a linear amplitude analyzer for nuclear charge analysis, was installed aboard the Cosmos 228 satellite. Preliminary results of measurements obtained using this instrument were presented in [44].

In conclusion, the authors wish to express their thanks to V. V. Beletskiy, I. G. Khatskevich, V. V. Golubkov, A. F. Sidorov, and I. A. Buterina for analysis of the Proton 2 AES orientation data.

References

1. Freier, Ph., E. Lofgren, E. Ney, F. Oppenheimer, H. Bradt and B. Peters. Phys. Rev., Vol. 74, 1948, p. 213. /136

2. Freier, Ph., E. Lofgren, E. Ney and F. Oppenheimer. Phys. Rev., Vol. 74, 1948, p. 1818.

3. Volodichev, N. N., N. L. Grigorov, O. V. Kislyakov, Yu. V. Mineyev, V. Ye. Nesterov, O. Yu. Nechayev, I. D. Rapoport, I. A. Savenko, A. V. Smirnov and B. M. Yakovlev. Kosmicheskiye issledovaniya, Vol. 5, No. 1, 1967, p. 119.

4. Quenby, J. and G. T. Wenk. Philos. Mag., Vol. 7, 1962, p. 1457.

5. Webber, W. R. Handbuch der Physik, 46/2, 1967, p. 181.

6. Murayama, T. Planet. Space Sci., Vol. 15, 1967, pp. 1169 - 1180.

7. Volodichev, N. N., N. L. Grigorov, V. Ye. Nesterov, I. D. Rapoport, I. I. Savenko and B. M. Yakovlev. Izvestiya AN SSSR, seriya fiz., Vol. 30, No. 11, 1966, p. 1763.

8. Volodichev, N. N. Dissertation, Moscow, NIIYaF, Moscow State University, 1969.

9. Ginzburg, V. L. and S. I. Syrovatskiy. Proiskhozhdeniye kosmicheskikh luchey (Origin of Cosmic Rays). Moscow, Izdatel'stvo AN SSSR, 1963.

10. Webber, W. R. and J. F. Ormes. Journ. Geophys. Res., Vol. 72, 1967, p. 5957.

11. Vernov, S. N., Ye. V. Gorchakov, I. V. Getselev, P. P. Ignat'yev and M. V. Ternovskaya. Kosmicheskiye issledovaniya, Vol. 7, No. 2, 1969, p. 273.

12. Volodichev, N. N., N. L. Grigorov, V. Ye. Nesterov, I. D. Rapoport, I. A. Savenko, G. A. Skuridin and A. F. Titenkov. Doklad na vsesoyuznoy konferentsii po fizike kosmicheskikh luchey v Alma-ate v 1966 (Report at All-Union Conference on Cosmic Ray Physics at Alma Ata in 1966). Preprint, Moscow, NIIYaF, Moscow State University, 1966.

13. Volodichev, N. N., N. L. Grigorov, V. Ye. Nesterov, O. Yu. Nechayev, A. N. Podorol'skiy, I. D. Rapoport and I. A. Savenko. Kosmicheskiye issledovaniya, Vol. 5, No. 1, 1967, p. 115.

14. Volodichev, N. N., N. L. Grigorov, V. Ye. Nesterov, I. D. Rapoport and I. A. Savenko. Izvestiya AN SSSR, seriya fiz., Vol. 31, No. 8, 1967, p. 1229.

15. Volodichev, N. N., N. L. Grigorov and I. A. Savenko. Kosmicheskiye issledovaniya, Vol. 5, No. 3, 1967, p. 436.

16. Waddington, C. J. Prog. Nuclear Phys., Vol. 8, 1960, p. 1.

17. Ginzburg, V. L., L. V. Kurnosova, L. A. Razorenov and M. I. Fradkin. UFN, Vol. 82, 1964, p. 585.

18. Webber, W. R., J. F. Ormes and T. von Rosenvinge. IX PICCR, London, Vol. 1, 1965, p. 407.

19. Webber, W. R. IX PICCR, London, Vol. 1, 1965, p. 403.

20. Singer, S. F. Progr. Elem. Particle and Cosmic Ray Phys., Vol. 4, Amsterdam, 1958.

21. Syrovatskiy, S. I. Astronomicheskiy zhurnal, Vol. 43, 1966, p. 340.

22. Ormes, J. F. and W. R. Webber. IX PICCR, London, Vol. 1, 1965, p. 349.

23. Fan, C. Y., G. Gloeckler and J. A. Simpson. Canad. J. Phys., Vol. 46, 1968, p. 548.

24. Balasubrahmanyan, V. K., et al. IX PICCR, London, Vol. 1, 1965, p. 427.

25. Blokh, Ya. L., L. I. Dorman', L. V. Kurnosova, V. I. Logachev, G. F. Platonov, L. A. Razorenov, V. G. Sinitsyna, A. S. Suslov and M. I. Fradkin. Issledovaniya kosmicheskogo prostranstva (Study of Cosmic Space). Moscow "Nauka" Press, 1965, p. 514.

26. Suslov, A. A. Dissertation, Moscow, FIAN SSSR, 1966.

27. Lezniak, J. A., W. R. Webber and J. Rockstroh. XIth Int. Conf. on Cosmic Rays. Budapest, 1969 (Mo-68).

28. Hsieh, K. C. Univ. of Chicago, Preprint EFI 69-26, 1969.

29. Friedlander, M. W. and J. Klarmann. Planet. Space Sci., Vol. 15, 1967, pp. 619 - 625.

30. Fody, S. A., M. W. Friedlander, H. Hasegawa and J. Klarmann. Planet. Space Sci., Vol. 16, 1968, pp. 253 - 254.

31. McDonald, F. B. and W. R. Webber. Journ. Geophys. Res., Vol. 67, 1962, p. 2119.

32. Balasubrahmanyan, V. K. and F. B. McDonald. Journ. Geophys. Res., Vol. 69, 1964, p. 3289.

33. Aizu, H., Y. Fujimoto, S. Hasegawa, M. Koshiba, I. Mito, J. Nishimura and K. Yokoi. Progress in Theor. Phys. Suppl., Vol. 16, 1960, p. 54.

34. Koshiba, M., E. Lohrman, H. Aizu and E. Tamai. Phys. Rev., Vol. 131, 1963, p. 2692.

35. Evans, D. E. Nuovo Cimento, Vol. 27, 1963, p. 394. /137

36. Webber, W. R. and J. F. Ormes. VIII PICCR, Jaipur, 1964.

37. Appa Rao, M. V. Nuovo Cimento, Vol. 32, 1964, p. 1158.

38. Badhwar, G. D., et al. Journ. Geophys. Res., Vol. 79, 1965, p. 1005.

39. Ginzburg, V. L. and S. I. Syrovatskiy. Izvestiya AN SSSR, seriya fiz., Vol. 29, No. 10, 1965, p. 1819.

40. Ginzburg, V. L. and S. I. Syrovatskiy. UFN, Vol. 88, 1966, p. 485.

41. Charakhch'yan, A. N. and T. N. Charakch'yan. Geomagnetizm i aeronomiya, Vol. 4, 1964, p. 643.

42. Kurnosova, L. V., L. A. Rezorenov and M. I. Fradkin. Izvestiya AN SSSR, seriya fiz., Vol. 29, No. 10, 1965, p. 1846.

43. Kaplon, M. F. and G. Skadron. Nuovo Cimento, Vol. 34, 1964, p. 1687.

44. Volodichev, N. N., N. L. Grigorov, O. Yu. Nechayev, I. A. Savenko, A. A. Suslov and R. M. Tul'skiy. Geomagnetizm i aeronomiya, Vol. 11, 1971, p. 144.

PROCESSING PROTON SPACE STATION SCIENTIFIC INFORMATION

V. V. Akimov, V. V. Beletskiy, V. V. Golubkov,
G. N. Zlotin, S. I. Karmanov, I. N. Kiknadze,
V. Ye. Nesterov, V. M. Pokras, V. L. Prokhin,
I. D. Rapoport, and I. G. Khatskevich

Introduction

The primary objective of the experimenter in conducting measurements aboard satellites is rapid and effective acquisition of information on the measured parameters. Leaving aside questions associated with formulation of the scientific experiment itself and quality (or validity) of measurement of the parameters being investigated by the scientific apparatus sensors, we shall examine those characteristics which are associated with the specifics of conducting experiments aboard satellites and must be considered in processing the scientific information. /138

The questions are associated both with the nature of the measured parameter output to the telemetry system, technique of data transmission and reception by the ground stations, techniques for correlating the measured parameters with the time and the data on satellite motion along its orbit and around its center of mass (i.e., questions of the design of certain satellite systems), and with the methods for processing the scientific information using ground-based

special-purpose and general-purpose computers. These characteristics are general, and must be considered in the design of most scientific experiments aboard satellites. Therefore, it seems to us that the experience accumulated in planning and carrying out scientific data processing for the Proton AES will be of considerable interest to both the physicist-experimenters and the satellite system designers.

1. Proton AES Experiment Formulation and Data Processing

The basic task posed in carrying out scientific experiments aboard the Proton AES was to ensure interaction between the scientific equipment, satellite systems, and ground processing facilities which would permit rapid automatic analysis of all the information. Here, all the indicated elements were considered component parts of the Proton AES integrated instrumentation-information complex, including: scientific instrument sensors; system for gathering information and feeding it to the telemetry system; telemetry system proper; scientific measurement support system (timing, trajectory, and orientation measurement); the systems for receiving, recording, decoding, and inputting the telemetry information to the general-purpose computers; and the data processing system. /139

The first four elements formed the onboard components, and the last two elements — the ground-based components of the satellite instrumentation-information complex.

The scientific equipment description, procedures, and measurement results were reported in [1 - 4]; the characteristic features of instrument indication output to the telemetry system, description of the system for telemetry information input to the computers, and some other elements of the complex are presented below.

We shall note the basic operating characteristics of the Proton AES data measurement complex.

1. The scientific apparatus parameters are recorded every eight seconds continuously throughout the entire flight by a high-scan-rate telemetry system using about 150 channels. The total volume of measurements subject to processing is about 10^7 bits per day, or 10^9 bits during the entire satellite lifetime.

2. Processing of the scientific apparatus parameters requires simultaneous decoding of many channels in each scan frame (the frame is the eight-second cycle, corresponding to scanning all the telemetry channels).

3. Requirement for time correlation, not only of each frame, but also of many channels within the frame.

4. Requirement for correlation of each frame to the navigational data (trajectory and orientation).

5. The Proton satellite is nonorientable, and its orientation is determined by a circular scan optical sensor (accuracy about $\pm 3^\circ$) and a three-component ferrosonde magnetometer. However, statistical reduction of the orientation data is required because of the large measurement errors and inadequate number of measurements.

6. The necessity for storing the raw recording data requires re-recording all the data on synoptic charts.

7. Requirement for hardware tie-in between the telemetry system and the general-purpose computer.

8. Breakdown of the scientific information processing technological cycle into: processing the scientific equipment indications, determinining the navigation parameters, combined processing of the scientific information, and the navigational data.

The designers of this system were faced with two basic tasks: 1) the technical organization task, including organization of the overall processing system and its individual elements; 2) the

scientific methods task, including the development and introduction of methods and programs for processing the scientific information and navigational data. In order to solve these rpoblems, it was necessary to develop: /140

1) methods for machine processing of the radiotelemetry information, including the technique for ground-based recorder data input into the general-purpose digital computers;

2) methods for organizing the multistep process of processing large and varied information streams;

3) method for determining vehicle orientation;

4) rational forms for output of the large volume of numerical data for their use by the experimenters;

5) methods for checking the validity of the results generated in the automatic data reduction process.

To this end, a mathematical support complex consisting of several programs was developed and implemented for the Ural-11 and M-20 general-purpose digital computers:

1) program for input to the Ural-11 general-purpose digital computer of information from the ground-based telemetry system recorders and preparation of the magnetic tape in the format of the given general-purpose digital computer ("Artur" system);

2) program for initial data processing with time correlation and voltage scaling;

3) program for logical processing and output of the instrument indications for the various output groups;

4) program for determining law of satellite motion around the center of mass from the measurement data;

5) program for calculating the navigational parameters at specified moments of time.

As a result of formal division of the information streams into arrays which can be assigned characteristics, serial processing of selected arrays with fixed data format output for each of them was organized. Thus, for each reproduction seance entering for serial processing, a set of volumes was generated with instrument indications — eight books having the same format, which facilitated search for and comparison of the values of the various parameters at the same moments of time.

In the process of debugging the processing system, we developed methods for output of intermediate synoptic materials characterizing the quality and composition of the information ("tabular", "dropout matrix", and "level number" methods), which made possible stage-by-stage checking of the results, and resolution of the question of controlling the course of the subsequent data processing.

II. Techniques for Instrument Indication Output to Telemetry System

The telemetry system transmits a voltage in the range of 0 - 6 V over each of the telemetry channels. This means that the output signals of all the equipment installed aboard the satellite must be presented in the form of discretely or continuously varying voltages. /141 In this case, it is usually necessary that the time during which the output voltages run through the entire variation range be longer than the telemetry channel scan period. Otherwise, it becomes impossible to follow the output voltage variation process.

The information comes from the outputs of the scientific equipment installed aboard the satellite in the form of voltage pulses, formed by the electronic logic circuits and corresponding to the various forms of events recorded by the instruments. The numbers or repetition frequencies of the pulses from all the scientific equipment

outputs must be transmitted over the telemetry system. The pulse repetition frequency is converted into voltage by a rate meter having linear or logarithmic scale. The reconversion from voltage level to rate at the moment of telemetry channel sampling is accomplished on the basis of the rate meter calibration curve.

When transmission of a number of pulses is required, use is made of an output unit consisting of one, two, or three output triggers and a summer. The summer has three inputs, with transmission coefficients such that the application of voltage from the trigger to the first input yields a voltage increment at the summer output of about 0.85 V, application to the second input yields an increment of about 1.7 V, and application to the third input yields an increment of about 3 V. In the absence of voltages at the inputs, the voltage at the summer output is equal to zero. Thus eight discrete voltage levels can appear at the summer output, each of which is uniquely associated with the state of the output triggers. Conversion from level number to trigger state is accomplished with the aid of Table 1.

TABLE 1

Level no.	U_{out}, V	Trigger state at summer inputs			Level no.	U_{out}, V	Trigger state at summer inputs		
		1	2	3			2	2	3
0	0	0	0	0	4	3.4	0	0	1
1	0.85	1	0	0	5	4.25	1	0	1
2	1.7	0	1	0	6	5.1	0	1	1
3	2.55	1	1	0	7	5.95	1	1	1

Figure 1 shows various techniques for connecting the output triggers to the outputs A, B, C of the scientific equipment.

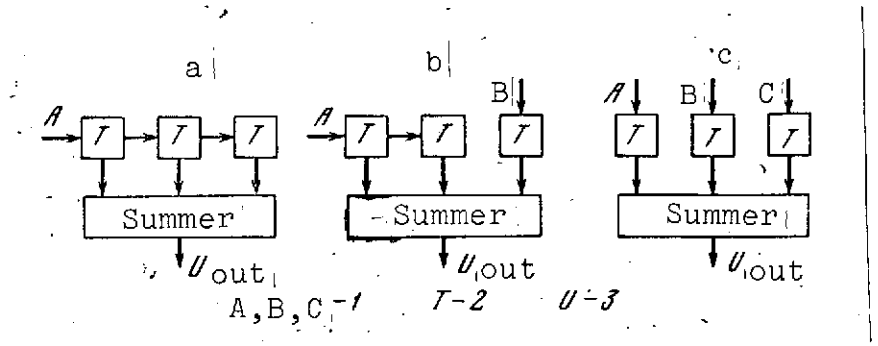

Figure 1. Connection of scientific equipment out uts
a — scientific equipment outputs; b — trigger; c — output to telemetry system

In order to determine the number of pulses arriving from the scientific equipment output during the time between two successive (n^{th} and (n + 1st)| telemetry channel scans, it is necessary to know the number of the voltage levels at the summer output for these scans (N_n and N_{n+1}).|

Conversion from the level numbers N_n and N_{n+1} to number of /142
pulses is accomplished using tables like Table 2, which serve for determining the number of type A pulses, with connection of the output units in the various schemes (Figure 1), respectively.

Each of the output unit connection techniques is characterized by the maximal uniquely reproducible number of pulses between two successive channel scans. For pulses A in schemes a, b, c of Figure 1, the maximal numbers of pulses are equal to 7, 3, 1, respectively. If there is a higher pulse repetition rate, counting losses will occur, leading to distortion of the information. Prescaling of the pulses from the scientific equipment outputs is used to ensure an acceptable pulse repetition rate at the inputs of the output units. Thus, each of the scientific equipment outputs is characterized by: 1) prescaling value; 2) output unit connection technique.

When processing the scientific information, it is necessary to /144
use the data of magnetometers and times installed aboard the satellite. Voltages varying in the 0 - 6 V range are applied to the

TABLE 2

a)

	0	1	2	3	4	5	6	7
0	0	7	6	5	4	3	2	1
1	1	0	7	6	5	4	3	2
2	2	1	0	7	6	5	4	3
3	3	2	1	0	7	6	5	4
4	4	3	2	1	0	7	6	5
5	5	4	3	2	1	0	7	6
6	6	5	4	3	2	1	0	7
7	7	6	5	4	3	2	1	0

b)

	0	1	2	3	4	5	6	7
0	0	3	2	1	0	3	2	1
1	1	0	3	2	1	0	3	2
2	2	1	0	3	2	1	0	3
3	3	2	1	0	3	2	1	0
4	0	3	2	1	0	3	2	1
5	1	0	3	2	1	0	3	2
6	2	1	0	3	2	1	0	3
7	3	2	1	0	3	2	1	0

c)

	1	0	2	3	4	5	6	7
0	0	1	0	1	0	1	0	1
1	1	0	1	0	1	0	1	0
2	0	1	0	1	0	1	0	1
3	1	0	1	0	1	0	1	0
4	0	1	0	1	0	1	0	1
5	1	0	1	0	1	0	1	0
6	0	1	0	1	0	1	0	1
7	1	0	1	0	1	0	1	0

Telemetry system from the magnetometers. With the aid of calibration curves, the voltages can be converted to magnetic field intensity component values.

A voltage of about 5 V appears at the timer output at the end of each one-minute (in the direct transmission mode) or 10-minute (in the memory mode) time interval, and serves as a reference point for time code transmission initiation. In the subsequent 10 timer channel scans, the 10 binary digits of the time code are read out. The value "0" corresponds to 0 V, the value "1" corresponds to $\sim$ 5 V. At the next timer channel scan, the reference for end of time code transmission is read out, expressed by a voltage of $\sim$ 5 V. Between such series of 12 scans, a voltage equal to zero is maintained in the timer channel.

1. General Scheme of Processing System

A general scheme of the Proton data instrumentation and information processing system is shown in Figure 2.

The ground-based telemetry recording magnetic tapes and information on satellite flight control enter the system in the data collection and processing center.

At the system output, the processing results appear in the form of systematized documentation, which form the Data Bank of the given cosmic experiment, and is destined for subsequent storage with repeated access to the data for analysis and scientific interpretation of the measurement values.

We see from the schematic that the information material passes through several processing stages. After systematization of the materials and determining their characteristics, the data processing proceeds in two directions:

1) summary re-recording from the magnetic types, which is used for examination, preliminary analysis, manual processing using simplified programs, and subsequent long-term storage; re-recording is performed on special-purpose computers and individual-channel paper graphs of the voltages are generated; this re-recording is fast and is performed for all measurement seances;

2) frame-by-frame processing of the data on general-purpose digital computers with output of the instrument indications and navigation parameter values for each telemetry system scan point. This processing is considerably more time-consuming, and is performed only for selected measurement seances. The output in tabular form is bound into volumes, also subject to long-term storage.

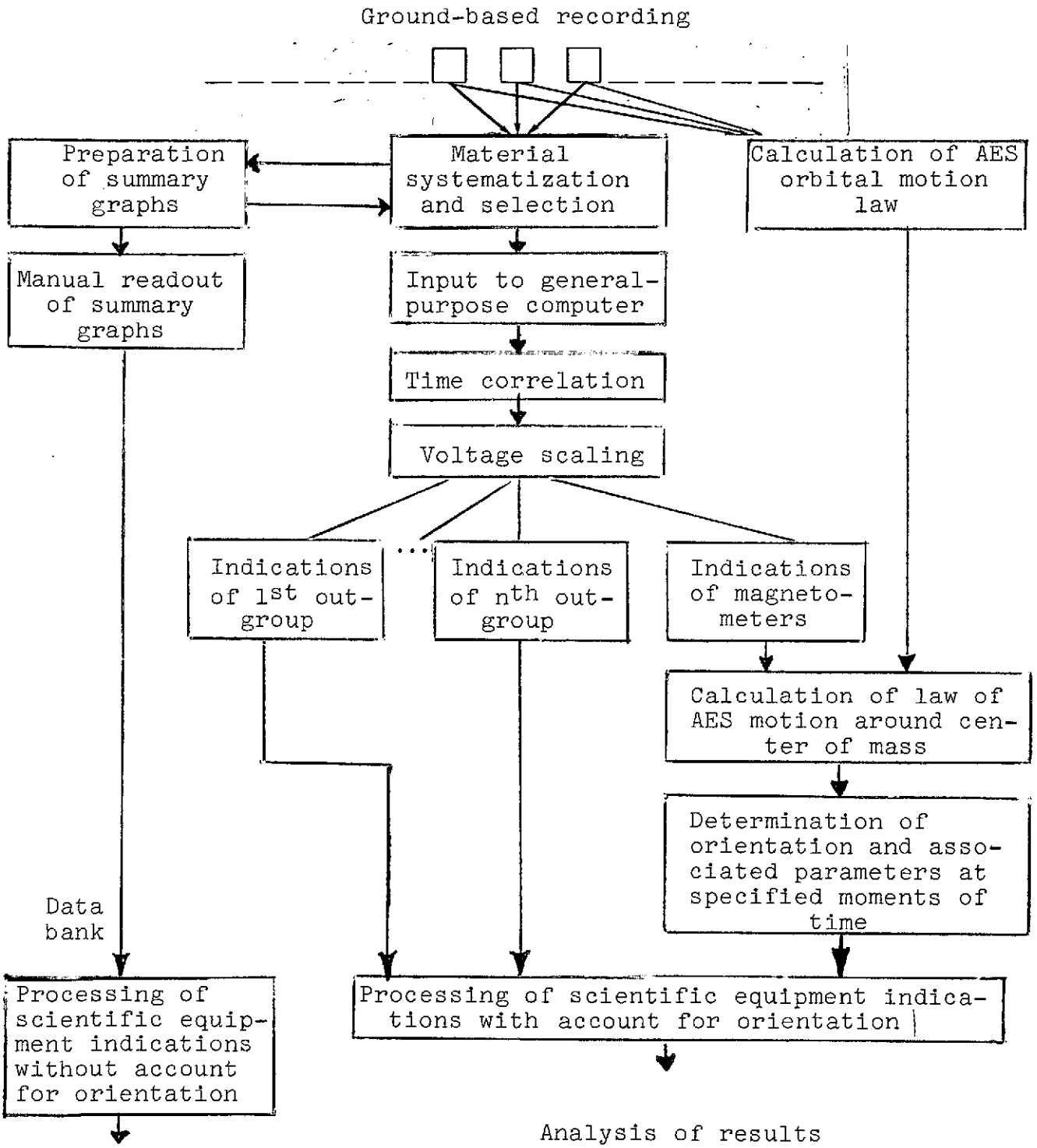

Figure 2. Proton data processing system

2. Telemetry Data Input to General-Purpose Digital Computer and Data Preparation for Processing

The scientific instrument telemetry indications had very little /145
statistical redundancy; therefore, it was necessary to process every telemetry word. This circumstance in itself made it difficult to perform the processing on specialized computers. The great variety and complexity of the algorithms which would have had to be realized during processing excluded the possibility of constructing a complete processing system using special-purpose computers.

In order to process the data on a general-purpose digital computer (GPDC), it was necessary to prepare the data recorded on the radiotelemetry system (RTS) magnetic tape, performing the following steps:

1) input of the data recorded on the radiotelemetry system magnetic types to the GPDC;

2) localization and marking of synchronization dropouts and restoration of the standard telemetry frame structure;

3) compiling reference information tables;

4) representing the radiotelemetry data and additional information in a formalized structure, input of these data to the GPDC magnetic tape;

5) monitoring the quality of the data prepared for processing.

The data input to the GPDC from the magnetic tape was accomplished using the method for direct input of large data arrays recorded on magnetic tapes into GPDC which had been developed at the Institute of Space Studies of the Academy of Sciences of the USSR. This method permitted data input to the computer without any transformation.

Localization and marking of the synchronization dropouts and restoration of the standard telemetry frame structure are necessary for telemetry channel separation and time correlation of the data. In restoring the structure, we used both a priori information on radiotelemetry system frame standard structure and the statistical characteristics of the data being processed. Algorithms were developed which localized synchronization dropouts of up to three telemetry words and detected and marked dropouts of longer durations.

In preparing the data, each array which could be processed independently — one second in the reproduce mode — was provided in the GPDC a table of reference information. This table, generated by the computer, contained information on data quality, time and point of reception, and locations of service marks necessary for subsequent processing. The table also includes information used for automatic tuning of the programs for subsequent processing.

After performing these steps, the data were recorded on the GPDC magnetic tapes in formalized form (Figure 3). This means that the data on the GPDC magnetic tape always has the standard structure, regardless of possible radiotelemetry system magnetic tape structure deviations as a consequence of various interferences, for example, because of dropout or the appearance of redundant telemetry words, dropout of data segments because of magnetic tape breakages, and so on. The specific characteristics of the

/146

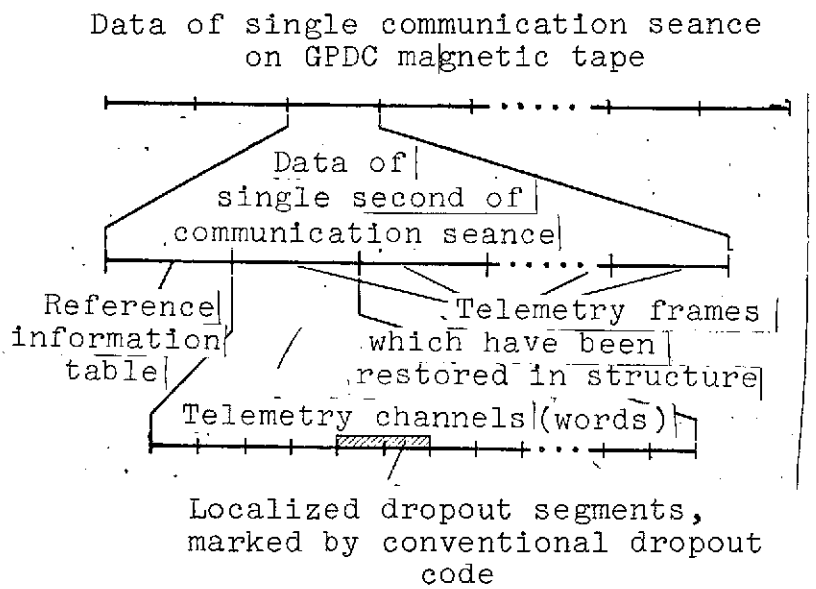

Figure 3. Structure of data on GPDC magnetic tape

given RTS (number of channels, location of service marks, number of frames per second) are reflected only in the reference information table.

Check of the quality of the data prepared for processing is accomplished using the a priori known form of the value distribution in the channels. Such channels were the RTS calibration channels and all the channels with 8- and 16-level structure of possible values. Additional analysis of the quality of the data prepared for processing was performed on a check printout of the reference information tables. All the steps of the preparation for processing were performed on a Ural-11B GPDC using the system developed at the Institute of Space Studies for input and preparation for processing of information recorded on RTS magnetic tapes. The time expenditures in this system, called the "Artur" system, for input and preparation for processing of the data obtained during the time of a single communication seance (approximately 1.5 million telemetry words) amounted to two hours of Ural-11 GPDC time, and one man-day, for preparation of the initial data and analysis of the results obtained.

3. Systematization of Recording Materials

Selection of the seances for carrying out complete frame-by-frame processing is made on the basis of several factor characterizing the seance and determined in the systematization stage. Such factors were: recording quality, rate of satellite rotation around its center of mass, orientation of axis of rotation in relation to /147
the axes of the scientific instruments, position of interchangeable filter in the SEZ-14 instrument, duration of satellite passage through magnetic anomaly regions.

An information characteristic, a sample of which is shown in Figure 4, was prepared for each seance.

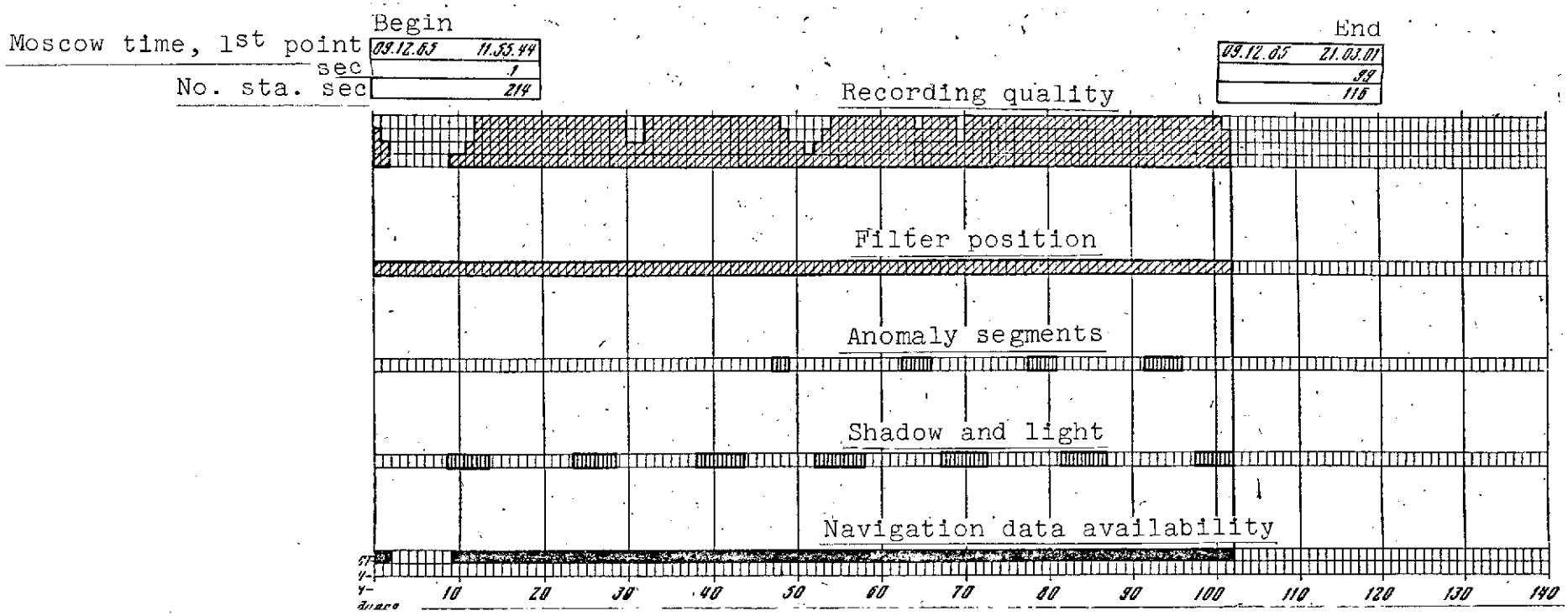

Figure 4. Information characteristic of seance:

5 — no loss
4 — loss of 1 - 2 points
3 — loss of 3 - 4 points
2 — loss of 4 or more points
1 — complete loss

Graphite
Undetermined position
Polyethylene
Without filter

Anomaly segments $\lambda = 270-40$, $\varphi = 0-65$
Shadow
Light
Information available

Navigation data not available

Eval. of sec from summary graphs

(Figure caption completed on following page)

Figure 4 (continued):

TM memory scan period

τ_{min} - - 8.45 - - sec

τ_{max} - - 8.57 - - sec

τ_{av} - - 8.51 - - sec

$\tau = 600/n$, where n is number of scan points between 10-min on-board ID timing marks (channel 401)

General evaluation of recording quality

1 2 3 4 5

5 — good, no dropouts
4 — small number of dropouts, little effect on results
3 — large number of dropouts, considerable deterioration of results
2 — practially unsuitable for processing
1 — no information

Rotation nature

Rotation period from 3.5 to 5.7 min

from 2.5 to 4.0 scan points

Rotation type M

A — fast, $\leq$ 30 points/period
M — slow, $\geq$ 30 points/period
x (index) — axis of rotation close to instrument longitudinal axis
(Period of Hx sign variation close to rotation half period)

An evaluation of seance quality was made by the operator on the basis of the summary graphs. The number of missing frames during discrete intervals —one second of reception — was determined, and a local evaluation of each second was made using a 5-point system (shown in graph form). An overall evaluation of the seance was also made using the 5-point system.

Orbital segments, involving passage through an anomaly, were determined from the increased count rate of individual parameters. The approximate rate of rotation around the center of mass and the position of the rotation axis were determined from the magnetometer indication graphs.

Such a characteristic accompanied the output documentation of each seance, and served as reference material for determining data validity.

4. Obtaining the Summary Recording

A special-purpose computer was used to re-record the telemetry information from the RTS magnetic tape onto summary graphs. The summary graph may contain one, two, or four tracks, on which the information from eight telemetry channels can be recorded. The general arrangement of the summary graphs is determined prior to beginning the summary re-recording. In so doing, the number of tracks on the summary graph is selected with account for the required voltage readout accuracy in each of the telemetry channels.

The requirements on timewise resolution determine the re-recording tape drive speed. It is desirable to configure the graphs so that the channels belonging to a single measurement program will be on the same summary graph. It is convenient to locate the channels servicing events between which there is a simple logical connection on the same summary graph. The necessity for calibration voltage (0 | and 100%) recording is indicated for each of the channels.

A sample summary graph is shown in Figure 5. It contains four tracks, on each of which the information of a single telemetry channel is recorded. The channel number is located below the lower track opposite the channel marker. Recording of the information of each channel is accompanied by recording of the calibration voltages. Numbered vertical marks are placed at the end of each information reception section. Second marks of the Master Time Service are also recorded on the graph.

The use of the special-purpose computer ensures high reliability /149 of the summary re-recording process. This makes it possible to use the summary graphs to monitor each computer information processing stage. The availability of the summary recording makes it possible to process the information manually using simplified programs, and make a rapid qualitative evalutation of the information.

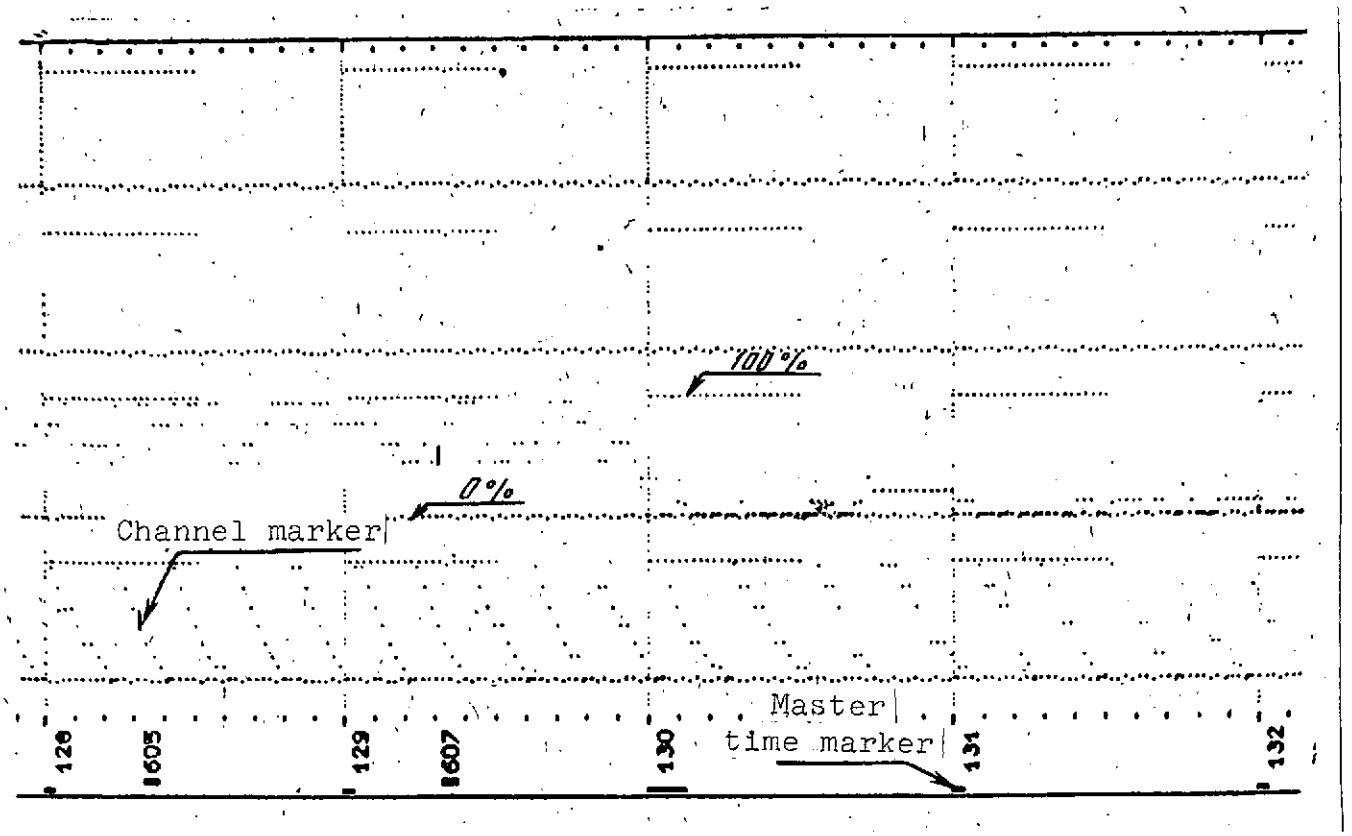

Figure 5. Scientific equipment parameter summary graph

5. Time Correlation of Information

Time correlation of the instrument indications obtained — determination of the second measurement coordinate — had two purposes.

The first purpose was introduction of an arbitrary time scale for numbering the measurements, in order to compare the indications of the various channels with one another (relative scale). For example, the generation of tables with the instrument indications was carried out in arbitrary time units: seance number, second number, frame number in given second. These units were determined by the recording structure.

The second purpose was the use of an absolute time scale, for example, Moscow time (date, hour, minute, second), for sequential calculation of satellite location in orbit at the measurement times.

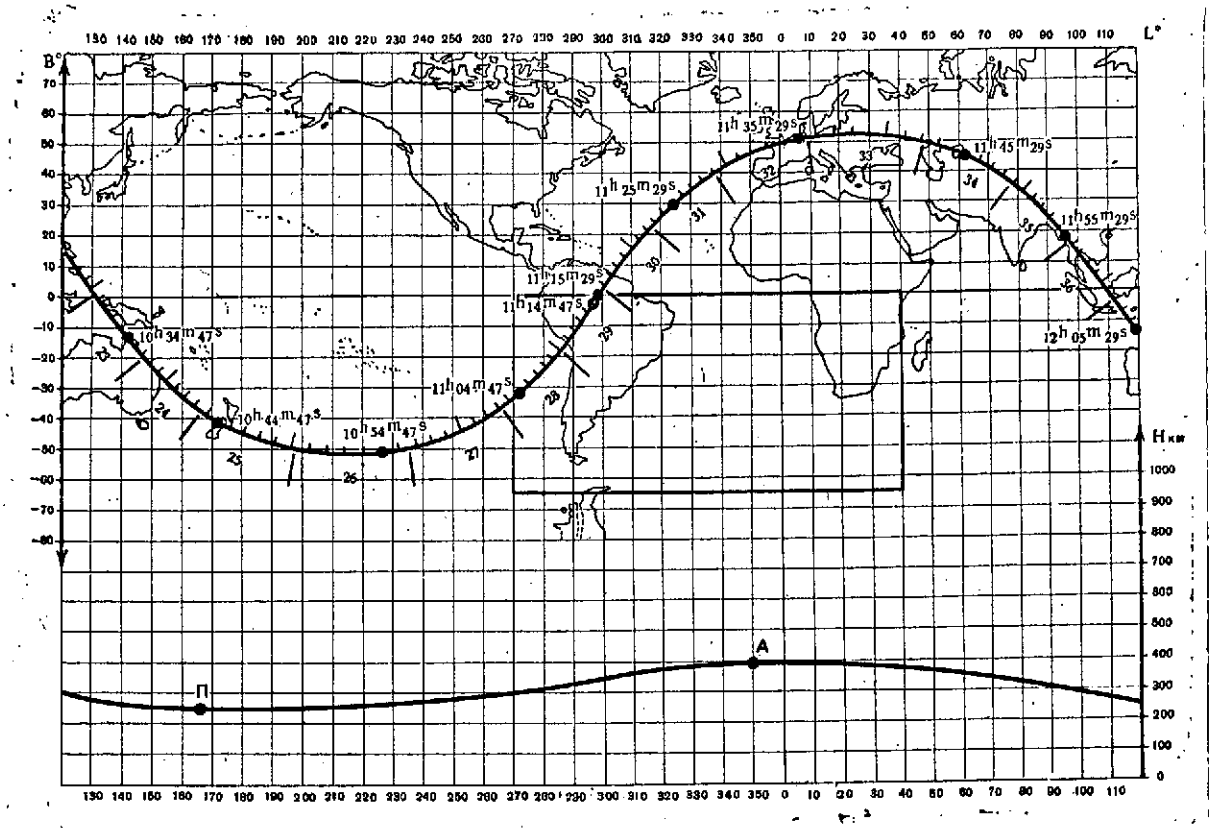

Figure 6. Map of AES geodesic coordinates and flight altitudes

This time was also calculated for each telemetry frame scan, and was presented in the tables, together with the other navigational parameters.

Figure 6 shows a map of the geographical coordinates and satellite flight altitudes with the arbitrary and absolute time scale noted. The indications of the onboard timer, which generates a marker signal each minute (or every 10 minutes), which is recorded by the telemetry system, are used to convert from one scale to the other. The timer indications are also recorded in the form of coded markers in the direct data transmission mode, which makes it possible to determine the time of their occurrence on the master time scale (MTS), which is shown on all the ground-based recording materials.

6. Voltage Scaling

Calibration tables, prepared for each recording seance (Figure 7), were used to convert the telemetry channel digital codes to step numbers (level numbers).

Groups of channels having the same nature of their variation are formed on the basis of the known parameter distribution in the telemetry system channels. For each group, we examine the code values in all the channels in each scan frame and determine the number of measurements taking the given code value. The resulting distribution functions are printed out, and from them the operator specifies the "larger-smaller" tables for determining the level number. The code values which do not fit into any of the specified tables are defined as erroneous values. After conversion into level numbers, the scientific instrument indications are formed into a new frame, where 4 binary units are assigned to each channel (0 - 7 is the level number, 8 is the error symbol).

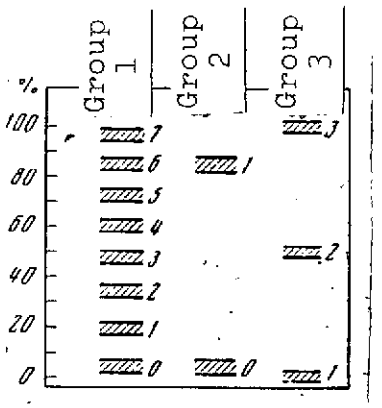

Figure 7. "Tables" for determining level number

/151

7. Instrument Indication Output

Output of the instrument indications was accomplished in the form of Ural-11 alphanumerical printer tables (Table 3), combined into a bound volume. The tables contained information obtained at various processing stages. Both the level numbers for each channel and the number of parameter conversions per single scan period, which is determined from the level numbers, were generated.

The framewise data structure was maintained at all the processing stages. Either the instrument indication or the absence of information — the dropout symbol — was indicated for each scan frame.

TABLE 3. INDICATIONS OF SEZ-14 INSTRUMENT

71—0052—14—1I sec 116

Point no.	Level no.	—1	—2	—3	—4	—5	—6	—7	№	№	EC	Logic events
		012	012	012	012	012	01	0	1	23456789	6789	EC
1	3030522303021	000	000	000	010	000	00	0	0	00000000	0000	
2	3030522303021	000	000	000	000	000	00	0	0	00000000	0000	
3	3030522303021	000	000	000	000	000	00	0	0	00000000	0000	
4	3030522303021	000	000	000	000	000	00	0	0	00000000	0000	
5	3131532303021	000	000	011	000	000	00	0	0	00000000	1000	X
6	3131532303020	000	000	000	000	000	00	0	0	00000000	0000	
7	3115546310020	000	000	000	011	000	00	0	0	11100000	1110	444 48
8	3115546310022	000	000	000	100	000	00	0	0	00000000	0000	
9	3115546310022	000	000	000	000	000	00	0	0	00000000	0000	
10	3115546310022	000	000	000	000	000	00	0	0	00000000	0000	
11	3115546310022	000	000	000	000	000	00	0	0	00000000	0000	
12	3115546310022	000	000	000	000	000	00	0	0	00000000	0000	
13	3151556323022	000	000	000	000	010	00	0	0	11100000	1000	054 46
14	3151556323022	000	000	000	000	000	00	0	0	00000000	0000	
15	3151556323022	000	000	000	000	000	00	0	0	00000000	0000	
16	3151556323022	000	000	000	000	000	00	0	0	00000000	0000	
17	3151556323022	000	000	000	000	000	00	0	0	00000000	0000	
18	3151556323022	000	000	000	000	000	00	0	0	00000000	0000	

71—0052—14—1I sec 116

Point no.	Level no.	—1	—2	—3	—4	—5	—6	—7	№	№	EC	Logic events
19	3151156323000	001	000	000	100	000	00	0	0	00000000	0000	
20	3151556323022	001	000	000	100	000	00	0	0	00000000	0000	
21	3151556323022	000	000	000	000	000	00	0	0	00000000	0000	
22	3151556323022	000	000	000	000	000	00	0	0	00000000	0000	
23	3171556323022	000	000	000	010	000	00	0	0	00000000	0000	
24	3171556323022	000	000	000	000	000	00	0	0	00000000	0000	
25	3171556323022	000	000	000	000	000	00	0	0	00000000	0000	
26	3133564323022	000	000	000	000	011	00	0	0	00000001	1000	X
27	3171574303722	000	000	000	000	011	00	0	0	00001110	1000	X
28	3150544303722	000	000	001	010	000	00	0	0	00000000	1000	043 36
29	3150544312722	000	000	000	000	000	00	0	0	11000000	0000	
30	3150544312722	000	000	000	000	000	00	0	0	00000000	0000	
31	3150544312722	000	000	000	000	000	00	0	0	00000000	0000	
32	3150545312722	000	000	000	000	000	00	0	0	00000000	0001	
33	3150545312722	000	000	000	000	000	00	0	0	00000000	0000	
34	3150545312722	000	000	000	000	000	00	0	0	00000000	0000	
35	3150545312722	000	000	000	000	000	00	0	0	00000000	0000	
36	3150545312722	000	000	000	000	000	00	0	0	00000000	0000	
37	3170545312722	000	000	000	000	000	00	0	0	00000000	0000	

The dropouts are differentiated on the basis of the stage of their appearance, for example:

1) structural dropouts of telemetry recording, detected by the "Artur" input system, usually framewise or secondwise;

2) frequent channelwise dropouts, detected upon conversion to level numbers using the given tables;

3) other dropouts, detected by checking the instrument counting circuit triggering logic.

The data output was accomplished without omission of the dropout segments. Although this increased the printout volume, it also facilitated considerably the data readout and search, since it permitted considering the vertical table measurement directly as a time scale.

8. Processing of Scientific Instrument Indications With Account for Orientation

The availability of the navigational data makes it possible to break the entire experiment time down into segments corresponding to different measurement conditions. In this case, the measurement /154
conditions for different event forms will be characterized by different sets of navigation parameters. For example, the zenith angle will be of essential importance for instruments having recording directivity, but will not enter into the measurement condition characteristic for the instruments not having directivity: the direction of the axis in the absolute coordinate system is essential for instruments recording the electromagnetic radiation, but is not important for instruments recording charged particles, etc.

Knowledge of the measurement conditions in each telemetry scan frame makes it possible to find the dependence of the characteristics of the events being recorded on each of these conditions. In order to construct these relations, it is necessary to take various samples

from the scientific information processing results. We first formulate tables of the time intervals, characterized by the required navigational parameter values. Table 4 is presented as an example. It contains, for several seconds of the seance, a listing of the numbers of the telemetry scan frames in which the values of the zenith angle α and magnetic rigidity P lie in the specified intervals.

Then we calculate the number of events, for which me must find the dependence on the indicated parameters in the scan frames, characterized by the given values $\alpha + \Delta\alpha$ and $P + \Delta P$. We determine the average event rate and the mean-square error. The set of such values for different values of α and P makes it possible to construct the dependence of the various event rates on the zenith angle and magnetic reigidity. Sampling with respect to the other navigational parameters is performed similarly.

We should point out that the operation described above is possible only when the variation of the navigation parameter value during the telemetry scan frame is noticeably less than the magnitude of the selected parameter value interval. This leads to a situation in which part of the measurement time, characterized by high satellite rotation rates around the center of mass, is not suitable for processing the scientific equipment indications with account for orientation.

The availability of the navigation data was of decisive importance in processing several measurement programs. For example, acquiring information on the primary gamma quanta fluxes using the GG-1 instrument was impossible, in principle, without knowledge of the instrument axis orientation. The results obtained when processing the scientific information, together with the navigation data, are presented in [5 - 13].

TABLE 4. PROTON 2. MEASUREMENT SEANCE ON 44th ORBIT. INTERVAL P = 6 - 10 BV

Interval α° / No. sec	0—20	20—40	40—60	60—80	80—100	100—120	120—140	140—160	160—180
71				3,4	39—42				
72				3—10	11—15 30,31	32,33			
79						24—32	8—13		
80					35—37	7—12, 30—34			
81			21,22	19,20	16—18	14,15	9—13 32—38		
82		4—5	1—3 6—7	8—9	10—11	13—14			
87				28,29	10—14 30—33				
94						19—27	14—18 28—38		
95						21,22	15—20	43	
102				11—15	3—10 16—25				
109								25—33	
110								8—9	1—7
113				2—4	5—6				
117		7—27							

9. Processing of Scientific Equipment Indications Without Account for Orientation

Processing of the scientific information with account for orientation can be accomplished only for that portion of the flight time which satisfies the requirements of low satellite rotation velocities and good quality of the magnetometer information. Hence follows the requirement for having measurement programs and processing methods /156 which permit obtaining results without knowledge of the instrument orientation. For this purpose, either the recorded parameters must be insensitive to instrument orientation, or the processing must be performed over sufficiently long measurement times to ensure good averaging of the measurement conditions. The first of these requirements is satisfied by the measurement programs using nondirectional instruments, for example, the program for measuring the all-particle energy spectrum using the SEZ-14 instrument calorimeter. An example of satisfaction of the second condition is processing of the primary cosmic ray proton spectrum measurement using the SEZ-14 instrument. The instrument records protons directionally, and the proton count rate depends on the degree of instrument aperture shading by the Earth, but, as a consequence of random satellite rotation, for long measurement times we can use an average shading coefficient equal to $\omega/4\pi$, where ω is the average shadow cone solid angle.

Processing without account for orientation does not require knowledge of the number of events in each scan frame; therefore, in processing scientific information, it is sufficient, as a rule, to know the number of events per machine second (42 - 43 scan frames). Such processing, not requiring exact correlation of the information with the scan frame number, can be performed manually using the summary graphs. In the automated processing case, the sums of the events per second are generated at the end of each machine second.

In the case of processing without knowing the orientation, it is still possible to determine roughly the event count rate dependence on instrument orientation. To this end, we utilize information

having very clear-cut dependence on the orientation. An example is the recording of high-energy protons by the SEZ-14 instrument with directional detector aboard the Proton 3 AES. Figure 8 shows the counting rate of such events as a function of time. The ordinate is the number of events per machine second, the abscissa is the machine second number. The observed modulation is caused by instrument aperture shading by the Earth. Seconds with zero number of counts correspond to practially complete shading of the aperture. The maxima located between the segments with zero count rate correspond to the absence of shading. It is possible to compile a listing of seconds with zero and complete shading, and use this listing to process various measurement programs. /157

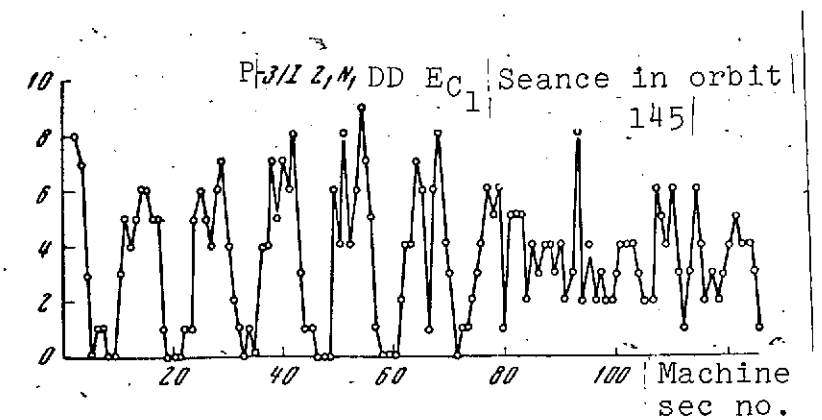

Figure 8. Count rate as function of time

Recording of the charged particles with minimal energy 100 - 400 MeV by the SEZ-1 (Proton 2) and DD (Proton 3) instruments made it possible to break measurement time down roughly into segments corresponding to the different geomagnetic latitudes. This then permitted construction of curves of various event count rates as functions of geomagnetic latitude.

III. Processing Magnetometer Information and Determining Orientation of "Proton" Satellite

Interpretation of the indications of the scientific equipment installed aboard the Proton satellite requires knowledge of instrument orientation in space, the angles which the instrument axes make with the direction to the Earth, and with the Earth's magnetic field intensity vector. For their calculation, it is sufficient to know

the position of the coordinate system fixed with the satellite (and in which the position of the instrument axes is known) relative to the coordinate system in which the physical quantities of interest to us are calculated.

Finding the relative position of these coordinate systems is the task of satellite orientation determination. The indications of magnetometers installed aboard the satellite are used in determining AES rotation and orientation. Since the measurements are made with errors, the statistical approach is the natural one for determination of satellite orientation and rotation. Moreover, the measurement information available at each fixed moment of time does not permit determining satellite orientation; therefore, it is necessary to use additional information on the nature of AES rotation around its center of mass, i.e., the mathematical model of the motion, containing the unknown parameters, is specified. Then the problem of rotation and orientation determination reduces to finding the unknown parameters from the available information.

The mathematical model of the motion was taken in differential equation form. In this case, the unknown parameters are the initial values. They were determined by the least squares method. The technique for determining artificial satellite orientation using a given system of measurements was presented in detail in [14, 15]. The /158
results of application of this technique to the Proton 2 satellite are described in [16]. Individual aspects of the problem are also discussed in [17]. The experimentally determined dynamic effects in Proton 2 satellite rotation and orientation are analyzed in [18, 19]. This analysis made it possible to draw definite conclusions on the nature of the interaction of the aerodynamic flow with the satellite. Several questions discussed in [14 - 19] are described in more detail in the collection of papers [20].

1. Problem Formulation

We introduce three coordinate systems:

1) the absolute geocentric coordinate system with X axis, directed toward the vernal equinox point, the Z axis directed along the Earth's rotation axis, and the Y axis completing the right hand system;

2) the Koenig axis system with origin at the satellite center of mass, the axes are colinear to the axes of the preceding system;

3) the body coordinate system with origin at the satellite center of mass and axes directed along its principal central axes of inertia.

We examine the vehicle center-of-mass motion in the absolute coordinate system, which is completely defined by its radius vector $\mathbf{R}(X, Y, Z)$ and velocity vector $\mathbf{V}(V_X, V_Y, V_Z)$, and the satellite motion around its center of mass, which is the rotation of the body coordinate system relative to the Koenig system. We shall describe the motion around the center of mass by the kinetic moment vector $\mathbf{L}(L_1, L_2, L_3)$ in the Koenig axis system and the Rodrigues-Hamilton parameters $\lambda_0, \lambda_1, \lambda_2, \lambda_3$.

It is assumed that the center-of-mass motion is known, and is independent of the motion around the center of mass. We examine only those segments of the satellite center-of-mass motion trajectory on which the disturbing moments of the external forces are small and have no significant effect on the motion around the center of mass. Analysis of the distrubances acting on the Proton satellite showed that only small vicinities of the perigee, where the aerodynamic moment influence is large, do not belong to such segments. Then the motion around the center of mass is described by the system of differential equations:

$$\frac{d\mathbf{L}}{dt}=0, \tag{1.1}$$

$$\frac{d\boldsymbol{\lambda}}{dt}=\frac{1}{2}[\lambda_0\cdot\boldsymbol{\omega}+\boldsymbol{\omega}\times\boldsymbol{\lambda}], \quad \frac{d\lambda_0}{dt}=-\frac{1}{2}(\boldsymbol{\omega}\cdot\boldsymbol{\lambda}), \tag{1.2}$$

where $\omega = m\Lambda^{-1}m\mathbf{L}$ is the angular velocity vector, Λ^{-1} is a diagonal matrix of dimension 3 × 3 with elements $1/A, 1/B, 1/C$ (A, B, C are the principal central moments of inertia), $\lambda = \{\lambda_1, \lambda_2, \lambda_3\}$;

$$m = \begin{pmatrix} \lambda_0^2+\lambda_1^2-\lambda_2^2-\lambda_3^2 & 2(\lambda_0\lambda_3+\lambda_1\lambda_2) & 2(-\lambda_0\lambda_2+\lambda_1\lambda_3) \\ 2(-\lambda_0\lambda_3+\lambda_1\lambda_2) & \lambda_0^2+\lambda_2^2-\lambda_1^2-\lambda_3^2 & 2(\lambda_0\lambda_1+\lambda_2\lambda_3) \\ 2(\lambda_0\lambda_2+\lambda_1\lambda_3) & 2(-\lambda_0\lambda_1+\lambda_2\lambda_3) & \lambda_0^2+\lambda_3^2-\lambda_1^2-\lambda_2^2 \end{pmatrix}$$

is the conversion matrix from the Koenig axes to the body coordinate system; m' is the transposed matrix. /159

The choice of components of the kinetic moment vector L and the Rodrigues-Hamilton parameters as the variables characterizing the motion is explained by the fact that they permit avoiding the singularity characteristic of the angular variables. The system of equations of motion written in these variables, while having the same simplicity as the Poisson equation system (containing only algebraic operations), at the same time has lower order, which is essential for processing tasks.

Since the System (1.1) - (1.2) is known, the motion around the center of mass is determined uniquely by specifying the initial values $L_1^0, L_2^0, L_3^0, \lambda_1^0, \lambda_2^0, \lambda_3^0$ at the moment of time t_0. It is known that the Rodrigues-Hamilton parameters are connected by the relation

$$\sum_{i=0}^{3} \lambda_i^2 = 1,$$

which is used to find

$$\lambda_0^0 = \sqrt{1-\lambda_1^{02}-\lambda_2^{02}-\lambda_3^{02}}.$$

We denote the ensemble of these parameters by

$$\mathbf{Q}\{Q_k\} = \{L_j^0, \lambda_r^0\},$$
$$(j = 1, 2, 3;\ r = 1, 2, 3;\ k = 1, \ldots, 6).$$

Then the problem of finding the motion around the center of mass reduces to finding the unknown Q-parameters. For its solution at the

moment of time t_i, we measure the functions ψ_i of the motion parameters Q_k

$$\psi_i = \psi_i(\mathbf{L}(\mathbf{Q}),\ \lambda(\mathbf{Q}, t_i)).$$

We denote the measured values of the functions ψ_i by $\bar{\psi}_i$.

2. Solution Method

Assuming that the measurement errors are random, we use the least squares method to solve the posed problem. In accord with this method, the parameters Q are determined from the condition of minimum of the function

$$\Phi(\mathbf{Q}) = \sum_{i=1}^{N} \frac{1}{\sigma_i^2} \xi_i^2, \qquad (2.1)$$

where $\xi_i = \bar{\psi}_i(\mathbf{Q}) - \langle \psi_i \rangle$ are the discrepancies, and σ^2_i — the variance of the measurement errors. The sought parameters Q, for which the minimum of Φ (Q) is reached, must satisfy the system of nonlinear equations

/160

$$\frac{\partial \Phi}{\partial Q_k} = \sum_{i=1}^{N} \frac{1}{\sigma_i^2} \xi_i \frac{\partial \psi_i}{\partial Q_k} = 0. \qquad (2.2)$$

The solution of (2.2) is made by the iteration method: starting from the known zero approximation $\mathbf{Q}^0$, we construct the successive approximation algorithm $\mathbf{Q}^{(S)} = \mathbf{Q}^{(S-1)} + \delta\mathbf{Q}^{(S)}$ (S is the iteration number), which is a modification of the algorithm described in [21]. In each iteration, we calculate the "Newtonian" corrections $\delta\mathbf{Q}_н$, satisfying the system of normal equations:

$$\left.\begin{aligned} &A^{(S-1)}\delta\mathbf{Q}_{\text{н}}^{(S)} = \mathbf{B}^{(S-1)}, \\ &A^{(S-1)} = \left\| A_{jk}^{(S-1)} \right\|_{j,k=1}^{n}, \quad \mathbf{B}^{(S-1)} = \left\| B_l^{(S-1)} \right\|_{l=1}^{n}, \\ &A_{jk}^{(S-1)} = \left(\sum_{i=1}^{N} \frac{1}{\sigma_i^2} \frac{\partial \psi_i}{\partial Q_j} \frac{\partial \psi_i}{\partial Q_k} \right)_{\mathbf{Q}^{(S-1)}}, \\ &B_l^{(S-1)} = \left(\sum_{i=1}^{N} \frac{1}{\sigma_i^2} \frac{\partial \psi_i}{\partial Q_l} \xi_i \right)_{\mathbf{Q}^{(S-1)}} \end{aligned}\right\} \qquad (2.3)$$

We shall consider a measurement set such that the problem has a unique solution. Then we find from (2.3), $\delta\mathbf{Q}_н = -[A^{(S-1)}]^{-1}\mathbf{B}^{(S-1)}$, since $\det A^{(S-1)} \neq 0$. We seek the correction $\delta\mathbf{Q}^{(S)}$ in the form $\delta\mathbf{Q}^{(S)} = \alpha_s \delta\mathbf{Q}_н^{(S)}$, where α_s is the iteration step, subject to determination. To ensure monotonic convergence of the process, we must select α_s in optimal fashion.

The algorithm for selecting α_s is based on approximating the function $\Phi(\alpha_s)$ being minimized along the direction $\delta\mathbf{Q}_н$ by a cubic parabola in α_s.

The zero approximation Q^0 to the values of the sought parameters, which is necessary for the iteration process, is found with the aid of the algorithm described in [15].

In order to form the normal Equations (2.3), it is necessary to know at the measurement time t_i the calculated values of the functions $\psi_i[\mathbf{L}(\mathbf{Q}), \lambda(\mathbf{Q}), \lambda_0(\mathbf{Q})]$ being measured, and the derivatives of the calculated values of the measurements with respect to the parameters being determined $d\psi_i/dQ_k$. The derivatives are calculated from the formula

$$\frac{\partial\psi_i}{\partial Q_k} = \sum_{l=1}^{3} \frac{\partial\psi_i}{\partial L_l}\frac{\partial L_l}{\partial Q_k} + \sum_{r=0}^{3} \frac{\partial\psi_i}{\partial\lambda_r}\frac{\partial\lambda_r}{\partial Q_k}, \tag{2.4}$$

where $d\psi_i/dL_l$ and $d\psi_i/d\lambda_r$ can be calculated explicitly, since the form of the function $\psi_i(\mathbf{L}, \lambda, \lambda_0)$ is known.

The quantities $\mathbf{L}, \lambda, \lambda_0$ and derivatives $\partial L_i/\partial Q_k$, $\partial\lambda_r/\partial Q_k$ necessary for calculating ψ_i and $d\psi_i/dQ_k$ are found as a result of combined integration of Equations (1.1) and (1.2), and the corresponding system of variational equations, which may be written as follows: /161

$$\frac{dD}{dt} = DP, \tag{2.5}$$

where D is the matrix of derivatives of the variables $\mathbf{L}, \lambda, \lambda_0$ with respect to the parameters Q_k of dimension $n \times 7$; P is the matrix of

derivatives of the right sides of (1.1) - (1.2) with respect to the variables $\mathbf{L}, \lambda, \lambda_0$| of dimension 7 × 7.

3. Magnetometric Information and Its Characteristics, Quality Analysis

Three-component magnetometers from which indications are taken at the successive moments of time t_i of the projections of the Earth's magnetic field intensity vector along the magnetometer axes, rigidly connected with the satellite, are installed aboard the Proton satellites in order to determine the orientation. In this case, we took the following as the measured functions ψ_i:

$$\psi_i = (m(Q_k, t_i)\mathbf{H}(t_i), \mathbf{l}_i), \quad (3.1)$$

where $H(t_i)$ is the vector of the Earth's magnetic field intensity at the moment t_i in the absolute coordinate system, $\mathbf{l}_i$| is the unit vector directed along the magnetometer axis corresponding to the measurement being made.

In order to calculate the vector $\dot{H}(t_i)$, we used its expansion into a series of Legendre functions [22]. The coefficients of the expansion were taken from [23]. The vehicle coordinates necessary for determining $H(t_i)$ were calculated using the formulas presented in [21]. /162

Specimens of the magnetometer indications, specifically the record of the positive component along the longitudinal axis

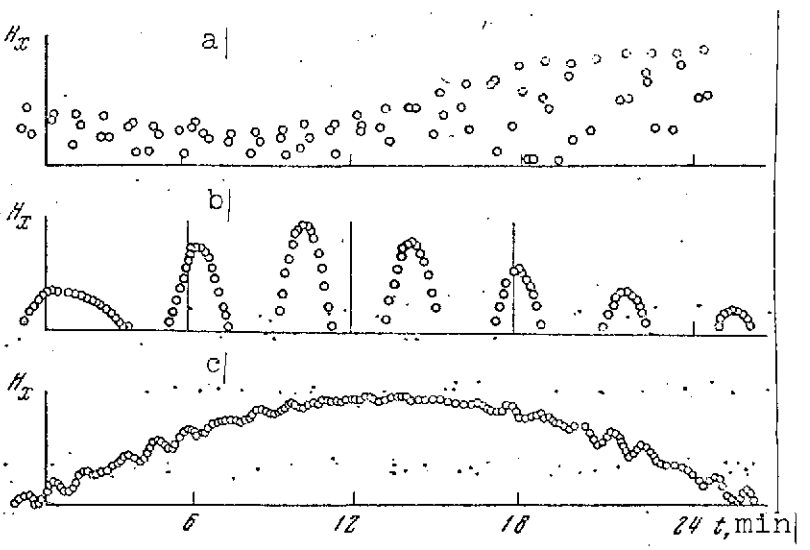

Figure 9. Specimens of magnetograms from Proton 2 satellite

(+ H_x) of the Proton 2 satellite, are shown in Figure 9, and correspond to the characteristic regimes of satellite rotation around its center of mass. Figure 9c corresponds to a regime close to vehicle spin around the longitudinal axis. Figure 9a corresponds to a regime close to spin about the transverse axis. In case 9a, the angular velocity of rotation is considerably larger than in case 9b, which is intermediate between 9a and 9c. The reliability of orientation determination algorithm operation and the accuracy of the results obtained depend significantly on the quality of the raw information, on the form and magnitude of the errors present in this information.

The quality of the magnetometric information was checked by comparing the modulus of the calculated and measured Earth's magnetic field intensity vector, which made it possible to determine the errors in time correlation of the information and find the dropout segments.

4. Results of Proton 2 Satellite Orientation Determination

Mass processing of the information on Proton satellite orientation was performed using the described technique at SOMI of the Academy of Sciences of the USSR (A. F. Sidorov, I. A. Buterina, S. A. Sarapkina). The processing results are navigational data tables.

For the Proton 2 satellite, these tables contained: time to which the navigation data are referred; two angles (α, ψ) defining instrument axis position in the coordinate system fixed with the local vertical; number of the instrument axis location zone as a function of the angle α (the entire range of values of the angle α of the instrument with the local vertical is broken down into several zones); two angles defining instrument axis position in the absolute coordinate system; two angles defining the instrument axis in position in the coordinate system fixed with the magnetic force line; the magnetic rigidity P_H, which depends on orientation; orbital data:

satellite latitude and longitude; and Earth's magnetic field intensity (Tables 5 and 6).

TABLE 5. NAVIGATION DATA AS FUNCTION OF SCAN POINTS

Dump 113 sec 102

Zone no.	Point no.	Time, hr/min/sec	H km	φ deg	λ deg	P_H	α°	ψ	BV	κ°	θ°	φ°	H	gamma.	lol ε°
+++01	2—	0113102	02	2—0113102		03	2—0113102		04	2—0113102		05	2—011		102
+++04	01	180549	03	426—30299		01	189060294		00	118—67321		04	2235		297
+++04	02	180557	03	424—30299		01	154065289		00	121—70328		04	2224		292
+++04	03	181605	03	422—33299		01	131060286		00	126—72342		04	2214		289
+++04	04	180614	03	420—33299		01	129073284		00	131—70354		04	2204		289
+++04	05	180622	03	417—32300		01	151078286		00	136—65358		04	2195		293
+++05	06	180631	03	415—32300		01	196080290		00	138—60355		04	2186		300
+++05	07	180639	03	413—30300		01	258082295		00	137—57348		04	2178		308
+++05	08	180648	03	411—30301		01	316080300		00	133—55339		04	2171		311
+++04	09	180656	03	409—30301		01	346075302		00	129—56329		04	2163		310
+++04	10	181704	03	407—30301		01	333070302		00	126—60321		04	2157		305
+++04	11	180713	03	404—29302		01	285066297		00	125—65316		04	2151		299
+++04	12	180721	03	402—29302		01	228066291		00	128—70319		04	2145		292
+++04	13	180730	03	400—29302		01	186069285		00	133—70335		04	2140		286
+++04	14	180738	03	398—24302		01	174075283		00	140—72355		04	2135		285
+++05	15	180747	03	396—24303		01	199080284		00	147—67002		04	2131		290
+++05	16	180755	03	394—27303		01	258086289		00	150—60359		04	2128		301
+++05	17	180804	03	391—27303		01	343087295		00	148—56351		04	2125		312
+++05	18	180812	03	389—26303		01	427080301		00	143—50341		04	2122		317
+++04	19	180820	03	387—26304		01	471078304		00	138—55330		04	2120		315
+++04	20	180829	03	385—25304		01	450073303		00	134—54321		04	2119		308
+++04	21	180837	03	383—25304		01	381069298		00	134—60315		04	2118		300
+++04	22	180846	03	381—20305		01	306068291		00	137—70317		04	2117		291
+++04	23	180854	03	378—20305		01	254072286		00	143—74332		04	2117		285
+++04	24	180903	03	376—23305		01	240078283		00	150—73353		04	2118		283
+++05	25	180911	03	374—23305		01	267080285		00	157—68001		04	2119		290
+++05	26	180920	03	372—20306		01	333089280		00	159—60359		04	2120		306
+++05	27	180928	03	370—22306		01	424090295		00	157—57352		04	2122		320
+++05	28	180936	03	368—20306		01	513087300		00	152—55342		04	2124		324
+++05	29	180945	03	365—20306		01	561083303		00	148—56333		04	2127		320
+++04	30	180953	03	363—20307		01	546078302		00	145—50324		04	2131		313
+++04	31	182002	03	361—20307		01	483070298		00	146—53319		04	2134		304
+++04	32	182010	03	359—18307		01	410070293		00	149—68320		04	2139		296

As an example, Figure 10 shows the values obtained for P_H and the angles α and ψ on the 52nd orbit of the Proton 2 satellite. Table 7 and Figure 11 given an idea of the orientation determination accuracy [20]. The notations in Table 7 and Figure 11 are: P_α is the confidence level (with probability no less than P_α, the error in determining the parameters does not exceed the values shown in Table

TABLE 6. NOTATIONS IN NAVIGATION DATA TABLES

Measurement time		Instrument orientation in space		Physical parameters	
	No. orbit in which stored information was reproduced	α^0	Angle of instrument longitudinal axis with vertical (with direction from center of Earth), 0-180°	H, gamma·10¹ (read as 47500)	Value of magnetic field intensity is determined from geomagnetic field data IZMIRAN for 1964
sec	No. of reproduction second interval	$\psi°$	Angle between projections of instrument longitudinal axis on horizontal plane and direction to the East, 0 - 360°		
Point no.	Sequential no. of scan point in given second interval	Zone no.	Zones of instrument axis position with respect to angle 1— 0°—42° 5— 80°—115° 2—42°—53° 6—115°—138° 3—53°—64° 7—138°—154° 4—64°—80° 8—154°—180°	P_H 1345 (Read as 13.45)	Geomagnetic cutoff threshold rigidity is calculated with account for vehicle orientation, geographic position, and altitude from the formula $P_H = P_0/r^2$, where r is satellite distance from center of Earth, referred to Earth's radius; P_0, magnetic rigidity at surface of Earth in direction of axis (for given angles α, ψ) at geomagnetic latitude ϕ_m. is determined from
Time, hr, min, sec	Measurement time (Moscow)	$\theta°$	Angles determining position of instrument longitudinal axis in absolute coordinate system ± 90°)		$P_0 = P_{0\,vert} = 4\{1+(1-\sin\alpha\cos\psi\cos^3\varphi_m^{\frac{1}{2}}\}^{-2}$,
AES position in orbit		$\Phi°$	0 - 360°		

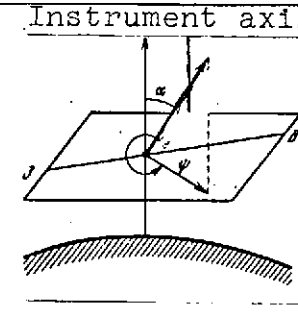

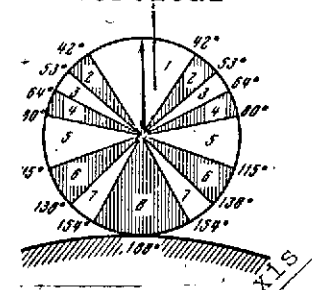

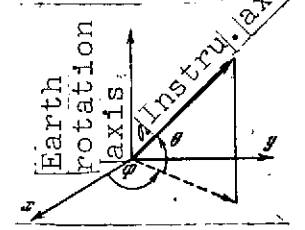

Direction to vernal equinox point

(Figure continued on following page)

TABLE 6. (continued)

Measurement time		Instrument orientation in space		Physical parameters
H, km	Satellite ht. above Earth's surface			where $P_{0\ vert}$, magnetic rigidity along the vertical at Earth's surface, is found from the Qwenby-Wenk tables; ϕ_m, the geomagnetic latitude is calculated from $\cos\varphi_m = \left[1-\frac{r^3}{R^3}(\sin\varphi\cos 11^\circ - \cos\varphi\sin\lambda^*\sin 11^\circ)\right]^{1/2}$, where $\lambda^* = \lambda - 21^\circ$ and $R = r^3 + 0{,}0499 + r\cdot 0{,}1413(\cos\varphi\cdot\sin\lambda^*\cdot\cos 11^\circ - \sin\varphi\times\sin 11^\circ)$
ϕ, deg		χ° Angle between direction of instrument axis and magnetic force line, 0 - 180°	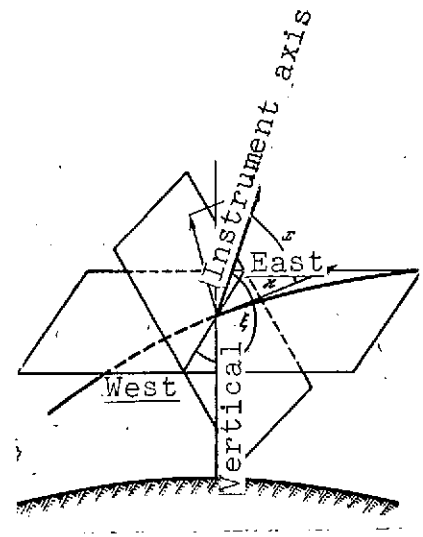	
λ, deg	Geographic longitude 0 - 360°	ξ° Angle between projection of instrument axis on plane perpendicular to the magnetic field intensity vector and line of intersection of this plane with horizontal plane, 0 - 360°		

TABLE 7. ACCURACY OF ANGLE Δ AND ANGULAR VELOCITY Δω/ω DETERMINATION*

	T = 10 min		T = 15 - 20 min, or more	
	Poor information $\sigma_H^* =$ 3500 gamma	Typical information $\sigma_H^* =$ 1850 gamma	Poor information $\sigma_H^* =$ 3800 gamma	Typical information $\sigma_H^* =$ 2200 gamma
$P_\alpha = 0,99$	Δ~15° Δω/ω~0,5%	Δ~3° Δω/ω~0,3%	Δ~5° Δω/ω~0,2%	Δ~3° Δω/ω~0,1
$P_\alpha = 0,95$	Δ~5° Δω/ω~0,4%	Δ~3° Δω/ω~0,2%	Δ~2° Δω/ω~0,1%	Δ<1° Δω/ω~0,05%

*Translator's note: Commas represent decimal points.

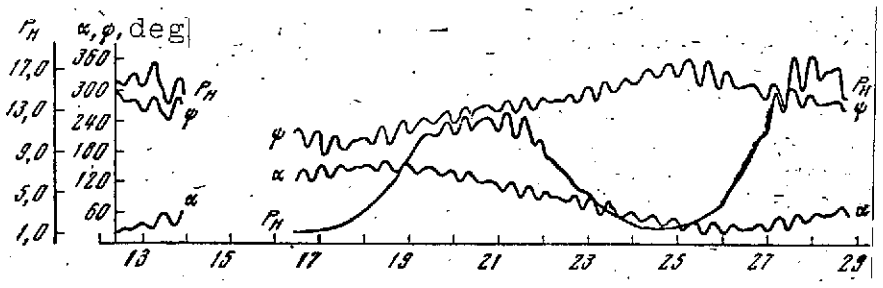

Figure 10. Variations of navigation parameters (from data of statistical processing of Proton 2 satellite information)

One division along abscissa axis corresponds to time interval 6.2 minutes

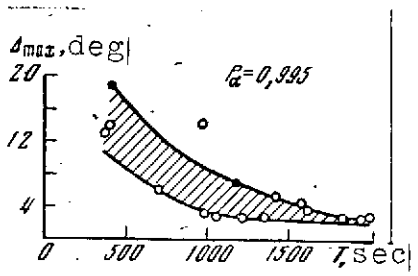

Figure 11. Accuracy of orientation determination as function of processed interval length

7), Δ is the angle determination error; Δω/ω is the relative angular velocity determination error; σ_H^* is the mean-square measurement error; T is the duration of the flight segment from which the simultaneously processed information was taken. Most typical are the numbers in the last column of Table 7. The accuracy improves with increase of the processed interval length. /163

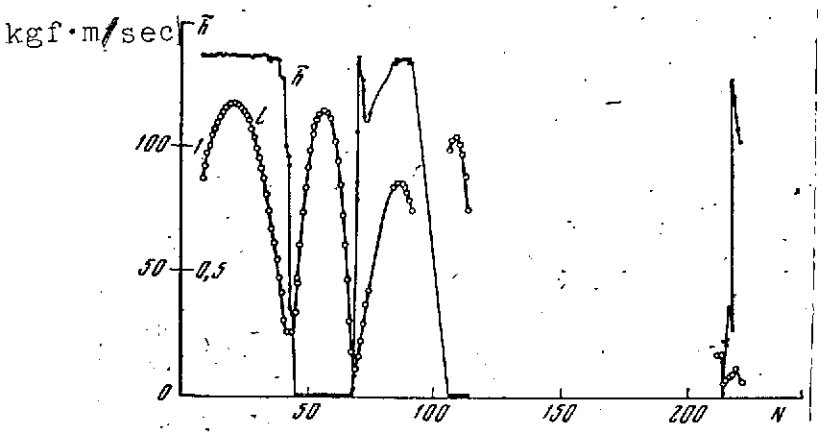

Figure 12. Variation of Proton 2 satellite kinetic moment vector modulus L and rotation energy $\tilde{h}$ from statistical processing data

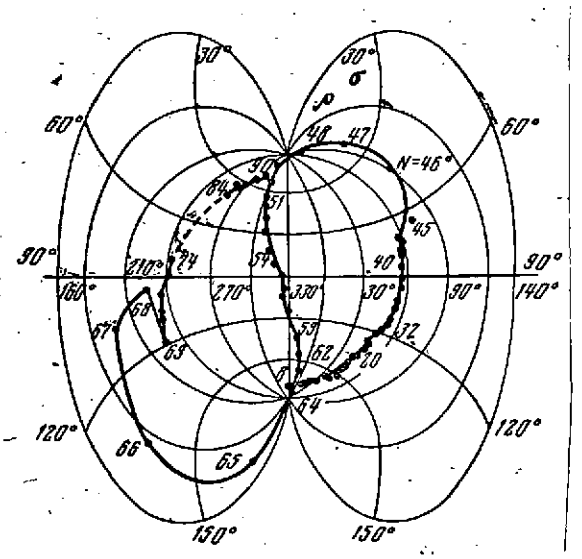

Figure 13. Trajectory of Proton 2 satellite kinetic moment vector in space (from statistical processing data)

Some results of determination of the orientation and rotation of the Proton 2 satellite in the first few dozen orbits are shown in Figure 12 and 13. These results make it possible to represent completely the nature of Proton 2 satellite rotation evolution during the indicated time interval. In Figure 12, the abscissa is the number N of orbits, the ordinate is the magnitude of the kinetic moment L and the dimensionless kinetic energy $\tilde{h}$ of rotation of the Proton 2 satellite. We observe deep long-period modulation of these quantities. L varies from 115 kgf · m · sec to ∿ 10 - 20 kgf · m · sec, /164 i.e., by a factor of 5 - 10. The quantity L determines the angular velocity of rotation, which, therefore, also changes several fold. The quantity $\tilde{h}$ determines the satellite rotation regime. For $\tilde{h} \sim 1.3$ "tumbling" (rotation around the transverse axis) of the satellite takes place. This stage lasts for several dozen orbits; the angular velocity (or L) is maximal in this case. Then there is rapid (4 - 5 orbits) transition to the axial rotation regime ($\tilde{h} \sim 0$) (at the midpoint of the transition segment the angular velocity is minimal); the satellite travels for several dozen orbits in the axial rotation regime ($\tilde{h} \sim 0$), again with maximal angular velocity, and then again transitions rapidly to the tumbling regime, and so on. Synchronously /165 with these long-period oscillations, there is also long-period change

of the position of the kinetic moment vector **L** in space (Figure 13). The figure shows the trajectory of **L** in space with orbit numbers along the trajectory; ρ is the angular distance of **L** from the North Pole of the world; σ is the latitude of **L**, measured from the vernal equinox point ($\sigma^* = 0°$). We see that **L** describes loops with broad /166
amplitude (loop span is $\sim 180°$), and periodically passes in the vicinity of the world poles (alternately through the North and South Poles).

5. Dynamic Analysis of Proton Satellite Rotation and Orientation Evolution. Evaluation of Nature of Interaction of Aerodynamic Flow with the Satellite

The experimentally discovered evolutionary effects in the motion of the Proton 2 satellite around its center of mass have a specific, previously unstudied nature. It was shown in [20 - 22] that these effects are caused by the aerodynamic flow influence on the solar battery paddles mounted skew-symmetrically on the satellite. A propellering aerodynamic moment is created, which spins the satellite like the windmill arms. In combination with the satellite orientation change relative to this flow, this creates the discovered long-period angular velocity modulations and nature of the rotation (axial spin or tumbling). Torques of any other nature cannot create such effects in the evolution of satellite motion around its center of mass [24]. Therefore, the observed propellering effects are easily distinguished from other effects.

On the other hand, it was found [19] that the propellering effects are sensitive to the nature of stream molecule reflection from the satellite surface. This makes it possible to evaluate the nature of molecular reflection on the basis of experimental data on Proton 2 satellite motion evolution around its center of mass. To date, very little is known concerning the real nature of molecular flow interaction with a satellite under cosmic conditions, yet the entire aerodynamics of the satellite depend on this interaction.

Therefore, determination of the reflection parameters is of considerable interest.

It was suggested in [19] that the reflection is purely diffusive with symmetric (relative to the normal to an elementary area) molecular scattering diagram. Then ambiguity in the nature of the reflection reduces to ignorance of only a single parameter — the probability mean reflection velocity C_r. It was shown that the experimental data on Proton 2 satellite orientation evolution lead to the value $C_r \sim 70$ m/sec, or $C_r/v \sim 10^{-2}$, where v is the incident flow velocity. Thus, the nature of the reflection was very close to absolutely inelastic impact. However, this conclusion is subject to refinement by introducing more complex molecule scattering models.

The described technique makes it possible to determine reliably and with adequate accuracy the orientation of artificial satellites for different types of motion. The technique works even in the case of low accuracy and incomplete information measurement complex, and also with a poor zero approximation. This indicates high reliability of the method. The technique is quite universal, and is applicable for determining the orientation of a broad class of satellites. It makes it possible to predict motion with definite accuracy on segments without instrumental information, and also makes it possible to determine the disturbances acting on the satellite. Processing by this technique of information from the Proton 2 satellite (more than 200 flight time orbits) made it possible to generate the series of navigation data for interpreting the indications of the scientific equipment installed aboard the satellite, and also made it possible to discover new dynamic effects in satellite orientation evolution and draw definite conclusions on the nature of aerodynamic flow interaction with the satellite.

Conclusion

The described techniques for processing Proton AES scientific information made it possible to automate the data reduction process to a considerable degree and obtain the scientific measurements results rapidly.

The systematic development of the described system took place in 1965 - 1968, practically simultaneously with the data reduction. The introduction of computer programs was carried out gradually, as the algorithms were worked out. Thus, in the initial stage, the Ural-11 general-purpose computer was used only for logic processing and generation of the instrument indications. Data input to the general-purpose computer was accomplished using punched cards, prepared manually from intermediate materials obtained from the special-purpose computers. By the time automatic data input development was completed, the programs for logic processing of the instrument indications had already been tested repeatedly on a large number of seances, and the only thing required was to mate them with the input program.

The described technique can be used for processing the scientific information of other space vehicles. In so doing, it is necessary to consider that the processing system preparation process is very tedious, and preparation must be initiated as early as possible, no later than the satellite production design stage. The design of the scientific measurements aboard satellites must take into consideration the possibility of automated information processing. The development of optimal facilities for compressing and selecting scientific information on board satellites is an urgent problem at the present time.

References

1. Grigorov, N. L., G. P. Kakhidze, et al. Kosmicheskiye issledovaniya, Vol. 5, No. 3, 1967, p. 383.

2. Grigorov, N. L., V. Ye. Nesterov, et al. Kosmicheskiye issledovaniya, Vol. 5, No. 3, 1967, p. 420.

3. Grigorov, N. L., V. Ye. Nesterov, et al. Izvestiya AN SSSR, seriya fiz., Vol. 31, 1967, p. 1225.

4. Grigorov, N. L., V. Ye. Nesterov, I. D. Rapoport, et al. /168
Kosmicheskiye issledovaniya, Vol. 5, No. 3, 1967, p. 395.

5. Basilova, R. N., N. L. Grigorov and I. A. Savenko. Kosmicheskiye issledovaniya, Vol. 7, No. 6, 1969, p. 895.

6. Basilova, R. N. and I. A. Savenko. On Energetic Charged Particle Angular Intensity Distribution Above the Atmosphere In the Cosmic Ray Equatorial Region. Geomagnetizm i aeronomiya, Vol. 11, No. 4, 1971.

7. Bratolyubova-Tsulukidze, L. S., N. L. Grigorov, L. F. Kalinkin, A. S. Melioranskiy, Ye. A. Pryakhin and I. A. Savenko. Measurement of High-Energy γ-Quanta in the Primary Cosmic Radiation Aboard the Proton 2 AES" Proceedings of All-Union Conference on Cosmic Ray Physics, Tashkent, Vol. 2, 1968. Moscow, FIAN, 1969.

8. Bratolyubova-Tsulukidze, L. S., N. L. Grigorov, L. F. Kalinkin, A. S. Melioranskiy, Ye. A. Pryakhin, I. A. Savenko and V. Ya. Yufarkin. Results of High-Energy γ-Quanta Measurement in the Primary Cosmic Radiation Aboard the Proton 2 and Kosmos 208 AES. Acta Phys. Acad. Sci. Hungaricae, 29, Vol. 29, Suppl. 1, 1970, p. 123.

9. Nesterov, V. Ye., I. V. Petrova, I. A. Savenko and K. N. Sharvina. Issledovaniye azimutal'noy uglovoy zavisimosti zakhvachennykh magitnym polem zemli protonov s energiey bol'she 400 Mev na malykh vysotakh (Study of the Azimuthal Angular Dependence of Protons with Energy More than 400 MeV Captured by the Earth's Magnetic Field at Low Altitudes). Proceedings of the All-Union Converence on Cosmic Ray Physics, Tashkent, Vol. 2, 1968. Moscow, FIAN, No. 1, 1969, p. 38.

10. Petrova, I. V., I. A. Savenko, O. I. Savun and K. N. Sharvina. Longitudinal Variation of the Inner Radiation Band Particle Intensity at Low Altitudes from Data of Proton 2 AES. Geomagnetizm i aeronomiya, Vol. 11, No. 2, 1971.

11. Volodichev, N. N., N. L. Grigorov and I. A. Savenko. Izucheniye spektra po zhestkostyam zaryadovykh grupp pervichnogo kosmicheskogo izlucheniya na kosmicheskoy stantsii "Proton-2" (Study of rigidity Spectrum of Primary Cosmic Radiation Charge Groups Aboard the Proton 2 Cosmic Station). Proceedings of All-Union Conference on Cosmic Ray Physics, Tashkent, Vol. 2. Moscow, FIAN, No. 1, 1969, p. 6.

12. Volodichev, N. N., N. L. Grigorov and I. A. Savenko. Rigidity Spectra of Primary Cosmic Ray Nuclear Groups. Acta Phys. Acad. Sci. Hungaricae, Vol. 29, Suppl. 1, 1970, p. 395.

13. Grigorov, N. L., N. N. Volodichev I. A. Savenko, and A. A. Suslov. Study of the Chemical Composition and Energy Spectra of Galactic Cosmic Rays Aboard AES. Present volume, p. 166.

14. Golubkov, V. V. and I. G. Khatskevich. Kosmicheskiye issledovaniya, Vol. 7, No. 4, 1969, p. 510.

15. Khatskevich, I. G. Kosmicheskiye issledovaniya, No. 1, 1971, p. 3.

16. Beletskiy, V. V., V. V. Golubkov, Ye. A. Stepanova and I. G. Khatskevich. Kosmicheskiye issledovaniya, Vol. 7, No. 4, 1969, p. 522.

17. Beletskiy, V. V., V. V. Golubkov, E. K. Lavrovskiy, S. I. Trushin and I. G. Khatskevich. Kosmicheskiye issledovaniya, Vol. 5, No. 5, 1967, pp. 686 - 702.

18. Beletskiy, V. V., V. V. Golubkov and I. G. Khatskevich. XVIII International Astronautic Congress, Belgrade, 1967. Pergamon Press: Oxford and New York, PWN-Polish Scientific Publisher, 1968.

19. Beletskiy, V. V. Kosmicheskiye issledovaniya, Vol. 8, No. 2, 1970.

20. Beletskiy, V. V., V. V. Golubkov, Ye. A. Stepanova and I. G. Khatskevich. Opredeleniye orientatsii iskusstvennykh sputnikov po dannym izmereniy (Determination of Artificial Satellite Orientation from Measurement Data). Rotaprint edition, Institute of Problems of Mechanics, Part 1, Moscow, 1967.

21. Akim, E. L. and T. M. Eneyev. Kosmicheskiye issledovaniya, Vol. 1, No. 1, 1963, p. 5.

22. Chapman, S and G. Bartels. Geomagnetism, 2. Oxford Univ. Press, London, 1946.

23. Adam, N. V., N. P. Ben'kova, V. P. Orlov, I. K. Osipov and L. O. Tyurmina. Geomagnetizm i aeronomiya, Vol. 2, No. 5, 1962, p. 949.

24. Beletskiy, V. V. Dvizheniye iskusstvennogo sputnika otnositel'no tsentra mass (Motion of Artificial Satellite Around Its Mass Center). Moscow, Nauka Press, 1965.

Abstracts

UDC 537.591

Prospects for Studying High-Energy Cosmic Ray Particles Aboard Heavy AES. N. L. Grigorov. /170

We examine the fundamental questions of the technique for studying superhigh-energy cosmic ray particles (energy interval 10^{10} - 10^{15} eV) and show that such particles can be observed and studied by direct methods with satisfactory statistical validity only beyond the limits of the Earth's atmosphere, using heavy artificial Earth satellites. With the aid of results obtained aboard the Proton 1, 2, 3 AES, we examine specific problems of high-energy particle physics and cosmic ray physics. We discuss some ways to study experimentally the subject problems using heavy AES.

UDC 537.591

Measurement of Effective Inelastic Interaction Sections of Proton with Carbon and Hydrogen Nuclei in the Energy Interval 20 - 600 GeV Aboard Proton 1, 2, 3 Space Stations. N. L. Grigorov, V. Ye. Nesterov, I. D. Rapoport, I. A. Savenko and G. A. Skuridin.

The values of σ^{in}_{p-C} in the energy interval 20 - 600 GeV have been measured aboard the Proton 1, 2, 3 AES utilizing primary cosmic ray protons with accuracy from 2 to 4.5%. The measured σ^{in}_{p-C} value increases by 20 $\pm$ 5% with energy increase from 20 to 200 GeV. The values of σ^{in}_{p-p} are obtained with errors from 8 to 20% by a difference method using polyethylene and carbon targets. The resulting energy dependence of σ^{in}_{p-p} does not contradict the same section growth obtained for σ^{in}_{p-C} in the same energy interval. Analysis of the various

systematic and physical effects influencing the measured section magnitude showed that these effects cannot explain the observed section increase.

UDC 537.591

Energetic Distribution of Primary Cosmic Ray Particles in the 10^{10} - 10^{14} Energy Interval Measured Aboard Proton 1, 2, 3, Space Stations. N. L. Grigorov, V. Ye. Nesterov, I. D. Rapoport, I. A. Savenko and G. A. Skuridin.

The energy spectrum of all primary cosmic ray particles in the energy interval 10^{10} - 10^{14} eV, and the energy spectrum of protons in the energy interval 10^{14} - 10^{1} eV, have been measured aboard the Proton 1, 2, 3 AES. The measured all-particle spectrum is a power-law spectrum over the entire energy interval. The proton energy spectrum becomes steeper at energies of 10^{12} - 10^{13} eV. The calculated nucleon spectra at various atmospheric depths based on the primary cosmic ray spectra obtained aboard the Proton AES agree with the gamma-ray, neutron, and nuclear-active particle spectra measured at the same atmospheric depths.

UDC 537.591

Apparatus for Studying Cosmic Rays Aboard the Proton 4 Scientific Station. N. L. Grigorov, I. D. Rapoport, I. A. Savenko, L. F. Kalinkin and G. P. Kakhidze.

A detailed systematic description is given of an experiment studying high-energy primary cosmic radiation undertaken aboard the Proton 4 scientific space station. The instrument for recording particles with energies $\gtrsim 10^{11}$ eV contained an ionization calorimeter with lead and iron absorber with overall thickness equal to about 7.5 nuclear interaction ranges, two large-area Cherenkov detectors for determining particle charges, carbon and polyethylene targets, and a nuclear interaction detector. With the aid of this equipment, we studied the energy and charge spectra of particles up to 10^{15} eV and measured the effective inelastic interaction section of protons with light and heavy nuclei. Two other instruments were used to record the electron component and seek fractionally charged particles.

UDC 537.591

Calibration of the SEZ-14 Instrument Installed Aboard Proton 1, 2, 3 Cosmic Stations on ITEP [Institute of Theoretical and Experimental Physics] Synchrotron. V. V. Akimov, B. S. Borisov, G. V. Veselova, L. L. Gol'din, L. N. Kondrat'yev, V. Ye. Nesterov, I. D. Rapoport N. G. Ryabova and G. K. Tumanov.

Results are presented of calibration of the SEZ-14* instrument /171 used aboard the Proton AES for measuring σ^{in}_{p-C} and σ^{in}_{p-p} at energies 20 - 600 GeV, and also for measuring the primary cosmic ray energy spectra on the ITEP synchrotron at proton energy 5 GeV. With proton entry into the instrument from the "exit window" side at energy 5 GeV, the measured value of $\sigma^{in}_{p-C} = 204 \pm 6$ mb, which is $8 \pm 6\%$ less than the σ^{in}_{p-C} value measured at energy 21.5 GeV on a particle accelerator. With entry of the protons into the instrument from the opposite side, the measured section becomes 167 ± 10 mb, i.e., the value decreases by 18%. In this case, the counting rate decreases by a factor of four. On the basis of the data obtained, we can conclude that when measuring σ^{in}_{p-C} aboard a satellite at energy 5 GeV, particle entry into the instrument from the back would reduce the measured section by 4% in comparison with the value measured for particle entry from the "entrance window" side.

UDC 537.591

Study of High-Energy Electrons in Near-Earth Cosmic Space Aboard Proton 1 and 2 AES. N. L. Grigorov, L. F. Kalinkin, E. I. Kogan-Laskina and I. A. Savenko.

Results are presented of measurements of the electron energy spectrum in the energy interval 20 MeV to 5 GeV and the distribution with respect to zenith angle of electrons with energies above 500 MeV, performed aboard the Proton 2 scientific space station. The data of several studies of properties of the "excess radiation" observed in the stratosphere and at heights of 10^2 - 10^3 km are analyzed. From the ensemble of results obtained by various authors in experiments involving balloon and satellite flights, we can conclude that there are significant fluxes of electrons with energies 10 - 10^3 MeV in the "excess radiation" composition in near-Earth cosmic space. The natural source of such electrons may be "albedo" particles which arise in the matter of the atmosphere under the influence of the primary cosmic rays. The large variations in time of the high-energy electron fluxes observed in the stratosphere may be considered

*Translator's note: Inadvertently given in foreign text as "SEZ-4".

confirmation of the hypothesis of capture and relatively long-term retention of these particles by the Earth's magnetic field, which had been proposed earlier on the basis of measurements aboard the Proton 1 and 2 AES.

UDC 537.591

Study of High-Energy Electrons in the Stratosphere. V. A. Bezus, A. M. Gal'per, N. L. Grigorov, V. V. Dmitrenko, L. F. Kalinkin, V. G. Kirillov-Ugryumov, B. I. Luchkov, A. S. Melioranskiy, I. A. Savenko and E. M. Shermanzon.

Results are presented of an experimental study of the intensity and energy spectra of the direct (toward the Earth) and albedo (away from the Earth) electrons with energy more than 100 MeV at various heights in the atmosphere. The measurements were made at geomagnetic latitude 46° N, where the cutoff rigidity is 3.5 GeV/c. The experiment was conducted during 1967 - 1968 aboard high-altitude balloons using an instrument with multilayer spark chamber. Large variations (by a factor of 2 - 3) of the direct electron flux which correlate with the state of the Earth's magnetosphere were discovered at small depths in the atmosphere ($h \lesssim 50$ g/cm^2). The effect is explained on the basis of the assumption of the existence in the Earth's magnetosphere of trapped electrons with energy more than 100 MeV, which "spill out" during disturbances of the magnetic field. The intensity of the "spilling" electron flux in the energy interval 100 - 1500 MeV is $(6.2 \pm 0.8) \cdot 10^{-2}$ (cm^2 · sec · sr)$^{-1}$. The exponent of the "spilling" flux is differential energy spectrum 1.56 ± 0.22.

UDC 537.591

Study of Chemical Composition and Energy Spectra of Galactic Cosmic Rays Aboard AES. N. L. Grigorov, N. N. Volodichev, I. A. Savenko and A. A. Suslov.

Results of flux measurements of primary ray cosmic nuclear groups with energy $\sim 10^9 - 10^{10}$ eV, obtained aboard the Proton 2 space station using a Cherenkov spectrometer with zero shading of the instrument by the Earth, are presented and discussed. Information on stable operation of the instrument permitted averaging the data obtained over a long time interval. The intensity values for the nuclear groups presented in the article exceed by a factor of two or more the intensities measured by several investigators, primarily aboard balloons during the same time period. On the other hand, studies performed aboard satellites and interplanetary stations in which the intensities obtained of particles with $Z \geq 1$ and $Z \geq 2$ are close to the intensities measured aboard the Proton 2 AES in the rigidity interval $\geq 1 - 2$ GeV/c are presented. The data obtained

/172

relate to the second half of 1965. We examine the advantages and disadvantages of the Cherenkov-scintillation method used and the prospects for further study of primary cosmic ray nuclear fluxes.

UDC 629.78.06

Processing Proton Space Station Scientific Information. V. V. Akimov, V. V. Beletskiy, V. V. Golubkov, G. N. Zlotin, S. I. Karmonov, I. N. Kikhadze, V. Ye. Nesterov, V. M. Pokras, V. L. Prokhin, I. D. Rapoport, and I. G. Khatskevich.

The characteristic features of Proton AES instrumentation data complex operation defined the tasks of designing the data processing system and its mathematical support. It was necessary to develop both methods and algorithms for processing the Proton AES scientific information which would permit a significant degree of automation of the data handling processes. The general scheme of the data processing system consists of several elements: material collection and systematization; data input into the general-purpose digital computer; obtaining the quick-look scientific recording, processing, and output of the scientific and navigation instrument telemetry indications. The techniques for statistical processing of the magnetometer information and satellite orientation determination are presented in greater detail. The processing of the scientific instrument indications with account for their attitude in space is the basic preliminary data processing result.

Translated for National Aeronautics and Space Administration under contract No. NASw 2483, by SCITRAN, P. O. Box 5456, Santa Barbara, California, 93108